

Ecophysiology of mercury-methylating microorganisms in freshwater ecosystems

By

Benjamin D. Peterson

A dissertation submitted in partial fulfillment of
the requirements for the degree of

Doctor of Philosophy

(Environmental Chemistry and Technology Program)

at the

UNIVERSITY OF WISCONSIN – MADISON

2021

Date of final oral examination: 2021-07-19

The dissertation is approved by the following members of the Final Oral Committee:

Dr. Katherine McMahon, Professor, Environmental Chemistry and Technology

Dr. David Krabbenhoft, Senior Research Scientist, U.S. Geological Survey

Dr. James Hurley, Professor, Environmental Chemistry and Technology

Dr. Eric Roden, Professor, Environmental Chemistry and Technology

Dr. Christina Remucal, Associate Professor, Environmental Chemistry and Technology

I believe that above all else, a scientist, especially a publicly funded environmental PhD student at a public university, is a public servant. To honor that, this thesis is dedicated to those who live, work, eat, and play in the places where this work was done. May the work described herein and the work I do in the future someday play a role in restoring environmental quality and improving the quality of life for those who are closest to and most dependent on their natural resources.

Table of Contents

Acknowledgements.....	iii
Abstract.....	viii
Chapter 1: Introduction.....	1
Chapter 2: Mercury methylation genes identified across diverse anaerobic microbial guilds in a eutrophic sulfate-enriched lake.....	11
Chapter 3: Metagenomic insights into hydrological and biogeochemical constraints on mercury methylation under suboxic conditions in a hydroelectric reservoir.....	76
Chapter 4: Microbial constraints on methylmercury production along a sulfate gradient in the Florida Everglades.....	124
Chapter 5: Influence of sulfate reduction on methylmercury production in a eutrophic freshwater lake.....	170
Chapter 6: Conclusions and future directions.....	209

Acknowledgements

This dissertation would not have been possible without a village of people. First and foremost, I'd like to thank Trina for welcoming me into the McMahon Lab family and for her unending support and encouragement over the last six years. Reading your work got me interested in microbial ecology and biogeochemistry before I really even knew what those words meant. I've learned so much about the scientific method and microbial ecology from you, but also a great deal about making science fun and having a good work-life balance. Joining your lab was one of the best decisions I've ever made, thank you for everything. Huge thanks also to Dave Krabbenhoft, who was essentially a co-advisor throughout my graduate work. Half of my research chapters were only possible because you welcomed me into ongoing research projects. I learned a great deal about how to identify and ask the important questions, the strength of collaborating with a large, interdisciplinary group of people, and the importance of seeing and getting a sense for the field site. Thanks for welcoming me into the USGS MRL family.

Thanks also to the rest of my committee. Jim, thanks for always being willing to chat, I learned so much about the Hg cycle from you, especially early on. Someday we'll take a look at those anoxic phototrophs! Eric, I miss swinging by your office in Geosciences and talking science, you were always great about challenging me to look at things from a different perspective. Christy, I've always looked up to your dedication to good science and attentiveness to detail, whether it was going over writing assignments in class, meeting about DOM collaborations, or just catching up on research. Karthik, your help in getting me started on metagenomic analyses was critical.

I have been fortunate enough to have had great collaborators throughout my work as well. Thanks to Brett Poulin for help and guidance on the Everglades and Hells Canyon projects.

I learned a great deal from you, not only about geochemistry, but about integrating pieces of information into a larger conceptual understanding of the processes. I look forward to working more with you in the future. Thanks to Sarah Janssen for guidance on pretty much every step of the scientific method throughout my time at UW. Your ability to see from the smallest details up to the big picture has taught me a lot about being a complete scientist. The incubations project would not have come together without your help. Thanks also to the Hells Canyon research team for welcoming me in and being supportive of my work. In particular, thanks to the Idaho Power Company folks that I've worked with, Jesse Naymik, Nick Gastelecutto, Ralph Myers, Chris Larsen, Chuck Hoovestal and the rest of the crew. Special thanks too to Austin Baldwin, Greg Clark, Collin Eagle-Smith, James Willacker, and Mark Marvin-DiPasquale, I've learned a great deal from all of you and have had a lot of fun working in the field and throwing around ideas with all of you. I'm sure I missed names in here... you know who you are, and I thank you for your help and support.

Thanks also to the entire Mercury Research Lab. Jake Ogorek, you're an excellent teacher, a better friend, and an even better cook. Thanks for all the extra time you put in teaching me to analyze my samples, and the analyses that you did yourself. Much of this work would not have come together without you. Thanks also to Mike Tate, John DeWild, Chris Babiarz, and Evan Routhier for your help with analyses and sampling, your feedback, and just generally making me feel like a part of the lab. Huge thanks to Ryan Lepak for getting me off the ground when I started. From helping me get started sampling when I was a rookie grad student, to extensive feedback on anything I send you, to long discussions about the Hg field at 2AM on the streets of Poland, to just getting a drink and having a good time, you've been a great mentor and friend throughout this process. Tylor Rosera, thanks for all the brainstorming sessions and help

in the field, hoping we get to work together more soon. Grace Armstrong, thanks for your help with the Mn and Fe analyses.

I also would not have made it this far without the support of the McMahon Lab family. Ben Oyserman, you helped get me started on this path, thanks for all the guidance, encouragement, and spit-balling, especially when we overlapped in the lab. Big thanks to Chris Lawson and Elizabeth McDaniel, you two were kind of my “cohort” for the lab and having two great scientists like you to look up to was invaluable. Chris, you’re one of the smartest and most enthusiastic scientists I know, and those long office conversations have really shaped my vision of what it means to be a good scientist. Can’t wait to come and work scrubbing your lab floors in Toronto! I hope we get the chance to collaborate in the future. Elizabeth, I admire your dedication to all facets of being a scientist. Please keep your github page updated so I can continue stealing code from you and expect emails asking for help in the future. Pancho, thanks for all your help getting started on the bioinformatics work! Amber, if you were not in the lab, I might still be on Mendota trying to get the incubations to work, your inability to say no to helping out with sampling knows no bounds. Thank you so much. Extra special thanks to Anna Schmidt and Robert Marick, working with you two over these last few years has been an amazing experience. You two are an inspiration, you are going to go on to do great things and I’m proud to have worked with you both. Thanks also to all the undergraduates I’ve mentored who have helped with sampling and analyses, Mykala Sobieck, Diana Mendez, Ariel Sorg, and Anna Schwendinger. For all the other McMahonites, I have learned something from each and every one of you. Beyond that, you have all been very supportive, having a crew like you to go through this with is irreplaceable. Thank you.

One of the best parts of working at UW – Madison is the opportunity to interact with people from all different departments. Thanks to all the graduate students in the EC&T, you are a great community. Thanks to James Lazarcik for not only putting up with me breaking equipment but going above and beyond in teaching me how the instruments work and how to troubleshoot them, and for reminding me to wear my safety glasses. Thanks also to everyone over at the CFL that took me in and let me pretend to be a limnologist. In particular thanks to Vince Butitta for all his help with, well, just about everything, including rescuing me off the lake at 1AM... multiple times. Martin Perales, talking with you through the dredges of year 3 kept me going at times. Luke Loken, you always had the little fix when I was in need, whether it was an R script, a suggestion for sampling, replacing a starter in the Taurus, or a new car in California. Thanks to Emily Stanley as well, for all your help over the years, your excitement for science is an inspiration.

Many thanks to my past mentors as well. To George Briggs, Eric Helms, and Janice Lovett from SUNY-Geneseo, thanks for letting me in to your labs to blunder around. Even if I didn't get much done, I learned some invaluable lessons from you all. Eric, thanks also for being a great mentor as I was tutoring students and generally being a great teacher. Carmen Vivar, you are one of the smartest scientists I've ever worked with, and those long brainstorming sessions have taught me the value of just spending time throwing ideas out there. Henriette van Praag, I'm still inspired by your commitment to good, clean scientific design, you have shaped my approach to building an experiment. Davide, thank you, for everything. Denise Ferkey, thank you for giving me my first exposure to full-time research.

Every grad student needs some distractions, and I was fortunate enough to have just the right number of them. Thanks to my climbing partners, especially Loris, those trips to Devil's

Lake this last year got me through some rough patches. Thanks to Tyler Hoecker, having a great friend with just a little bit of scientific expertise overlap made for some very fun science discussions. Also enjoyed the climbing, camping adventures, and all-around good times. Thanks as well to my friends and colleagues with MTR Magic Key, having some art projects to focus on helped get my brain reset for science. Thanks especially to Colin Keenan, not sure if you know how much the late-night editing room or filming sessions, rounds of Suburbia or Splendor, and Pokemon battles helped me get through at times. Thanks also for being my very first labmate at Geneseo... I will never forget those days. Thanks to the Milwaukee Bucks for waiting to win the Finals until the day after I defended. #BucksInSix!

No one deserves more credit for this thesis than my parents. Mom and Dad, your endless patience with my endless questions and constant encouragement to find the answers for myself has led me directly to where I am now, asking questions for a living. You have always supported me and celebrated me for who I am and the effort I put in rather than the outcome. I can't tell you how important that has been to me and the lesson I have learned from that. You are the best parents anyone could ask for; I love you both. Thanks also to my siblings, I'm so proud of and inspired by everything that you all are doing. Thank you for always being supportive and interested in whatever I'm doing. Spending time with you all rejuvenates my spirit. I also got the best set of siblings anyone could ask for... guess I'm just a lucky guy that way!

Thanks to my fuzzleball officemates for the last year and half, Bertrand and Fitzpatrick. And of course, thanks to my wife, Hannah. Thank you for getting me out of my head when I needed to the most and thank you for sticking by my side for this whole crazy adventure and loving me when I was at my most stressed, at the bottom of the thesis writing hole. We made it! I'm looking forward to sharing the next round of adventures with you.

Abstract

The goal of this dissertation is to investigate the ecophysiology of mercury (Hg)-methylating organisms in freshwater ecosystems in order to probe how biogeochemical cycles influence the production of toxic methylmercury (MeHg). MeHg production is an important step in food web accumulation of MeHg, but the microbial community that mediates this process in the environment is poorly understood. By linking the Hg methylation gene *hgcA* to genes encoding metabolic pathways and pairing this with geochemical measurements and targeted Hg methylation assays, we sought to illuminate the mechanisms underlying the Hg methylation capacity of microbial communities in multiple freshwater ecosystems.

In **Chapter 1**, I provide a brief overview of the field as it stands today. I provide a background on transport and transformations of Hg in aquatic ecosystems, constraints on bioavailability of inorganic Hg, and what is known about Hg-methylating organisms in culture and in the environment. I also review the molecular sequencing methods and Hg-methylation assays used in this dissertation. In **Chapter 2**, we used shotgun metagenomic sequencing and genome reconstruction to identify and characterize the genomes of Hg-methylators in a eutrophic, sulfate-enriched freshwater lake. This data showed that non-canonical Hg-methylating organisms, particularly fermentative organisms from the Kiritimatiellaeota phylum, are numerically dominant throughout the anoxic hypolimnion in Lake Mendota. In **Chapter 3**, we again used shotgun metagenomics and genomic reconstruction paired with extensive hydrological and geochemical data to identify Hg-methylating organisms in a highly dynamic hydroelectric reservoir over three years. We showed that the extent of MeHg production and accumulation is heavily dependent on the hydrologic regime of the system and suggest that MeHg production is occurring under suboxic conditions not previously thought to facilitate Hg-

methylation. Again, the Hg-methylating community was dominated by non-canonical Hg-methylators. In **Chapter 4**, we isolated the impact of the microbial community on MeHg production using a stable-isotope enriched Hg tracer experiment in parallel with characterization of the Hg-methylating microbial community. We showed that the Hg methylation capacity increased with decreasing levels of sulfate and was closely correlated to *hgcA* abundance. Despite evidence for active sulfate reduction, there were no sulfate-reducing bacteria (SRB) with *hgcA*. In **Chapter 5**, we revisited the sulfate-enriched eutrophic lake from Chapter 2 to pair metagenomic sequencing with Hg methylation assays to investigate the role of sulfate reduction in MeHg production. We observed significant decreases in MeHg production in response to inhibition of SRB, despite the low abundance of SRB with *hgcA*. Finally, in **Chapter 6**, I summarize the findings of this thesis and discuss future directions that will expand upon these findings.

Overall, this thesis expands our knowledge of the metabolic and taxonomic diversity of Hg-methylating organisms and how these communities are shaped by limnological conditions. It also shows how the Hg methylation capacity of the microbial community can impact the *in situ* production and accumulation of MeHg. It provides a framework for using insights into the ecophysiology of the Hg methylators to predict the impact of different biogeochemical cycles on Hg methylation. It also highlights the need to expand upon these findings using geochemical characterization, molecular sequencing, Hg methylation assays, next-generation physiology experiments, and additional functional analysis of the microbial community to further understand how organisms with *hgcA* are mediating the production of MeHg in aquatic ecosystems.

Chapter 1: Introduction

Mercury (Hg) is a well-known and near-ubiquitous public health threat.¹ Hg levels in the environment have increased 3-4 times since the start of the Industrial Revolution, largely due to anthropogenic sources such as coal-fired power plants and small-scale artisanal gold mining.² Hg pollution can be locally discharged to aquatic environments as inorganic Hg(II) (iHg) or released into the atmosphere, primarily as elemental Hg(0).³ It can remain in the atmosphere for up to a year, which allows it to be distributed globally, before being oxidized to iHg and deposited onto terrestrial or aquatic ecosystems.³ The iHg can then complex with a wide range of ligands, which will help determine the fate of the Hg, whether it is transformed and taken up by aquatic organisms, bound to particulate matter and buried in the sediments, or reduced back to Hg(0) and possibly released into the atmosphere.^{2,4,5}

Hg contamination in aquatic ecosystems is problematic due to its ability to bioaccumulate and biomagnify.⁶ This leads to high levels of Hg contamination in aquatic food webs, which can have deleterious neurotoxic and developmental effects on organisms at the top of the food web, including humans who rely on Hg-contaminated fish or other animals for sustenance.¹ This bioaccumulation and biomagnification of Hg only occurs as organic methylmercury (MeHg). MeHg is produced intracellularly by bacteria and archaea, typically in anoxic environments, then exported back to the environment.^{7,8} Once in the environment, it can enter the aquatic food web by uptake into algal cells.⁹ Because MeHg is most often produced in anoxic environments and the base of the food web tends to be in oxic environments, the proximity of MeHg production to oxic regions and MeHg transport post-production are critical elements in determining the extent of MeHg accumulation in the food web.

MeHg production is primarily controlled by two factors, the bioavailability of iHg for uptake and the Hg methylation capacity of the microbial community.¹⁰ Both factors have been shown to be limiting under different circumstances.^{11–13} The bioavailability of iHg for uptake and subsequent methylation has been well-studied but is still not fully understood. Sulfide binds strongly to iHg, forming HgS complexes that can aggregate into particles and precipitate, leading to Hg loss to the sediments.¹⁴ When dissolved organic matter (DOM) is present alongside sulfide, it can limit the formation of particulate HgS and enhance iHg bioavailability.¹⁵ This works through a number of possible mechanisms, such as precluding or preventing HgS complexes^{16,17}, usually associated with the aromaticity of the DOM¹⁸, or by Hg binding to the S-moieties in the DOM. Interactions between the two factors, such as the sulfurization of the DOM¹⁹, complicates the relationship between the two. Furthermore, there is still uncertainty over whether iHg speciation is largely due to kinetic constraints or thermodynamic equilibrium.^{4,20,21} This, coupled with the uncertainty in binding constants and solubility measurements of some complexes, makes it difficult to accurately model and predict iHg complexation in natural ecosystems.⁴ The other primary factor influencing MeHg production, the Hg methylation capacity of the microbial community, is still poorly understood in natural systems. This is the primary focus of this thesis and is discussed more below.

Microbial Hg methylation is mediated by the *hgcAB* genes.⁸ The *hgcA* gene is a distant homologue of the corrinoid iron-sulfur gene within the acetyl-CoA synthase complex.⁸ HgcA uses methyl-tetrahydrofolate as a methyl group donor in the methylation reaction, which links it to the tetrahydrofolate (THF) cycle and the Wood-Ljungdahl pathway.^{8,22,23} HgcB appears to reduce the cobalamin co-factor in HgcB, thus assisting in turnover of the protein.⁸ Uptake of iHg is active for some organisms⁷ and may be linked to Zn uptake pathways²⁴. Once the iHg is

methylated, it is rapidly exported from the cell, suggesting a role in Hg detoxification.⁷ However, microbes with an *hgcA* deletion do not suffer reduced fitness under laboratory conditions.^{8,25} Thus, the physiological role of this process is still unknown; in fact, Hg methylation is widely suspected to not be the native function of the *hgcA* gene. Understanding the role of Hg methylation and HgcA function in cell physiology will help explain the distribution of these genes in the environment and where and when the Hg methylation pathways are active in natural ecosystems.

The microbial Hg-methylation capacity in natural ecosystems is linked to the identity of the microbial guilds that are producing MeHg under environmental conditions. Early studies relied on isolation of Hg-methylators or stimulation/inhibition of Hg-methylating activity, which identified sulfate-reducing bacteria as the dominant Hg-methylating organisms.^{26,27} Iron-reducing *Geobacter*^{28,29} and methanogenic archaea³⁰ were also identified as relevant Hg-methylators. The discovery of *hgcA*⁸ facilitated rapid identification of putative Hg-methylating organisms in cultured organisms with sequenced genomes^{31,32} and publicly available metagenomes³³ and metagenome-assembled genomes^{34,35}, thus expanding the known diversity of putative Hg-methylating organisms. In the environment, molecular sequencing methods have identified diverse *hgcA* sequences in rice paddy soils^{36,37}, pristine³⁸ and impacted^{39,40} lake sediments, periphyton-associated biofilms^{41,42}, wetland soils⁴³⁻⁴⁵, and the water column of freshwater⁴⁶ and marine ecosystems⁴⁷⁻⁵¹. However, the links between geochemical conditions, microbial metabolic activity, and MeHg production are still poorly understood.

Parallel with these advancements in the Hg methylation field, molecular sequencing techniques have become much more powerful, further fueling our ability to investigate the microbial community under environmental conditions. Several PCR primer sets have been built

for amplicon sequencing of *hgcA* in environmental samples.^{35,36,43,44,52} While this approach does provide deep sequencing of the microbes with *hgcA*, it does not identify sequences highly divergent from the reference sequences used to build the primers and does not provide additional information about the gene content of organism containing the *hgcA* gene.^{34,46} Additionally, the *hgcA* gene is highly divergent and is thought to have been widely distributed through horizontal gene transfer^{33,34}, which limits our ability to identify and characterize organisms based solely on their *hgcA* gene. On the other hand, shotgun metagenomics involves sequencing random strands of DNA from the sample, which reduces amplification bias and enables the identification of highly divergent *hgcA* genes. The strands of DNA can be “assembled” into longer contigs, which enables the recovery of full-length gene sequences and provides additional genomic context for the gene. Subsequently these genes can be “binned” into population genomes, or “bins”, which provides further metabolic and taxonomic information about the Hg-methylating organism.⁵³ This has become an extremely powerful technique that allows researchers to reconstruct the genomes of organisms of interest and predict their metabolic function *in situ*. The rapidly decreasing cost of sequencing, the expanding toolbox for metagenomic analyses, and the increasing size and availability of reference datasets suggest that shotgun metagenomic sequencing will continue to play an increased role in Hg methylation studies. Additionally, shotgun metagenomics can be combined with more advanced measurements such as metatranscriptomics/metaproteomics or stable isotope probing to further probe the impact of different organisms with *hgcA* on MeHg production in the environment.

While the diversity of Hg-methylating organisms is beginning to be appreciated, we still have little understanding of how this diversity impacts MeHg production under environmental conditions. Even in controlled laboratory conditions, there is a wide range in MeHg production

capacity of different organisms with *hgcA*^{31,32,54}, and this can change with changing conditions or an added metabolic partner^{55,56}. Many other factors could influence MeHg production capacity as well. For example, transcriptional regulation of *hgcA* has only been tested under a narrow range of laboratory conditions, but these results do suggest it is constitutive despite the presence of an *arsC*-like regulator in the tested organisms.^{56,57} While *hgcA* has been shown to be expressed in the water column of a marine inlet, expression was not compared to the abundance of the organisms.⁵⁰ In thawing permafrost, RNA levels of *hgcA* was unlinked to *hgcA* abundance in the DNA.^{34,58} Translational regulation could further modify Hg methylation activity. Additionally, the uncertainty about the role of *hgcA* in microbial metabolism and its reliance on a metabolic cycle heavily involved in an array of energy conserving, carbon fixing, and biosynthetic pathways means we cannot predict why and/or when Hg-methylators find it advantageous to produce MeHg.

Thus, pairing these shotgun metagenomic methods with other molecular sequencing methods and functional measurements of Hg methylation and microbial metabolism is an important step in understanding how the microbial community underlies the observed MeHg production and accumulation in the environment. A key method is the stable isotope-enriched Hg tracer incubations, in which Hg species that are highly enriched in one isotope are added to an environmental sample under either ambient or modified conditions, incubated for a set period of time, and then preserved and analyzed using inductively coupled plasma mass spectrometry.^{59,60} This technique has been widely used to measure MeHg production in cultures, but also has been used to measure MeHg production potential in environments such as the water column of freshwater lakes^{46,61,62}, wastewater impacted freshwater sediments³⁸, and wetland soils^{44,45}.

Overall, there is a major knowledge gap in understanding which microbial processes are driving Hg methylation in natural systems, which leads to a limited understanding of how geochemical factors drive MeHg production capacity. In this thesis, we first set out to identify and characterize Hg-methylating organisms in two separate freshwater lacustrine systems using shotgun metagenomic techniques (Chapters 2 and 3). We then paired targeted stable isotope-enriched Hg methylation assays with shotgun metagenomic sequencing to isolate the Hg methylation capacity and investigate the Hg methylating organisms underlying the observed trends (Chapter 4). Finally, we paired these two methods again to probe how the microbial community mediates the impact of sulfate reduction on MeHg production (Chapter 5). These studies lay the foundation for more targeted studies investigating how the microbial mechanisms underlying the Hg methylation capacity link biogeochemical cycling and water quality to MeHg production in aquatic ecosystems.

References

1. UN. *Global mercury assessment*. (2018).
2. Amos, H. M., Jacob, D. J., Streets, D. G. & Sunderland, E. M. Legacy impacts of all-time anthropogenic emissions on the global mercury cycle. *Global Biogeochem. Cycles* **27**, 410–421 (2013).
3. Krabbenhoft, D. P. & Sunderland, E. M. Global Change and Mercury. *Science* **341**, 1457–1458 (2013).
4. Hsu-Kim, H., Kucharzyk, K. H., Zhang, T. & Deshusses, M. A. Mechanisms regulating mercury bioavailability for methylating microorganisms in the aquatic environment: A critical review. *Environ. Sci. Technol.* **47**, 2441–2456 (2013).
5. Morel, F. M. M., Kraepiel, A. M. L. & Amyot, M. The chemical cycle and bioaccumulation of mercury. *Annu. Rev. Ecol. Syst.* **29**, 543–566 (1998).
6. Watras, C. J. *et al.* Bioaccumulation of mercury in pelagic freshwater food webs. *Science of The Total Environment* **219**, 183–208 (1998).
7. Schaefer, J. K. *et al.* Active transport, substrate specificity, and methylation of Hg(II) in anaerobic bacteria. *Proceedings of the National Academy of Sciences* **108**, 8714–8719 (2011).
8. Parks, J. M. *et al.* The genetic basis for bacterial mercury methylation. *Science* **339**, 1332–1335 (2013).
9. Mason, R. P., Reinfelder, J. R. & Morel, F. M. M. Bioaccumulation of mercury and methylmercury. *Water, Air, and Soil Pollution* **80**, 915–921 (1995).
10. Regnell, O. & Watras, C. J. Microbial mercury methylation in aquatic environments: A critical review of published field and laboratory studies. *Environ. Sci. Technol.* **53**, 4–19 (2019).
11. Zhang, T., Kucharzyk, K. H., Kim, B., Deshusses, M. A. & Hsu-Kim, H. Net methylation of mercury in estuarine sediment microcosms amended with dissolved, nanoparticulate, and microparticulate mercuric sulfides. *Environ. Sci. Technol.* **48**, 9133–9141 (2014).
12. Kucharzyk, K. H., Deshusses, M. A., Porter, K. A. & Hsu-Kim, H. Relative contributions of mercury bioavailability and microbial growth rate on net methylmercury production by anaerobic mixed cultures. *Environ. Sci.: Processes Impacts* **17**, 1568–1577 (2015).
13. Liem-Nguyen, V. *et al.* Effects of Nutrient Loading and Mercury Chemical Speciation on the Formation and Degradation of Methylmercury in Estuarine Sediment. *Environ. Sci. Technol.* **50**, 6983–6990 (2016).
14. Benoit, J. M., Gilmour, C. C., Mason, R. P. & Heyes, A. Sulfide controls on mercury speciation and bioavailability to methylating bacteria in sediment pore waters. *Environ. Sci. Technol.* **33**, 951–957 (1999).
15. Graham, A. M., Aiken, G. R. & Gilmour, C. C. Dissolved organic matter enhances microbial mercury methylation under sulfidic conditions. *Environ. Sci. Technol.* **46**, 2715–2723 (2012).
16. Ravichandran, M., Aiken, G. R., Ryan, J. N. & Reddy, M. M. Inhibition of precipitation and aggregation of metacinnabar (mercuric sulfide) by dissolved organic matter isolated from the Florida Everglades. *Environ. Sci. Technol.* **33**, 1418–1423 (1999).
17. Ravichandran, M., Aiken, G. R., Reddy, M. M. & Ryan, J. N. Enhanced dissolution of cinnabar (mercuric sulfide) by dissolved organic matter isolated from the Florida Everglades. *Environ. Sci. Technol.* **32**, 3305–3311 (1998).

18. Waples, J. S., Nagy, K. L., Aiken, G. R. & Ryan, J. N. Dissolution of cinnabar (HgS) in the presence of natural organic matter. *Geochimica et Cosmochimica Acta* **69**, 1575–1588 (2005).
19. Graham, A. M. *et al.* Sulfurization of dissolved organic matter increases Hg–sulfide–dissolved organic matter bioavailability to a Hg-methylating bacterium. *Environ. Sci. Technol.* **51**, 9080–9088 (2017).
20. Jiskra, M. *et al.* Kinetics of Hg(II) exchange between organic ligands, goethite, and natural organic matter studied with an enriched stable isotope approach. *Environ. Sci. Technol.* **48**, 13207–13217 (2014).
21. Jonsson, S. *et al.* Mercury methylation rates for geochemically relevant Hg^{II} species in sediments. *Environ. Sci. Technol.* **46**, 11653–11659 (2012).
22. Choi, S.-C., Chase, T. & Bartha, R. Metabolic pathways leading to mercury methylation in *Desulfovibrio desulfuricans* LS. *Appl Environ Microbiol* **60**, 4072–4077 (1994).
23. White, D., Drummond, J. & Fuqua, C. *The Physiology and Biochemistry of Prokaryotes*. (Oxford University Press, 2012).
24. Schaefer, J. K., Szczuka, A. & Morel, F. M. M. Effect of Divalent Metals on Hg(II) Uptake and Methylation by Bacteria. *Environ. Sci. Technol.* **48**, 3007–3013 (2014).
25. Qian, C. *et al.* Global proteome response to deletion of genes related to mercury methylation and dissimilatory metal reduction reveals changes in respiratory metabolism in *Geobacter sulfurreducens* PCA. *J. Proteome Res.* **15**, 3540–3549 (2016).
26. Gilmour, C. C., Henry, E. A. & Mitchell, R. Sulfate stimulation of mercury methylation in freshwater sediments. *Environ. Sci. Technol.* **26**, 2281–2287 (1992).
27. Compeau, G. C. & Bartha, R. Sulfate-reducing bacteria: Principal methylators of mercury in anoxic estuarine sediment. *Appl Environ Microbiol* **50**, 498–502 (1985).
28. Fleming, E. J., Mack, E. E., Green, P. G. & Nelson, D. C. Mercury Methylation from Unexpected Sources: Molybdate-Inhibited Freshwater Sediments and an Iron-Reducing Bacterium. *Appl Environ Microbiol* **72**, 457–464 (2006).
29. Kerin, E. J. *et al.* Mercury methylation by dissimilatory iron-reducing bacteria. *Appl Environ Microbiol* **72**, 7919–7921 (2006).
30. Hamelin, S., Amyot, M., Barkay, T., Wang, Y. & Planas, D. Methanogens: principal methylators of mercury in lake periphyton. *Environ. Sci. Technol.* **45**, 7693–7700 (2011).
31. Gilmour, C. C. *et al.* Mercury methylation by novel microorganisms from new environments. *Environ. Sci. Technol.* **47**, 11810–11820 (2013).
32. Gilmour, C. C., Bullock, A. L., McBurney, A., Podar, M. & Elias, D. A. Robust mercury methylation across diverse methanogenic *Archaea*. *mBio* **9**, 1–13 (2018).
33. Podar, M. *et al.* Global prevalence and distribution of genes and microorganisms involved in mercury methylation. *Sci. Adv.* **1**, 1–12 (2015).
34. McDaniel, E. A. *et al.* Expanded phylogenetic diversity and metabolic flexibility of mercury-methylating microorganisms. *mSystems* **5**, 1–21 (2020).
35. Gionfriddo, C. M. *et al.* An improved hgcAB primer set and direct high-throughput sequencing expand Hg-methylator diversity in nature. *Front. Microbiol.* **11**, 1–23 (2020).
36. Liu, Y.-R., Yu, R.-Q., Zheng, Y.-M. & He, J.-Z. Analysis of the microbial community structure by monitoring an Hg methylation gene (hgcA) in paddy soils along an Hg gradient. *Appl Environ Microbiol* **80**, 2874–2879 (2014).
37. Liu, Y.-R. *et al.* Unraveling microbial communities associated with methylmercury production in paddy soils. *Environ. Sci. Technol.* **52**, 13110–13118 (2018).

38. Bravo, A. G. *et al.* Methanogens and iron-reducing bacteria: the overlooked members of mercury-methylating microbial communities in boreal lakes. *Appl Environ Microbiol* **84**, e01774-18, /aem/84/23/e01774-18.atom (2018).
39. Bravo, A. G. *et al.* Geobacteraceae are important members of mercury-methylating microbial communities of sediments impacted by waste water releases. *ISME J* **12**, 802–812 (2018).
40. Bravo, A. G. *et al.* Persistent Hg contamination and occurrence of Hg-methylating transcript (*hgcA*) downstream of a chlor-alkali plant in the Olt River (Romania). *Environ Sci Pollut Res* **23**, 10529–10541 (2016).
41. Bae, H.-S., Dierberg, F. E. & Ogram, A. Periphyton and Flocculent Materials Are Important Ecological Compartments Supporting Abundant and Diverse Mercury Methylator Assemblages in the Florida Everglades. *Appl Environ Microbiol* **85**, e00156-19, /aem/85/13/AEM.00156-19.atom (2019).
42. Carrell, A. A. *et al.* Nutrient exposure alters microbial composition, structure, and mercury methylating activity in periphyton in a contaminated watershed. *Front. Microbiol.* **12**, 647861 (2021).
43. Schaefer, J. K., Kronberg, R.-M., Morel, F. M. M. & Skjellberg, U. Detection of a key Hg methylation gene, *hgcA*, in wetland soils. *Environ Microbiol Reports* **6**, 441–447 (2014).
44. Bae, H.-S., Dierberg, F. E. & Ogram, A. Syntrophs dominate sequences associated with the mercury methylation-related gene *hgcA* in the Water Conservation Areas of the Florida Everglades. *Appl Environ Microbiol* **80**, 6517–6526 (2014).
45. Schaefer, J. K., Kronberg, R., Björn, E. & Skjellberg, U. Anaerobic guilds responsible for mercury methylation in boreal wetlands of varied trophic status serving as either a methylmercury source or sink. *Environ Microbiol* **22**, 3685–3699 (2020).
46. Jones, D. S. *et al.* Molecular evidence for novel mercury methylating microorganisms in sulfate-impacted lakes. *ISME J* (2019) doi:10.1038/s41396-019-0376-1.
47. Villar, E., Cabrol, L. & Heimbürger-Boavida, L. Widespread microbial mercury methylation genes in the global ocean. *Environ Microbiol Reports* 1–11 (2020) doi:10.1111/1758-2229.12829.
48. Capo, E. *et al.* Deltaproteobacteria and Spirochaetes-like bacteria are abundant putative mercury methylators in oxygen-deficient water and marine particles in the Baltic Sea. *Front. Microbiol.* **11**, 1–11 (2020).
49. Tada, Y., Marumoto, K. & Takeuchi, A. Nitrospina-Like Bacteria Are Potential Mercury Methylators in the Mesopelagic Zone in the East China Sea. *Front. Microbiol.* **11**, 1369 (2020).
50. Lin, H. *et al.* Mercury methylation by metabolically versatile and cosmopolitan marine bacteria. *ISME J* (2021) doi:10.1038/s41396-020-00889-4.
51. Gionfriddo, C. M. *et al.* Microbial mercury methylation in Antarctic sea ice. *Nature Microbiology* **1**, 1–12 (2016).
52. Christensen, G. A. *et al.* Development and validation of broad-range qualitative and clade-specific quantitative molecular probes for assessing mercury methylation in the environment. *Appl Environ Microbiol* **82**, 6068–6078 (2016).
53. Tyson, G. W. *et al.* Community structure and metabolism through reconstruction of microbial genomes from the environment. *Nature* **428**, 37–43 (2004).

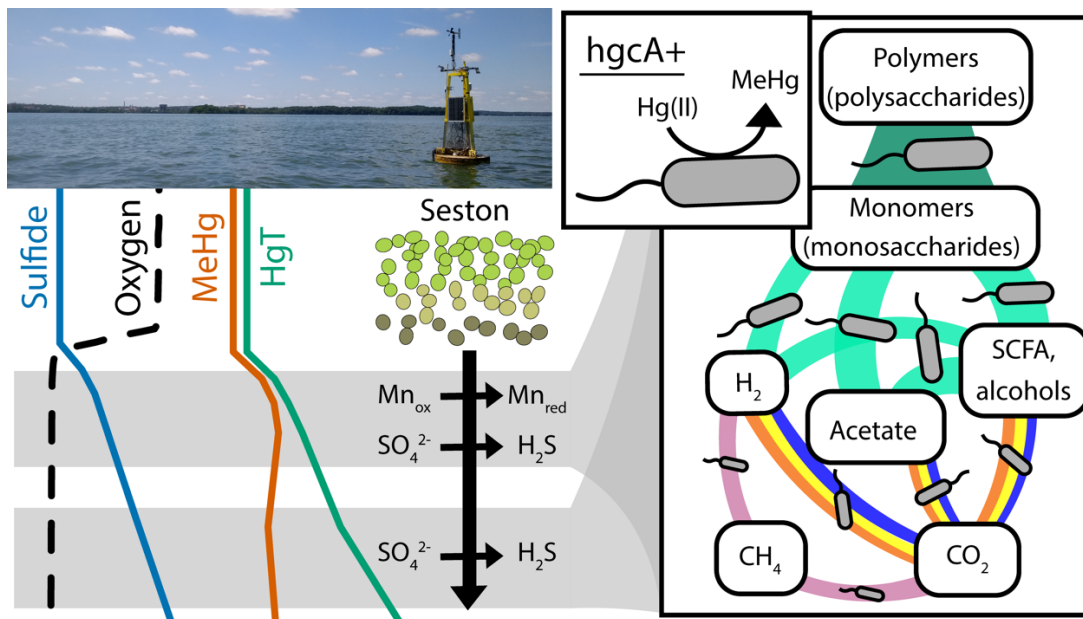
54. Ranchou-Peyruse, M. *et al.* Overview of mercury methylation capacities among anaerobic bacteria including representatives of the sulphate-reducers: implications for environmental studies. *Geomicrobiology Journal* **26**, 1–8 (2009).
55. Yu, R.-Q., Reinfelder, J. R., Hines, M. E. & Barkay, T. Syntrophic pathways for microbial mercury methylation. *ISME J* **12**, 1826–1835 (2018).
56. Goñi-Urriza, M. *et al.* Relationships between bacterial energetic metabolism, mercury methylation potential, and *hgcA/hgcB* gene expression in *Desulfovibrio dechloroacetivorans* BerOc1. *Environ Sci Pollut Res* **22**, 13764–13771 (2015).
57. Gilmour, C. C. *et al.* Sulfate-reducing bacterium *Desulfovibrio desulfuricans* ND132 as a model for understanding bacterial mercury methylation. *Appl. Environ. Microbiol.* **77**, 3938–3951 (2011).
58. Singleton, C. M. *et al.* Methanotrophy across a natural permafrost thaw environment. *ISME J* **12**, 2544–2558 (2018).
59. Hintelmann, H. & Evans, R. D. Application of stable isotopes in environmental tracer studies - Measurement of monomethylmercury (CH₃Hg⁺) by isotope dilution ICP-MS and detection of species transformation. *Fresenius' Journal of Analytical Chemistry* **358**, 378–385 (1997).
60. Hintelmann, H., Keppel-Jones, K. & Evans, R. D. Constants of mercury methylation and demethylation rates in sediments and comparison of tracer and ambient mercury availability. *Environ Toxicol Chem* **19**, 2204–2211 (2000).
61. Eckley, C. S. *et al.* Mercury methylation in the hypolimnetic waters of lakes with and without connection to wetlands in northern Wisconsin. *Can J Fish Aquat Sci* **62**, 400–411 (2005).
62. Eckley, C. S., Luxton, T. P., Knightes, C. D. & Shah, V. Methylmercury production and degradation under light and dark conditions in the water column of the Hells Canyon Reservoirs, USA. *Environ Toxicol Chem* etc.5041 (2021) doi:10.1002/etc.5041.

Chapter 2: Mercury methylation genes identified across diverse anaerobic microbial guilds in a eutrophic sulfate-enriched lake.

This chapter has been published in Environmental Science and Technology. Citation:

Peterson, Benjamin D., Elizabeth A. McDaniel, Anna G. Schmidt, Ryan F. Lepak, Sarah E. Janssen, Patricia Q. Tran, Robert A. Marick, Jacob M. Ogorek, John F. DeWild, David P. Krabbenhoft, Katherine D. McMahon. (2020) “Mercury methylation genes identified across diverse anaerobic microbial guilds in a eutrophic sulfate-enriched lake.” *Environmental Science & Technology* 54, no. 24: pg. 15840–51. <https://doi.org/10.1021/acs.est.0c05435>.

Table of contents art from the paper:



Abstract

Mercury (Hg) methylation is a microbially mediated process that converts inorganic Hg into bioaccumulative, neurotoxic methylmercury (MeHg). The metabolic activity of methylating organisms is highly dependent on biogeochemical conditions, which subsequently influences MeHg production. However, our understanding of the ecophysiology of methylators in natural ecosystems is still limited. Here we identified potential locations of MeHg production in the anoxic, sulfidic hypolimnion of a freshwater lake. At these sites, we used shotgun metagenomics to characterize microorganisms with the Hg-methylation gene *hgcA*. Putative methylators were dominated by *hgcA* sequences divergent from those in well-studied, confirmed methylators. Using genome-resolved metagenomics, we identified organisms with *hgcA* (*hgcA*⁺) within the Bacteroidetes and the recently described Kiritimatiellaeota phyla. We identified *hgcA*⁺ genomes derived from sulfate-reducing bacteria, but these accounted for only 22% of *hgcA*⁺ genome coverage. The most abundant *hgcA*⁺ genomes were from fermenters, accounting for over half of the *hgcA* gene coverage. Many of these organisms also mediate hydrolysis of polysaccharides, likely from cyanobacterial blooms. This work highlights the distribution of the Hg-methylation genes across microbial metabolic guilds and suggests that primary degradation of polysaccharides and fermentation may play an important but unrecognized role in MeHg production in the anoxic hypolimnion of freshwater lakes.

Introduction

Environmental Hg levels have increased 3-4 times compared to pre-development times, largely due to human activity.¹ Much of this anthropogenically released Hg is gaseous-elemental Hg, which can later be oxidized to Hg(II) and deposit to terrestrial and aquatic ecosystems.² Microorganisms can then convert Hg(II) to methylmercury (MeHg) in various low redox environments, including sediments, periphyton, rice paddy soils, and sub- or anoxic regions of freshwater and marine water columns.³⁻⁹ MeHg bioaccumulates and biomagnifies up the food web, making Hg-methylation an important process in food web Hg accumulation.¹⁰ In freshwater lakes, MeHg accumulation has historically been attributed to production in sediments followed by diffusion across the sediment-water interface.^{5,11,12} However, Hg-methylation also occurs in the water column, under both anoxic and oxic conditions, and can account for the bulk of water column MeHg accumulation in some lakes.^{4,6,9,13-15}

Biogeochemical conditions, like redox status and carbon bioavailability, can indirectly drive MeHg production by fueling metabolic activity of Hg-methylating microorganisms.^{12,16} Inhibition of sulfate reduction in cultured isolates and *in situ* assays have linked sulfate-reducing bacteria (SRBs) activity to MeHg production.^{11,12} Many subsequent studies have linked sulfate reduction to Hg-methylation across many ecosystems, suggesting that SRBs are the primary drivers of MeHg production *in situ*.¹⁷⁻²⁰ Later studies identified iron-reducing bacteria (FeRB) and methanogenic archaea that can also produce MeHg, expanding the terminal electron-accepting processes (TEAPs) associated with MeHg production.^{21,22} We know little about how primary degradation of organic molecules, syntrophy, or fermentation influence MeHg production, but some fermentative and syntrophic microbes, such as Clostridia, are known to methylate.^{23,24} On the community level, Hg-methylation rates increase with increasing overall

heterotrophic activity, suggesting that simply increasing carbon and energy flux through microbial communities can promote MeHg production.^{9,25} To date, most of our understanding of microbial Hg-methylation relies on reductionist monoculture experiments or on amendment/inhibition studies with environmental samples that lack information about the microbial community supporting MeHg production.

The identification of the *hgcAB* gene cluster has provided a molecular marker for MeHg production, allowing for the in-depth examination of microbial communities and conditions that promote Hg-methylation in the environment.^{23,26} Surveys of publicly available genomes, metagenomes and metagenome-assembled genomes have expanded the known phylogenetic and metabolic diversity of organisms with *hgcA* (*hgcA*+).^{23,27–32} Using polymerase chain reaction (PCR)-based amplicon sequencing, several studies have demonstrated that *hgcA*+ communities are phylogenetically distinct and linked to geochemical conditions across different environments.^{33–37} While this approach generally captures the deep diversity of *hgcA* sequences in complex communities, PCR primers are subject to amplification bias and do not provide additional phylogenetic or metabolic information.^{14,29,30} Shotgun metagenomics, which involves sequencing random small strands of DNA from a sample, reduces amplification biases and enables assembly of longer DNA segments that provide additional genetic context for identified genes. This method also offers a more robust identification of novel *hgcA* sequences from environmental samples, since computational tools such as Basic Local Alignment Search Tool (BLAST) and Hidden Markov Models (HMMs) are better equipped to identify divergent sequences.^{31,38,39} To provide further genetic context for *hgcA*, genome-resolved metagenomics can be used to generate population genomes (bins) from the assembled DNA, enabling phylogenetic identification using conserved genes and metabolic characterization.^{14,40,41} This

approach has been used to identify prominent novel Hg-methylators from the Aminicenantes and Kiritimatiellaeota phyla in the water column of a sulfate-enriched lake.¹⁴ The ability to not only identify Hg-methylators but also describe their metabolic potential *in situ* makes genome-resolved metagenomics an important tool in closing the gap between culture work and *in situ* assays or observations and in understanding how nutrient and biogeochemical conditions influence Hg-methylation.

In this study we applied genome-resolved metagenomics to identify the metabolic pathways linking biogeochemical cycling to MeHg production in the hypolimnion of Lake Mendota, Wisconsin, USA, a large, well-studied, freshwater eutrophic lake. During stratification, >50% of the total Hg (HgT) in the hypolimnion is MeHg, yet it is unclear which microbial communities are contributing to these high MeHg levels. Mendota has elevated sulfate concentrations due to watershed geology, which supports sulfate reduction in the anoxic hypolimnion; thus, we hypothesized that the *hgcA*⁺ community is dominated by sulfate-reducing organisms.^{42,43} We used Hg speciation and redox profiles to identify sites with suspected *in situ* MeHg production and selected a subset of these for shotgun metagenomic sequencing. This approach allowed us to identify novel methylators and examine their metabolic pathways, place the methylators in the context of the broader microbial community, and ultimately provide insight into how biogeochemical cycles may influence MeHg production. Historically, TEAPs such as sulfate reduction and methanogenesis have been identified as drivers of MeHg production, but this work suggests that primary degradation and fermentation may drive *in situ* MeHg production in this system.

Materials and Methods

Field sampling. Lake Mendota is a large dimictic lake located in Madison, Wisconsin, USA. Sampling was conducted at the deepest part of the lake, near the North Temperate Lakes Long-Term Ecological Research (NTL-LTER) buoy. The lake is approximately 24 meters deep at this site. Samples were collected approximately monthly in 2017 from the onset of hypolimnetic anoxia in June until stratification broke down and the water column mixed. Profiles of temperature, dissolved oxygen, and turbidity were collected with a multi-parameter sonde (YSI Incorporated, Yellow Springs, OH). Samples were collected through acid-washed Teflon sampling line using a peristaltic pump. Samples for total sulfide analysis were preserved in 1% zinc acetate. Water samples for dissolved metal (non-Hg) analysis were filtered through a 0.45 μm PES Acrodisc filter (Pall Corp., Port Washington, NY) and acidified to 1% hydrochloric acid (HCl). Hg samples were collected using trace-metal-clean methods in 2.5L bottles.⁴⁴ These bottles were allowed to overflow before capping to minimize oxygen exposure within the sample, then were double-bagged and stored in a cooler. Water was filtered through ashed quartz fiber filter (QFF) within 24 hours and preserved to 1% HCl for filter-passing Hg and MeHg analysis.⁴⁴ The QFF filters were frozen for particulate Hg analysis.⁴⁴ DNA samples were collected by filtering 300-400 ml of sample water onto 0.22 μm pore-size PES filters (Pall Corp., Port Washington, NY) and were flash-frozen on liquid nitrogen within 90 seconds of collection.

Geochemical analyses. Sulfide was quantified spectrophotometrically using the Cline method.⁴⁵ Iron and manganese were quantified by inductively coupled plasma optical emission spectrometry. Processing and analysis of Hg samples was done at the U.S. Geological Survey (USGS) Mercury Research Laboratory (MRL), Middleton, WI. Filter-passing and particulate HgT samples were oxidized using bromine monochloride (BrCl) and quantified using tin

reduction coupled to cold vapor atomic fluorescence spectrometry.^{46,47} Filter-passing and particulate MeHg samples were distilled to remove matrix interferences and then quantified by inductively coupled plasma mass spectrometry following US EPA method 1630 modified by quantification via isotope dilution.⁴⁸⁻⁵⁰ All HgT and MeHg analyses passed required quality assurance and control standards. Geochemical data can be found in Table S1a.

DNA extraction, sequencing, and assembly. We selected five samples for shotgun metagenomic DNA sequencing and analysis. Three of these samples were selected to coincide with the chemocline and are referred to as CHE1, CHE2, and CHE3 (Table S2). The other two samples are from the deep euxinic hypolimnion and are referred to as EUX1 and EUX2 (Table S2). DNA was extracted by enzymatic and physical lysis followed by phenol-chloroform extraction and isopropanol precipitation.⁵¹ DNA library preparation was done at the Functional Genomics Lab and sequencing was done in the Vincent J. Coates Genomics Sequencing Lab (QB3-Berkeley, Berkeley, CA). Library preparation was done with a Kapa Biosystem Library Prep kit, targeting inserts ~600bp in length (Roche Sequencing and Life Science, Kapa Biosystems, Wilmington, MA). The five libraries were pooled and run on a single lane on an Illumina HiSeq4000 with 150bp paired-end sequencing (Illumina, Inc., San Diego, CA). Raw reads were trimmed using Sickle (v1.33) and assembled using metaSPADes (v3.12) (Table S3).^{52,53} Assembly-based analyses were run on all scaffolds >500bp long. Open reading frames (ORFs) were predicted using Prodigal (v2.6.2).⁵⁴ Reads were mapped to the scaffolds of each assembly using BBMap (v35) with default settings.⁵⁵ Scaffold abundance is defined as the mean value of the read coverage at each nucleic acid residue in a scaffold. Gene abundances are defined as the abundance of the corresponding scaffold. Scaffold abundances in each metagenome were normalized by calculating the ratio of reads in the smallest metagenome to the

number of reads in that metagenome, then multiplying the abundance of each scaffold by this ratio.

Metagenomic binning and annotation. Automatic binning was done for each assembly on scaffolds >1000bp in length. Bins were generated using Metabat2 (v2.12.1), MaxBin (v2.1.1), and CONCOCT (v0.4.1), then aggregated using Das Tool.^{56–59} Bins across assemblies were clustered into “high matching sets” (HMSs) if they shared at least 98% ANI over at least 50% of the genome. CheckM (v1.1.2) was used to estimate the completeness and redundancy of each bin.⁶⁰ One bin from each HMS was selected for further analysis. We retrieved 228 medium quality bins that were more than 75% complete and less than 10% redundant (Table S6).⁶¹ These bins accounted for only 33% of the total number of reads. Bins were then decontaminated using Anvi'o (v5.2), reassembled with SPADes, and re-binned in Anvi'o.^{53,62} Taxonomy of each bin was estimated using GTDB-TK (v0.3.2).⁶³ Preliminary metabolic annotations were done using MetaPathways.⁶⁴ Annotations of metabolic genes of interest were confirmed using Hidden Markov Models (HMMs) from TIGRFAM and PFAM, gene neighborhoods, and phylogenies.³⁸

hgcA identification. A custom HMM for HgcA amino acid sequences was built with hmmbuild from hmmer (v3.1b2) using experimentally verified HgcA amino acid sequences (Table S4).^{23,65} Putative HgcA sequences were identified using hmmsearch (v3.1b2) (Table S5).⁶⁵ Each hit was manually screened for the cap helix domain and at least 4 transmembrane domains.²⁶ HgcA sequences were dereplicated across assemblies using CD-HIT (v4.8.1) with a 97% identity cut-off.⁶⁶

Phylogenetic analyses. Bin phylogenies were based on 16 ribosomal protein (rp16) sequences.⁶⁷ For rp16 and HgcA phylogenies, amino acid sequences were aligned using MUSCLE (v3.8.31).⁶⁸ Each rp16 gene was aligned individually, then all alignments were

concatenated. Sequences with less than half of the aligned residues were manually removed. Alignments were inspected in Geneious and trimmed using BMGE1.1 with the BLOSUM30 substitution matrix.⁶⁹ The final HgcA alignment included 181 residues and the final rp16 alignment included 2217 residues. RAxML (v8.2.11) was used to generate a maximum likelihood (ML) tree under the GAMMA distribution with the LG model.⁷⁰ Branch support was generated by rapid bootstrapping. For HgcA phylogenies, RogueNaRok (v1.0) was used to remove “rogue taxa” interfering with proper tree generation.⁷¹ Rogue taxa were classified using pplacer and included in the analysis.⁷² The best-scoring ML tree for HgcA was mid-point rooted using the Phangorn R package and visualized using ggtree.^{73,74} For unbinned HgcA sequences, taxonomy was assigned to each HgcA sequence based on phylogenetic clustering with HgcA reference sequences from NCBI and bin phylogenies of binned HgcA sequences. HgcA sequences that did not fall into a monophyletic cluster are marked as “unknown”. The rp16 ML tree was rooted using an archaeal outgroup.

Data availability. Trimmed metagenomes and metagenomic assemblies can be found under BioProject PRJNA646991. The scaffolds and the ORFs for the bins, can be found at the project page on the Open Science Framework (OSF), here: <https://osf.io/9vwgt/>. The nucleic acid and amino acid sequence files for the confirmed *hgcA*/HgcA sequences and the HgcA HMM used in this study can be found on the same OSF page.

Results and Discussion

Redox and Hg biogeochemistry in Lake Mendota. Microbial anaerobic respiration is regulated by terminal electron acceptor availability, which continually evolves vertically in

Mendota's hypolimnion throughout the summer-fall season as negative redox conditions strengthen due to high biochemical oxygen demand (Fig. 2.1, S2.1). We monitored limnological and biogeochemical conditions in the hypolimnion to identify likely TEAPs at play (Table S1). Anoxia developed in the hypolimnion as early as June, likely due to senescence and decomposition of biomass from spring phytoplankton blooms (Fig. S2.1). Nitrate/nitrite levels reached 6 μM at the oxic/anoxic interface in August, but by September were nearly undetectable (Fig. S2.1). Dissolved iron (Fe) transiently accumulated (5 μM) in the hypolimnion immediately following anoxia, but was quickly precipitated out by sulfide and was unlikely to serve as an electron acceptor in the water column (Fig. S2.1).⁷⁵

Manganese (Mn) also accumulated shortly after anoxia developed and remained in the hypolimnion throughout the anoxic period, ranging from 4-6 μM . In June and August, the near-bottom hypolimnetic accumulation of Mn and linear profile suggests that Mn was being reduced in the surficial sediments and diffusing into the hypolimnion.⁷⁶ During September and October, there was a peak in dissolved Mn near the oxic/anoxic interface (Fig. S2.1, S2.2). Particulate Mn was detected (1.4 μM) just above the peak in dissolved Mn in late September (Fig. S2.2). While this peak was not detected in October, this could be due to insufficient sampling resolution, since the profile from September suggests that particulate Mn is localized to a thin band in the water column (Fig. S2.2). Together, these data suggest localized reduction, just below the oxic-anoxic interface, of settling Mn oxides that were produced by the downward migration of the thermocline, as previously shown to occur in Lake Mendota and other lakes.^{75,76} This indicates that Mn reduction could be an important TEAP near the oxic/anoxic interface during late anoxia.⁷⁷

Sulfate reduction, commonly implicated in MeHg production, has been documented in the water column of Lake Mendota.⁴³ During early stratification, under relatively high redox conditions, sulfate levels were approximately 180 μM throughout the water column (Fig. S2.1, S2.2). Sulfide was first detected in August and accumulated to over 150 μM by October (Fig. 2.1, S2.1, S2.2). Sulfate depletion mirrored sulfide accumulation, with sulfate levels falling to 21 μM in the deep hypolimnion by October. Sulfate levels have previously been shown to be limiting below 100 μM in Lake Mendota sediments, and other work has shown that SRB require >60 μM sulfate to outcompete methanogens.^{43,78} Taken together, these data suggest that sulfate reduction is likely an important TEAP in driving anaerobic metabolism throughout the hypolimnion during late fall, but may slow in the deep hypolimnetic waters during late stratification.

Once oxygen was depleted, both HgT and MeHg began accumulating in the hypolimnion (Fig. 2.1, S2.1). We discuss here total MeHg and HgT levels, calculated by summing the dissolved and particulate fractions, but the dissolved and particulate fractions are shown in Fig. S2.1. The lower hypolimnetic buildup of MeHg and HgT during June and August suggests that diffusion of Hg from sediments is important. This persists in September and October for HgT, which reached 1.86 ng/L in the deep hypolimnion. However, during this time, MeHg increased in the metalimnion up to 0.63 ng/L, while hypolimnetic MeHg remained between 0.4 and 0.5 ng/L. Correspondingly, the percent MeHg (the MeHg:HgT ratio) peaked at the oxic/anoxic interface (52%). The late fall peak in MeHg and percent MeHg near the oxic-anoxic interface is likely due to elevated MeHg production in the metalimnion relative to the hypolimnion. Other potential explanations of this MeHg enrichment include increased demethylation of MeHg in the deep hypolimnion, which to our knowledge has not been shown to occur in lakes; or MeHg

diffusion from above, which is unlikely because MeHg levels are low in the epilimnion. Elevated MeHg production just beneath the oxycline has been shown in other freshwater lakes^{9,13} and in other redox transition zones, such as hyporheic zones and Sphagnum moss mats.¹⁹ There are likely two concurrent reasons for this elevated MeHg production in this region. First, high sulfide levels can strongly inhibit MeHg production by reducing the bioavailability of Hg to methylators.⁷⁹ While sulfide concentrations are high enough in the deep hypolimnion to inhibit Hg-methylation, sulfide levels near the oxycline are relatively low. However, some of the highest MeHg levels recorded were at 17.8 m in October, when dissolved MeHg was 0.63 ng/L and sulfide was over 100 μM (Fig. 2.1). Second, overall microbial metabolism is often elevated near strong redox gradients.⁹ During late stratification, the percent MeHg maxima also coincided with peaks in turbidity, which has been previously shown to co-localize with elevated microbial activity and MeHg production.¹⁵ It is most likely that a combination of these two factors (abiotic speciation and Hg-methylator activity) led to elevated MeHg production near the oxic-anoxic interface.

HgcA identification. Metagenomic approaches were used to identify *hgcA* genes that corresponded with metalimnetic peaks of MeHg and hypolimnetic euxinic regions. We identified 108 unique *hgcA* genes on assembled scaffolds recovered from the five samples (Fig. S2.3). While we used *hgcA* as our marker for Hg-methylation, the *hgcB* gene is also required for methylation activity.²⁶ Ninety of the identified *hgcA* genes also had a downstream *hgcB* gene, confirming that these are likely functional Hg-methylation genes. Seven of the 18 *hgcA*+ scaffolds lacking *hgcB* ended just downstream of *hgcA*, and it is possible that *hgcB* did not assemble into the scaffold. The remaining 11 *hgcA* genes with no *hgcB* partner had a similar phylogenetic and coverage distribution to those with a downstream *hgcB* (Fig. S2.4, Table S5).

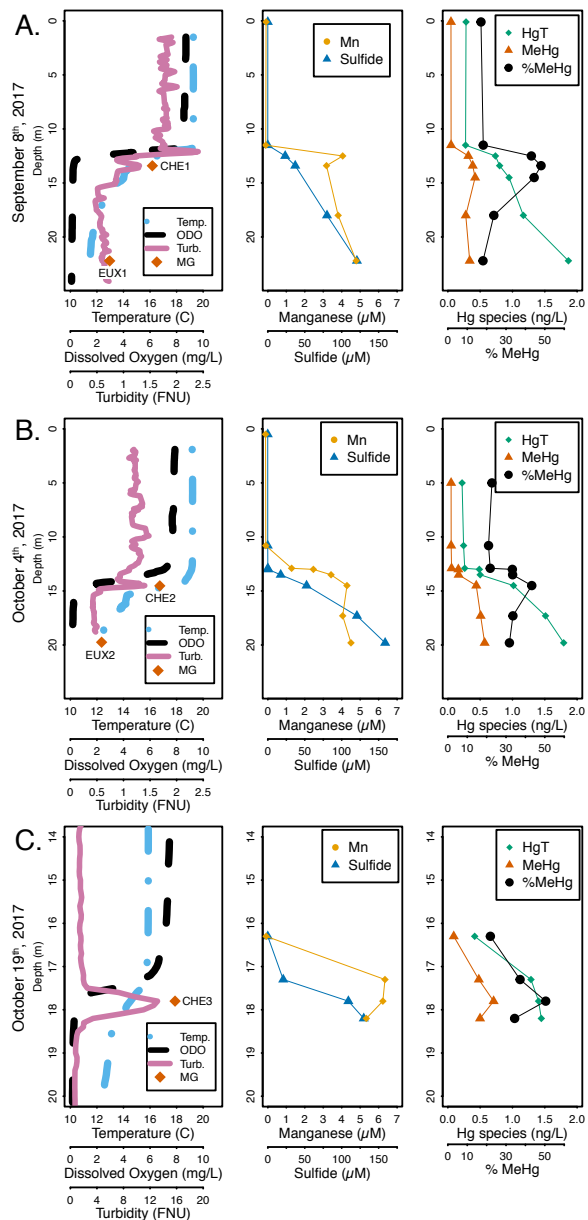


Figure 2.1: Physical and geochemical profiles of Lake Mendota from 2017 on September 8th (A), October 4th (B) and October 19th (C). Column 1: Parameters measured continuously with a sonde and includes orange diamonds where samples for metagenomic sequencing were collected, names denoted next to symbol. Column 2: Total sulfide and filter-passing manganese values at discrete depths. Column 3: HgT and MeHg values, as sum total of the dissolved and particulate fractions. Dissolved and particulate fractions are plotted individually in Figure S1. Note the changed scale for depth on the y-axis and for turbidity on the x-axis in the October 19th profiles (C). The metagenomic samples collected near the metalimni-on for October 4th and October 19th were both collected coincident with the observed spike in turbidity. Abbreviations: Temp. - Temperature ($^{\circ}\text{C}$), ODO - Optical dissolved oxygen in mg/L, Turb. - Turbidity in Formazin Nephelometric Units (FNU), MG - metagenome sample

Notably, Hg-methylation has been experimentally verified in *Desulfovibrio africanus* sp. Walvis Bay and *Desulfovibrio inopinatus*, in which *hgcA* is separated from *hgcB* by a single gene and 29kbp, respectively.^{26,80,81} Since we cannot rule out that the corresponding *hgcB* gene is elsewhere in the genome for these 11 sequences, we included all 108 *hgcA* genes in our analysis.

While our biogeochemical data shows greater MeHg accumulation in the metalimnion than in the hypolimnion, *hgcA* abundance did not vary substantially between the metalimnion and hypolimnion (Fig. 2.2b). This is consistent with a lack of correlation between *hgcA* abundance and Hg-methylation activity or MeHg levels in the literature.⁷⁹ Relating overall abundance of *hgcA* genes from metagenomes to MeHg levels is problematic due to the fact that metagenomic data is compositional rather than absolute.⁸² In addition, culture experiments show there is a wide range of Hg-methylation activity by different *hgcA*⁺ organisms.²³ Finally, as discussed above, abiotic factors such as sulfide complexation also likely play a large role in determining MeHg production in the water column.⁷⁹

We then searched for the *hgcA* gene in the 228 reconstructed metagenomic bins. We identified 41 *hgcA*⁺ bins that were representative of the overall *hgcA* genetic diversity. All but three of these genomes had an *hgcB* sequence paired with *hgcA*, and no bins were found with *hgcB* but no *hgcA*. One of these bins (LEN_0031) included two copies of the *hgcA* gene. However, bins represent composite population genomes rather than individual genomes.⁸³ Thus, we cannot confirm that the two *hgcA* sequences were present together in a single organism, which, to our knowledge, has not been demonstrated. These 41 bins accounted for 51% of the total *hgcA* coverage in our assemblies. This limited coverage highlights an inability to recover genomes for 13 out of the 30 most abundant *hgcA* sequences, including the most abundant *hgcA* gene (Fig. S2.5). Efforts to recover these abundant *hgcA*⁺ bins through read subsampling, contig

curation using assembly graphs, reassembly, and manual binning and curation were unsuccessful. Many of these scaffolds had highly abundant sequence nucleotide variants, suggesting there were multiple closely related strains, which can interfere with the binning process. While this means our view of the metabolic diversity of *hgcA*⁺ bins in these metagenomes is incomplete, we did successfully bin *hgcA*⁺ scaffolds corresponding to most of the HgcA phylogenetic clusters, suggesting that most of the methylator diversity is represented in our bins (Fig. 2.2). The *hgcA*⁺ bins accounted for 17% of the total read coverage from all bins and included some of the most abundant bins from our metagenomes (Fig. S2.6a). The *hgcA*⁺ bins were slightly less abundant than bins without *hgcA* (*hgcA*⁻) bins, but this could be due to the greater degree of manual curation of the *hgcA*⁺ bins (Fig. S2.6b). Overall, the *hgcA*⁺ bins recruited 6% of the total number of reads from our metagenomic datasets. Because the *hgcA*⁺ bins accounted for only 51% of the total coverage of all recovered *hgcA* sequences, we estimate that *hgcA*⁺ genomes account for ~12% of the total metagenomic reads across our five samples, which is consistent with previous work applying this technique in similar systems.¹⁴

Phylogenetic diversity of *hgcA*⁺ community. Most of the identified *hgcA* genes from this study are not representative of well-characterized and experimentally verified methylating organisms. Of the 108 HgcA sequences, only 43 clustered with HgcA sequences from experimentally verified methylators (Fig. 2.2, S2.4). The majority of these sequences are associated with the Deltaproteobacteria class. The most abundant of these, accounting for 12% of the *hgcA*⁺ coverage, belong to the Syntrophobacterales order, which includes both syntrophic and sulfate-reducing organisms (Fig. S2.4, S2.7). The two other Deltaproteobacteria orders are Geobacterales and Desulfobacterales, both of which are metabolically diverse but commonly associated with iron reduction and sulfate reduction, respectively. Notably, no sequences

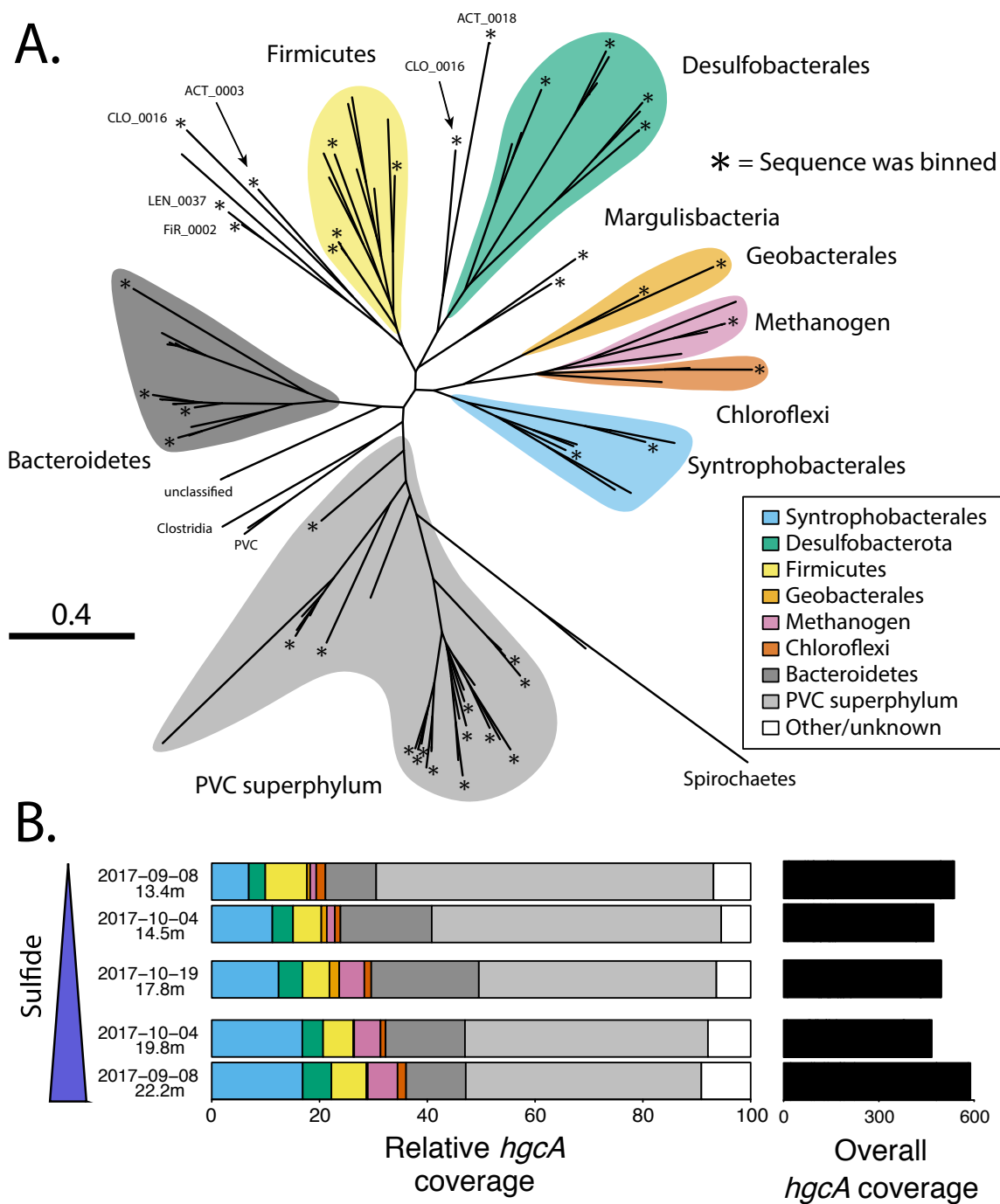


Figure 2.2: A) Phylogenetic tree of *HgcA* sequences from this study and B) fractional coverage of *HgcA* sequences within predicted taxonomic groups. Unconfirmed methylators dominate *HgcA* gene diversity in Lake Mendota, both numerically (A) and by coverage (B). For panel A, asterisks at the end of branches indicate sequence was binned, while all other branches are unbinned *HgcA* sequences from this study. Sequences were assigned a predicted taxonomic group based on phylogenetic clustering with *HgcA* reference sequences from NCBI and bin phylogenies of binned *HgcA* sequences (for detailed tree with reference sequences, see Figure S3). Binned sequences outside of a monophyletic cluster are labeled with their bin name. In panel B, the black bars on the right refer to the overall coverage of all *HgcA* genes in each metagenome. Samples are arranged in order of increasing sulfide levels.

associated with Desulfovibrionales or Pseudodesulfovibrionales, two well-studied orders that include the model sulfate-reducing methylator *Desulfovibrio desulfuricans* ND132, were detected.⁸⁴ We also detected *hgcA* genes from the other two common groups of confirmed methylators, the phylum Firmicutes and methanogenic Archaea. However, both of these also constituted a small percentage of the total *hgcA* coverage (<7% each). Overall, *hgcA* sequences associated with confirmed methylators only accounted for about 27% of the total *hgcA* coverage. While abundance does not necessarily correlate to activity, this suggests that novel unconfirmed methylators may play a larger than expected role in MeHg production in Lake Mendota.

The majority of *hgcA* read coverage was accounted for by two large *hgcA* clusters, neither of which are associated with experimentally verified methylators. Fourteen of these sequences, accounting for 13% of the total *hgcA* coverage, formed a monophyletic cluster with substantial bootstrap support (Fig. S2.4). Taxonomic and phylogenetic analysis of the four bins with *hgcA* genes from this cluster placed them in the Bacteroidales order (phylum Bacteroidetes) (Table S6, Fig. S2.7, S2.8). The other large cluster of HgcA sequences included 33 sequences and accounted for 50% of the total *hgcA* coverage. We could only recover a few genes from the NCBI NR database that clustered with these sequences, and none from reference isolate genomes (Fig. S2.4). Phylogenetic analysis of the 15 bins with these *hgcA* genes identified them as members of the Planctomycetes-Verrucomicrobia-Chlamydia (PVC) superphylum, 11 of which are members of the recently proposed Kiritimatiellaeota phylum (Fig. S2.7, S2.9).⁸⁵ The PVC superphylum dominates the overall read coverage of our bins as well, with 79 PVC bins accounting for 42% of total bin coverage, with 30% coming from Kiritimatiellaeota alone (Fig. S2.9, Table S6). There are very few publicly available Kiritimatiellaeota genomes and only three cultured representatives.^{85,86} Notably, a recent paper also identified several *hgcA*+ bins

associated with the Kiritimatiellaeota phylum in a sulfate-enriched lake, but neither the HgcA sequences nor the rp16 sequences from those bins clustered closely with those from the current study (Fig. S2.4).¹⁴ This suggests that the Kiritimatiellaeota phylum is far more diverse than our current reference databases indicate and that the *hgcA* gene could be widely distributed throughout it. For both the Kiritimatiellaeota and the Bacteroidales, the presence of *hgcA* within bins was not phylogenetically conserved (Fig. S2.8, S2.9). We also identified several other novel putative methylators that were lower in number and abundance, including Margulisbacteria, Firestonebacteria, and Actinobacteria. The dominance of highly diverse and novel *hgcA*⁺ organisms in these samples highlights the value of using genome-resolved shotgun metagenomics (as compared to amplicon sequencing) to identify methylators in a new study system, as it allows for the identification of divergent *hgcA* lineages and taxonomic classification of the associated bins.

Metabolic potential of methylating bins. Many of the *hgcA*⁺ lineages we identified can employ a wide variety of metabolic strategies, while others have few closely related reference genomes; thus, it was vital to examine their metabolic pathways to determine which TEAPs and other biogeochemical cycles could be potentially linked to Hg-methylation. While most of the literature has focused on both SRBs and methanogens as the dominant methylators, due to the sulfate/sulfide abundance in Lake Mendota and documentation of sulfate reduction in the water column,⁴³ we hypothesized that most *hgcA*⁺ genomes in Lake Mendota harbor genes enabling sulfate reduction. The ability to respire sulfate to sulfide is encoded by the *dsrABD*, *aprAB*, *sat*, and *qmoABC* genes; bins with this complete set of genes were termed SR⁺.^{87,88} Three of the four Desulfobacterales *hgcA*⁺ bins and both of the Syntrophobacterales *hgcA*⁺ bins, including the most abundant *hgcA*⁺ bin (SYN_0007), were SR⁺ (Fig. S2.10, S2.11). SR⁺ methylators are

slightly more abundant in the euxinic samples (25-26% of *hgcA*⁺ bin coverage) than the chemocline samples (14-21%) (Fig. 2.3). Overall, SR⁺ bins (*hgcA*⁺ and *hgcA*⁻) account for only 7% of the total bin coverage. Sulfate reduction is not the only respiratory pathway reliant on sulfur redox reactions, though. Three *hgcA*⁺ bins that are not SR⁺ contained polysulfide reductase (*psr*) homologues, which provide the ability to respire partially reduced sulfur compounds such as tetrathionate or thiosulfate (Fig. S2.10, S2.12).⁸⁹ However, these three bins were relatively low in abundance and may also rely on other TEAPs for respiration (Fig. S2.10). Methanogenic methylators were even less abundant, with only a single bin (MET_0028) accounting for 2% of the *hgcA*⁺ bin coverage, mostly in the deep euxinic sites where MeHg production is suspected to be lower (Fig. 2.3). No *hgcA*⁻ methanogens were identified. MET_0028 is a member of the hydrogenotrophic Methanomicrobiales order.⁹⁰ Overall, the fraction of methylators relying on metabolic pathways historically associated with Hg-methylation (sulfate reduction and methanogenesis) was far lower than we expected.

We also identified several *hgcA*⁺ bins corresponding to potential Mn-reducing organisms. While reduced Mn has been correlated to MeHg levels,⁹¹ Mn reduction has not, to our knowledge, been linked directly to MeHg production *in situ* and has even been proposed as a method for limiting MeHg production in sediments.⁹² Organisms that respire insoluble metal oxides often use porin-cytochrome C complexes (PCCs) to mediate extracellular electron transfer (EET).⁹³ We recovered genomes for several Verrucomicrobia, Bacteroidetes, and Kiritimatiellaeota with PCC-like gene clusters, but they were not closely related to PCCs experimentally verified to conduct EET (Fig. S2.10, S2.13). However, both *hgcA*⁺ Geobacterales bins had a PCC operon homologous to the *extEFG* operon from *Geobacter sulfurreducens*, which has been shown to mediate both Fe and Mn oxide reduction (Fig. S2.10,

S2.13).⁹⁴ These bins both had low read coverage, but were most abundant in CHE3, where we saw evidence for enhanced Mn cycling and peaks in fraction MeHg (Fig. 2.3). Notably, there is little evidence for Fe redox cycling, suggesting that these organisms were unlikely to rely on Fe reduction (Fig. S2.2). While Mn levels are low in the water column relative to sulfate (<5 μM), previous work has shown that low Fe levels can drive substantial carbon oxidation in regions with a steep redox gradient.⁹⁵ Combined with observations that Geobacterales methylators often produce MeHg at a high rates in culture, this suggests that Mn cycling at the oxic-anoxic interface may play a role in MeHg production in Lake Mendota.^{22,23,96}

We also detected genes for nitrogen species reduction in *hgcA*+ bins (Fig. S2.10). While nitrite-oxidizing *Nitrospinae* have been identified as potential methylators,³⁹ reduction of nitrogen species has not, to our knowledge, been linked to MeHg production. In fact, nitrate amendment has been shown to reduce MeHg levels in lakes.⁹⁷ While many bins, both *hgcA*+ and *hgcA*-, encoded genes required for dissimilatory nitrate/nitrite reduction to ammonia (DNRA), these proteins can detoxify nitrite or disperse reducing equivalents during fermentation in addition to respiration..^{98,99} This, in combination with low nitrate/nitrite levels in the water column during this time of year and the presence of other respiratory pathways in these bins suggest that nitrogen-based respiration does not play a major role in overall community metabolism or MeHg production in this system. However, we cannot rule out the potential role of cryptic N cycling, especially near the chemocline.

The remaining 27 *hgcA*+ bins are likely to be derived from fermentative or syntrophic organisms, based on their lack of canonical genes for TEAPs. Bins linked to obligate fermentation were also common in the total microbial community, as they represent 106 of the 228 bins, accounting for almost 50% of the bin coverage. This is likely an underestimate of the

organisms relying on fermentation, as it does not include the many bins containing genes for dissimilatory nitrate/nitrite reduction or oxidases that were likely maintaining fermentative metabolism at these anoxic depths. These bins possess an array of genes for pyruvate fermentation and aldehyde and alcohol dehydrogenases for fermentative production of short chain fatty acids (Fig. S2.14). They also had genes that could facilitate syntrophy through hydrogen or formate evolution.¹⁰⁰ Hydrogenases used for H₂ uptake and formate dehydrogenases were present in many respiratory bins (*hgcA*⁺ and *hgcA*⁻), further suggesting that this community may rely on syntrophic metabolism. Many of these fermentative/syntrophic bins correspond to organisms specialized in polysaccharide degradation, with 13 *hgcA*⁺ bins having at least 40 glycoside hydrolases (GHs). The highly abundant Kiritimatiellaeota appear particularly suited to polysaccharide degradation, with bins carrying up to 468 GHs. In fact, 100 total bins carried over 40 GH genes each, suggesting that primary polysaccharide degradation is a common metabolic strategy in the anoxic water column in Lake Mendota. Of these, 49 represent obligate fermenters, while 50 are thought to represent facultative aerobes. Together, these data indicate that fermentative and syntrophic processes may play a much larger role in MeHg production than we had hypothesized.

Our data show that *hgcA* is widely distributed throughout members of the anaerobic microbial food web. Overall, typical metabolic pathways associated with Hg-methylation such as sulfate reduction, methanogenesis, and iron reduction are outnumbered by fermentative, polysaccharide-degrading *hgcA*⁺ organisms, which predominated at both meta- and hypolimnetic sites. The dissolved organic carbon pool in Lake Mendota is dominated by autochthonous inputs and primary production at this time of year is controlled by cyanobacteria, which have a high proportion of exopolysaccharides in their biomass.^{42,101,102} Together, this suggests that the supply

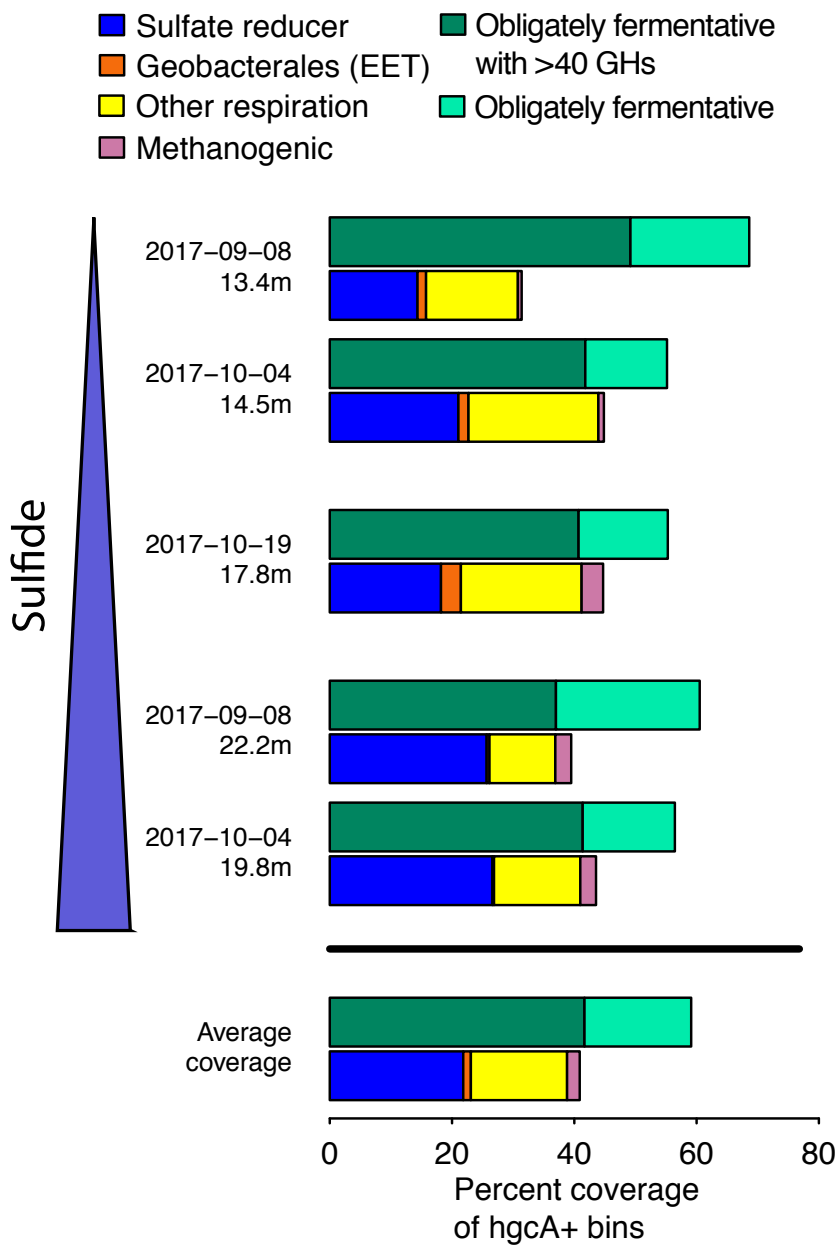


Figure 2.3. Fractional coverage of metabolic functional groups within *hgcA*+ community. Fermentative organisms are the most abundant *hgcA*+ organisms in Lake Mendota. Coverage of each functional group has been normalized to the coverage of all *hgcA*+ bins in each metagenome. Plots of coverage in the different metagenomes are arranged by decreasing redox potential, which corresponds to increasing sulfide concentrations. Abbreviations: GHs - glucoside hydrolases, EET - external electron transfer.

of large organic molecules, particularly polysaccharides from cyanobacterial blooms in the epilimnion, may contribute directly to MeHg production. A previous study in a eutrophic lake reported abundant polysaccharide-degrading, fermentative *hgcA*⁺ Kiritimatiellaeota, suggesting these organisms may link polysaccharide degradation to Hg-methylation in many eutrophic systems.¹⁴ Similar *hgcA* sequences were also identified in the Baltic sea on marine snow in oxygen-depleted waters, although at lower relative abundances.²⁷ It is unclear whether these novel *hgcA* sequences will be amplified by existing primers so we cannot comment on their presence/absence in other systems where PCR-based amplicon sequencing methods are used. On the other hand, respiratory *hgcA*⁺ organisms are much less abundant in Lake Mendota and are dominated by SRB in the meta- and hypolimnion during late stratification, likely due to the elevated levels of sulfate in the lake. Sulfate reduction in general appears to be the dominant form of anaerobic respiration in the hypolimnion. At the onset of stratification, sulfate levels are approximately 160 μM , well above what they need to outcompete methanogens [Loveley and Klug, 1983]. Interestingly, Jones et al reported similar levels of *hgcA*⁺ SRB in the water column of two lakes heavily enriched in sulfate ($\sim 3\text{mM}$ and $\sim 0.5\text{mM}$), suggesting that in water columns both heavily and moderately impacted by sulfate loading, SRBs still account for a relatively small portion of the *hgcA*⁺ community.¹⁴ Other TEAPs, such as Mn reduction, may be linked to Hg-methylation under certain conditions in Lake Mendota as well, since the *hgcA*⁺ Geobacterales appeared in the metalimnion during late stratification where we saw evidence for enhanced Mn cycling. However, we still do not know which of these *hgcA*⁺ organisms are active methylators or how rapidly they produce MeHg. Additional work using more functional measurements such as metatranscriptomics or metaproteomics will help identify which of these *hgcA*⁺ organisms are metabolically active and expressing *hgcA* under in situ conditions.

It is also important to consider that each of these *hgcA*-carrying organisms is a member of the anaerobic microbial food web and is thus influenced by the overall levels of community metabolism. For example, while there is little information on mass flux constraints on carbon degradation in freshwater anoxic water columns, in other anoxic environments such as marine sediments, hydrolysis and primary fermentation are the rate-limiting steps in community metabolism.^{103–105} Additionally, syntrophic organisms require that respiratory partners consume their metabolic end-products, such as hydrogen.¹⁰⁰ Thus, the supply of terminal electron acceptors and/or carbon substrates and the corresponding activity of flanking microbial community members controls the flux of carbon and energy through the anaerobic microbial food web, influencing the metabolism of individual *hgcA*⁺ organisms and presumably their methylation rates. This is supported by data that show that overall levels of heterotrophic activity correlate to MeHg production.^{9,25} This highlights the need for further research on complex natural communities to probe not only which organisms have and express the *hgcAB* genes or what metabolic pathways they have, but also how biogeochemical conditions and the overall flux of carbon and energy through different levels of the microbial anaerobic food web can directly and indirectly influence MeHg production *in situ*.

Acknowledgements

The authors acknowledge extensive analytical support from the USGS Toxic Substances Hydrology Program. We also acknowledge the North Temperate Lakes Long Term Ecological Research (NTL-LTER) site, Lake Mendota Microbial Observatory field crews, and UW Center for Limnology for field and logistical support. In particular we thank graduate students Tylor Rosera, Stephanie Berg, and Marissa Kneer for sampling assistance, and Joseph Skarlupka for computational assistance. We also thank undergraduate researchers Mykala Sobieck, Diana Mendez, and Ariel Sorg for sampling design and sampling assistance. Geochemical analyses were performed at the Water Science and Engineering Laboratory at the University of Wisconsin – Madison. Mercury analyses were performed in the Mercury Research Laboratory in the Upper Midwest Water Science Center at the U.S. Geological Survey in Middleton, WI. Computational work was performed in part using the Wisconsin Energy Institute computing cluster, which is supported by the Great Lakes Bioenergy Research Center as part of the U.S. Department of Energy Office of Science. Any use of trade, product, or firm names in this publication is for descriptive purposes only and does not imply endorsement by the U.S. Government.

Funding Sources

Katherine D. McMahon received funding from the United States National Science Foundation Microbial Observatories program (MCB-0702395), the Long-Term Ecological Research Program (NTL-LTER DEB-1440297), and an INSPIRE award (DEB-1344254), the Wisconsin Alumni Research Foundation. Funding for sequencing was provided by the National Oceanic and Atmospheric Administration (NA10OAR4170070 via the Wisconsin Sea Grant College Program Project #HCE-22). Benjamin Peterson was supported by the National Science Foundation Graduate Research Fellowship Program during this research.

References

1. Amos HM, Jacob DJ, Streets DG, Sunderland EM. Legacy impacts of all-time anthropogenic emissions on the global mercury cycle. *Global Biogeochem Cycles*. 2013;27(2):410-421. doi:[10.1002/gbc.20040](https://doi.org/10.1002/gbc.20040)
2. UN. *Global Mercury Assessment*.; 2018.
3. Cleckner LB, Gilmour CC, Hurley JP, Krabbenhoft DP. Mercury methylation in periphyton of the Florida Everglades. *Limnol Oceanogr*. 1999;44(7):1815-1825. doi:[10.4319/lo.1999.44.7.1815](https://doi.org/10.4319/lo.1999.44.7.1815)
4. Gascón Díez E, Loizeau J-L, Cosio C, Bouchet S, Adatte T, Amouroux D, Bravo AG. Role of settling particles on mercury methylation in the oxic water column of freshwater systems. *Environ Sci Technol*. 2016;50(21):11672-11679. doi:[10.1021/acs.est.6b03260](https://doi.org/10.1021/acs.est.6b03260)
5. Jensen S, Jernelöv A. Biological methylation of mercury in aquatic organisms. *Nature*. 1969;223:753-754. doi:[10.1038/223754b0](https://doi.org/10.1038/223754b0)
6. Lepak RF, Janssen SE, Yin R, Krabbenhoft DP, Ogorek JM, DeWild JF, Tate MT, Holsen TM, Hurley JP. Factors affecting mercury stable isotopic distribution in piscivorous fish of the Laurentian Great Lakes. *Environ Sci Technol*. 2018;52(5):2768-2776. doi:[10.1021/acs.est.7b06120](https://doi.org/10.1021/acs.est.7b06120)
7. Rothenberg SE, Feng X. Mercury cycling in a flooded rice paddy. *J Geophys Res*. 2012;117(G3003). doi:[10.1029/2011JG001800](https://doi.org/10.1029/2011JG001800)
8. Sunderland EM, Krabbenhoft DP, Moreau JW, Strode SA, Landing WM. Mercury sources, distribution, and bioavailability in the North Pacific Ocean: Insights from data and models. *Global Biogeochem Cycles*. 2009;23(2):1-14. doi:[10.1029/2008GB003425](https://doi.org/10.1029/2008GB003425)
9. Watras CJ, Bloom NS, Claas SA, Morrison KA, Gilmour CC, Craig SR. Methylmercury production in the anoxic hypolimnion of a dimictic seepage lake. *Water, Air, and Soil Pollution*. 1995;80:735-745.
10. Bloom NS. On the chemical form of mercury in edible fish and marine invertebrate tissue. *Can J Fish Aquat Sci*. 1992;49(5):1010-1017. doi:[10.1139/f92-113](https://doi.org/10.1139/f92-113)
11. Compeau GC, Bartha R. Sulfate-reducing bacteria: Principal methylators of mercury in anoxic estuarine sediment. *Appl Environ Microbiol*. 1985;50(2):498-502.
12. Gilmour CC, Henry EA, Mitchell R. Sulfate stimulation of mercury methylation in freshwater sediments. *Environ Sci Technol*. 1992;26(11):2281-2287. doi:[10.1021/es00035a029](https://doi.org/10.1021/es00035a029)
13. Eckley CS, Watras CJ, Hintelmann H, Morrison K, Kent AD, Regnell O. Mercury methylation in the hypolimnetic waters of lakes with and without connection to wetlands in northern Wisconsin. *Can J Fish Aquat Sci*. 2005;62(2):400-411. doi:[10.1139/f04-205](https://doi.org/10.1139/f04-205)

14. Jones DS, Walker GM, Johnson NW, Mitchell CPJ, Coleman Wasik JK, Bailey JV. Molecular evidence for novel mercury methylating microorganisms in sulfate-impacted lakes. *ISME J.* February 2019. doi:[10.1038/s41396-019-0376-1](https://doi.org/10.1038/s41396-019-0376-1)
15. Watras CJ, Bloom NS. The vertical distribution of mercury species in Wisconsin lakes: Accumulation in plankton layers. In: *Mercury Pollution: Integration and Synthesis*. Lewis Publications; 1994:137-151.
16. Warner KA, Roden EE, Bonzongo J-C. Microbial mercury transformation in anoxic freshwater sediments under iron-reducing and other electron-accepting conditions. *Environ Sci Technol.* 2003;37(10):2159-2165. doi:[10.1021/es0262939](https://doi.org/10.1021/es0262939)
17. Jeremiason JD, Engstrom DR, Swain EB, Nater EA, Johnson BM, Almendinger JE, Monson BA, Kolka RK. Sulfate addition increases methylmercury production in an experimental wetland. *Environ Sci Technol.* 2006;40(12):3800-3806. doi:[10.1021/es0524144](https://doi.org/10.1021/es0524144)
18. King JK, Saunders FM, Lee RF, Jahnke RA. Coupling mercury methylation rates to sulfate reduction rates in marine sediments. *Environmental Toxicology and Chemistry.* 1999;18(7):1362-1369. doi:[10.1002/etc.5620180704](https://doi.org/10.1002/etc.5620180704)
19. Regnell O, Watras CJ. Microbial mercury methylation in aquatic environments: A critical review of published field and laboratory studies. *Environ Sci Technol.* 2019;53(1):4-19. doi:[10.1021/acs.est.8b02709](https://doi.org/10.1021/acs.est.8b02709)
20. Willacker JJ, Eagles-Smith CA, Ackerman JT. Mercury bioaccumulation in estuarine fishes: Novel insights from sulfur stable isotopes. *Environ Sci Technol.* 2017;51(4):2131-2139. doi:[10.1021/acs.est.6b05325](https://doi.org/10.1021/acs.est.6b05325)
21. Hamelin S, Amyot M, Barkay T, Wang Y, Planas D. Methanogens: Principal methylators of mercury in lake periphyton. *Environ Sci Technol.* 2011;45(18):7693-7700. doi:[10.1021/es2010072](https://doi.org/10.1021/es2010072)
22. Kerin EJ, Gilmour CC, Roden E, Suzuki MT, Coates JD, Mason RP. Mercury methylation by dissimilatory iron-reducing bacteria. *Appl Environ Microbiol.* 2006;72(12):7919-7921. doi:[10.1128/AEM.01602-06](https://doi.org/10.1128/AEM.01602-06)
23. Gilmour CC, Podar M, Bullock AL, Graham AM, Brown SD, Somenahally AC, Johs A, Hurt RA, Bailey KL, Elias DA. Mercury methylation by novel microorganisms from new environments. *Environ Sci Technol.* 2013;47(20):11810-11820. doi:[10.1021/es403075t](https://doi.org/10.1021/es403075t)
24. Yu R-Q, Reinfelder JR, Hines ME, Barkay T. Syntrophic pathways for microbial mercury methylation. *ISME J.* 2018;12(7):1826-1835. doi:[10.1038/s41396-018-0106-0](https://doi.org/10.1038/s41396-018-0106-0)
25. Guimarães JRD, Mauro JBN, Meili M, Sundbom M, Haglund AL, Coelho-Souza SA, Hylander LD. Simultaneous radioassays of bacterial production and mercury methylation in the periphyton of a tropical and a temperate wetland. *Journal of Environmental Management.* 2006;81(2):95-100. doi:[10.1016/j.jenvman.2005.09.023](https://doi.org/10.1016/j.jenvman.2005.09.023)
26. Parks JM, Johs A, Podar M, Bridou R, Hurt RA, Smith SD, Tomanicek SJ, Qian Y, Brown SD, Brandt CC, Palumbo AV, Smith JC, Wall JD, Elias DA, Liang L. The genetic basis for

bacterial mercury methylation. *Science*. 2013;339(6125):1332-1335.
doi:[10.1126/science.1230667](https://doi.org/10.1126/science.1230667)

27. Capo E, Bravo AG, Soerensen AL, Bertilsson S, Pinhassi J, Feng C, Andersson AF, Buck M, Björn E. Deltaproteobacteria and Spirochaetes-like bacteria are abundant putative mercury methylators in oxygen-deficient water and marine particles in the Baltic Sea. *Front Microbiol*. 2020;11:1-11. doi:[10.3389/fmicb.2020.574080](https://doi.org/10.3389/fmicb.2020.574080)

28. Gilmour CC, Bullock AL, McBurney A, Podar M, Elias DA. Robust mercury methylation across diverse methanogenic *Archaea*. *mBio*. 2018;9(2):1-13. doi:[10.1128/mBio.02403-17](https://doi.org/10.1128/mBio.02403-17)

29. Gionfriddo CM, Wymore AM, Jones DS, Wilpiseski RL, Lynes MM, Christensen GA, Soren A, Gilmour CC, Podar M, Elias DA. An improved hgcAB primer set and direct high-throughput sequencing expand Hg-methylator diversity in nature. *Front Microbiol*. 2020;11:1-23. doi:[10.3389/fmicb.2020.541554](https://doi.org/10.3389/fmicb.2020.541554)

30. McDaniel EA, Peterson BD, Stevens SLR, Tran PQ, Anantharaman K, McMahon KD. Expanded phylogenetic diversity and metabolic flexibility of mercury-methylating microorganisms. Kent AD, ed. *mSystems*. 2020;5(4):1-21. doi:[10.1128/mSystems.00299-20](https://doi.org/10.1128/mSystems.00299-20)

31. Podar M, Gilmour CC, Brandt CC, Soren A, Brown SD, Crable BR, Palumbo AV, Somenahally AC, Elias DA. Global prevalence and distribution of genes and microorganisms involved in mercury methylation. *Sci Adv*. 2015;1:1-12. doi:[10.1126/sciadv.1500675](https://doi.org/10.1126/sciadv.1500675)

32. Villar E, Cabrol L, Heimbürger-Boavida L. Widespread microbial mercury methylation genes in the global ocean. *Environ Microbiol Reports*. February 2020:1-11. doi:[10.1111/1758-2229.12829](https://doi.org/10.1111/1758-2229.12829)

33. Bae H-S, Dierberg FE, Ogram A. Syntrophs dominate sequences associated with the mercury methylation-related gene *hgcA* in the Water Conservation Areas of the Florida Everglades. *Appl Environ Microbiol*. 2014;80(20):6517-6526. doi:[10.1128/AEM.01666-14](https://doi.org/10.1128/AEM.01666-14)

34. Bravo AG, Zopfi J, Buck M, Xu J, Bertilsson S, Schaefer JK, Poté J, Cosio C. Geobacteraceae are important members of mercury-methylating microbial communities of sediments impacted by waste water releases. *ISME J*. 2018;12(3):802-812. doi:[10.1038/s41396-017-0007-7](https://doi.org/10.1038/s41396-017-0007-7)

35. Christensen GA, Wymore AM, King AJ, Podar M, Hurt RA, Santillan EU, Soren A, Brandt CC, Brown SD, Palumbo AV, Wall JD, Gilmour CC, Elias DA. Development and validation of broad-range qualitative and clade-specific quantitative molecular probes for assessing mercury methylation in the environment. *Appl Environ Microbiol*. 2016;82(19):6068-6078. doi:[10.1128/AEM.01271-16](https://doi.org/10.1128/AEM.01271-16)

36. Liu Y-R, Yu R-Q, Zheng Y-M, He J-Z. Analysis of the microbial community structure by monitoring an Hg methylation gene (*hgcA*) in paddy soils along an Hg gradient. *Appl Environ Microbiol*. 2014;80(9):2874-2879. doi:[10.1128/AEM.04225-13](https://doi.org/10.1128/AEM.04225-13)

37. Schaefer JK, Kronberg R-M, Morel FMM, Skjellberg U. Detection of a key Hg methylation gene, *hgcA*, in wetland soils. *Environ Microbiol Reports*. 2014;6(5):441-447. doi:[10.1111/1758-2229.12136](https://doi.org/10.1111/1758-2229.12136)
38. Eddy SR. Hidden Markov Models. *Current Opinion in Structural Biology*. 1996;6:361-365.
39. Gionfriddo CM, Tate MT, Wick RR, Schultz MB, Zemla A, Thelen MP, Schofield R, Krabbenhoft DP, Holt KE, Moreau JW. Microbial mercury methylation in Antarctic sea ice. *Nature Microbiology*. 2016;1(10):1-12. doi:[10.1038/nmicrobiol.2016.127](https://doi.org/10.1038/nmicrobiol.2016.127)
40. Lin H, Ascher DB, Myung Y, Lamborg CH, Hallam SJ, Gionfriddo CM, Holt KE, Moreau JW. Mercury methylation by metabolically versatile and cosmopolitan marine bacteria. *bioRxiv*. 2020:[preprint]. doi:[10.1101/2020.06.03.132969](https://doi.org/10.1101/2020.06.03.132969)
41. Tyson GW, Chapman J, Hugenholtz P, Allen EE, Ram RJ, Richardson PM, Solovyev VV, Rubin EM, Rokhsar DS, Banfield JF. Community structure and metabolism through reconstruction of microbial genomes from the environment. *Nature*. 2004;428(6978):37-43. doi:[10.1038/nature02340](https://doi.org/10.1038/nature02340)
42. Brock TD. *A Eutrophic Lake: Lake Mendota, Wisconsin*. 1st ed. Springer; 1985.
43. Ingvorsen K, Zeikus JG, Brock TD. Dynamics of bacterial sulfate reduction in a eutrophic lake. *Appl Environ Microbiol*. 1981;42(6):1029-1036. doi:[10.1128/AEM.42.6.1029-1036.1981](https://doi.org/10.1128/AEM.42.6.1029-1036.1981)
44. Olson ML, DeWild JF. Techniques for the collection and species-specific analysis of low levels of mercury in water, sediment, and biota. In: *U.S. Geological Survey Water-Resources Investigations Report*. Vols 99-4018B. Washington, D.C.; 1999.
45. Cline JD. Spectrophotometric determine of hydrogen sulfide in natural waters. *Limnol Oceanogr*. 1969;14(3):454-458. doi:[10.4319/lo.1969.14.3.0454](https://doi.org/10.4319/lo.1969.14.3.0454)
46. *U.S EPA Method 1631, Revision E: Mercury in Water by Oxidation, Purge and Trap, and Cold Vapor Atomic Fluorescence Spectrometry*. Washington, D.C.: U.S. Environmental Protection Agency; 2002.
47. Olund SD, DeWild JF, Olson ML, Tate MT. Methods for the preparation and analysis of solids and suspended solids for total mercury. In: *U.S. Geological Survey Techniques of Water-Resources Investigations, Book 5, Chapter A8*. Techniques and Methods.; 2004.
48. DeWild JF, Olson ML, Olund SD. *Determination of Methyl Mercury by Aqueous Phase Ethylation, Followed by Gas Chromatographic Separation with Cold Vapor Atomic Fluorescence Detection*. Open-File Report. Reston, VA: U. S. Geological Survey; 2002.
49. Horvat M, Bloom NS, Liang L. Comparison of distillation with other current isolation methods for the determination of methyl mercury compounds in low level environmental samples. *Analytica Chimica Acta*. 1993;281:135-152. doi:[10.1016/0003-2670\(93\)85348-N](https://doi.org/10.1016/0003-2670(93)85348-N)
50. Lepak RF, Krabbenhoft DP, Ogorek JM, Tate MT, Bootsma HA, Hurley JP. Influence of *Cladophora*–quagga mussel assemblages on nearshore methylmercury production in Lake Michigan. *Environ Sci Technol*. 2015;49(13):7606-7613. doi:[10.1021/es506253v](https://doi.org/10.1021/es506253v)

51. Lever MA, Torti A, Eickenbusch P, Michaud AB, Å antl-Temkiv T, JÃ,rgensen BB. A modular method for the extraction of DNA and RNA, and the separation of DNA pools from diverse environmental sample types. *Front Microbiol.* 2015;6. doi:[10.3389/fmicb.2015.00476](https://doi.org/10.3389/fmicb.2015.00476)
52. Joshi N, Fass J. *Sickle: A Sliding-Window, Adaptive, Quality-Based Trimming Tool for FastQ Files.*; 2011. <https://github.com/najoshi/sickle>.
53. Nurk S, Meleshko D, Korobeynikov A, Pevzner PA. metaSPAdes: A new versatile metagenomic assembler. *Genome Research.* 2017;27(5):824-834. doi:[10.1101/gr.213959.116](https://doi.org/10.1101/gr.213959.116)
54. Hyatt D, Chen G-L, LoCascio PF, Land ML, Larimer FW, Hauser LJ. Prodigal: Prokaryotic gene recognition and translation initiation site identification. *BMC Bioinformatics.* 2010;11(1):119. doi:[10.1186/1471-2105-11-119](https://doi.org/10.1186/1471-2105-11-119)
55. Bushnell B. *BBMap Short Read Aligner.*; 2015. <https://sourceforge.net/projects/bbmap/>.
56. Alneberg J, Bjarnason BS, de Bruijn I, Schirmer M, Quick J, Ijaz UZ, Lahti L, Loman NJ, Andersson AF, Quince C. Binning metagenomic contigs by coverage and composition. *Nat Methods.* 2014;11(11):1144-1146. doi:[10.1038/nmeth.3103](https://doi.org/10.1038/nmeth.3103)
57. Kang DD, Li F, Kirton E, Thomas A, Egan R, An H, Wang Z. MetaBAT 2: An adaptive binning algorithm for robust and efficient genome reconstruction from metagenome assemblies. *PeerJ.* 2019;7:1-13. doi:[10.7717/peerj.7359](https://doi.org/10.7717/peerj.7359)
58. Sieber CMK, Probst AJ, Sharrar A, Thomas BC, Hess M, Tringe SG, Banfield JF. Recovery of genomes from metagenomes via a dereplication, aggregation and scoring strategy. *Nat Microbiol.* 2018;3(7):836-843. doi:[10.1038/s41564-018-0171-1](https://doi.org/10.1038/s41564-018-0171-1)
59. Wu Y-W, Simmons BA, Singer SW. MaxBin 2.0: An automated binning algorithm to recover genomes from multiple metagenomic datasets. *Bioinformatics.* 2016;32(4):605-607. doi:[10.1093/bioinformatics/btv638](https://doi.org/10.1093/bioinformatics/btv638)
60. Parks DH, Imelfort M, Skennerton CT, Hugenholtz P, Tyson GW. CheckM: Assessing the quality of microbial genomes recovered from isolates, single cells, and metagenomes. *Genome Res.* 2015;25(7):1043-1055. doi:[10.1101/gr.186072.114](https://doi.org/10.1101/gr.186072.114)
61. Bowers RM, Stepanauskas R, Harmon-Smith M, Doud D, Reddy TBK, Schulz F, Jarett J, Rivers AR, Eloe-Fadrosh EA, Tringe SG, Ivanova NN, Copeland A, Clum A, Becraft ED, Malmstrom RR, Birren B, Podar M, Bork P, Weinstock GM, Garrity GM, Dodsworth JA, Yooseph S, Sutton G, Glöckner FO, Gilbert JA, Nelson WC, Hallam SJ, Jungbluth SP, Ettema TJG, Tighe S, Konstantinidis KT, Liu W-T, Baker BJ, Rattei T, Eisen JA, Hedlund B, McMahon KD, Fierer N, Knight R, Finn R, Cochrane G, Karsch-Mizrachi I, Tyson GW, Rinke C, Consortium TGS, Lapidus A, Meyer F, Yilmaz P, Parks DH, Murat Eren A, Schriml L, Banfield JF, Hugenholtz P, Woyke T. Minimum information about a single amplified genome (MISAG) and a metagenome-assembled genome (MIMAG) of bacteria and archaea. *Nat Biotechnol.* 2017;35(8):725-731. doi:[10.1038/nbt.3893](https://doi.org/10.1038/nbt.3893)

62. Eren AM, Esen ÖC, Quince C, Vineis JH, Morrison HG, Sogin ML, Delmont TO. Anvi'o: An advanced analysis and visualization platform for 'omics data. *PeerJ*. 2015;3:1-29. doi:[10.7717/peerj.1319](https://doi.org/10.7717/peerj.1319)
63. Chaumeil P-A, Mussig AJ, Hugenholtz P, Parks DH. GTDB-Tk: A toolkit to classify genomes with the Genome Taxonomy Database. *Bioinformatics*. 2019;36(6):1925-1927. doi:[10.1093/bioinformatics/btz848](https://doi.org/10.1093/bioinformatics/btz848)
64. Konwar KM, Hanson NW, Pagé AP, Hallam SJ. MetaPathways: A modular pipeline for constructing pathway/genome databases from environmental sequence information. *BMC Bioinformatics*. 2013;14(202):1-10. doi:[10.1186/1471-2105-14-202](https://doi.org/10.1186/1471-2105-14-202)
65. Eddy SR. *Hmmer.*; 2015. <http://hmmer.org/>.
66. Fu L, Niu B, Zhu Z, Wu S, Li W. CD-HIT: Accelerated for clustering the next-generation sequencing data. *Bioinformatics*. 2012;28(23):3150-3152. doi:[10.1093/bioinformatics/bts565](https://doi.org/10.1093/bioinformatics/bts565)
67. Anantharaman K, Brown CT, Hug LA, Sharon I, Castelle CJ, Probst AJ, Thomas BC, Singh A, Wilkins MJ, Karaoz U, Brodie EL, Williams KH, Hubbard SS, Banfield JF. Thousands of microbial genomes shed light on interconnected biogeochemical processes in an aquifer system. *Nat Commun*. 2016;7(13219):1-11. doi:[10.1038/ncomms13219](https://doi.org/10.1038/ncomms13219)
68. Edgar RC. MUSCLE: A multiple sequence alignment method with reduced time and space complexity. *BMC Bioinformatics*. 2004;5(113):1-19. doi:[10.1186/1471-2105-5-113](https://doi.org/10.1186/1471-2105-5-113)
69. Criscuolo A, Gribaldo S. BMGE (Block Mapping and Gathering with Entropy): A new software for selection of phylogenetic informative regions from multiple sequence alignments. *BMC Evol Biol*. 2010;10(210):1-21. doi:[10.1186/1471-2148-10-210](https://doi.org/10.1186/1471-2148-10-210)
70. Stamatakis A. RAxML version 8: A tool for phylogenetic analysis and post-analysis of large phylogenies. *Bioinformatics*. 2014;30(9):1312-1313. doi:[10.1093/bioinformatics/btu033](https://doi.org/10.1093/bioinformatics/btu033)
71. Aberer AJ, Krompass D, Stamatakis A. Pruning rogue taxa improves phylogenetic accuracy: An efficient algorithm and webservice. *Systematic Biology*. 2013;62(1):162-166. doi:[10.1093/sysbio/sys078](https://doi.org/10.1093/sysbio/sys078)
72. Matsen FA, Kodner RB, Armbrust EV. Pplacer: Linear time maximum-likelihood and Bayesian phylogenetic placement of sequences onto a fixed reference tree. *BMC Bioinformatics*. 2010;11(538):1-16. doi:[10.1186/1471-2105-11-538](https://doi.org/10.1186/1471-2105-11-538)
73. Schliep KP. Phangorn: Phylogenetic analysis in R. *Bioinformatics*. 2011;27(4):592-593. doi:[10.1093/bioinformatics/btq706](https://doi.org/10.1093/bioinformatics/btq706)
74. Yu G, Smith DK, Zhu H, Guan Y, Lam TT. Ggtree: An R package for visualization and annotation of phylogenetic trees with their covariates and other associated data. *Methods Ecol Evol*. 2017;8:28-36. doi:[10.1111/2041-210X.12628](https://doi.org/10.1111/2041-210X.12628)
75. Stauffer RE. Cycling of manganese and iron in Lake Mendota, Wisconsin. *Environ Sci Technol*. 1986;20(5):449-457. doi:[10.1021/es00147a002](https://doi.org/10.1021/es00147a002)

76. Chadwick SP, Babiarz CL, Hurley JP, Armstrong DE. Influences of iron, manganese, and dissolved organic carbon on the hypolimnetic cycling of amended mercury. *Science of The Total Environment*. 2006;368(1):177-188. doi:[10.1016/j.scitotenv.2005.09.039](https://doi.org/10.1016/j.scitotenv.2005.09.039)
77. Tebo BM, Rosson RA, Nealson KH. Potential for Manganese(II) Oxidation and Manganese(IV) Reduction to Co-Occur in the Suboxic Zone of the Black Sea. In: İzdar E, Murray JW, eds. *Black Sea Oceanography*. Dordrecht: Springer Netherlands; 1991:173-185. doi:[10.1007/978-94-011-2608-3_10](https://doi.org/10.1007/978-94-011-2608-3_10)
78. Lovley DR, Klug MJ. Sulfate reducers can outcompete methanogens at freshwater sulfate concentrations. *Appl Environ Microbiol*. 1983;45(1):187-192.
79. Hsu-Kim H, Kucharzyk KH, Zhang T, Deshusses MA. Mechanisms regulating mercury bioavailability for methylating microorganisms in the aquatic environment: A critical review. *Environ Sci Technol*. 2013;47(6):2441-2456. doi:[10.1021/es304370g](https://doi.org/10.1021/es304370g)
80. Goñi-Urriza M, Klopp C, Ranchou-Peyruse M, Ranchou-Peyruse A, Monperrus M, Khalfaoui-Hassani B, Guyoneaud R. Genome insights of mercury methylation among *Desulfovibrio* and *Pseudodesulfovibrio* strains. *Research in Microbiology*. 2020;171(1):3-12. doi:[10.1016/j.resmic.2019.10.003](https://doi.org/10.1016/j.resmic.2019.10.003)
81. Ranchou-Peyruse M, Monperrus M, Bridou R, Duran R, Amouroux D, Salvado JC, Guyoneaud R. Overview of mercury methylation capacities among anaerobic bacteria including representatives of the sulphate-reducers: Implications for environmental studies. *Geomicrobiology Journal*. 2009;26(1):1-8. doi:[10.1080/01490450802599227](https://doi.org/10.1080/01490450802599227)
82. Gloor GB, Macklaim JM, Pawlowsky-Glahn V, Egozcue JJ. Microbiome datasets are compositional: And this is not optional. *Front Microbiol*. 2017;8:1-6. doi:[10.3389/fmicb.2017.02224](https://doi.org/10.3389/fmicb.2017.02224)
83. Sczyrba A, Hofmann P, Belmann P, Koslicki D, Janssen S, Dröge J, Gregor I, Majda S, Fiedler J, Dahms E, Bremges A, Fritz A, Garrido-Oter R, Jørgensen TS, Shapiro N, Blood PD, Gurevich A, Bai Y, Turaev D, DeMaere MZ, Chikhi R, Nagarajan N, Quince C, Meyer F, Balvočiūtė M, Hansen LH, Sørensen SJ, Chia BKH, Denis B, Froula JL, Wang Z, Egan R, Don Kang D, Cook JJ, Deltel C, Beckstette M, Lemaitre C, Peterlongo P, Rizk G, Lavenier D, Wu Y-W, Singer SW, Jain C, Strous M, Klingenberg H, Meinicke P, Barton MD, Lingner T, Lin H-H, Liao Y-C, Silva GGZ, Cuevas DA, Edwards RA, Saha S, Piro VC, Renard BY, Pop M, Klenk H-P, Göker M, Kyrpides NC, Woyke T, Vorholt JA, Schulze-Lefert P, Rubin EM, Darling AE, Rattei T, McHardy AC. Critical assessment of metagenome interpretation—a benchmark of metagenomics software. *Nat Methods*. 2017;14(11):1063-1071. doi:[10.1038/nmeth.4458](https://doi.org/10.1038/nmeth.4458)
84. Gilmour CC, Elias DA, Kucken AM, Brown SD, Palumbo AV, Schadt CW, Wall JD. Sulfate-reducing bacterium *Desulfovibrio Desulfuricans* NDI32 as a model for understanding bacterial mercury methylation. *Appl Environ Microbiol*. 2011;77(12):3938-3951. doi:[10.1128/AEM.02993-10](https://doi.org/10.1128/AEM.02993-10)
85. Spring S, Bunk B, Spröer C, Schumann P, Rohde M, Tindall BJ, Klenk H-P. Characterization of the first cultured representative of Verrucomicrobia subdivision 5 indicates the proposal of a novel phylum. *ISME J*. 2016;10(12):2801-2816. doi:[10.1038/ismej.2016.84](https://doi.org/10.1038/ismej.2016.84)

86. van Vliet DM, Palakawong Na Ayudthaya S, Diop S, Villanueva L, Stams AJM, Sánchez-Andrea I. Anaerobic degradation of sulfated polysaccharides by two novel Kiritimatiellales strains isolated from black sea sediment. *Front Microbiol.* 2019;10:1-16. doi:[10.3389/fmicb.2019.00253](https://doi.org/10.3389/fmicb.2019.00253)
87. Anantharaman K, Hausmann B, Jungbluth SP, Kantor RS, Lavy A, Warren LA, Rappé MS, Pester M, Loy A, Thomas BC, Banfield JF. Expanded diversity of microbial groups that shape the dissimilatory sulfur cycle. *ISME J.* 2018;12(7):1715-1728. doi:[10.1038/s41396-018-0078-0](https://doi.org/10.1038/s41396-018-0078-0)
88. Pereira IAC, Ramos AR, Grein F, Marques MC, da Silva SM, Venceslau SS. A comparative genomic analysis of energy metabolism in sulfate reducing bacteria and archaea. *Front Microbio.* 2011;2:1-22. doi:[10.3389/fmicb.2011.00069](https://doi.org/10.3389/fmicb.2011.00069)
89. Rothery RA, Workun GJ, Weiner JH. The prokaryotic complex iron–sulfur molybdoenzyme family. *Biochimica et Biophysica Acta.* 2008;1778:1897-1929. doi:[10.1016/j.bbamem.2007.09.002](https://doi.org/10.1016/j.bbamem.2007.09.002)
90. Thauer RK, Kaster A-K, Seedorf H, Buckel W, Hedderich R. Methanogenic archaea: Ecologically relevant differences in energy conservation. *Nat Rev Microbiol.* 2008;6(8):579-591. doi:[10.1038/nrmicro1931](https://doi.org/10.1038/nrmicro1931)
91. Alpers CN, Fleck JA, Marvin-DiPasquale M, Stricker CA, Stephenson M, Taylor HE. Mercury cycling in agricultural and managed wetlands, Yolo Bypass, California: Spatial and seasonal variations in water quality. *Science of The Total Environment.* 2014;484:276-287. doi:[10.1016/j.scitotenv.2013.10.096](https://doi.org/10.1016/j.scitotenv.2013.10.096)
92. Vlassopoulos D, Kanematsu M, Henry EA, Goin J, Leven A, Glaser D, Brown SS, O'Day PA. Manganese(IV) oxide amendments reduce methylmercury concentrations in sediment porewater. *Environ Sci: Processes Impacts.* 2018;20(12):1746-1760. doi:[10.1039/C7EM00583K](https://doi.org/10.1039/C7EM00583K)
93. Richardson DJ, Butt JN, Fredrickson JK, Zachara JM, Shi L, Edwards MJ, White G, Baiden N, Gates AJ, Marritt SJ, Clarke TA. The “porin-cytochrome” model for microbe-to-mineral electron transfer: Microbe-to-mineral electron transfer. *Molecular Microbiology.* 2012;85(2):201-212. doi:[10.1111/j.1365-2958.2012.08088.x](https://doi.org/10.1111/j.1365-2958.2012.08088.x)
94. Jiménez Otero F, Chan CH, Bond DR. Identification of different putative outer membrane electron conduits necessary for Fe(III) citrate, Fe(III) oxide, Mn(IV) oxide, or electrode reduction by *Geobacter Sulfurreducens*. *J Bacteriol.* 2018;200(19):1-20. doi:[10.1128/JB.00347-18](https://doi.org/10.1128/JB.00347-18)
95. Berg JS, Michellod D, Pjevac P, Martinez-Perez C, Buckner CRT, Hach PF, Schubert CJ, Milucka J, Kuypers MMM. Intensive cryptic microbial iron cycling in the low iron water column of the meromictic Lake Cadagno: A cryptic microbial iron cycle. *Environmental Microbiology.* 2016;18(12):5288-5302. doi:[10.1111/1462-2920.13587](https://doi.org/10.1111/1462-2920.13587)
96. Schaefer JK, Morel FMM. High methylation rates of mercury bound to cysteine by *Geobacter sulfurreducens*. *Nature Geosci.* 2009;2(2):123-126. doi:[10.1038/ngeo412](https://doi.org/10.1038/ngeo412)

97. Todorova SG, Driscoll CT, Matthews DA, Effler SW, Hines ME, Henry EA. Evidence for regulation of monomethyl mercury by nitrate in a seasonally stratified, eutrophic lake. *Environ Sci Technol*. 2009;43(17):6572-6578. doi:[10.1021/es900887b](https://doi.org/10.1021/es900887b)
98. Simon J. Enzymology and bioenergetics of respiratory nitrite ammonification. *FEMS Microbiol Rev*. 2002;26(3):285-309. doi:[10.1111/j.1574-6976.2002.tb00616.x](https://doi.org/10.1111/j.1574-6976.2002.tb00616.x)
99. Simon J, Kern M, Hermann B, Einsle O, Butt JN. Physiological function and catalytic versatility of bacterial multihaem cytochromes c involved in nitrogen and sulfur cycling. *Biochemical Society Transactions*. 2011;39(6):1864-1870. doi:[10.1042/BST20110713](https://doi.org/10.1042/BST20110713)
100. Sieber JR, McInerney MJ, Gunsalus RP. Genomic insights into syntrophy: The paradigm for anaerobic metabolic cooperation. *Annu Rev Microbiol*. 2012;66(1):429-452. doi:[10.1146/annurev-micro-090110-102844](https://doi.org/10.1146/annurev-micro-090110-102844)
101. Bertocchi C, Navarini L, Cesaro A, Anastasio M. Polysaccharides from cyanobacteria. *Carbohydrate Polymers*. 1990;12:127-153. doi:[10.1016/0144-8617\(90\)90015-K](https://doi.org/10.1016/0144-8617(90)90015-K)
102. Beversdorf LJ, Miller TR, McMahon KD. The role of nitrogen fixation in cyanobacterial bloom toxicity in a temperate, eutrophic lake. *PLoS ONE*. 2013;8(2):1-11. doi:[10.1371/journal.pone.0056103](https://doi.org/10.1371/journal.pone.0056103)
103. Billen G. Modelling the processes of organic matter degradation and nutrients recycling in sedimentary systems. In: *Sediment Microbiology (Special Publications of the Society for General Microbiology, Book 7)*. 1st ed. Academic Press Inc; 1982:15-52.
104. Boschker HTS. Decomposition of organic matter in the littoral sediments of a lake. 1997.
105. Meyer-Reil L-A. Seasonal and spatial distribution of extracellular enzymatic activities and microbial incorporation of dissolved organic substrates in marine sediments. *Appl Environ Microbiol*. 1987;53(8):1748-1755. doi:[10.1128/AEM.53.8.1748-1755.1987](https://doi.org/10.1128/AEM.53.8.1748-1755.1987)

Appendix to Chapter 2: Supplementary tables, methods and results, and figures

Supplementary Tables: All supplementary data and tables can be found here:

<https://figshare.com/account/home#/projects/117342>

Table S2.1. A) Geochemical data table. B) Sonde profile data.

Table S2.2. Summary of metadata and geochemical data associated with metagenomic samples.

Table S2.3. Assembly statistics for each of the assemblies, after removing all scaffolds <500bp in length.

Table S2.4. Metadata for 30 HgcA amino acid sequences from confirmed methylators.

Table S2.5. Aggregated information for each *hgcA* gene from the dereplicated set. Classification of *hgcA* is based on the bin phylogenies, for the binned genes, and on the HgcA phylogenies, for the unbinned genes. “Rogue taxa” indicates that the HgcA sequence was interfering with phylogenetic reconstruction. These sequences were classified using pplacer with the *hgcA* phylogeny. The *hgcB* column indicates whether or not there was an *hgcB* gene immediately downstream of the *hgcA* gene on the scaffold. The abundance of each sequence is presented as the percentage of *hgcA* coverage within a metagenome that each gene accounts for.

Table S2.6. Bin information and statistics. Completeness and redundancy estimates are based on universal conserved proteins set in CheckM. Inferred taxonomy is based on a rp16-based ML-tree tree with a large reference data set. Coverage of each bin in each metagenome has been normalized to the number of reads in the smallest metagenome.

Supplementary Methods and Results: Includes additional details on sampling efforts, Hg analyses, DNA extractions, and bioinformatics workflows.

Sampling site and methods. Lake Mendota is a dimictic lake covering almost 40 km² located in Madison, Wisconsin, USA. It is heavily eutrophic due to heavy agricultural land use in the watershed and is elevated in sulfate. All sampling was done at the Deep Hole, a large basin that is the deepest part of the lake. Profiles were collected within 100m of the North Temperate Lakes Long-Term Ecological Research buoy (GPS coordinates: 43.0989, -89.4055). Water-quality profiles and depth-discrete samples were collected once a month throughout the ice-off season in 2017. Sampling was more frequent in the late fall and focused on the oxic-anoxic interface. Water temperature, dissolved oxygen saturation,

and turbidity were measured with a YSI Exo2 multiparameter sonde (YSI Incorporated, Yellow Springs, OH). Sonde data can be found in Table S1b. The profiles of these constituents were viewed in real-time to guide selection of sampling depth. The sonde was then attached to 100ft of acid-washed Teflon sampling line, with the intake positioned at equal depth to the sensors. The anchor line was loosened and the boat moved back ~10 meters. The sampling line was flushed with 2L (~6x of the volume of the tubing) of sample water at the first sampling depth and flushed with 1L of sample water at each subsequent depth.

Water for sulfate and sulfide analysis was collected into a 15ml Falcon tube and immediately preserved in 1% zinc acetate. Samples for dissolved iron and manganese analysis were filtered through a 0.45 μ m PES Acrodisc filter and then also collected into 15ml Falcon tubes and preserved with 1% HCl. DNA samples were collected with an in-line 0.22 μ m pore-size PES filter (Pall Corp.) housed in an Advantec polypropylene filter holder. The filter cartridges were rinsed with ~200ml of site water before filtration. Sample was collected until the filter began to clog (~350-500ml of water). When finished, all remaining water was flushed through the filter cartridge and the filter was removed, folded, placed into a 2ml cryotube, and flash-frozen with liquid nitrogen, all within 90 seconds of completing filtration. Water for Hg analyses were collected using clean hands/dirty hands methods.¹ Raw water was collected into new triple-rinsed PETG 2.5L bottles and allowed to overflow before capping to eliminate headspace and minimize oxygen diffusion into the samples. In the field, samples were double-bagged, then stored in a cooler on ice. After collection, samples were brought to the U.S. Geological Survey (USGS) Mercury Research Laboratory (MRL) within 24 hours for filtration. Raw water was filtered through a quartz

fiber filter (QFF) and preserved with HCl to a final concentration of 1% for dissolved total mercury (HgT) and methylmercury (MeHg) analysis. Particulate matter retained on QFFs was frozen and retained for particulate-bound Hg analysis.

QA/QC for biogeochemical analyses. For both sulfide and sulfate, the daily detection limit (DDL) for each analytical set was required to be below 2 μM for the run to pass. The r^2 of the calibration curve was required to be > 0.995 . Every tenth sample was analyzed in triplicate, and the relative standard deviation (RSD) was within 10%. The detection limits for manganese and iron were approximately 1 μM . Every tenth sample was analyzed in duplicate and the relative percent difference was $< 10\%$.

Mercury analyses. Analysis of the Hg samples were conducted at the USGS MRL. All analytical methods for HgT and MeHg are described in detail at the MRL website (<https://wi.water.usgs.gov/mercury-lab/research/analysis-methods.html>), but are described briefly here. Quality assurance and control objectives of the MRL can also be found on the MRL website (<https://wi.water.usgs.gov/mercury-lab/research/quality.html>). Briefly, all replicates were within 10% deviation (for duplicates) or 10% RSD (for triplicates), check standards were between 90-110%, and matrix spikes were between 90-110%. The reporting limit for both HgT and MeHg is 0.04 ng/L. HgT in aqueous and particulate samples were quantified by cold vapor atomic fluorescence spectrometry (CVAFS). Aqueous HgT determination followed EPA Method 1631, revision E: oxidation with bromine monochloride, neutralization with hydroxylamine, reduction with tin chloride, purge and trap with dual stage gold amalgamation, and finally quantification by CVAFS on a Tekran Model 2500 Mercury

Detector.² All aqueous samples were analyzed in duplicate, and passed all required quality assurance and control objectives as stated by the USGS MRL. Particulate-bound HgT was analyzed using similar methods and is fully described in USGS Techniques and Methods 5 A-8.³

Filter-passing and particulate MeHg were analyzed following a modified version of US EPA method 1630 and passed all required quality assurance and control objectives as stated by the USGS MRL. The modified method includes analyte quantification with isotope dilution, automated sample preparation by the Brooks Rand Merx-M, and inductively coupled plasma mass spectrometry (ICP-MS) detection.⁴⁻⁶ Samples for analyses were first spiked with Me¹⁹⁹Hg, amended with copper sulfate (CuSO₄) (for aqueous samples) or a dilute CuSO₄/sulfic acid/potassium chloride solution (for filters), and distilled at 121°C under N₂ gas. The distillate was then treated with sodium tetraethylborate to ethylate ionic mercury species. On the Merx-M, the resulting gaseous ethylated mercury was purged from the distillate with argon gas, retained on Tenax, thermally desorbed, mass-separated by gas chromatography, and introduced to the ICP-MS (Thermo Fisher Scientific iCAP-RQ).

DNA extraction protocol. DNA was extracted using a modified protocol involving enzymatic and physical cell disruption, phenol-chloroform extraction, and purification by isopropanol/ethanol precipitation. Frozen filters were placed into a tube with a zirconium sphere and garnet flakes (Lysing Matrix A, MP Biomedical). Filters were treated with 250µl of 1mg/ml lysozyme for 10 min at room temperature. Proteins were then digested with 250µl of 1mg/ml proteinase K in a 2XS buffer (2% xanthogenate, 40mM EDTA, 1.6M ammonium acetate, 2% SDS, in a 200mM Tris buffer, pH7.5) for 3 minutes at room

temperature. Filters were then mechanically shredded by 3 minutes of beadbeating. Polysaccharides were precipitated out by addition of 125 μ l of 5M NaCl followed by 125 μ l of 10% CTAB. Samples were incubated in a 70°C water bath for 20 minutes. The supernatant was then extracted twice with 750 μ l of phenol:chloroform:isoamylalcohol (25:24:1), followed by a single wash extraction with 750 μ l of chloroform. Each extraction consisted of addition of reagent, mixing by inversion for 2-3 minutes, centrifugation at 13200 rpm for 5 minutes, and the transfer of the supernatant to a new 1.5ml Eppendorf tube. After the chloroform wash, DNA was precipitated by addition of 800 μ l 100% cold isopropanol. DNA was precipitated at -20°C overnight, then spun down at 13200 rpm for 15 minutes. The supernatant was removed and the DNA washed with 1ml 70% ethanol, then spun down for another 15 minutes at 13200 rpm. The supernatant was removed and the DNA dried for ~2 hrs, before resuspending in 50 μ l of TE buffer. DNA was quantified using a Qubit Fluorometer and quality was assessed on a Nanodrop.

Sequencing and assembly. DNA library preparation was performed at the Functional Genomics Lab and DNA sequencing at the Vincent J. Coates Genomics Sequencing Lab, both within the California Institute for Quantitative Biosciences (QB3-Berkeley, Berkeley, CA). A Kapa Biosystem Library Prep kit was used to generate libraries with an approximate insert size of ~600bp (Roche Sequencing and Life Science, Kapa Biosystems, Wilmington, MA). Libraries were pooled and sequenced on a single lane of an Illumina HiSeq4000 for paired-end reads of 150bp (Illumina, Inc., San Diego, CA). Sickle (v1.33) was used to trim the raw reads to maintain a QC score of 20 over a sliding window of 15 and reads shorter than 100bp after trimming were cut.⁷ Quality of the trimmed reads was assessed using FastQC.⁸ Metagenomes were assembled both individually and together

using metaSPADes (v3.12) with kmer sizes of 21, 33, 55, 77, 99, and 127.⁹ The quality of the assembly was assessed using the assembly contiguity perl script `abyss-fac.pl` associated with the Abyss assembler.¹⁰ [Prodigal](#) was used to predict open reading frames (version 2.6.2).¹¹

Initial binning. Reads from each metagenome were mapped to the scaffolds from each assembly using BMap (v35).¹² All default settings were used. Assemblies were initially binned using tetranucleotide frequency and differential coverage using three different binning algorithms: Metabat2 (v2.12.1), MaxBin (v2.1.1), and CONCOCT (v0.4.1).¹³⁻¹⁵ For each individual assemblies, CONCOCT was run with a maximum of 350 clusters, based on iterative rounds of binning. The coassembly was not binned with CONCOCT due to duration and intensity of computing power. Maxbin and Metabat2 were both run using default parameters. The bins from these three binning algorithms (two for the coassembly) were then aggregated using [DAS Tool](#) with a score threshold of 0.4.¹⁶ Final completeness, contamination, and other quality factors of the aggregated bins were determined using CheckM (v1.1.2).¹⁷ To dereplicate the bins across the individual assemblies and the coassembly, pairwise ANI comparisons were made between every bin using a [pipeline written by Sarah Stevens](#) that uses the Joint Genome Institute's ANI calculator.¹⁸ Bins with greater than 98% ANI over 50% alignment (criteria based on drop-off points in values for both ANI and alignment) were grouped into a "high matching set" (HMS). The "best" bin of the HMS was chosen to be the representative sequence, based primarily on percent completeness, size of bin, and quality of the assembly. Contamination was also considered, but to a lesser degree due to the following decontamination efforts.

Bin refinement and curation. All hgcA+ bins were decontaminated using the anvi-refine interface in Anvi'o (v5.2).¹⁹ Manual binning was conducted based on differential coverage and clustering of contigs by tetranucleotide frequency. These bins were then reassembled to improve bin quality. All reads mapping back to each bin were extracted and reassembled individually using SPADes (kmer length of 21, 33, 55, 77, 99, and 127). This assembly was then manually binned in anvi'o based on differential coverage and tetranucleotide frequency using CONCOCT.^{13,19} Manual comparison of the %GC content, tetranucleotide frequency, differential coverage, and taxonomy of adjacent genes according to Kaiju was conducted on binned hgcA+ scaffolds, relative to other scaffolds in the bin, to confirm the inclusion of these scaffolds within the bin.²⁰ Open reading frames (ORFs) were predicted for each bin using Prodigal (v2.6.2) on "single" mode.¹¹

Hidden Markov Model construction. To facilitate accurate identification of HgcA sequences in our metagenomes, a Hidden Markov Model (HMM) of the HgcA sequence was built. Thirty HgcA protein sequences from publicly available genomes of confirmed methylating organisms were aligned using MUSCLE (Table S4) (v3.8.31).²¹ This alignment was imported into Geneious and manually curated as follows. The ends of the alignment were trimmed so that the alignment started at a well-conserved domain and all residues that were not covered by at least 50% of the sequences were masked. The aligned fasta file was then used to build the HMM using the hmmbuild function in hmmer (v3.1b2).²² The HMM can be found on the Open Science Framework project page, here:

<https://osf.io/9vwgt/>.

To determine the trusted and noise cut-off, the PFAM database was searched using the reference HgcA sequences. Only PF03699, the PFAM in which HgcA was originally discovered, returned any hits. All sequences in PFAM03599 were downloaded and aligned using MUSCLE (v3.8.31).²¹ Sequences that contained the characteristic cap-helix domain of HgcA and at least four transmembrane domains (predicted by TMHMM in Geneious) were categorized as 'HgcA-like' and all other sequences were classified as 'CFeSP-like'. The newly built HMM was used to search these two groups of sequences. The lowest score from the 'HgcA-like' group was 131.8, and this was added as the trusted cutoff score. The highest score from the 'CFeSP-like' group was 93.0, which was added as the noise cutoff score.

Identification of hgcAB. Potential HgcA sequences were identified in the ORFs using the custom HgcA HMM, using the trusted cut-off score of 131.8, with *hmmsearch* from the *hmmer* (v3.1b2) program.²² Putative hgcA sequences were aligned using MUSCLE (v3.8.31), and this alignment was manually inspected in Geneious.²¹ Sequences without the cap helix domain (N(V/I)WCA(A/G)(A/G)(K/R)) or at least four transmembrane domains, as predicted by TMHMM in Geneious, were discarded.²³ We next looked at the location of the *hgcA* gene on the scaffold. Genes that overlapped the beginning or end of the scaffold were manually examined. If the gene had lost some of the conserved regions due to overhanging the end of the scaffold, the sequence was discarded. All HgcA sequences were dereplicated using a 97% identity cutoff based on CD-HIT (v4.8.1), resulting in a final set of 108 *hgcA* genes.²⁴

The genes immediately downstream of each *hgcA* gene were extracted and aligned to a reference dataset of hgcB sequences. Sequences that aligned well and contained the

conserved CM/IECGAC motif were scored as *hgcB* genes. The corresponding amino acid sequences of these genes were used to build an HgcB HMM, following the protocol outlined above for HgcA. This HMM was used to search all the bins for *hgcB*, but did not detect any *hgcB* sequences in any of the bins that were not immediately downstream of an *hgcA* gene. If there was no predicted ORF within 500bp of an *hgcA* gene, we BLASTed the 500bp immediately downstream of the *hgcA* gene against the nr database using blastx. This identified 3 *hgcB*-like sequences that were not predicted as ORFs by Prodigal. These *hgcA* sequences were counted as having a downstream *hgcB* partner.

Phylogenetic analysis of HgcA. This workflow was used for generating the phylogenetic trees of HgcA sequences from both the assemblies and the bins. The amino acid sequences of the final HgcA sequences were aligned, using MUSCLE (v3.8.31), with 31 reference HgcA proteins from confirmed methylating organisms (Table S4).²¹ This alignment was manually inspected in Geneious and then trimmed using BMGE1.1 (on the Galaxy [web server](#)) with the BLOSUM30 substitution.²⁵ The remaining options were left at the default settings (sliding window = 3, maximum entropy level = 0.5, gap rate cutoff = 0.5, and minimum block size = 5). The RAxML software was used to generate a maximum likelihood tree. The GAMMA distribution was used, and automatic determination of the protein substitution model was made.²⁶ For all HgcA analyses, the LG substitution matrix was used. Rapid bootstrapping was called and was allowed to run until sufficient bootstrap analysis was detected under extended majority rule. The script was called as follows:

```
raxmlHPC-PTHREADS -f a -p 283976 -m PROTGAMMAAUTO -N autoMRE -x 2381 -T 20 -s
hgcA_for_phylogeny.afa -n hgcA.
```

For the assembly-based HgcA analysis, we generated HgcA-based phylogenies in an iterative fashion, removing highly divergent sequences that interfered with the bootstrapping analysis. Once the ML tree was selected and the bootstrapping complete, we used RogueNaRok (v1.0) to identify “rogue taxa” that interfered with the quality and reliability of the trees.²⁷ Sequences identified as rogue were removed from the original FASTA file and the tree was built again using the above workflow. In this second tree, one sequence was manually identified as highly divergent and removed from the analysis. After trimming with BMGE1.1, the alignment contained 181 residues. The automatic bootstrapping algorithm in RAxML ran 100 bootstrap replicates. The best-scoring ML tree was mid-point rooted in R using the Phangorn package and visualized using ggtree.^{28,29}

The *hgcA* gene sequences from the assemblies were assigned a taxonomic classification in an iterative process. If the *hgcA* gene was binned, it was classified by the rp16-based phylogeny of the bin. Unbinned sequences in a monophyletic group with HgcA sequences from confirmed methylators or other *hgcA*+ bins were classified according to the nearest references. Some sequences did not cluster with others definitively and were classified as unknown. Sequences identified as “rogue” during the phylogenetic reconstruction were placed onto the resulting tree using pplacer.³⁰ Based on their placement, they were assigned a taxonomy as described above.

Metabolic reconstruction:

Sulfur metabolism: Potential polysulfide reductase (*psr*) homologues were identified using an HMM for the catalytic unit of the complex iron–sulfur molybdoenzyme (CISM). Phylogenetic trees were used to identify likely *psr* candidate. These candidates

were confirmed to have the classic complex iron–sulfur molybdoenzyme (CISM) architecture and include the common sulfur-trafficking rhodanese domain-containing proteins (Fig. S2.11).^{31,32} We also searched for the anaerobic sulfite reductase gene cluster (*asr*), which can also mediate sulfate reduction, but did not find any genomes with those genes.

Nitrogen metabolism: GEO_0030 and DES_0034 each have at least one nitrate reductase and *nrfA*, suggesting they are capable of mediating dissimilatory nitrate reduction to ammonia (DNRA). Three other *hgcA*+ bins (PLA_0021, KIR_0036, DES_0019) have only the *nrfHA* gene cluster, and thus likely support nitrite reduction to ammonia. Each of these bins had other respiratory pathways (reduction of S, PCCs) that could be active instead. The various DNRA and denitrifying genes, as well as oxidases, were also wide-spread throughout the *hgcA*- bins we recovered.

Fermentative and syntrophic metabolism. Several of the 27 *hgcA*+ bins marked as fermentative do have *cyd* (cytochrome bd oxidases) or *nrfHA* operons, but the lack of other respiratory genes suggests that these are used to minimize oxidative stress or for nitrite detoxification. Twenty-four of the fermentative *hgcA*+ bins have hydrogenases commonly involved in fermentative H₂ evolution, mostly [FeFe] Group A hydrogenases, with some from [NiFe] Group 4.³³ Fourteen of these, including all of the highly abundant Kiritimatiellaeota *hgcA*+ bins, also have the Rnf complex, which can facilitate reverse electron transport to drive electron dispersal through H₂ production and is commonly used in syntrophy.^{34,35} Hydrogenases for H₂ uptake are widespread throughout bins with respiratory genes, suggesting that they would be viable syntrophic partners. Syntrophic

metabolism can also be mediated by formate transfer. Eight hgcA+ bins had pyruvate formate lyase (*pflB*), through which pyruvate is fermented to acetyl-CoA and formate. The formate can be exported and used by respiratory organisms with formate dehydrogenase (FDH) as an electron donor.³⁶

References

1. Olson ML, DeWild JF. Techniques for the collection and species-specific analysis of low levels of mercury in water, sediment, and biota. In: *U.S. Geological Survey Water-Resources Investigations Report*. Vols 99-4018B. Washington, D.C.; 1999.
2. *U.S EPA Method 1631, Revision E: Mercury in Water by Oxidation, Purge and Trap, and Cold Vapor Atomic Fluorescence Spectrometry*. Washington, D.C.: U.S. Environmental Protection Agency; 2002.
3. Olund SD, DeWild JF, Olson ML, Tate MT. Methods for the preparation and analysis of solids and suspended solids for total mercury. In: *U.S. Geological Survey Techniques of Water-Resources Investigations, Book 5, Chapter A8*. Techniques and Methods.; 2004.
4. DeWild JF, Olson ML, Olund SD. *Determination of Methyl Mercury by Aqueous Phase Ethylation, Followed by Gas Chromatographic Separation with Cold Vapor Atomic Fluorescence Detection*. *Open-File Report*. Reston, VA: U. S. Geological Survey; 2002.
5. Horvat M, Bloom NS, Liang L. Comparison of distillation with other current isolation methods for the determination of methyl mercury compounds in low level environmental samples. *Analytica Chimica Acta*. 1993;281:135-152. doi:[10.1016/0003-2670\(93\)85348-N](https://doi.org/10.1016/0003-2670(93)85348-N)
6. Lepak RF, Krabbenhoft DP, Ogorek JM, Tate MT, Bootsma HA, Hurley JP. Influence of *Cladophora*-*Quagga* Mussel Assemblages on Nearshore Methylmercury Production in Lake Michigan. *Environ Sci Technol*. 2015;49(13):7606-7613. doi:[10.1021/es506253v](https://doi.org/10.1021/es506253v)
7. Joshi N, Fass J. *Sickle: A Sliding-Window, Adaptive, Quality-Based Trimming Tool for FastQ Files*; 2011. <https://github.com/najoshi/sickle>.
8. Andrews S. *FastQC: A Quality Control Tool for High Throughput Sequence Data*.; 2010.
9. Nurk S, Meleshko D, Korobeynikov A, Pevzner PA. metaSPAdes: A new versatile metagenomic assembler. *Genome Research*. 2017;27(5):824-834. doi:[10.1101/gr.213959.116](https://doi.org/10.1101/gr.213959.116)
10. Simpson JT, Wong K, Jackman SD, Schein JE, Jones SJM, Birol I. ABySS: A parallel assembler for short read sequence data. *Genome Research*. 2009;19(6):1117-1123. doi:[10.1101/gr.089532.108](https://doi.org/10.1101/gr.089532.108)

11. Hyatt D, Chen G-L, LoCascio PF, Land ML, Larimer FW, Hauser LJ. Prodigal: Prokaryotic gene recognition and translation initiation site identification. *BMC Bioinformatics*. 2010;11(1):119. doi:[10.1186/1471-2105-11-119](https://doi.org/10.1186/1471-2105-11-119)
12. Bushnell B. *BBMap Short Read Aligner*; 2015. <https://sourceforge.net/projects/bbmap/>.
13. Alneberg J, Bjarnason BS, de Bruijn I, et al. Binning metagenomic contigs by coverage and composition. *Nat Methods*. 2014;11(11):1144-1146. doi:[10.1038/nmeth.3103](https://doi.org/10.1038/nmeth.3103)
14. Kang DD, Li F, Kirton E, et al. MetaBAT 2: An adaptive binning algorithm for robust and efficient genome reconstruction from metagenome assemblies. *PeerJ*. 2019;7:e7359. doi:[10.7717/peerj.7359](https://doi.org/10.7717/peerj.7359)
15. Wu Y-W, Simmons BA, Singer SW. MaxBin 2.0: An automated binning algorithm to recover genomes from multiple metagenomic datasets. *Bioinformatics*. 2016;32(4):605-607. doi:[10.1093/bioinformatics/btv638](https://doi.org/10.1093/bioinformatics/btv638)
16. Sieber CMK, Probst AJ, Sharrar A, et al. Recovery of genomes from metagenomes via a dereplication, aggregation and scoring strategy. *Nat Microbiol*. 2018;3(7):836-843. doi:[10.1038/s41564-018-0171-1](https://doi.org/10.1038/s41564-018-0171-1)
17. Parks DH, Imelfort M, Skennerton CT, Hugenholtz P, Tyson GW. CheckM: Assessing the quality of microbial genomes recovered from isolates, single cells, and metagenomes. *Genome Res*. 2015;25(7):1043-1055. doi:[10.1101/gr.186072.114](https://doi.org/10.1101/gr.186072.114)
18. Varghese NJ, Mukherjee S, Ivanova N, et al. Microbial species delineation using whole genome sequences. *Nucleic Acids Res*. 2015;43(14):6761-6771. doi:[10.1093/nar/gkv657](https://doi.org/10.1093/nar/gkv657)
19. Eren AM, Esen ÖC, Quince C, et al. Anvi'o: An advanced analysis and visualization platform for 'omics data. *PeerJ*. 2015;3:e1319. doi:[10.7717/peerj.1319](https://doi.org/10.7717/peerj.1319)
20. Menzel P, Ng KL, Krogh A. Fast and sensitive taxonomic classification for metagenomics with Kaiju. *Nat Commun*. 2016;7(1):11257. doi:[10.1038/ncomms11257](https://doi.org/10.1038/ncomms11257)
21. Edgar RC. MUSCLE: A multiple sequence alignment method with reduced time and space complexity. *BMC Bioinformatics*. 2004;5(113):1-19. doi:[10.1186/1471-2105-5-113](https://doi.org/10.1186/1471-2105-5-113)
22. Eddy SR. *Hmmer*; 2015. <http://hmmer.org/>.
23. Parks JM, Johs A, Podar M, et al. The genetic basis for bacterial mercury methylation. *Science*. 2013;339(6125):1332-1335. doi:[10.1126/science.1230667](https://doi.org/10.1126/science.1230667)
24. Fu L, Niu B, Zhu Z, Wu S, Li W. CD-HIT: Accelerated for clustering the next-generation sequencing data. *Bioinformatics*. 2012;28(23):3150-3152. doi:[10.1093/bioinformatics/bts565](https://doi.org/10.1093/bioinformatics/bts565)
25. Criscuolo A, Gribaldo S. BMGE (Block Mapping and Gathering with Entropy): A new software for selection of phylogenetic informative regions from multiple sequence alignments. *BMC Evol Biol*. 2010;10(210):1-21. doi:[10.1186/1471-2148-10-210](https://doi.org/10.1186/1471-2148-10-210)

26. Stamatakis A. RAxML version 8: A tool for phylogenetic analysis and post-analysis of large phylogenies. *Bioinformatics*. 2014;30(9):1312-1313. doi:[10.1093/bioinformatics/btu033](https://doi.org/10.1093/bioinformatics/btu033)
27. Aberer AJ, Krompass D, Stamatakis A. Pruning rogue taxa improves phylogenetic accuracy: An efficient algorithm and webservice. *Systematic Biology*. 2013;62(1):162-166. doi:[10.1093/sysbio/sys078](https://doi.org/10.1093/sysbio/sys078)
28. Schliep KP. Phangorn: Phylogenetic analysis in R. *Bioinformatics*. 2011;27(4):592-593. doi:[10.1093/bioinformatics/btq706](https://doi.org/10.1093/bioinformatics/btq706)
29. Yu G, Smith DK, Zhu H, Guan Y, Lam TT. Ggtree: An R package for visualization and annotation of phylogenetic trees with their covariates and other associated data. *Methods Ecol Evol*. 2017;8:28-36. doi:[10.1111/2041-210X.12628](https://doi.org/10.1111/2041-210X.12628)
30. Matsen FA, Kodner RB, Armbrust EV. Pplacer: Linear time maximum-likelihood and Bayesian phylogenetic placement of sequences onto a fixed reference tree. *BMC Bioinformatics*. 2010;11(1):538. doi:[10.1186/1471-2105-11-538](https://doi.org/10.1186/1471-2105-11-538)
31. Cipollone R, Ascenzi P, Visca P. Common themes and variations in the rhodanese superfamily. *TBMB*. 2007;59(2):51-59. doi:[10.1080/15216540701206859](https://doi.org/10.1080/15216540701206859)
32. Thauer RK, Kaster A-K, Seedorf H, Buckel W, Hedderich R. Methanogenic archaea: Ecologically relevant differences in energy conservation. *Nat Rev Microbiol*. 2008;6(8):579-591. doi:[10.1038/nrmicro1931](https://doi.org/10.1038/nrmicro1931)
33. Greening C, Biswas A, Carere CR, et al. Genomic and metagenomic surveys of hydrogenase distribution indicate H₂ is a widely utilised energy source for microbial growth and survival. *ISME J*. 2016;10(3):761-777. doi:[10.1038/ismej.2015.153](https://doi.org/10.1038/ismej.2015.153)
34. Biegel E, Schmidt S, González JM, Müller V. Biochemistry, evolution and physiological function of the Rnf complex, a novel ion-motive electron transport complex in prokaryotes. *Cell Mol Life Sci*. 2011;68(4):613-634. doi:[10.1007/s00018-010-0555-8](https://doi.org/10.1007/s00018-010-0555-8)
35. Nobu MK, Narihiro T, Rinke C, et al. Microbial dark matter ecogenomics reveals complex synergistic networks in a methanogenic bioreactor. *ISME J*. 2015;9(8):1710-1722. doi:[10.1038/ismej.2014.256](https://doi.org/10.1038/ismej.2014.256)
36. Sieber JR, McInerney MJ, Gunsalus RP. Genomic Insights into Syntrophy: The Paradigm for Anaerobic Metabolic Cooperation. *Annu Rev Microbiol*. 2012;66(1):429-452. doi:[10.1146/annurev-micro-090110-102844](https://doi.org/10.1146/annurev-micro-090110-102844)

Supplementary Figures: Includes additional geochemical profiles, *hgcAB* alignments, detailed phylogenetic trees, and figures detailing metabolic pathways of methylators.

Figure S2.1. Representative profiles of Lake Mendota from across the open water season in 2017. The dissolved Hg species are operationally defined as everything that passes a quartz fiber filter (QFF), and the particulate fraction is what is retained on a QFF. Both iron and manganese are the dissolved fraction only (0.45 μ m PES filter). Abbreviations: Temp. - Temperature ($^{\circ}$ C), ODO - Optical dissolved oxygen in mg/L, Turb. - Turbidity in Formazin Nephelometric Units (FNU), NO_x - total nitrate and nitrite, HgT - Total mercury, MeHg - Methylmercury, %MeHg - Methylmercury concentration divided by total mercury concentration.

Figure S2.2. Geochemical profiles focused on metalimnion. On these two dates, we collected samples for biogeochemical gradients repeatedly over the metalimnion. We collected samples for particulate iron (Fe) and manganese (Mn) in these profiles in addition to the usual constituents from the other profiles. Abbreviations: Temp. - Temperature ($^{\circ}$ C), ODO - Optical dissolved oxygen in mg/L, Turb. - Turbidity in Formazin Nephelometric Units (FNU), Mn - manganese, Fe - iron, diss. - dissolved (passes through 0.45 μ m filter), part - particulate (retained on 0.45 μ m filter, calculated as difference between unfiltered and filter-passing samples).

Figure S2.3. Alignments of identified *hgcA* and *hgcB* amino acid sequences from all five metagenomes. Green bars indicate regions of predicted transmembrane domains in the alignments. The zoomed-in portion of the *hgcA* alignment highlights a portion of the corrinoid-binding domain for a subset of the sequences, and includes the characteristic highly conserved cap-helix domain. For *hgcB*, we highlighted a portion of the alignment that includes one of the two highly conserved ferredoxin-binding motifs from a subset of the sequences.

Figure S2.4. Maximum likelihood tree of *HgcA* sequences and overall coverage across five metagenomes. Names in black indicate unbinned *hgcA* sequences. For *hgcA* sequences that were binned, the scaffold name was replaced with the bin name (red names). Dark blue names indicate *hgcA* sequences from bins from a recent paper in a similar system.¹ These bins are followed by the IMG Taxon ID in parentheses. Grey names indicate *hgcA* sequences downloaded from NCBI's non-redundant database that did not come from the genome of a confirmed methylating organisms. Remaining colored names are from genomes of confirmed methylators and match the color scheme in Figure 2 (yellow - Firmicutes; green - Desulfobacterales; pink - methanogens; orange - Geobacterales; light blue - Syntrophobacterales). All reference sequence names are followed by their accession version number in parentheses. Scaffold coverage is the average coverage of nucleotides in the corresponding *hgcA*+ scaffold across all five metagenomes. Sequence names from this study that are followed by a pound sign do not have a trailing *hgcB* sequence.

Figure S2.5. Overview of binning of *hgcA* sequences. A: Rank abundance curve of *hgcA* sequences across all metagenomes. Bars colored in red indicate a binned sequence. B: Plot of average coverage of scaffold vs. length of scaffold of *hgcA*+ sequences, with red dots indicating that the sequence was binned.

Figure S2.6. Comparison of coverage between *hgcA*⁺ and *hgcA*⁻ bins. A: Rank abundance curve of all bins across all metagenomes. Bins encoding *hgcA* are colored green. B: Log coverage of *hgcA*⁺ vs. *hgcA*⁻ bins.

Figure S2.7. Maximum likelihood tree of *rp16* genes from all bacterial *hgcA*⁺ bins and reference genomes from NCBI. Bootstrap values below 50 have been removed. Tree was rooted using three archaeal bins from this study. Names in red correspond to bins identified in this study. Genome names in black were pulled from NCBI database and have the accession ID in parentheses.

Figure S2.8. Maximum likelihood tree of *rp16* gene from all Bacteroidales bins from this study. Bin names in green are *hgcA*⁻ bins, while those in orange are *hgcA*⁺ bins. Sequences in black are bins downloaded from NCBI, and bin names surrounded by asterisks are reference genomes from isolate cultures. The Bacteroidales tree was rooted using two Flavobacteriales reference genomes (*Owenweeksia hongkongensis* DSM 17368 and *Fluviicola taffensis* DSM 16823)

Figure S2.9. The *hgcA* gene is widespread in Mendota Kiritimatiellaeta bins, but is not phylogenetically conserved. Maximum-likelihood tree is based on a concatenated alignment of *rp16* proteins. Names in orange are *hgcA*⁺ bins from this study, and green names are *hgcA*⁻ bins from this study. Names in black are genomes or bins retrieved from the National Center for Biotechnology Information (NCBI), and genomes with the asterisks indicate cultured isolate reference genomes. The accession version numbers are in parentheses following the bin or genome name. The bin names in blue correspond to two *hgcA*⁺ bins from a recent publication.¹ The tree was generated in RAxML and rooted using the two Lentisphaerae genomes (*Lentisphaera araneosa* and *Victivallis vadensis*). Bootstrap values of less than 50 are not shown.

Figure S2.10. Heatmap of metabolic potential of *hgcA*⁺ bins with respiratory metabolic genes and overall bin abundance. Dissimilatory nitrogen cycling genes are in red: *narG* = membrane-bound nitrate reductase, *napA* = periplasmic nitrate reductase, *nrfHA* = cytochrome c nitrite reductase. Genes for nitrite reduction by denitrification were not identified in any *hgcA*⁺ bins. Putative external electron transfer proteins are in orange: PCC = Porin-cytochrome c complex. Sulfur cycling genes in blue: *dsrAB* = dissimilatory sulfite reductase; *psrA* = polysulfide-reductase homolog. Methanogenesis refers to the overall phenotype indicated by the bin. In green are complex I (the 11 and/or 14 subunit version) and complex II of the electron transport chain.

Figure S2.11. A: Rank abundance curve of *hgcA*⁺ bins across all five metagenomes, colored by predicted metabolic potential. The bin coverage is relativized to the total coverage of all the bins (both *hgcA*⁺ and *hgcA*⁻).

Figure S2.12. Phylogenetic tree of polysulfide reductase (*psr*) homologs from *hgcA*⁺ bins. In the branch labels, the bin names are followed by the scaffold number and ORF number in parentheses. Names in orange are from *hgcA*⁺ bins, green are from *hgcA*⁻ bins. Names in black correspond to reference sequences. The gene neighborhoods within 2500bp upstream and downstream of the corresponding MoOR from this study are shown to the right of the tree. The canonical complex iron-sulfur molybdoenzyme (CISM) architecture

includes the MoOR (shown in blue), a four-cluster protein (FCP) with four Fe-S clusters (shown in green), and a membrane anchor protein (MAP), such as the nrfD subunit from the nitrite reductase complex NrfABCD (shown in red). Rhodenase-domain proteins (RDP), involved in sulfur transport, are shown in purple.

Figure S2.13. Phylogenetic tree and gene neighborhoods of beta-barrel outer membrane protein (BB-OMP) genes from hgcA+ bins. Sequence names in red are from hgcA+ bins, and the following numbers in parentheses indicate the scaffold and ORF, respectively. The gene neighborhoods within 4000bp upstream and downstream of the BB-OMP genes are shown to the right of the tree. BB-OMP sequences are shown in blue, and the predicted number of transmembrane sheets within the protein are provided above the gene. Predicted multiheme cytochrome c proteins are shown in green, with the number of the heme-binding sites above the gene. The predicted localization of the protein is shown below the gene (E indicates extracellular, P indicates periplasmic).

Figure S2.14. Abundance and metabolic gene features of fermentative bins. The percentage of bin coverage is relative to the total coverage of all the bins from this study. Genes potentially involved in fermentative hydrogen evolution are shown in orange: Rnf = Rhodobacter nitrogen fixation complex; FeFe GA = [FeFe]-hydrogenase, group A; NiFe G4e = [NiFe]-hydrogenase, group 4e. Genes or gene clusters involved in fermentation of pyruvate are shown in green: PFL = pyruvate-formate lyase; FDH = formate dehydrogenase; PFOR = pyruvate-ferredoxin oxidoreductase; ackA = acetate kinase (ADP-forming); pta = phosphate acetyltransferase.

Figure S2.1

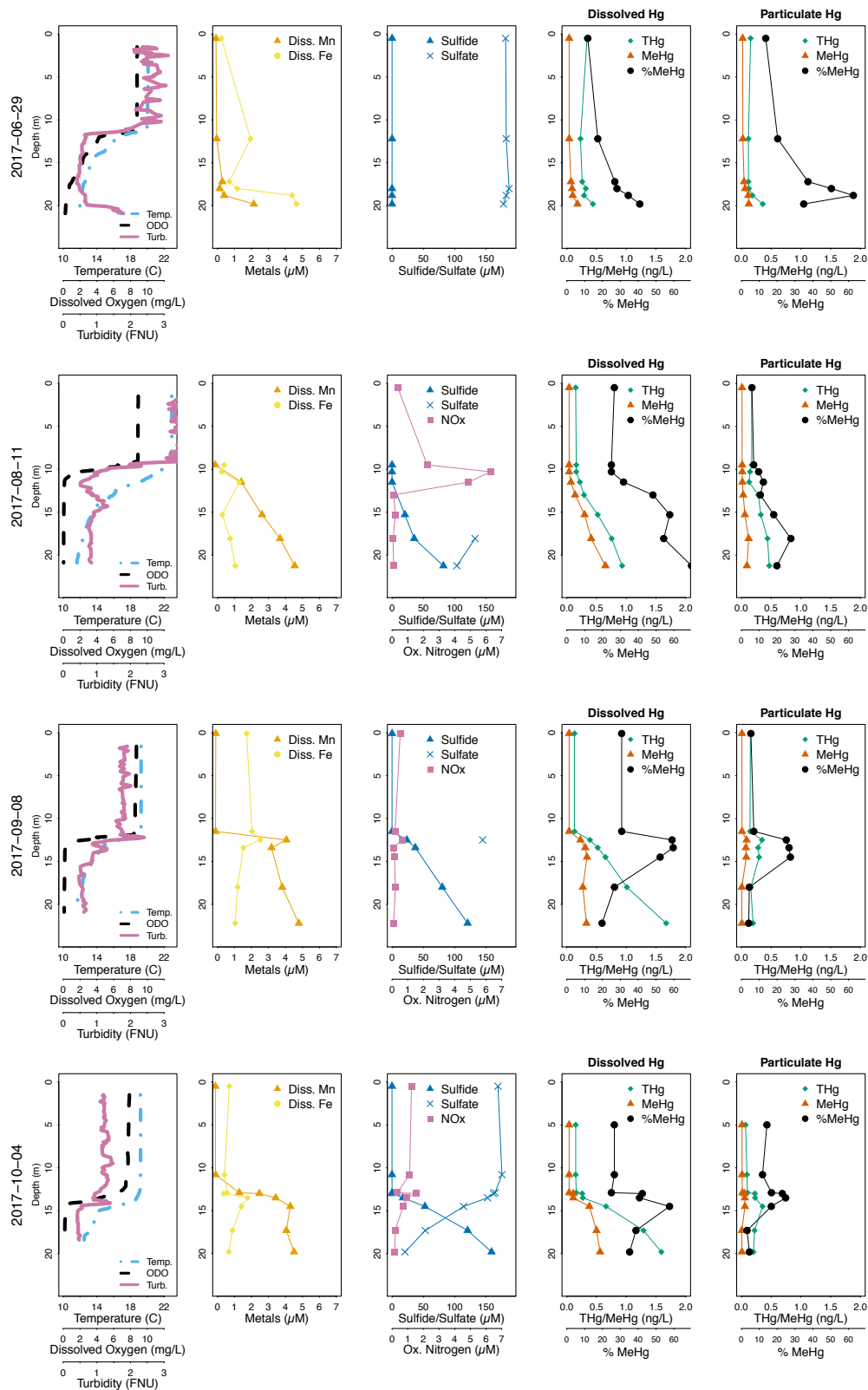


Figure S2.2

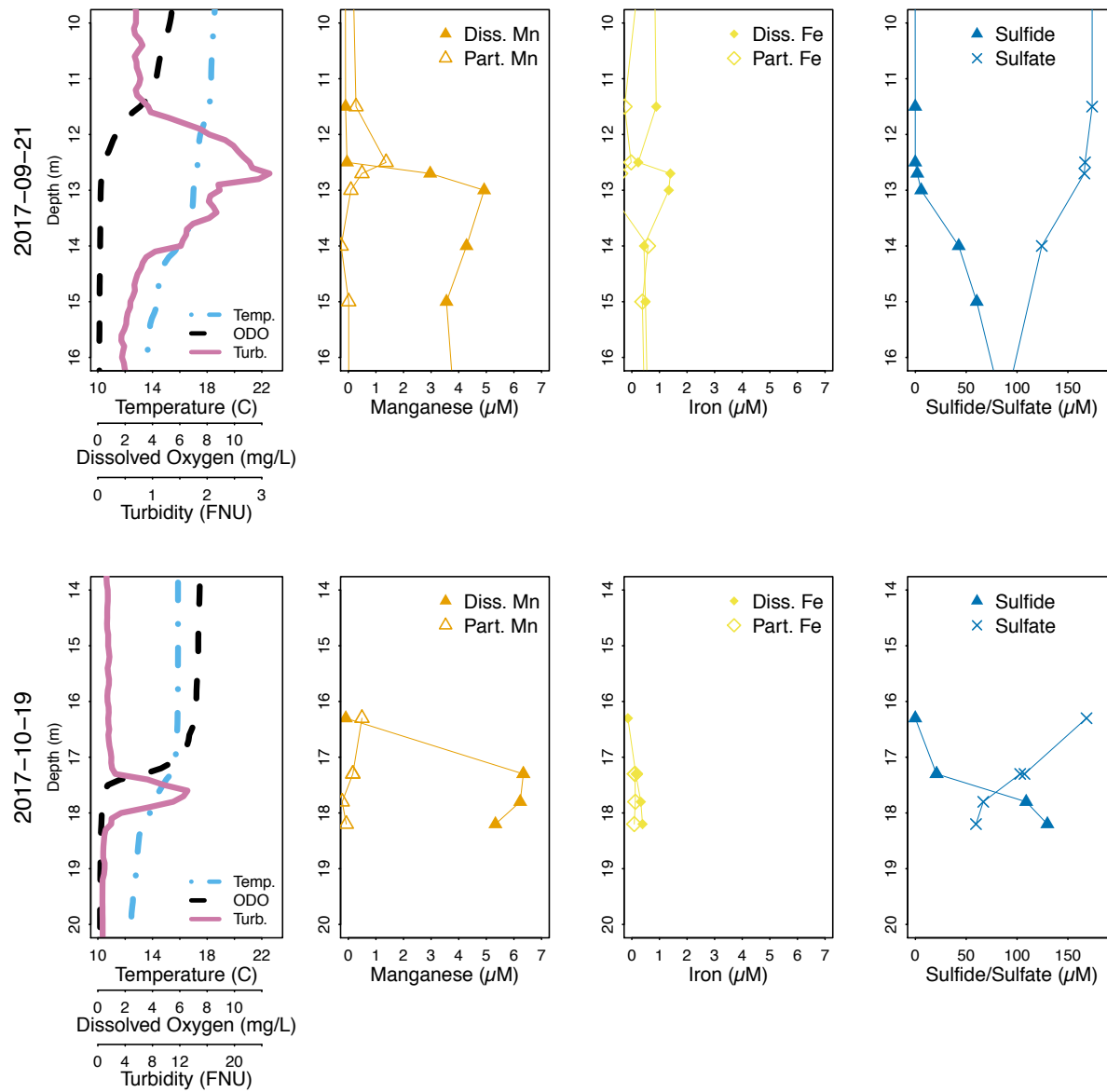


Figure S2.5

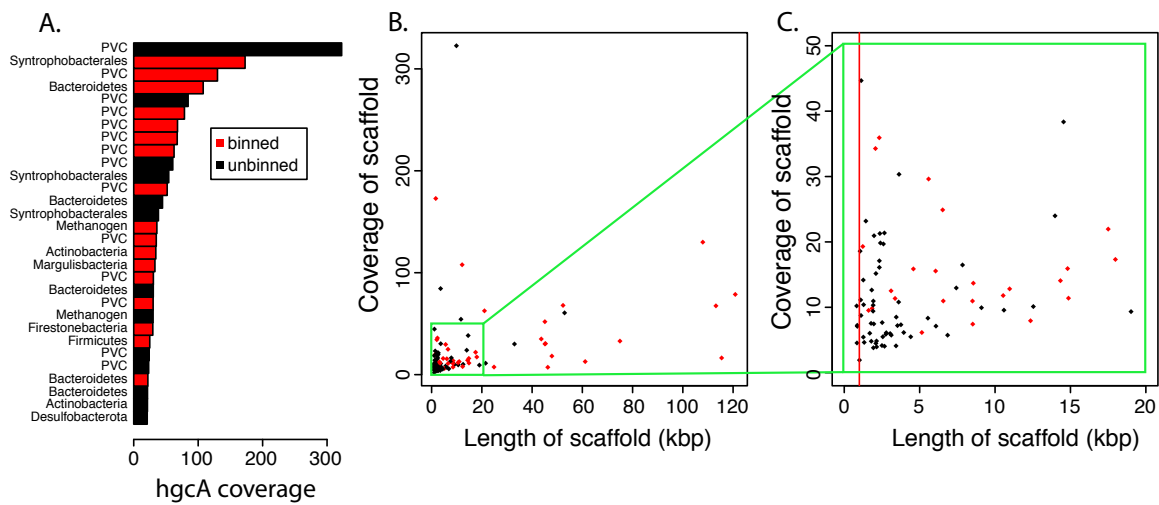


Figure S2.6

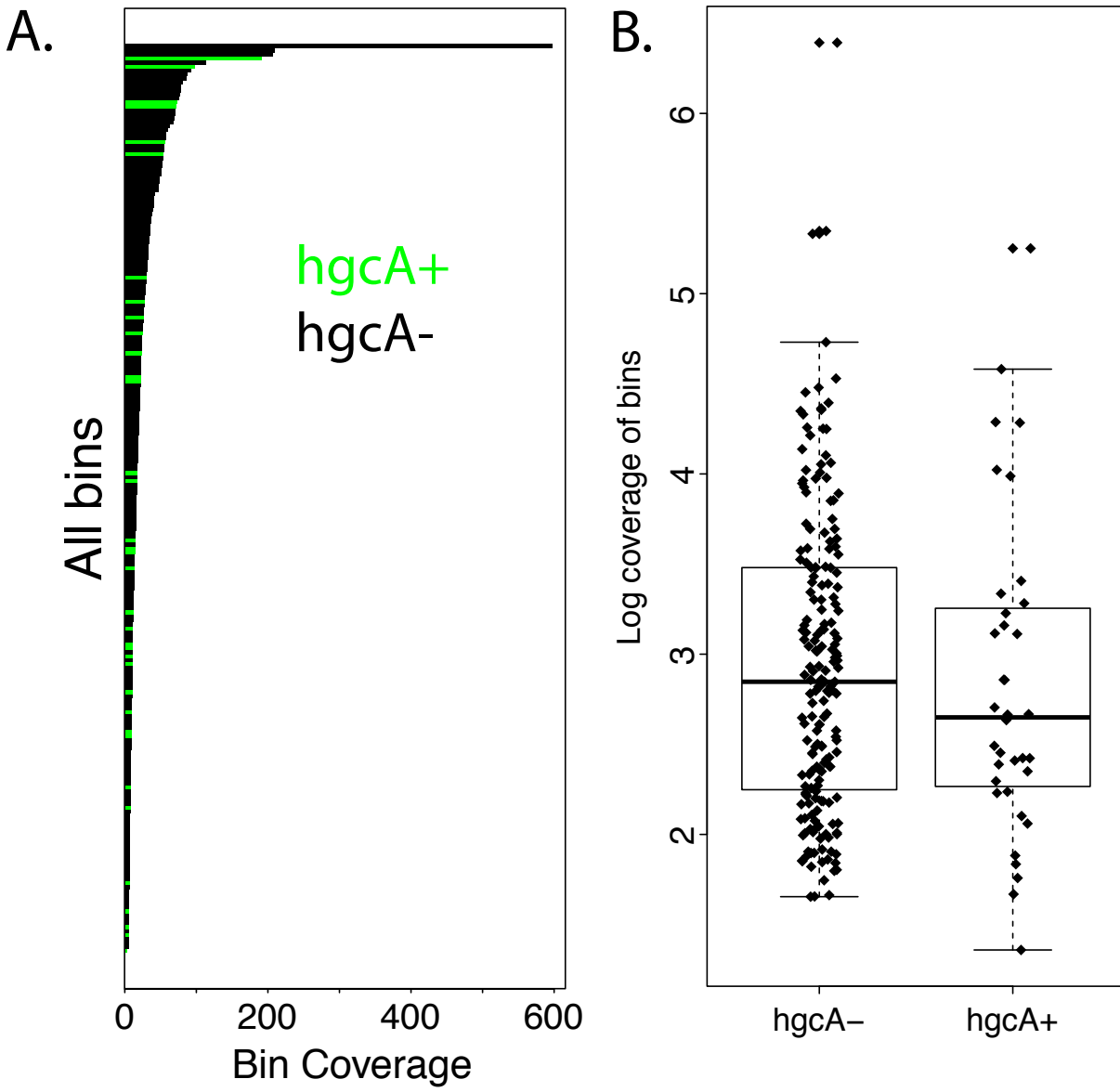


Figure S2.7

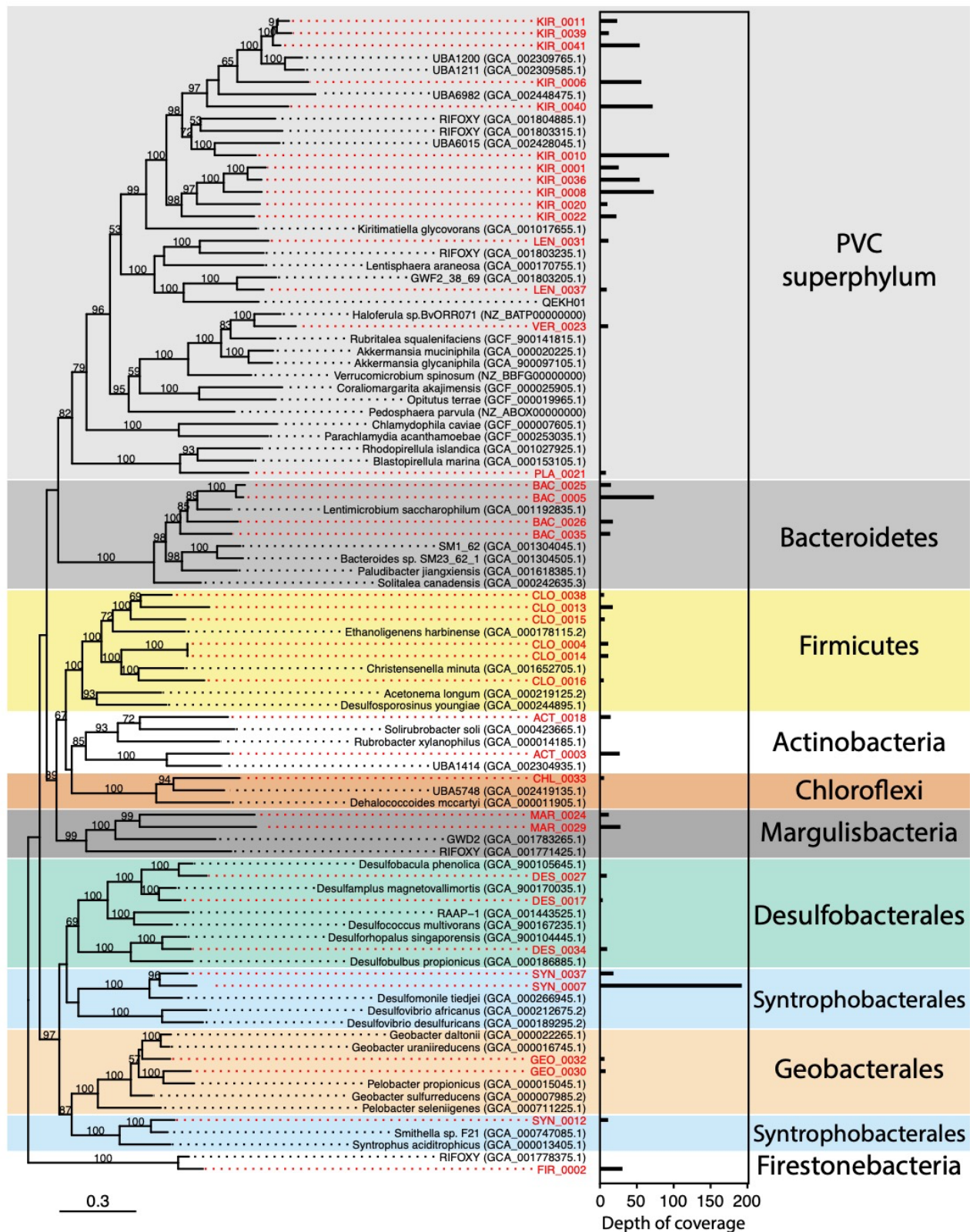


Figure S2.8

Reference genomes

Publicly available MAGs

hgcA+ bins

hgcA- bins

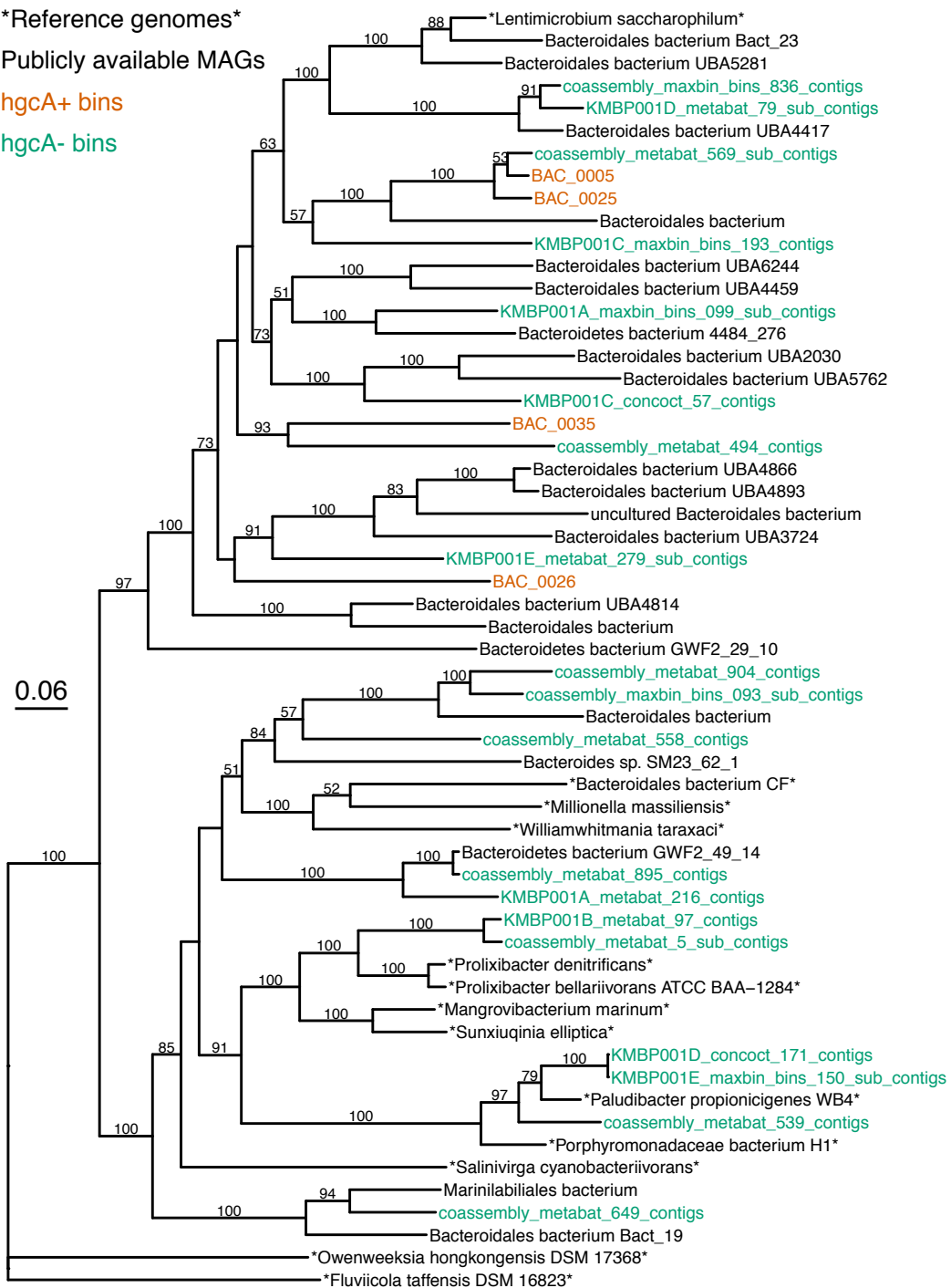


Figure S2.10

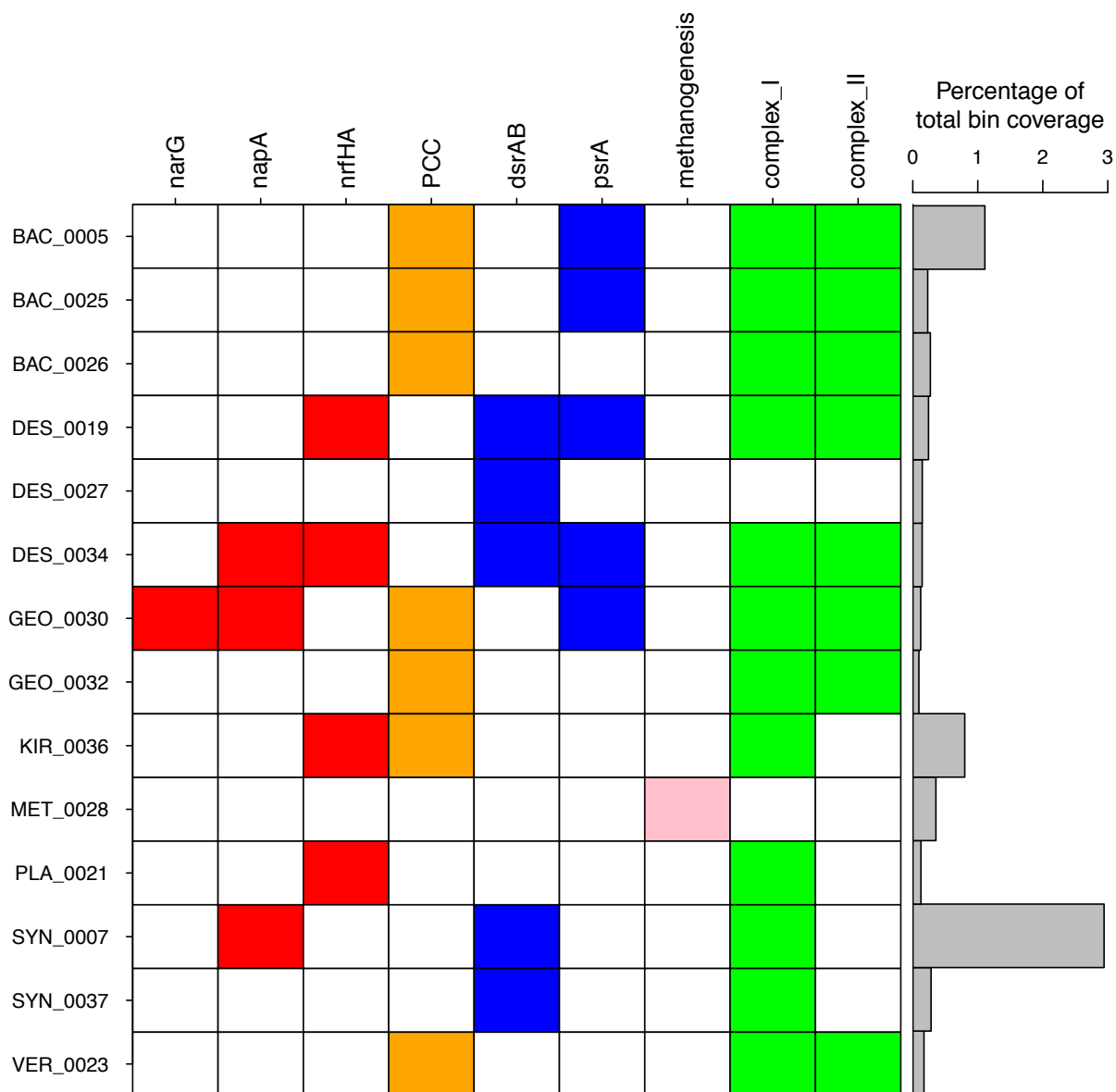


Figure S2.11

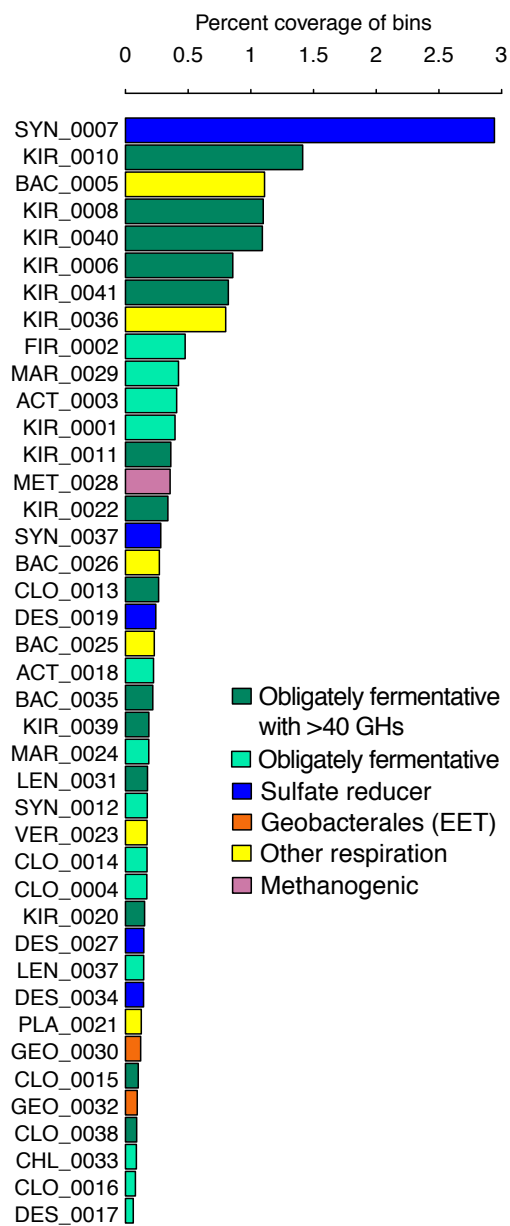


Figure S2.12

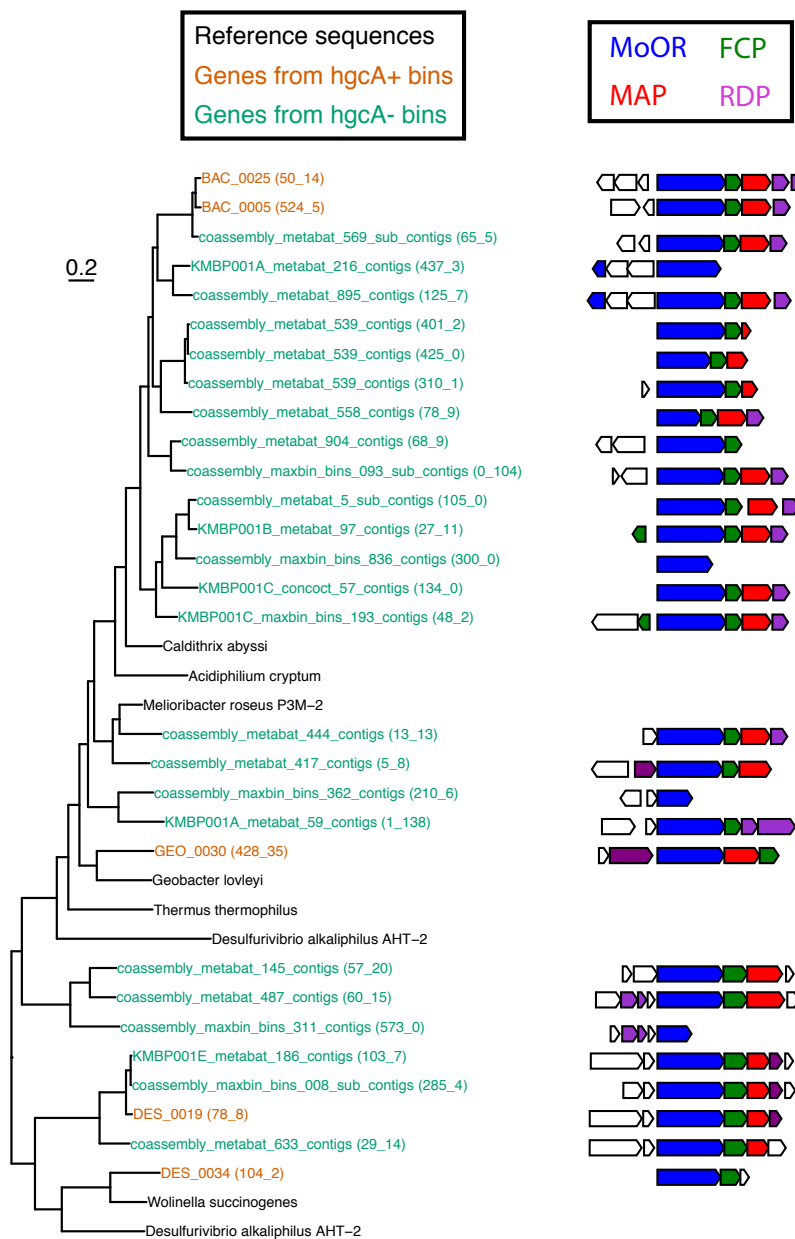


Figure S2.13

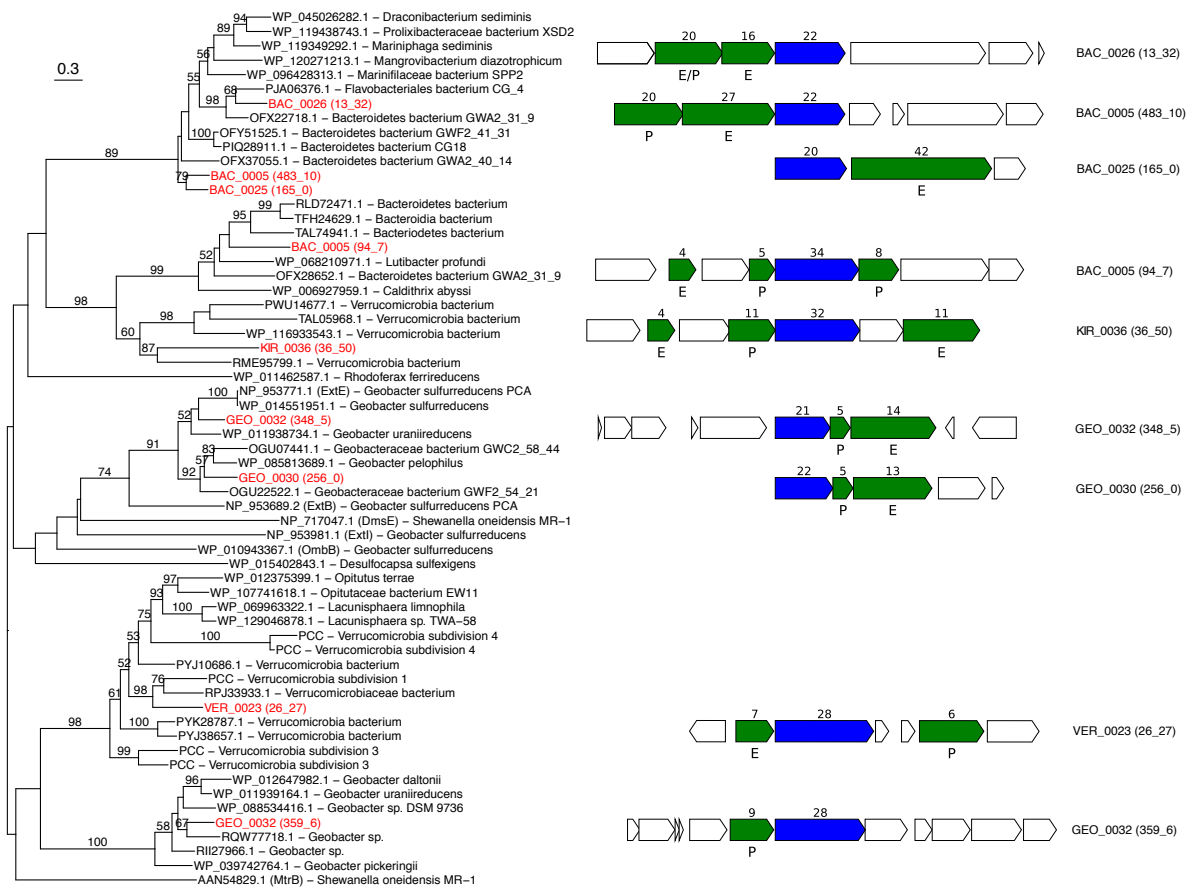
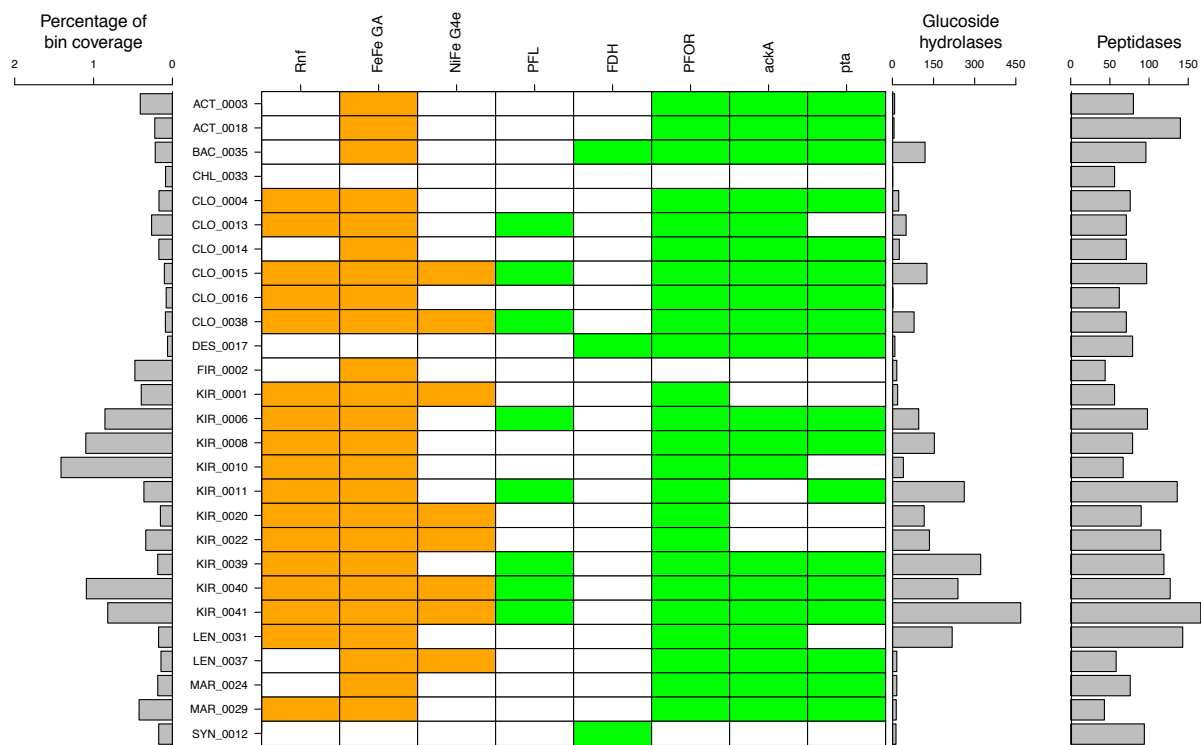


Figure S2.14



Chapter 3: Metagenomic insights into hydrological and biogeochemical constraints on mercury methylation under suboxic conditions in a hydroelectric reservoir.

This chapter has been prepared as a manuscript for submission for peer review and publication.

Co-authored with Brett A. Poulin, David Krabbenhoft, Charles N. Olmstead, and Katherine D. McMahon. The heatmap dissolved oxygen figures were made by Chris Larsen and Nick Gastelecutto.

Abstract

Brownlee Reservoir is a hydroelectric dam within the Hells Canyon Complex that, like many hydroelectric dams, experiences dynamic hydrological and geochemical conditions and is a known source of mercury to the aquatic food web within the impoundment. Methylmercury is produced efficiently in the system despite the predominance of suboxic rather than anoxic conditions. In this chapter, we collected a suite of geochemical measurements alongside samples for shotgun metagenomic sequencing to identify the likely locations of methylmercury production. We reconstructed genomic bins of mercury-methylating organisms to identify possible links between biogeochemical cycles and methylmercury production. We confirmed that much of the methylmercury was likely being produced in the water column in the more lacustrine portion of the reservoir. Hotspots for methylmercury production and accumulation were linked to locations in the reservoir where anoxia initially developed, suggesting that methylmercury accumulation and uptake into the food web is linked to hydrologic conditions in the reservoir and can be highly variable from year-to-year. Geochemical profiles and genomic reconstruction of Hg-methylating organisms indicated that methylmercury production occurs in this system under nitrate- or Mn-reducing conditions, which were previously thought to preclude Hg-methylation. This work also expands the known conditions conducive to producing methylmercury and suggest that the mercury-methylation mitigation efforts by nitrate- or Mn-amendment may be unsuccessful in some locations.

Introduction

Reservoirs are hotspots for methylmercury (MeHg) production and contamination in the food web.^{1,2} This elevated production is due to the replenishment of microbial substrates in anoxic environments. For example, drying/rewetting of sediment soils due to water level fluctuations can drive MeHg production by cycling between anoxic conditions, where MeHg production occurs, and oxic conditions, when terminal electron acceptors (TEAs) can be replenished. Elevated MeHg production can also occur in the water column and deeper sediments, where lotic inflow can provide a continuous supply of inorganic mercury (iHg), TEAs, and labile organic matter³, while stratification and hypolimnetic anoxia can develop in the downstream, more lentic portions of the reservoir⁴. The onset of anoxia is generally driven by the settling out of organic matter but is controlled by a complex array of hydrologic and geochemical factors.⁵ Once produced, MeHg can be taken up into the food web within the reservoir⁶, transferred to linked terrestrial food webs⁷, or exported downstream through the dam as the hypolimnion is eroded and the reservoir turns over⁷, which can lead to Hg accumulation in food webs downstream^{8,9}. In both situations, the extent of MeHg production within the reservoir is tightly linked to MeHg accumulation in the food web. A critical knowledge gap in understanding the Hg cycle in reservoirs is an accurate picture of how hydrologic and biogeochemical factors combine to control the timing and location of MeHg production.

MeHg production is typically associated with low-redox environments and was thought to be mediated primarily by sulfate-reducing bacteria (SRB)^{10,11}, iron-reducing bacteria (FeRB)^{12,13} and methanogens^{14,15}. These conclusions have encouraged efforts to mitigate MeHg production by increasing the redox status of the system¹⁶, either by hypolimnetic oxygenation¹⁷ or whole-lake addition of nitrate¹⁸ or manganese (Mn) oxide¹⁹. However, MeHg production has

been observed within oxic environments²⁰, including in the Hells Canyon sites described here.²¹ The *hgcAB* Hg-methylation marker genes have also been observed in suspected nitrite-oxidizers^{22,23} and nitrate-reducing/aerobic organisms.²⁴ Other links between MeHg production and the nitrogen (N) cycle have also been proposed, such as the occurrence of N-fixation in genomes with *hgcA*.²⁵ The *Geobacter* iron-reducing bacteria (FeRB) that produce MeHg are often capable of Mn-reduction as well.^{26,27} Hg-methylating Geobacterales bins with genes for external electron transfer (EET) pathways that mediate Fe- or Mn-reduction have been observed in a lake co-localized with a peak in Mn cycling.²⁸ Other *hgcA* sequences have been identified in oxic environments, although it is possible they are living in anoxic niches on falling particles.²⁹ Collectively, these data suggest that Hg-methylation may be possible under nitrate- or Mn-reducing conditions, which we will refer to as suboxic throughout this manuscript. However, there is still a knowledge gap in understanding the extent to which these high-redox respiratory bacteria (HRBB) influence MeHg production under suboxic conditions.

Brownlee Reservoir is a western arid reservoir in the Hells Canyon Complex (HCC) of hydroelectric dams along the Snake River.⁴ Within the HCC, MeHg levels in smallmouth bass tissue exceed the state human-health criteria for both Idaho and Oregon.⁴ Brownlee is a net source of dissolved MeHg, indicating that MeHg production *in situ* could be an important control on food web MeHg accumulation both within and downstream from the reservoir.³ Water column MeHg profiles and MeHg gradients above the sediment-water interface suggest that MeHg production appears to be occurring within the water column, especially in the more lentic areas, downstream of river mile 310.³⁰ Additionally, sulfide production is limited throughout the water column³⁰ and sediments³¹ in Brownlee, suggesting that MeHg production occurs under

suboxic conditions. Thus, this site presents a good opportunity to search for Hg-methylating organisms under various redox conditions within the water column.

In this study, we evaluated the water column of Brownlee reservoir for Hg-methylation potential over multiple years and hydrological/geochemical conditions. We collected depth-discrete samples at multiple stations for metagenomic sequencing and a full suite of physical and geochemical measurements over three years, under different stages of stratification or hydrologic conditions. We conducted shotgun metagenomic sequencing at a subset of these locations to identify and characterize *hgcA* genes. Using genome reconstruction, we identified multiple Hg-methylating organisms with the capacity for high-redox respiration. Fermentative Hg-methylators were also highly abundant. The microbial Hg-methylating community exhibited high intra-year variation, mostly linked to the biogeochemical gradients, and high inter-year variation, which could be linked to yearly differences in the hydrological and biogeochemical conditions of the water column. Overall, this work provides insight into the constraints on MeHg production in a dynamic western arid reservoir through the lens of the microbes and provides evidence for MeHg production under nitrate- and Mn-reducing conditions.

Materials and Methods

Site description and sampling: Brownlee Reservoir is a freshwater hydroelectric reservoir, the most upstream reservoir within the Hells Canyon Complex (HCC). It has a hydraulic retention time of 34 days³ and is one of the largest reservoirs in North America at 93 km long with an area of 61 km². The riverine to lacustrine transition occurs around river mile (RM) 305 to RM310 as the Snake River flows into the HCC. Nutrient inputs into the system are high due to agricultural land constituting a large percentage of the watershed. These inputs fuel

intense cyanobacterial blooms near the riverine-lacustrine transition, supplying large amounts of organic matter to Brownlee. This biomass ultimately creates high levels of biological oxygen demand in the hypolimnion, leading to anoxic conditions starting in May (Figs. 3.1-2). Flow rates have high intra- and interannual variation, resulting in drastically different hydrologic and physical characteristics from year to year.³ Sampling was done at RM286 and RM300 in September of 2017 and 2018, which spanned most of the lateral extent of the anoxic hypolimnion. In July 2019, we collected profiles spanning the reservoir from RM286 up to RM318. We selected RM300 and RM310 for metagenomic analysis based on the greater extent of Mn-accumulation and MeHg accumulation at those two stations, respectively. All sampling protocols were conducted using trace-metal-clean protocols.³² Sampling was conducted using a 5/8" inner diameter Teflon sampling line and a peristaltic pump outfitted with acid-washed C-Flex tubing. Samples for anion analysis were preserved by freezing on dry ice. Samples for dissolved Mn and Fe analysis were filtered with an in-line capsule filter (0.45 μ m) and preserved immediately in the field to 2% v/v nitric acid, while unfiltered water was acidified the same way for whole water Mn and Fe quantification. Samples for sulfide analysis were preserved using sulfide anti-oxidant buffer. Samples for mercury speciation analysis were processed within 12 hours of collection. For processing, the samples were filtered with quartz fiber filters (QFFs), the filtrate was acidified to 1% HCl for dissolved Hg and MeHg analysis, and the QFFs were frozen for particulate Hg and MeHg analysis. Samples for DNA sequencing were collected by filtering 300-800 ml of sample water onto 0.22 μ m pore-size Sterivex filters (Millipore, SVGP01050) with a peristaltic pump. Samples were preserved within 90 seconds by flash-freezing with liquid nitrogen.

Geochemical analyses: Detailed methods for geochemical analyses, including Hg analyses, have been previously published.³⁰ Briefly, Mn and Fe were analyzed by inductively coupled plasma optical emission spectroscopy, nitrate was measured using ion chromatography, and sulfide was measured using an ion-selective electrode. All Hg analyses were done at the U.S. Geological Survey (USGS) Mercury Research Laboratory (MRL) in Middleton, WI. Total Hg was measured by bromine monochloride oxidation followed by tin reduction coupled to cold vapor atomic fluorescence spectrometry for quantification.^{33,34} Samples for MeHg were first distilled, then quantified by isotope dilution (ID) using inductively coupled plasma mass spectrometry, following U.S. EPA method 1630, with modifications for ID.³⁵⁻³⁷ All Hg measurements met quality control and assurance standards set by the USGS MRL.

DNA extraction and sequencing: Filters were removed from the Sterivex cartridges using a sterile PVC cutter and sterilized razors and tweezers. Half of the filter was used for DNA extraction and half was archived. Cells were lysed using physical and chemical lysis methods, then the DNA was extracted twice using phenol:chloroform, washed with a chloroform extraction, and purified using isopropanol precipitation. Library preparation was done in the Functional Genomics Lab and sequencing done in the Vincent J. Coates Genomics Sequencing Lab (QB3, Berkeley, CA). Inserts approximately 600bp in length were used to generate sequencing libraries with a Kapa Biosystem Library Prep kit (Roche Sequencing and Life Science, Kapa Biosystems, Wilmington, MA). 150 bp paired-end reads were generated on an Illumina NovaSeq.

Metagenome assembly, binning, and annotation: Reads were trimmed and overlapping read pairs were merged using fastp (v0.20.1).³⁸ Metagenomes were clustered using Mash (v2.2.2), a kmer-based metric.³⁹ All assemblies were done using metaSPADes (v3.14.1).⁴⁰

Downstream analyses were only conducted on contigs longer than 1000 bp. Open reading frames (ORFs) were predicted using Prodigal⁴¹ (v2.6.3) on the metagenome mode and bowtie2⁴² (v2.6.3) was used to map reads back to the assembled contigs. Raw gene and bin abundances were calculated as the average “coverage”, which is the average number of reads mapping to each nucleotide in the gene/bin. To normalize abundance across metagenomes, we calculated the coverage of 16 different ribosomal genes (the rp16 genes) in each assembly.^{43,44} The coverage of each gene/bin within a metagenome was normalized to the mean coverage of the rp16 genes for that metagenome. Automatic binning was done using Metabat2⁴⁵ (v2:2.15) and MaxBin2⁴⁶ (v2.2.7), which were then aggregated using Das Tool⁴⁷ (v1.1.2). Bins containing an *hgcA* gene were then manually curated in anvi'o⁴⁸ (v6.2) using the automatic binning results as a reference. Bins were grouped into mOTUs that shared 98% ANI and had 50% alignment fraction. The taxonomy of each bin was estimated using GTDB-TK.⁴⁹ Metabolic genes in the assemblies were initially identified using Hidden Markov Models (HMMs) and confirmed using phylogenetic trees. Metabolic annotations of the bins were done using convergent approaches, including kofamscan⁵⁰, custom HMMs with hmmer⁵¹, METABOLIC⁵², and FEET. Major TEAP annotations were confirmed by phylogenetic reconstruction. Phylogenetic trees of bins were based on alignments of the rp16 genes.⁴³ References were identified from the GTDB tree and downloaded using NCBI's Entrez.

***hgcA* identification, identification, and classification:** HgcA sequences were identified in the ORFs from all assemblies using a custom HMM.²⁸ Putative HgcA sequences without a cap helix domain were removed. Truncated sequences without any transmembrane domains at the C-terminal end were not included in the phylogenetic and abundance calculations but are included in the supplementary information for completeness. The final set of *hgcA* genes were

dereplicated across all assemblies by clustering them at 97% identity using CD-HIT.⁵³ Amino acid sequences were aligned with MUSCLE⁵⁴ (v3.8.31) and then this alignment was aligned to the Hg-MATE database⁵⁵ (v1.01142021). Residues in the alignment that included gaps in at least 50% of the sequences were masked. A maximum-likelihood tree was generated from this alignment using RAxML⁵⁶ (v8.2.11) under the GAMMA distribution with the LG model, then mid-point rooted using the Phangorn⁵⁷ (v2.7.0) package in R and visualized using ggtree⁵⁸ (v3.1.1). Automatic rapid bootstrapping was used to generate branch support, with a final count of 550 bootstraps. HgcA sequences were also automatically classified using the Hg-MATE database and pplacer and guppy based on an established workflow^{59,60}. Using this autoclassification data, the phylogeny information from the binned *hgcA* sequences, and the inferred taxonomy based on the HgcA phylogeny, we assigned a taxonomic classification to each of our *hgcA* genes. If possible, we also assigned one of four predicted metabolic guilds to each *hgcA* gene: high-redox respiratory bacteria (HRRB), sulfate-reducing bacteria (SRB), methanogen (MET) or fermentative (FERM). The “high-redox respiratory” category includes all Pelobacteraceae and Bacteroidetes-associated *hgcA* sequences, since the two bins we recovered each contained respiratory pathways for nitrate reduction and EET. It should be noted that lateral gene transfer is thought to be common for *hgcA* genes and that phylogenetic similarity does not equate to functional similarity. Thus, these metabolic assignments are only estimations.

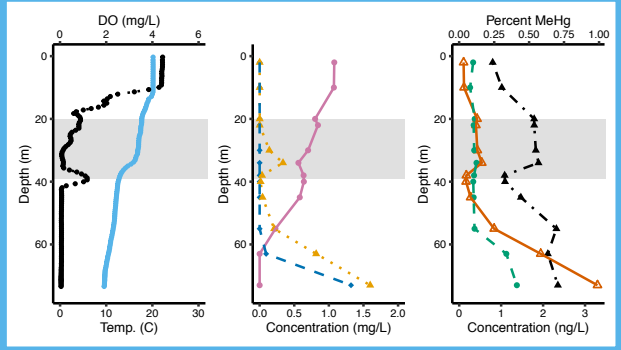
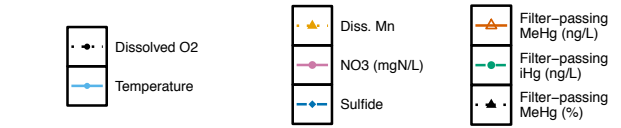
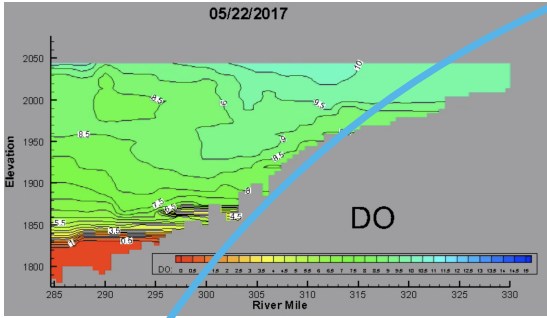
Results

Hydrologic conditions and redox gradients: Dissolved oxygen (DO) heatmaps from 2017 and 2018 based on sonde profiles collected every two weeks from April 1st to the end of December suggest different temporal and spatial variations in DO consumption (Figs. 3.1A-D,

3.2A-B). In 2017, anoxia initially developed in the deepest part of Brownlee reservoir, from approximately RM295 down to the dam (Fig. 3.1A). This initial location of anoxia expanded along the sediment-water interface upstream, reaching RM325 by mid-July. In 2018, anoxia developed near RM305 in mid-May and spread laterally both up- and downstream (Fig. 3.1B). By mid-July, the pattern of anoxia was similar to that in 2017. In both years, cooling inflows from the Snake River starting in late July resulted in interflow in which the inflowing water dives below the surface and flows between the epi- and hypolimnion. The plunging waters sheared off the top portions of the metalimnion and translocated them downstream. By the time of our sampling for metagenomic sequencing in 2017 and 2018, some of the anoxic metalimnion at RM300 had been eroded, while some of that water being transported downstream had appeared in the metalimnion at RM286.

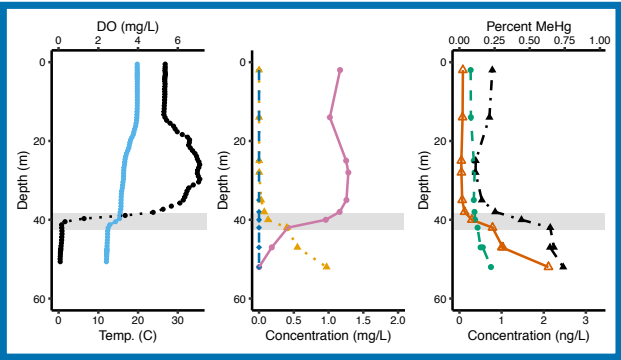
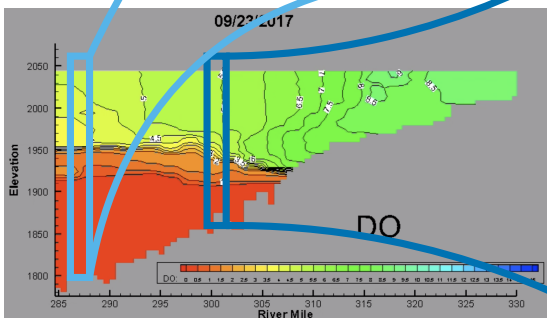
Overall, the meta- and hypolimnion in September 2017 at RM286 (2017-RM286) were more reduced than 2018-RM286 (Fig. 3.1E,G), but 2017-RM300 was less reduced than 2018-RM300 (Fig. 3.1E,H). At 2017-RM286, nitrate decreased irregularly from about 1 mgN/L in the epilimnion down to below detection by 62 m (Fig. 3.1E; App. B1). Dissolved Mn peaked in the metalimnion (0.34 mg/L) and at the bottom of the hypolimnion (1.6 mg/L). Sulfide appeared once nitrate was completely depleted, reaching 1.3 mg/L at 73 m. At 2018-RM286, however, nitrate was not completely depleted until just above the sediment-water interface, dissolved Mn was found at much lower concentrations, peaking near 1.0 mg/L in the mid-hypolimnion, and no sulfide was detected throughout the water column (Fig. 3.1G; App. B1). These trends were reversed upriver at RM300, where we observed complete nitrate depletion and sulfide accumulation, albeit only to 0.16 mg/L sulfide, in the hypolimnion in 2018, but in 2017 we only

A. May 22, 2017



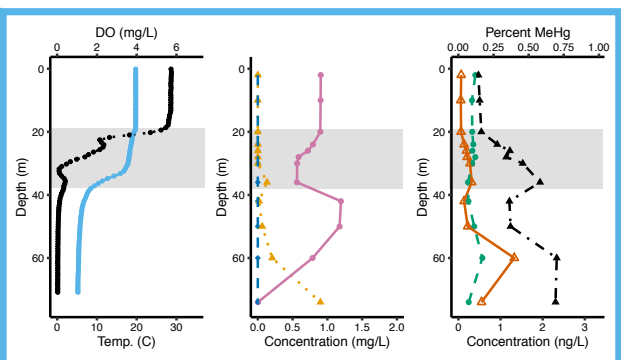
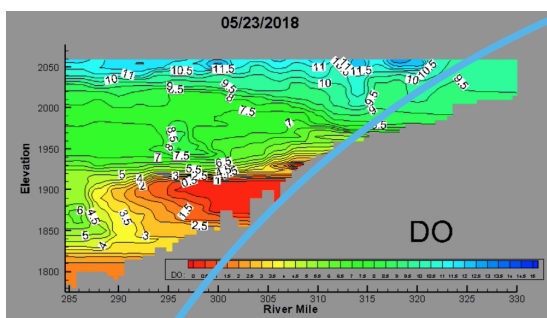
F. RM286

B. Sept 23, 2017



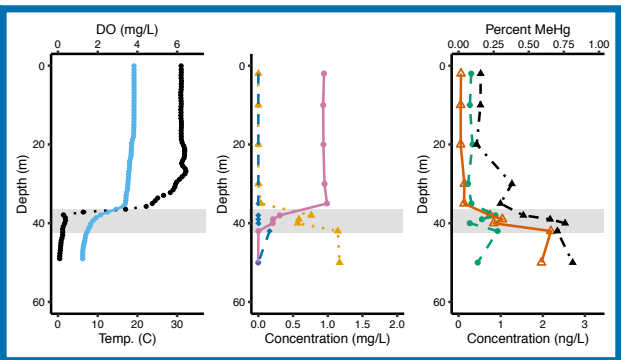
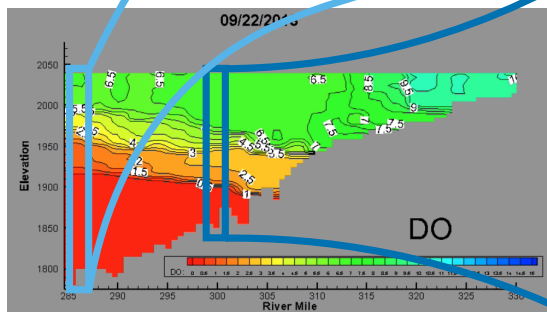
F. RM300

C. May 22, 2018



G. RM286

D. Sept 23, 2018



I. RM300

Figure 3.1: Initial site of oxygen depletion influences redox state and MeHg accumulation in late fall. Plots A-D are heatmaps of the interpolated dissolved oxygen (DO) profiles of Brownee reservoir. In 2017, oxygen was depleted initially in May in the deep hypolimnion from RM 295 down to the dam at RM284 (A), which then expanded to fill the hypolimnion by the time of sampling in September 2017 (B). In May of 2018, oxygen was initially depleted between RM300 and RM305 (C). By September (D), the entire hypolimnion from RM305 to the dam had no detectable oxygen. Plots E-H show vertical profiles of temperature, dissolved oxygen, manganese, nitrate, sulfide, inorganic Hg, MeHg, and percent MeHg in 2017 (E and F) and 2018 (G and H) at RM286 and RM300. Redox profiles show that even in September, the hypolimnion is more reduced at the site of initial oxygen depletion in these two years. Shaded gray boxes show approximate location of metalimnion.

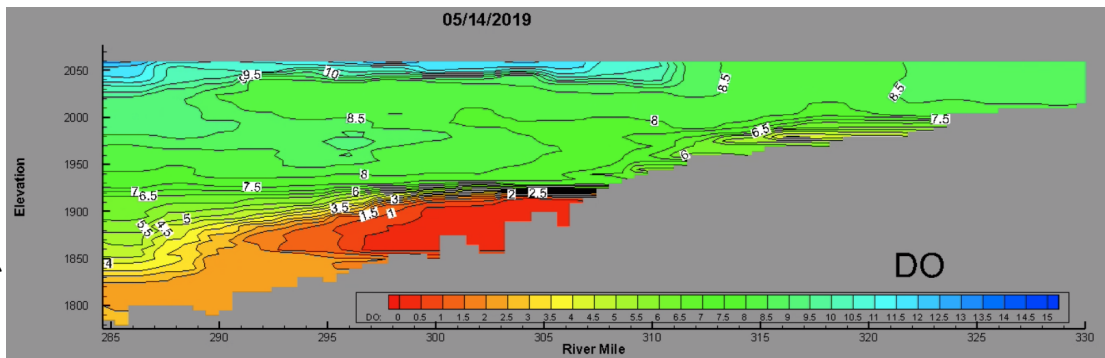
observed nitrate depletion at the lowest depth (52 m) and no sulfide accumulation (Figs. 3.1F,H; Fig. S3.2).

The progression of anoxia in 2019 was similar to that during 2018, with anoxia developing initially near RM305 (Fig. 3.2A). By the time of sampling in late July, anoxia had spread up- and down-stream, reaching over 100 km upstream from the dam up to RM325 (Fig. 3.2B). However, the hypolimnion at RM300 and RM310 at that time was far less reduced than it was during our previous years of sampling (Figs. 3.2C-D). While we do not have a sonde cast at RM300 for this sample date, examination of routine profiles collected by Idaho Power before and after this date suggest the thermocline and oxycline was at approximately 45 m. Nitrate was elevated at RM300 below the thermocline compared to RM310 (Figs. 3.2C-D). However, the nitrate to chloride ratio remained the same, suggesting this higher concentration was caused by transport from upstream rather than *in situ* production of nitrate.³⁰ Mn began to accumulate at 50 m, up to over 0.8 mg/L. At RM310, Mn had not accumulated as far up the water column, suggesting that the hypolimnion was less reduced at RM310 than at RM300 (Figs. 3.2C-D).

Hg speciation: Mid-water column maximums in MeHg in the metalimnion and the hypolimnion suggest MeHg production was occurring in the water column at multiple dates and locations. Filter-passing iHg is thought to be more available to Hg-methylators and the MeHg pool is dominated by the dissolved fraction at most sampling locations, so the results presented here will be focused on the dissolved fractions for both MeHg and iHg (Figs. 3.1 and 3.2). Both particulate and dissolved iHg and MeHg profiles are available in Fig. S3.4-6. Throughout all profiles, filtered iHg ranged mostly consistent, from approximately 0.2 ng/L to 0.4 ng/L, only increasing above that when sulfide appeared (Fig. 3.1E,H). On the other hand, MeHg exhibited differences across years and stations, but generally peaked in both the meta- and hypolimnion

A.

May 14th, 2019



B.

July 22nd, 2019

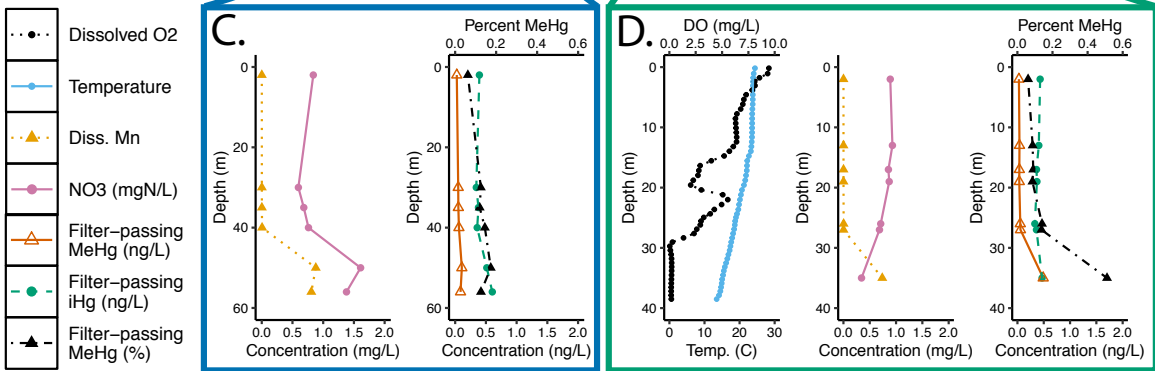
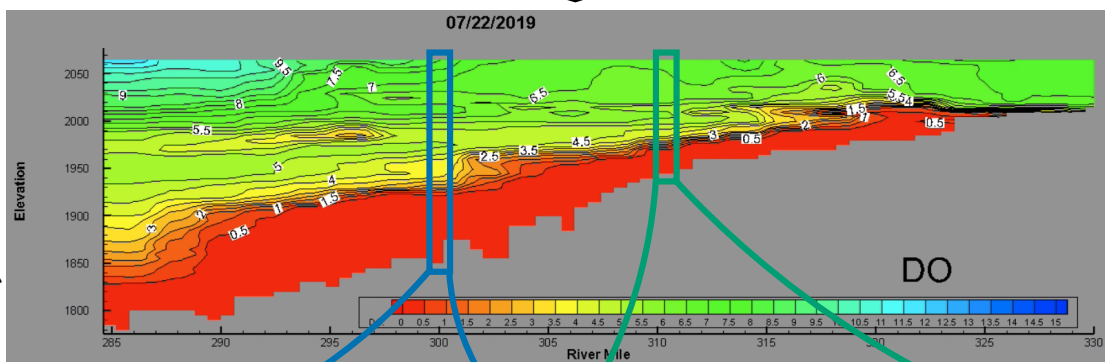


Figure 3.2: Early oxygen depletion leads to a more reduced water column but not necessarily more MeHg in summer 2019. Interpolated profiles of dissolved oxygen (DO) in Brownlee from May (A) and July (B) of 2019 are shown as heatmaps. Oxygen was initially depleted in May between RM300 and RM305 (A) and spread throughout most of the hypolimnion from RM325 down to the dam at RM286 (B). Vertical profiles of temperature, dissolved oxygen, manganese, nitrate, sulfide, inorganic Hg, MeHg, and percent MeHg show more reduced conditions at RM300 (C) than at RM310 (D). Despite more reduced conditions at RM300, MeHg levels were higher in the hypolimnion of RM310.

(Fig. 3.1E-H; 3.2C-D). Depths with detectable oxygen had very low MeHg levels. MeHg was higher under oxygen-depleted conditions, even while nitrate was still present. MeHg accumulated in the metalimnion of RM286 to higher levels in 2017 (0.5 ng/L) than 2018 (0.3 ng/L). There was also more MeHg in the hypolimnion at 2017-RM286 (>3 ng/L), as compared to 2018. Interestingly, MeHg levels at 2018-RM286 peaked to 1.2 ng/L in the middle of the hypolimnion. At RM300, MeHg was abundant in both the meta- and hypolimnion in both 2017 and 2018 but reached higher concentrations (>2 ng/L) in 2018. Due to the consistency of the iHg concentrations, the trends in fraction MeHg values matched the MeHg values closely, except for at the sulfidic depths, where the fraction MeHg began to level off (Fig. 3.1E-H; 3.2C-D). HCC is a remarkably efficient Hg-methylating system, with over 75% of the total Hg pool present at MeHg at some depths.

Metagenomic data: We generated shotgun metagenomes from 34 different samples collected at RM286 and RM300 in September 2017 and 2018 and at RM300 and RM310 in 2019. Before trimming and read merging, the metagenome read count ranged from 16 million to 478 million paired-end reads (Table S1). Metagenomes from 2017 and 2018 were grouped into clusters based on Mash similarity and coassembled within that cluster. Metagenomes from 2019 were assembled individually due to there being fewer metagenomes, each with a greater read count. Metagenomes from 2017 were also all coassembled together. The coassembly for 2018 was not completed due to memory constraints on the computing cluster. Assembly statistics are shown in Table S2.

Microbial metabolic potential: To confirm potential activity of terminal electron-accepting processes (TEAPs), we searched the assembled metagenomes for genes encoding TEAP pathways. In 2017 and 2018, *narG* gene was most abundant at the sharpest nitrate

gradients, at both RM286 and RM300, further suggesting that nitrate reduction was occurring at these locations (Fig. S3.1-2). These genes also appeared in the hypolimnetic depths during 2019, although there was not a substantial decrease in nitrate yet at this time (Fig. S3.3). Mn- and Fe-reduction can be mediated by a wide variety of protein complexes and there are likely many that have not yet been characterized. However, we did observe elevated abundance of homologs of *extE*, which is involved in Mn- and Fe-reduction²⁶, at 50 m at RM300 in 2019, coincident with a peak in dissolved Mn (Fig. S3.3). These genes were not present in the metalimnion at RM286 and RM300 in 2017 and 2018, despite the evidence for Mn reduction at those locations (Fig. S3.1-2). We also searched for reductive *dsrA* and *dsrD* genes as markers for sulfide reduction. At RM286, these genes were identified in the deep hypolimnion in 2017, coincident with the appearance of sulfide, but not in 2018, when there was no detectable sulfide (Fig. S3.1). At 2017-RM300, there was a small increase in *dsrAD* at the deepest two samples despite the lack of sulfide accumulation, whereas in 2018-RM300, *dsrAD* peaked just under the oxic/anoxic interface, which was coincident with a peak in sulfide (Fig. S3.2).

Assembly-based *hgcA* sequence abundance: We identified 26 unique HgcA amino acid sequences in the ORFs across all metagenomes (Fig. S3.7). Additional *hgcA* data is shown in Table S3. HgcA sequences were only analyzed further if they had the cap helix domain required for methylation activity and at least four transmembrane domains at the C-terminus end. Most *hgcA* genes had a *hgcB* gene immediately downstream. For four *hgcA* genes, the scaffold terminated immediately after the *hgcA*, suggesting the *hgcB* was simply not assembled into the contig. There were also three *hgcA* sequences that had ORFs downstream that were not *hgcB*. Because it has been shown that the *hgcB* gene can be located elsewhere on the genome and still be functional⁶¹⁻⁶³, we kept these sequences in the analyses. We observed similar trends in *hgcA*

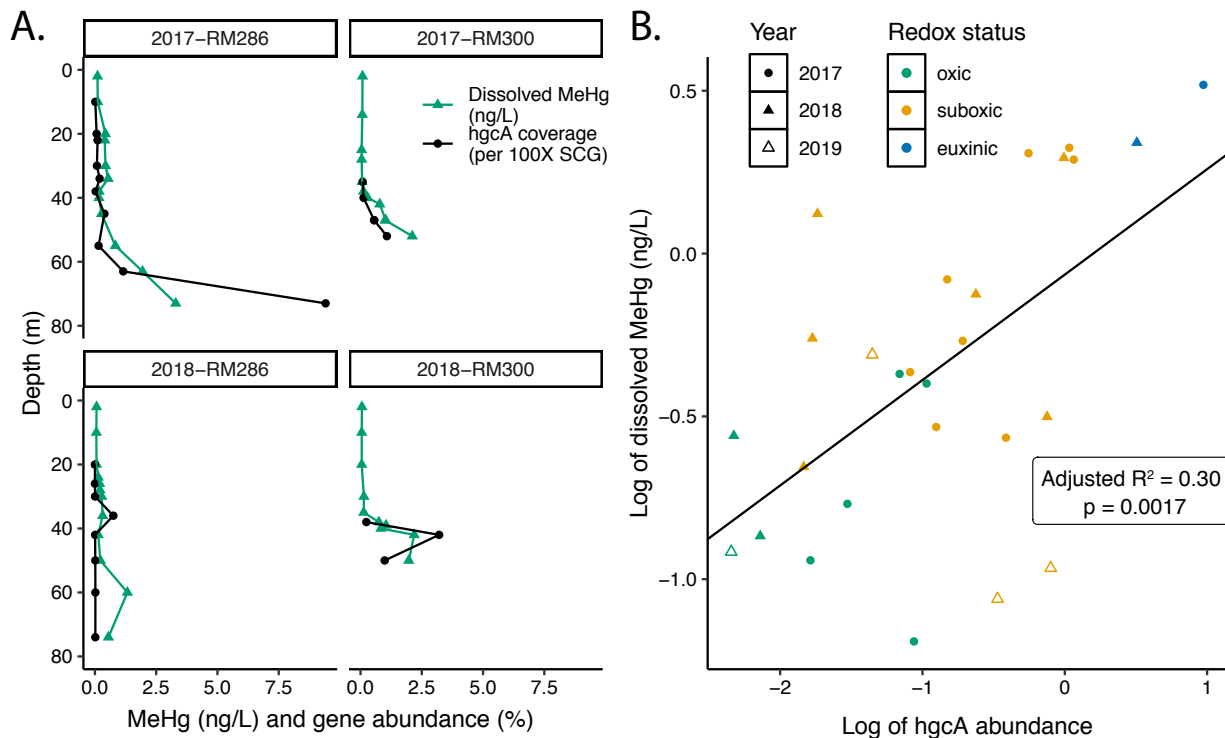


Figure 3.3: MeHg levels correlate to *hgcA* gene abundance in 2017 and 2018. Depth profiles of MeHg and *hgcA* gene abundance are shown in (A) for RM286 and RM300 from 2017 and 2018. The *hgcA* abundance is normalized to the mean abundance of 16 ribosomal protein genes. MeHg concentration were plotted against the *hgcA* coverage for all dates and depths (B). Values on both axes were log-transformed to achieve a normal distribution. Linear regression showed significant correlation between MeHg concentrations and *hgcA* ($p = 0.0017$).

gene abundance and MeHg concentrations across the different stations and years (Fig. 3.3A). Abundance of *hgcA* was highest in the two samples with sulfide accumulation, but *hgcA* was also present at all depths under suboxic conditions (Fig. 3.3A-B). There were few reads that mapped to the *hgcA* gene in oxygenated waters. The depth profiles for *hgcA* and MeHg tracked each other closely in 2017 and 2018, excluding one hypolimnetic sample in RM286 in 2018, where there was no peak in *hgcA* coverage in the upper hypolimnion despite a prominent MeHg peak (Fig. 3.3A). Overall, we observed a linear correlation ($p = 0.0017$, $R^2 = 0.30$) between *hgcA* and dissolved MeHg levels under log transformation (Fig. 3.3B).

Genome reconstruction of Hg-methylators: To assign taxonomy and predict metabolic potential of the *hgcA*⁺ organisms found in each section of the water column, we constructed and curated genomic bins containing *hgcA* (*hgcA*⁺). We identified 16 medium-quality⁶⁴ *hgcA*⁺ bins (> 50% completeness, < 10% redundant) that were grouped into 10 metagenome operational taxonomic units (mOTUs), within which bins shared >97% ANI and >50% gene alignment. Phylogenetic reconstruction and metabolic pathway identification returned nearly identical results for each of the bins within a mOTU, so here we will describe these results for one selected representative within each mOTU. Most phylogenetic clusters of *hgcA* included at least one binned *hgcA* sequence (Fig S.3.8). Metabolic gene content data can be found in Supplementary Data 2.

Fermentative Hg-methylators: We identified four mOTUs corresponding to putative fermentative organisms within the Planctomycetes-Verrucomicrobia-Chlamydia (PVC) superphylum (Fig. S3.9). Three of these were in the Kiritimatiellaeota phylum. Two, represented by anvio_*hgcA*_0261 and anvio_*hgcA*_0040, were recovered from the 2017 metagenomes and one (anvio_*hgcA*_0110) from the 2018 metagenomes (Fig. 3.4A). The mOTUs from the two

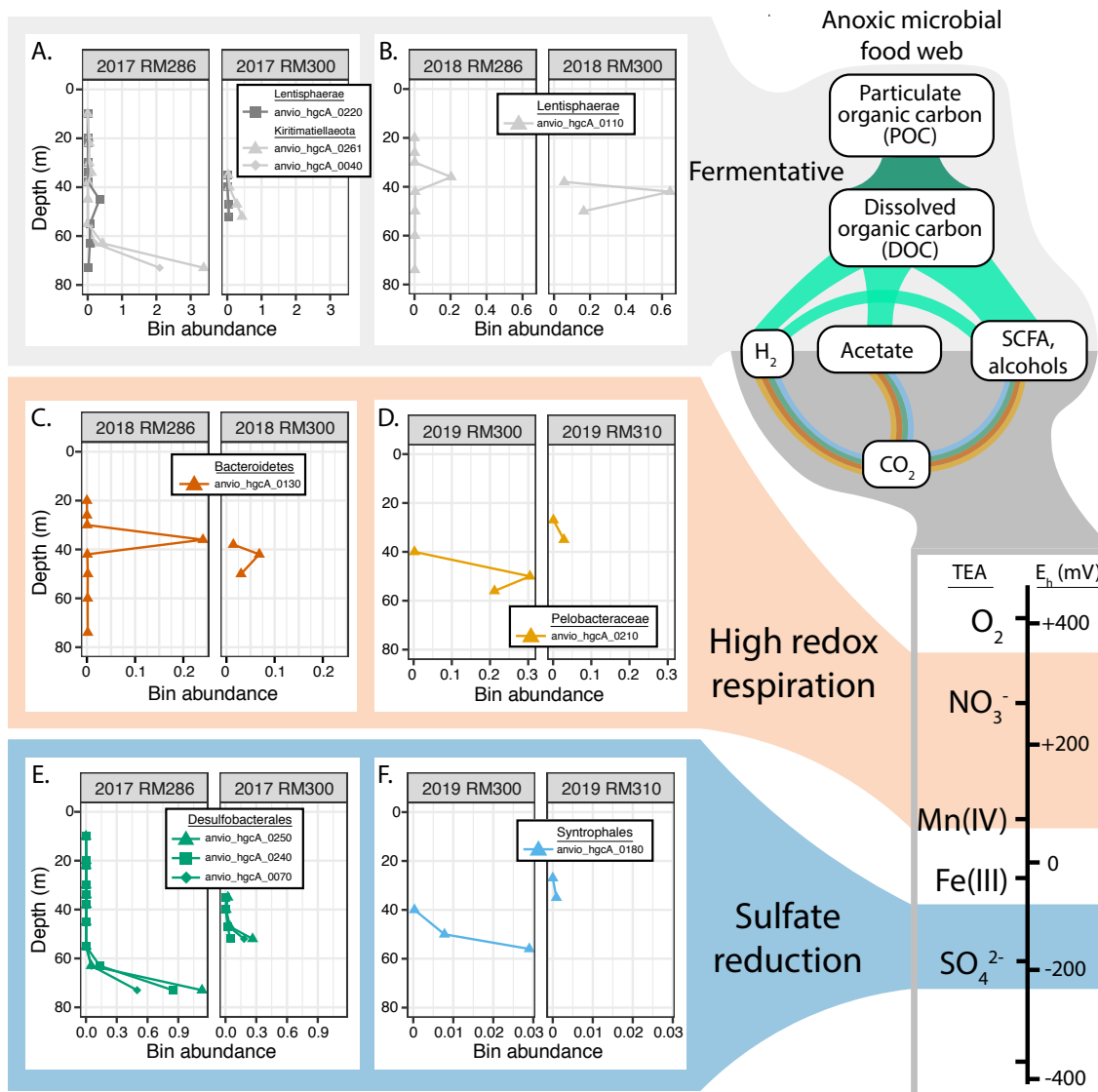


Figure 3.4: Depth profiles for hgcA+ bin from different metabolic guilds. We identified four fermentative bins, three from 2017 (A) and one from 2018 (B). These bins are thought to be involved in the breakdown of large organic matter and fermentation of the resulting products. We also identified two high redox respiration bacteria (HRRB) that can reduce Mn oxides and nitrate, one each in 2018 (C) and 2019 (D). Finally, we also identified four hgcA+ sulfate reducers, three Desulfobacterales from 2017 (E) and one Syntrophales from 2019 (F). These data show that different geochemical factors could be controlling MeHg production from year to year and at different depths.

separate years are phylogenetically separated, but both cluster with *hgcA*+ PVC mOTUs from the anoxic hypolimnion of a eutrophic freshwater lake²⁸ (Fig. S3.9). These three bins all correspond to obligately fermentative organisms. They appear to have been polysaccharide-degrading organisms, as each bin had at least 78 glycoside hydrolases (GHs). The main difference in metabolic genes between the two bins from 2017 is that *anvio_hgcA_0261* has the nitrite reductase operon *nrfAH*. Interestingly, these two bins also shared similar abundance patterns in 2017 except that *anvio_hgcA_0261*, with *nrfAH*, peaked in the metalimnion at RM286 in addition to the hypolimnion (Fig. 3.4A). This could indicate a greater tolerance of suboxic conditions, potentially due to the ability to detoxify nitrite. The fourth bin, *anvio_hgcA_0220*, was classified into the Lentisphaerae phylum. This bin was most abundant at 45 m at RM286 in 2017, where nitrate levels were still around 0.6 mg/L (Fig. 3.4B). This bin corresponds to an obligately fermentative organism, as it had no electron transport chain, but it did encode an anaerobic sulfite reductase and the *cydAB* terminal oxidase. Unlike the Kiritimatiellaeota bins, this bin did not appear to specialize in polysaccharide degradation with, only 22 GHs.

High-redox respiratory Hg-methylators: Two of the representative bins, *anvio_hgcA_0130* and *anvio_hgcA_0210*, encoded metabolic pathways for terminal electron accepting processes (TEAPs) at higher redox levels (more oxidized conditions) than commonly associated with Hg-methylation. The *anvio_hgcA_0130* bin was classified into the Prolixibacteraceae family within the Bacteroidales order (Fig. S3.10). A previous study identified *hgcA*+ Bacteroidales genomes from isolate genomes and environmental studies²⁵, but none within Prolixibacteraceae. This bin had a complete aerobic electron transport chain, multiple terminal oxidases, and nitrate reductase. It also had several genes that encode pathways

for external electron transfer (EET), including an outer-membrane multiheme cytochrome c (MHC) genes annotated as *extA*²⁶ with an adjacent periplasmic MHC. It also included the *imcH* gene, which has been shown to be used for EET to high-redox TEAs⁶⁵. This bin was recovered from the 2018 metagenomes and was most abundant in the metalimnion at RM286, only at the depth where reduced Mn was detected (Fig. 3.4C). It also had a small peak in abundance at RM300 in the metalimnion. The anvio_hgcA_0210 bin was reconstructed from 2019 metagenomes and was classified by GTDB as Pelobacteraceae, which is closely related to the Geobacteraceae. This bin is most abundant at 50m at RM300 in 2019, where dissolved Mn rapidly increases, suggesting a potential hotspot for Mn cycling (Fig. 3.4D). This bin contained several genes encoding pathways for EET, including *extE* homologues, which encoding a porin-cytochrome c complex²⁶ and *imcH* and *cbcL*, which facilitate EET to high and low redox TEAs, respectively⁶⁶. Overall, it includes 23 multiheme cytochrome c (MHC) genes, which are often linked to EET processes. This bin also encodes a *coxACDB* terminal oxidase and *nrfAH*. While these could be used for respiration of oxygen or nitrite, respectively, both genes can be found in metal-reducing Geobacteraceae and are thought to be involved in oxygen/nitrite detoxification⁶⁷.

Sulfate-reducing Hg-methylators: We also recovered four bins from 2017 and 2019 that correspond to sulfate-reducing bacteria (SRB). Three of these bins were classified as Desulfobacterales and the fourth was a Smithellaceae, within the Syntrophobacterales order. These bins each had at least partial reductive *dsr* operons and an electron transport chain, including either complex I or an *rnf* operon. In 2017, these bins were only present when sulfide was detected in the water column (Fig. 3.4E). However, in 2019, the Smithellaceae was detected at low abundance at 56 m at RM300, despite a lack of sulfide accumulation and about 1.4 mgN/L of nitrate present (Fig. 3.4F, 3.2C).

Abundance of Hg-methylating groups: Using the taxonomy of *hgcA*+ bins from this study and a phylogenetic reconstruction of the HgcA sequences along with HgcA sequences from the Hg-MATE database⁵⁵ and several recently published papers^{28,68}, we assigned a phylogenetic affiliation for each *hgcA* gene. However, it is important to note that prior work suggests that *hgcA* has likely undergone extensive horizontal gene transfer (HGT)^{25,59,69} and thus taxonomic assignment of an organism based on the phylogeny of this gene should be interpreted with caution. Using this inferred information, we generated profiles of the taxonomic composition of *hgcA* at each RM across the three years (Fig. 3.5). Each of these *hgcA* sequences was also assigned a metabolic function based on the metabolic reconstruction of bins with a closely related *hgcA* gene. We grouped sequences into four groups: fermentative (FERM); high-redox respiratory bacteria (HRRB), which included sequences associated with bins expected to reduce nitrate and/or Mn oxides; sulfate reducing bacteria (SRB); and methanogens (MET). These classifications should also be interpreted with caution, because in addition to the possibility of HGT, the metabolic potential of organisms can vary widely within phylogenetically similar groups based on differential gene content.

Overall, we observed drastic differences in the *hgcA* community from year-to-year, throughout the water column, and across different sites, even between locations with relatively similar redox states (Fig. 3.5). In 2017 at RM286, FERM sequences dominated the metalimnetic *hgcA* community, particularly the Kiritimatiellaeota (Fig. 3.5A). Lentisphaerae-associated FERM sequences were dominant in the upper hypolimnion. In the deep hypolimnion, where sulfide had begun to accumulate, *hgcA* abundance was much higher, which was about 2/3rd Kiritimatiellaeota and 1/3rd SRB from Desulfobacterales. Throughout the profile, there were low numbers of HRRB from Bacteroidetes and, surprisingly, methanogens. At RM300 in 2017, the

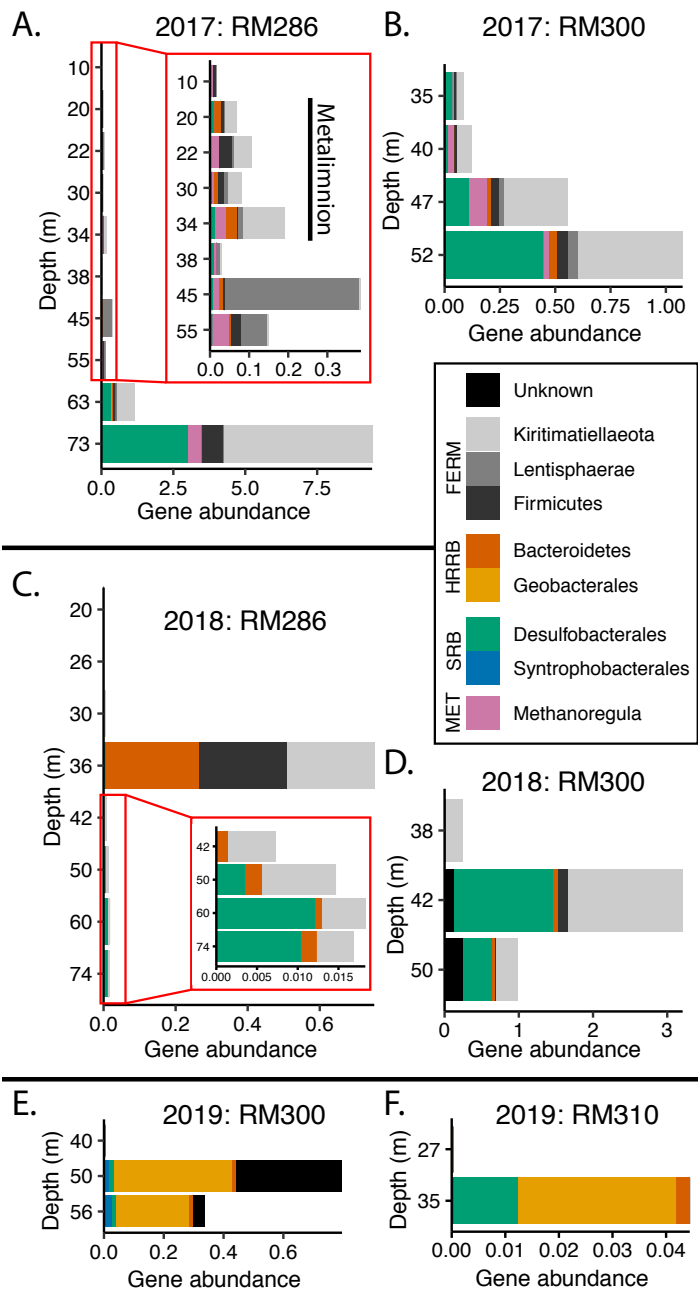


Figure 3.5: Bar charts showing taxonomic and metabolic diversity of *hgcA*⁺ organisms across three years of sampling. Insets for RM286 from 2017 (A) and 2018 (C) show zoomed-in view of metagenomes with lower abundance.

hypolimnion had a similar community to the deep hypolimnion at RM286 (Fig. 3.5B). In 2018, *hgcA* abundance at RM286 was much lower than in 2017 (Fig. 3.5C). It was most abundant in the metalimnion at 36 m, where there was a mix of FERM sequences from Firmicutes and Kiritimatiellaeota and HRRB from Bacteroidetes. The highest abundance of *hgcA* in 2018, however, was at RM300 in the upper hypolimnion (Fig. 3.5D). Here we observed a mix of SRB sequences and FERM sequences, again from Kiritimatiellaeota. In 2019, *hgcA* was even lower in abundance. At RM300, *hgcA* peaked in the middle of the hypolimnion (Fig. 3.5E). HRRB sequences from Pelobacterales were the most abundant, followed by several unknown sequences that did not cluster closely with any known *hgcA* sequences. The *hgcA* pool at RM310 was low in abundance, but what was there was mostly Pelobacterales again (Fig. 3.5F).

Discussion

While hypolimnetic MeHg accumulation has often been considered to occur primarily in the sediment and subsequently diffuse into the water column, a growing body of evidence^{28,68,70–72} indicates that MeHg production within the water column can be an important source of MeHg to freshwater lacustrine systems. Additionally, water column Hg methylation is likely more important for food web bioaccumulation than benthic Hg methylation due to its proximity to the epilimnion and zooplankton foraging habits. The data presented here suggest that water column MeHg production is an important source of MeHg production for this system. Across all sites, dates, and depths, we observed a linear correlation between the MeHg concentrations in the water column and the *hgcA* gene abundance (Fig. 3.3B). This provides strong evidence for the importance of water column Hg-methylation in either producing or maintaining the pool of MeHg in the water column. In 2017 at RM286 (Fig. 3.1E) and RM300 (Fig. 3.1F), MeHg

concentrations decreased nearly linearly coming out the sediments. While this could in theory be explained by diffusion or dispersal, the downward hydraulic gradient at these locations, with 60-80 meters of head, is likely pushing water into the sediments, which would overwhelm any diffusion or dispersal moving MeHg upwards. In 2018, the MeHg gradients at these two sites were very different, where there were clear mid-column peaks in MeHg concentrations, strongly suggesting *in situ* MeHg production rather than efflux from the sediments (Figs. 3.1G-H). One surprising finding, however, was the low abundance of *hgcA* genes at 60 meters at RM286 in 2018, where we observed high MeHg concentrations (Fig. 3.3A). Water column production is also backed up by “corewater” profiles, which are obtained by collecting a short sediment core and drawing off the water overlying the sediments at approximately 20 cm intervals to examine chemical gradients immediately overlying the sediments. The gradients in these corewater profiles show that in late fall, from approximately RM300 to the dam downstream at RM284, there is no MeHg flux out of the sediments.³⁰

In 2019, the MeHg concentrations and the *hgcA* abundance in the hypolimnion did not match up as we would have expected. MeHg was highest this year at RM310, where there was very low *hgcA* coverage (Fig. 3.2D, 3.5F). This suggests that the MeHg at RM310 was being produced in the sediments and diffusing into the bottom of the hypolimnion. This is also supported by the corewater data, which suggests that diffusive flux of MeHg out of the sediments occurs upstream of RM305.³⁰ On the other hand, at RM300, where corewater profiles suggest there is no diffusive flux out of the sediments³⁰, MeHg concentrations in the water column are very low despite the presence of *hgcA* (Fig. 3.2C, 3.5E). The lack of nitrate depletion suggests that this water had only recently become depleted in oxygen and that MeHg production in the water column at this site had just started (Fig. 3.2C). Collectively, this data suggests that the

relative importance of water column vs. sediment production of MeHg may vary spatially and temporally.

We also observed MeHg accumulation in the metalimnion at RM286 during 2017 and 2018 (Figs. 3.1E,G). Because the metalimnion sits above water that has much lower MeHg concentrations, this cannot be explained by diffusion from the sediments. During fall and early winter, the cooling riverine water flowing into Brownlee drops below the warmer epilimnion and becomes “interflow” moving through the metalimnion.⁷³ This interflow shears off layers of stratification in the hypolimnion, carrying the former hypolimnetic water down through the reservoir and ultimately through the dam.³ During both years, there was substantial interflow moving through the metalimnion, which indicates that at least some of that metalimnetic MeHg could have originated in hypolimnetic water upstream. However, the elevated MeHg at the bottom of this interflow, where *hgcA* is also highest, suggest that this region is still an important source for *in situ* Hg-methylation as it flows through the reservoir (Figs. 3.1E,G). While MeHg production and concentration may be higher in the hypolimnion than the metalimnion, aerobic zooplankton and fish are unlikely to migrate through 30-50 m of anoxic water to reach these high MeHg levels. The proximity of the metalimnion to the aerobic epilimnion and therefore to the base of the food web means this is an important source of MeHg to consider.⁷⁴

Reservoirs, particularly those used for hydroelectric power generation, are complicated and highly dynamic systems, which can have a major impact on Hg cycling in the system. In 2017, anoxia initially developed in the bottom water at RM286, due to incomplete flushing of the hypolimnion from 2016 (Fig. 3.1A). By September, RM286 had a lower redox status than RM300, as evidenced by the loss of nitrate and the appearance of sulfide and sulfate-reducing genes (Figs. 3.1E; Fig. S3.1A). Conversely, in 2018, anoxia developed between RM300 and

RM305 and by September of that year, the hypolimnion at RM300 was at a lower redox state relative to RM286 further downstream (Figs. 3.1C,G-H; Fig. S3.1B). This spatial difference in redox status between years is reflected in both the MeHg concentrations and *hgcA* abundance data, where we saw higher concentrations of MeHg and abundance of *hgcA* at RM286 than at RM300 in 2017, but in 2018 the MeHg and *hgcA* abundance were greater at RM300 (Figs. 3.1E-H, 3.3A). In 2019, when our sampling was much earlier in the year, anoxia initially developed near RM300 (Fig. 3.2A). At the time of sampling, the hypolimnion at RM300 had more Mn in the water column and had more hits to the EET and sulfite reductase genes, suggesting the water was in a much more reduced state than at RM310 (Fig. S3.3). Correspondingly, we saw much higher levels of *hgcA* at RM300, despite the higher levels of MeHg at RM310, which was likely due to MeHg diffusion out of the sediments (Figs. 3.2C-D, 3.5E-F). These variations in where MeHg is produced in the water column are likely to be translated to spatial differences in MeHg bioaccumulation in the food web throughout the reservoir. Additionally, when and where the Hg-methylating microbes are producing MeHg in the reservoir can also determine when and where it is mixed into the interflow and moved through the dam.^{3,7} While some of the MeHg production may have been produced after the water was mixed into the interflow, the “age” of anoxia of that water parcel is still related to the overall MeHg levels. Overall, the data presented here show how different hydrological conditions can impact the redox status of the water, which can impact the microbial community composition and metabolism, which subsequently determines the location and extent of MeHg production. This ultimately has major implications for how MeHg moves throughout the reservoir and accumulates in the food web and for how the reservoir acts as a MeHg source to downstream waters.

This work presents a strong case for the importance of MeHg production in suboxic environments rather than strictly in anoxic environments. The geochemical profiles presented here indicate that water column Hg-methylation is occurring at depths where nitrate is still present, which is confirmed by the presence of *hgcA* at these depths. Vertical gradients in nitrate suggest that nitrate reduction is actively occurring at these depths, which is also supported by the abundance of the *narG* genes in the metagenomes. We did not observe high concentrations of particulate Mn, presumed to be mostly Mn(IV) oxides, which are the TEA in Mn reduction. However, Mn oxides can cycle rather quickly at steep oxidic gradients.^{75,76} The presence of EET genes at some of these depths further suggests Mn reduction as an active TEAP in the Brownlee water column. Combined with the lack of sulfide accumulation or *dsr* genes at these depths and the evidence that MeHg is produced in the water column, the presence of nitrate and Mn reduction pathways indicates that the observed MeHg is produced under suboxic conditions.

While previous studies have identified MeHg production in suboxic environments, most have hypothesized that the actual Hg-methylation is occurring in anoxic niches.^{20,21} However, the metabolic gene data from the *hgcA*⁺ bins suggests that Hg-methylation can be facilitated by microorganisms living under true suboxic conditions. The *hgcA*⁺ mOTUs associated with Prolixibacteraceae and the Pelobacteraceae both contain genes for terminal oxidases, nitrate or nitrite reduction, and EET genes normally used for reduction of Mn and Fe oxides. While they contain all these pathways, both bins were not found in the epilimnion and peaked in abundance at the metalimnion, Prolixibacteraceae in 2018 at RM286 and RM300, Pelobacteraceae at RM300 in 2019 (Fig 3.4A-B). This suggests that despite their terminal oxidases, they are more competitive under suboxic rather than fully oxidic conditions. Previous work identified a *hgcA*⁺ Pelobacteraceae bin closely related to the one presented here that had a similar set of metabolic

genes.²⁸ The bin from that study also peaked in abundance at a site of suspected Mn cycling, just under the oxic/anoxic interface in the water column of a freshwater lake.²⁸ Bacteroidetes bins carrying *hgcA* and a similar diversity of TEAP pathways were reconstructed from that same lake, but were present throughout the anoxic hypolimnion.²⁸ Other studies have identified *hgcA* sequences likely from *Geobacter*, which are closely related to Pelobacteraceae and also often reliant on Fe or Mn reduction, or *Pelobacter* in rice paddy⁷⁷ and lake^{78,79} sediments. While Mn respiration has not yet been shown to be capable of driving MeHg production, Fe-reducing *Geobacter* are also capable of reducing Mn^{66,80} and are known to be rapid Hg-methylators^{81,82}. Additionally, several other studies have identified possible links between environmental Mn reduction and MeHg production^{83,84}. Nitrate reduction, on the other hand, has been identified in *hgcA*+ bins^{24,28} but has not been implicated in MeHg production. Experimental verification of these potential metabolic linkages in the lab and in the field is a critical next step for understanding the role of nitrate and Mn reduction in controlling MeHg.

One of the most abundant groups of *hgcA* genes in our samples was associated with the PVC superphylum. Three of the four *hgcA*+ bins belonged to the Kiritimatiellaeota phylum and one was associated with the Lentisphaerae phylum (Fig S3.9). These bins were phylogenetically and metabolically similar to the most abundant *hgcA*+ bins from the anoxic hypolimnion of a freshwater lake, where PVC-associated, mostly Kiritimatiellaeota-associated, *hgcA* sequences accounted for about 50% of the Hg-methylating population.²⁸ Two *hgcA*+ Kiritimatiellaeota bins were identified in another anoxic freshwater lake, although these two were quite phylogenetically distinct from the HCC bins (Fig S3.9).⁶⁸ Analysis of the metabolic pathways present in the PVC bins from this study indicate they represent obligately fermentative organisms with potential for polymer degradation, which is also consistent the two studies

discussed above^{28,68}. The Kiritimatiellaeota had more cellulases and oligosaccharide-degrading genes, while the Lentisphaerae included several chitinases and pullanases. Their likely role in these ecosystems is to initiate decomposition of phytoplankton biomass that is sinking through the redox cline, suggesting a particularly important role in eutrophic systems. Thus, these organisms could be a direct link between complex carbon degradation and fermentation to production of MeHg, regardless of TEAP activity. The emergence of Kiritimatiellaeota, and to a lesser extent Lentisphaerae, as abundant Hg-methylating organisms within the water column of freshwater lakes warrants further study. More generally, this study corroborates a growing body of evidence that fermentative organisms are often the most abundant putative Hg-methylating organisms in freshwater ecosystems.^{28,68} While fermentative organisms tend to produce less MeHg than respiratory organisms under laboratory conditions, these cultures are not closely related to what we see in the environment and these monoculture conditions are likely very different than what the organisms experience *in situ*, which may affect their MeHg production. Thus, additional work using functional assays to test the impact of these organisms on MeHg production will be key to clarifying if these organisms represent an overlooked direct link between carbon degradation and Hg-methylation.

Acknowledgements

Funding was provided by Idaho Power Company, the Idaho Department of Environmental Quality, the USGS Cooperative Funding, Toxics Substances Hydrology, and Contaminant Biology programs (Environmental Health Mission Area). Graduate student support was provided through the National Institute for Water Resource grant. Nick Gastelecutto, Jesse Naymik, Chuck Hoovestall, Chris Larsen provided extensive sampling support. Analytical support was provided by Mike Tate, John DeWild, Sarah Janssen, Jake Ogorek, Christopher Babiarz, and Ron Antweiler. Collin Eagles-Smith, James Willacker, and Mark Marvin-DiPasquale provided helpful feedback on data analysis.

References

1. Bodaly, R. A. *et al.* Bioaccumulation of mercury in the aquatic food chain in newly flooded areas. in *Metal ions in biological systems* vol. 34 259–288 (MARCEL DEKKER AG, 1997).
2. Brigham, M. E., Krabbenhoft, D. P., Olson, M. L. & DeWild, J. F. Methylmercury in flood-control impoundments and natural waters of northwestern Minnesota, 1997–99. **138**, 67–78 (2002).
3. Baldwin, A. K. *et al.* Seasonal Dynamics and Interannual Variability in Mercury Concentrations and Loads through a Three-Reservoir Complex. *Environ. Sci. Technol.* **54**, 9305–9314 (2020).
4. Clark, G. M. *et al.* Mercury cycling in the Hells Canyon Complex of the Snake River, Idaho and Oregon. (2016).
5. Friedl, G. & Wüest, A. Disrupting biogeochemical cycles – Consequences of damming. **64**, 11 (2002).
6. Willacker, J. J. *et al.* Reservoirs and water management influence fish mercury concentrations in the western United States and Canada. *Science of The Total Environment* **568**, 739–748 (2016).
7. Canavan, C. M., Caldwell, C. A. & Bloom, N. S. Discharge of methylmercury-enriched hypolimnetic water from a stratified reservoir. *The Science of The Total Environment* **260**, 159–170 (2000).
8. Kasper, D., Fernandes, E., Palermo, A., Branco, C. W. C. & Malm, O. Evidence of elevated mercury levels in carnivorous and omnivorous fishes downstream from an Amazon reservoir. *Hydrobiologia* **694**, 87–98 (2012).
9. Kasper, D. *et al.* Reservoir Stratification Affects Methylmercury Levels in River Water, Plankton, and Fish Downstream from Balbina Hydroelectric Dam, Amazonas, Brazil. *Environ. Sci. Technol.* **48**, 1032–1040 (2014).
10. Gilmour, C. C., Henry, E. A. & Mitchell, R. Sulfate stimulation of mercury methylation in freshwater sediments. *Environ. Sci. Technol.* **26**, 2281–2287 (1992).
11. Compeau, G. C. & Bartha, R. Sulfate-reducing bacteria: Principal methylators of mercury in anoxic estuarine sediment. *Appl Environ Microbiol* **50**, 498–502 (1985).
12. Fleming, E. J., Mack, E. E., Green, P. G. & Nelson, D. C. Mercury Methylation from Unexpected Sources: Molybdate-Inhibited Freshwater Sediments and an Iron-Reducing Bacterium. *Appl Environ Microbiol* **72**, 457–464 (2006).
13. Kerin, E. J. *et al.* Mercury methylation by dissimilatory iron-reducing bacteria. *Appl Environ Microbiol* **72**, 7919–7921 (2006).
14. Hamelin, S., Amyot, M., Barkay, T., Wang, Y. & Planas, D. Methanogens: principal methylators of mercury in lake periphyton. *Environ. Sci. Technol.* **45**, 7693–7700 (2011).
15. Gilmour, C. C., Bullock, A. L., McBurney, A., Podar, M. & Elias, D. A. Robust mercury methylation across diverse methanogenic *Archaea*. *mBio* **9**, 1–13 (2018).
16. Todorova, S. G. *et al.* Evidence for regulation of monomethyl mercury by nitrate in a seasonally stratified, eutrophic lake. *Environ. Sci. Technol.* **43**, 6572–6578 (2009).
17. Dent, S. R., Beutel, M. W., Gantzer, P. & Moore, B. C. Response of methylmercury, total mercury, iron and manganese to oxygenation of an anoxic hypolimnion in North Twin Lake, Washington. *Lake and Reservoir Management* **30**, 119–130 (2014).

18. Matthews, D. A. *et al.* Whole-lake nitrate addition for control of methylmercury in mercury-contaminated Onondaga Lake, NY. *Environmental Research* **125**, 52–60 (2013).
19. Vlassopoulos, D. *et al.* Manganese(IV) oxide amendments reduce methylmercury concentrations in sediment porewater. *Environ. Sci.: Processes Impacts* **20**, 1746–1760 (2018).
20. Gascón Díez, E. *et al.* Role of settling particles on mercury methylation in the oxic water column of freshwater systems. *Environ. Sci. Technol.* **50**, 11672–11679 (2016).
21. Eckley, C. S., Luxton, T. P., Knightes, C. D. & Shah, V. Methylmercury production and degradation under light and dark conditions in the water column of the Hells Canyon Reservoirs, USA. *Environ Toxicol Chem* etc.5041 (2021) doi:10.1002/etc.5041.
22. Gionfriddo, C. M. *et al.* Microbial mercury methylation in Antarctic sea ice. *Nature Microbiology* **1**, 1–12 (2016).
23. Tada, Y., Marumoto, K. & Takeuchi, A. Nitrospina-Like Bacteria Are Potential Mercury Methylators in the Mesopelagic Zone in the East China Sea. *Front. Microbiol.* **11**, 1369 (2020).
24. Lin, H. *et al.* Mercury methylation by metabolically versatile and cosmopolitan marine bacteria. *ISME J* (2021) doi:10.1038/s41396-020-00889-4.
25. McDaniel, E. A. *et al.* Expanded phylogenetic diversity and metabolic flexibility of mercury-methylating microorganisms. *mSystems* **5**, 1–21 (2020).
26. Jiménez Otero, F., Chan, C. H. & Bond, D. R. Identification of different putative outer membrane electron conduits necessary for Fe(III) citrate, Fe(III) oxide, Mn(IV) oxide, or electrode reduction by *Geobacter sulfurreducens*. *J Bacteriol* **200**, 1–20 (2018).
27. Lovley, D. R. & Phillips, E. J. P. Novel Mode of Microbial Energy Metabolism: Organic Carbon Oxidation Coupled to Dissimilatory Reduction of Iron or Manganese. *Applied and Environmental Microbiology* **54**, 1472–1480 (1988).
28. Peterson, B. D. *et al.* Mercury methylation genes identified across diverse anaerobic microbial guilds in a eutrophic sulfate-enriched lake. *Environ. Sci. Technol.* **54**, 15840–15851 (2020).
29. Capo, E. *et al.* Deltaproteobacteria and Spirochaetes-like bacteria are abundant putative mercury methylators in oxygen-deficient water and marine particles in the Baltic Sea. *Front. Microbiol.* **11**, 1–11 (2020).
30. Poulin, B. A. *et al.* *Chemical characterization of water and suspended sediment of the Snake River and Hells Canyon Complex (Idaho, Oregon)*. <https://doi.org/10.5066/P9DT2B6J> (2020).
31. Marvin-DiPasquale, M. *et al.* *Biogeochemical data for mercury and other constituents in surface sediment and deep cores from the Hells Canyon Reservoir Complex, Idaho and Oregon 2014-2018*. <https://doi.org/10.5066/P9L4XCD0> (2020).
32. Olson, M. L. & DeWild, J. F. Techniques for the collection and species-specific analysis of low levels of mercury in water, sediment, and biota. in *U.S. Geological Survey Water-Resources Investigations Report* vols 99-4018B (1999).
33. *U.S EPA Method 1631, Revision E: Mercury in Water by Oxidation, Purge and Trap, And Cold Vapor Atomic Fluorescence Spectrometry.* (2002).
34. Olund, S. D., DeWild, J. F., Olson, M. L. & Tate, M. T. Methods for the preparation and analysis of solids and suspended solids for total mercury. in *U.S. Geological Survey Techniques of Water-Resources Investigations, Book 5, Chapter A8* (2004).

35. DeWild, J. F., Olson, M. L. & Olund, S. D. *Determination of Methyl Mercury by Aqueous Phase Ethylation, Followed by Gas Chromatographic Separation with Cold Vapor Atomic Fluorescence Detection. Open-file Report.* (2002).
36. Horvat, M., Bloom, N. S. & Liang, L. Comparison of distillation with other current isolation methods for the determination of methyl mercury compounds in low level environmental samples. *Analytica Chimica Acta* **281**, 135–152 (1993).
37. Lepak, R. F. *et al.* Influence of *Cladophora*–quagga mussel assemblages on nearshore methylmercury production in Lake Michigan. *Environ. Sci. Technol.* **49**, 7606–7613 (2015).
38. Chen, S., Zhou, Y., Chen, Y. & Gu, J. fastp: an ultra-fast all-in-one FASTQ preprocessor. *Bioinformatics* **34**, i884–i890 (2018).
39. Ondov, B. D. *et al.* Mash: fast genome and metagenome distance estimation using MinHash. *Genome Biol* **17**, 132 (2016).
40. Nurk, S., Meleshko, D., Korobeynikov, A. & Pevzner, P. A. metaSPAdes: a new versatile metagenomic assembler. *Genome Research* **27**, 824–834 (2017).
41. Hyatt, D. *et al.* Prodigal: prokaryotic gene recognition and translation initiation site identification. *BMC Bioinformatics* **11**, 119 (2010).
42. Langmead, B. & Salzberg, S. L. Fast gapped-read alignment with Bowtie 2. *Nat Methods* **9**, 357–359 (2012).
43. Anantharaman, K. *et al.* Thousands of microbial genomes shed light on interconnected biogeochemical processes in an aquifer system. *Nat. Commun.* **7**, 1–11 (2016).
44. Sorek, R. *et al.* Genome-Wide experimental determination of barriers to horizontal gene transfer. *Science* **318**, 1449–1452 (2007).
45. Kang, D. D. *et al.* MetaBAT 2: an adaptive binning algorithm for robust and efficient genome reconstruction from metagenome assemblies. *PeerJ* **7**, 1–13 (2019).
46. Wu, Y.-W., Simmons, B. A. & Singer, S. W. MaxBin 2.0: an automated binning algorithm to recover genomes from multiple metagenomic datasets. *Bioinformatics* **32**, 605–607 (2016).
47. Sieber, C. M. K. *et al.* Recovery of genomes from metagenomes via a dereplication, aggregation and scoring strategy. *Nat Microbiol* **3**, 836–843 (2018).
48. Eren, A. M. *et al.* Anvi'o: an advanced analysis and visualization platform for 'omics data. *PeerJ* **3**, 1–29 (2015).
49. Chaumeil, P.-A., Mussig, A. J., Hugenholtz, P. & Parks, D. H. GTDB-Tk: a toolkit to classify genomes with the Genome Taxonomy Database. *Bioinformatics* **36**, 1925–1927 (2019).
50. Aramaki, T. *et al.* KofamKOALA: KEGG Ortholog assignment based on profile HMM and adaptive score threshold. *Bioinformatics* **36**, 2251–2252 (2020).
51. Eddy, S. R. *hmmer*. (2015).
52. Zhou, Z. *et al.* METABOLIC: High-throughput profiling of microbial genomes for functional traits, biogeochemistry, and community-scale metabolic networks. *bioRxiv (pre-print)* 30 (2020).
53. Fu, L., Niu, B., Zhu, Z., Wu, S. & Li, W. CD-HIT: accelerated for clustering the next-generation sequencing data. *Bioinformatics* **28**, 3150–3152 (2012).
54. Edgar, R. C. MUSCLE: a multiple sequence alignment method with reduced time and space complexity. *BMC Bioinformatics* **5**, 1–19 (2004).
55. Gionfriddo, C. M. *et al.* Hg-MATE-Db.v1.01142021. (2021).

56. Stamatakis, A. RAxML version 8: a tool for phylogenetic analysis and post-analysis of large phylogenies. *Bioinformatics* **30**, 1312–1313 (2014).
57. Schliep, K. P. phangorn: phylogenetic analysis in R. *Bioinformatics* **27**, 592–593 (2011).
58. Yu, G., Smith, D. K., Zhu, H., Guan, Y. & Lam, T. T. ggtree: an R package for visualization and annotation of phylogenetic trees with their covariates and other associated data. *Methods Ecol. Evol.* **8**, 28–36 (2017).
59. Gionfriddo, C. M. *et al.* An improved hgcAB primer set and direct high-throughput sequencing expand Hg-methylator diversity in nature. *Front. Microbiol.* **11**, 1–23 (2020).
60. Matsen, F. A., Kodner, R. B. & Armbrust, E. V. pplacer: linear time maximum-likelihood and Bayesian phylogenetic placement of sequences onto a fixed reference tree. *BMC Bioinformatics* **11**, 1–16 (2010).
61. Goñi-Urriza, M. *et al.* Genome insights of mercury methylation among *Desulfovibrio* and *Pseudodesulfovibrio* strains. *Research in Microbiology* **171**, 3–12 (2020).
62. Parks, J. M. *et al.* The genetic basis for bacterial mercury methylation. *Science* **339**, 1332–1335 (2013).
63. Ranchou-Peyruse, M. *et al.* Overview of mercury methylation capacities among anaerobic bacteria including representatives of the sulphate-reducers: implications for environmental studies. *Geomicrobiology Journal* **26**, 1–8 (2009).
64. Bowers, R. M. *et al.* Minimum information about a single amplified genome (MISAG) and a metagenome-assembled genome (MIMAG) of bacteria and archaea. *Nat Biotechnol* **35**, 725–731 (2017).
65. Levar, C. E., Chan, C. H., Mehta-Kolte, M. G. & Bond, D. R. An Inner Membrane Cytochrome Required Only for Reduction of High Redox Potential Extracellular Electron Acceptors. *mBio* **5**, e02034-14 (2014).
66. Levar, C. E., Hoffman, C. L., Dunshee, A. J., Toner, B. M. & Bond, D. R. Redox potential as a master variable controlling pathways of metal reduction by *Geobacter sulfurreducens*. *ISME J* **11**, 741–752 (2017).
67. Aklujkar, M. *et al.* The genome of *Geobacter bemidjiensis*, exemplar for the subsurface clade of *Geobacter* species that predominate in Fe(III)-reducing subsurface environments. *BMC Genomics* **11**, 490 (2010).
68. Jones, D. S. *et al.* Molecular evidence for novel mercury methylating microorganisms in sulfate-impacted lakes. *ISME J* (2019) doi:10.1038/s41396-019-0376-1.
69. Podar, M. *et al.* Global prevalence and distribution of genes and microorganisms involved in mercury methylation. *Sci. Adv.* **1**, 1–12 (2015).
70. Eckley, C. S. *et al.* Mercury methylation in the hypolimnetic waters of lakes with and without connection to wetlands in northern Wisconsin. *Can J Fish Aquat Sci* **62**, 400–411 (2005).
71. Watras, C. J. *et al.* Methylmercury production in the anoxic hypolimnion of a dimictic seepage lake. *Water, Air, and Soil Pollution* **80**, 735–745 (1995).
72. Lepak, R. F. *et al.* Factors affecting mercury stable isotopic distribution in piscivorous fish of the Laurentian Great Lakes. *Environ. Sci. Technol.* **52**, 2768–2776 (2018).
73. Ebel, W. J. & Koski, C. H. *Limnology of Brownlee Reservoir 1962 - 1964*. 42 (1964).
74. Watras, C. J. *et al.* Bioaccumulation of mercury in pelagic freshwater food webs. *Science of The Total Environment* **219**, 183–208 (1998).

75. Berg, J. S. *et al.* Intensive cryptic microbial iron cycling in the low iron water column of the meromictic Lake Cadagno: A cryptic microbial iron cycle. *Environmental Microbiology* **18**, 5288–5302 (2016).
76. Chadwick, S. P., Babiarz, C. L., Hurley, J. P. & Armstrong, D. E. Influences of iron, manganese, and dissolved organic carbon on the hypolimnetic cycling of amended mercury. *Science of The Total Environment* **368**, 177–188 (2006).
77. Liu, Y.-R. *et al.* Unraveling microbial communities associated with methylmercury production in paddy soils. *Environ. Sci. Technol.* **52**, 13110–13118 (2018).
78. Bravo, A. G. *et al.* Geobacteraceae are important members of mercury-methylating microbial communities of sediments impacted by waste water releases. *ISME J* **12**, 802–812 (2018).
79. Bravo, A. G. *et al.* Methanogens and iron-reducing bacteria: the overlooked members of mercury-methylating microbial communities in boreal lakes. *Appl Environ Microbiol* **84**, e01774-18, /aem/84/23/e01774-18.atom (2018).
80. Nealson, K. H. & Myers, C. R. Microbial reduction of manganese and iron: new approaches to carbon cycling. *Appl Environ Microbiol* **58**, 439–443 (1992).
81. Schaefer, J. K. & Morel, F. M. M. High methylation rates of mercury bound to cysteine by *Geobacter sulfurreducens*. *Nature Geosci* **2**, 123–126 (2009).
82. Gilmour, C. C. *et al.* Mercury methylation by novel microorganisms from new environments. *Environ. Sci. Technol.* **47**, 11810–11820 (2013).
83. Alpers, C. N. *et al.* Mercury cycling in agricultural and managed wetlands, Yolo Bypass, California: Spatial and seasonal variations in water quality. *Science of The Total Environment* **484**, 276–287 (2014).
84. Schaefer, J. K., Kronberg, R., Björn, E. & Skjellberg, U. Anaerobic guilds responsible for mercury methylation in boreal wetlands of varied trophic status serving as either a methylmercury source or sink. *Environ Microbiol* **22**, 3685–3699 (2020).

Appendix to Chapter 3: Supplementary tables and figures

Supplementary Tables: All supplementary data and tables can be found here:

<https://figshare.com/account/home#/projects/117342>

Supplementary Data 3.1: Includes all supplementary tables.

Table S1: Metagenome reads counts.

Table S2: Assembly statistics for all 12 assemblies used in analyses.

Table S3: *hgcA* information, including quality, classifications, binning, *hgcB* information and abundance.

Supplementary Data 3.2: Includes quality and subset of metabolic data for *hgcA*⁺ bins.

Supplementary Figures:

Figure S3.1: Profiles of physical and geochemical parameters and gene abundances of selected genes at RM286 in 2017 (A) and 2018 (B). Gene abundances for *narG*, *dsrA*, and *dsrD* are normalized to the mean abundance of 16 ribosomal proteins. *narG* is a respiratory nitrate reductase. *dsrA* and *dsrD* are two genes in the operon encode dissimilatory sulfite reductase. We only included *dsrA* were confirmed to be from the reductive class of *dsrA*.

Figure S3.2: Profiles of physical and geochemical parameters and gene abundances of selected genes at RM300 in 2017 (A) and 2018 (B). Gene abundances for *narG*, *dsrA*, and *dsrD* are normalized to the mean abundance of 16 ribosomal proteins. *narG* is a respiratory nitrate reductase. *dsrA* and *dsrD* are two genes in the operon encode dissimilatory sulfite reductase. We only included *dsrA* were confirmed to be from the reductive class of *dsrA*.

Figure S3.3: Profiles of physical and geochemical parameters and gene abundances of selected genes in 2019 at RM300 (A) and RM310 (B). Gene abundances for *narG*, *extE*, *dsrA*, and *dsrD* are normalized to the mean abundance of 16 ribosomal proteins. *narG* is a respiratory nitrate reductase. The *extE* genes all have adjacent multiheme cytochrome c genes and were phylogenetically closely related to *extE*. *dsrA* and *dsrD* are two genes in the operon encode dissimilatory sulfite reductase. We only included *dsrA* were confirmed to be from the reductive class of *dsrA*.

Figure S3.4: Profile of Hg species with supplementary geochemistry data from RM286 in 2017 (A) and 2018 (B). DO = dissolved oxygen in mg/L; Mn = dissolved manganese in mg/L; iHg = inorganic mercury in ng/L; MeHg = methylmercury in ng/L.

Figure S3.5: Profile of Hg species with supplementary geochemistry data from RM300 in 2017 (A) and 2018 (B). DO = dissolved oxygen in mg/L; Mn = dissolved manganese in mg/L; iHg = inorganic mercury in ng/L; MeHg = methylmercury in ng/L.

Figure S3.6: Profile of Hg species with supplementary geochemistry data in 2019 from RM300 (A) and RM310 (B). DO = dissolved oxygen in mg/L; Mn = dissolved manganese in mg/L; iHg = inorganic mercury in ng/L; MeHg = methylmercury in ng/L.

Figure S3.7: Alignment of HgcA amino acid sequences identified from this study. This includes all identified sequences before dereplication. The entire sequence is shown in (A), while (B) is zoomed in on the corrinoid-binding domain. Purple line outlines the highly conserved cap helix domain.

Figure S3.8: Maximum likelihood phylogenetic tree of HgcA amino acid sequences. Tree was generated using RAxML and was rooted using paralog sequences that were included in tree generation and removed later.

Figure S3.9: Maximum likelihood phylogenetic tree of concatenated alignment of 16 ribosomal proteins from bins within the Kiritimatiellaeota and Lentisphaerae phyla. References were obtained from NCBI RefSeq and GenBank databases. Tree was generated using RAxML and was rooted using two Planctomycetes genomes (shown in tree).

Figure S3.10: Maximum likelihood phylogenetic tree of concatenated alignment of 16 ribosomal proteins from bins within the Bacteroidales order. References were obtained from the NCBI RefSeq and GenBank databases. Tree was generated using RAxML and was rooted using two Flavobacteriales genomes (shown in tree).

Figure S3.1

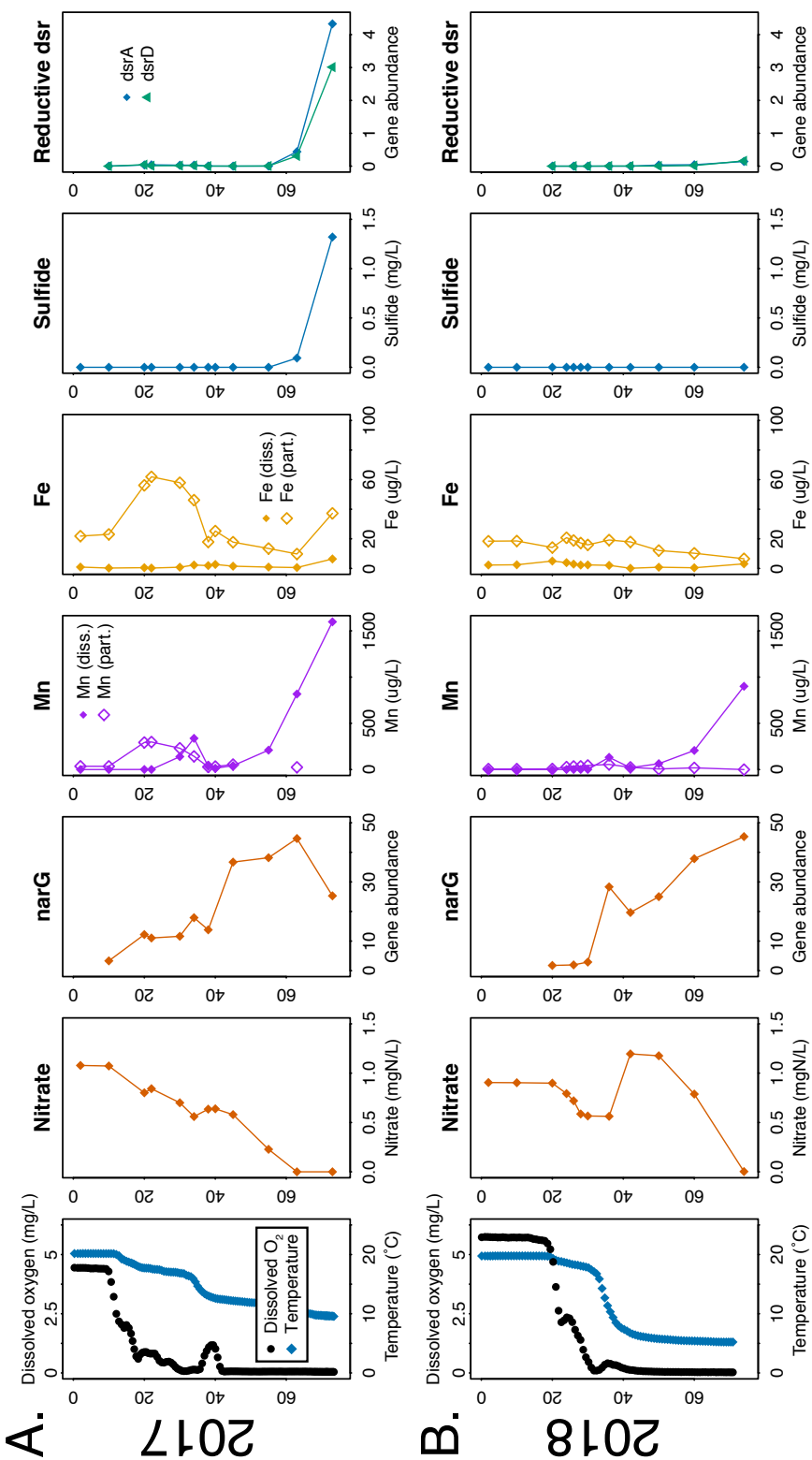


Figure S3.2

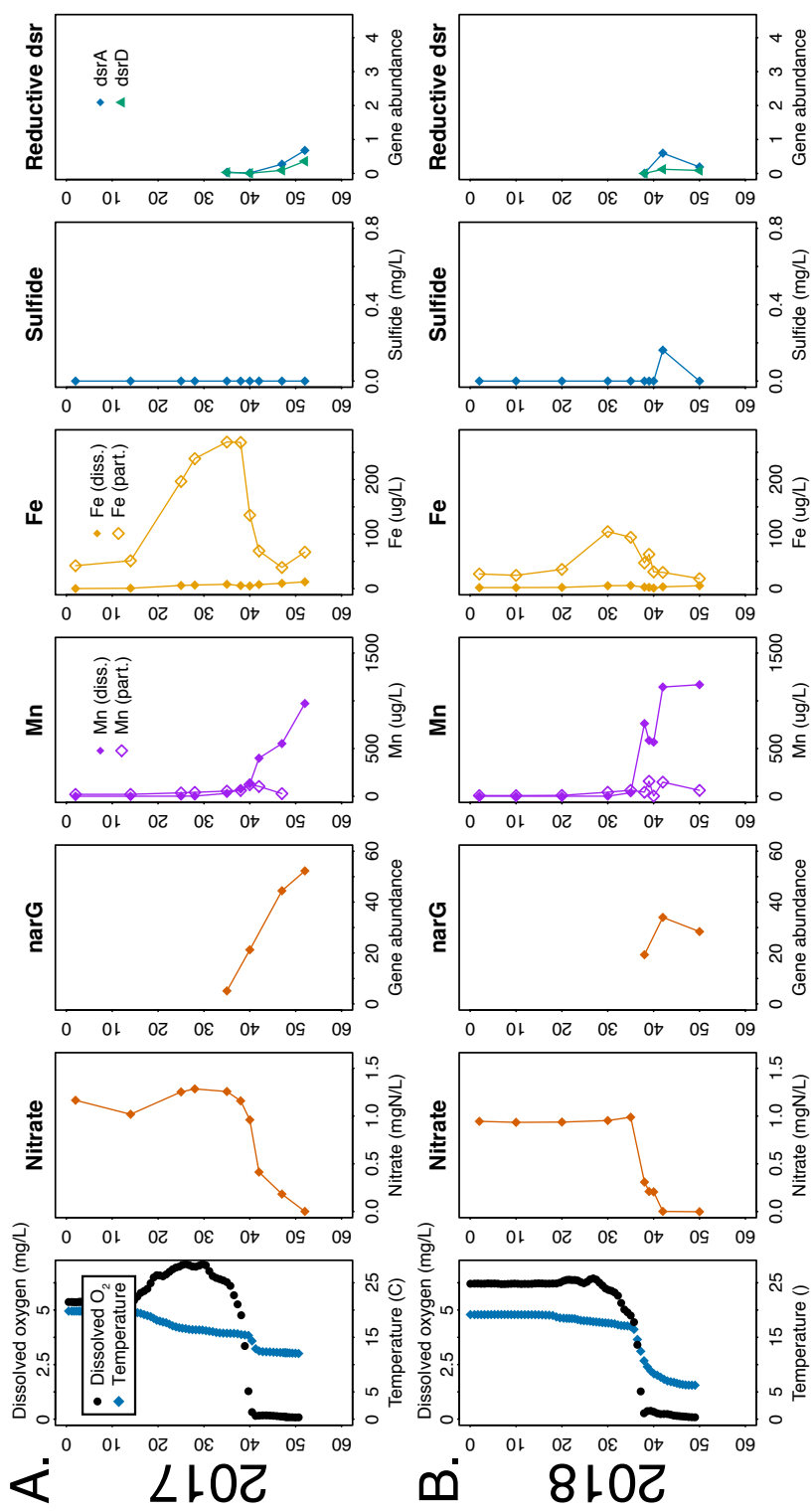


Figure S3.3

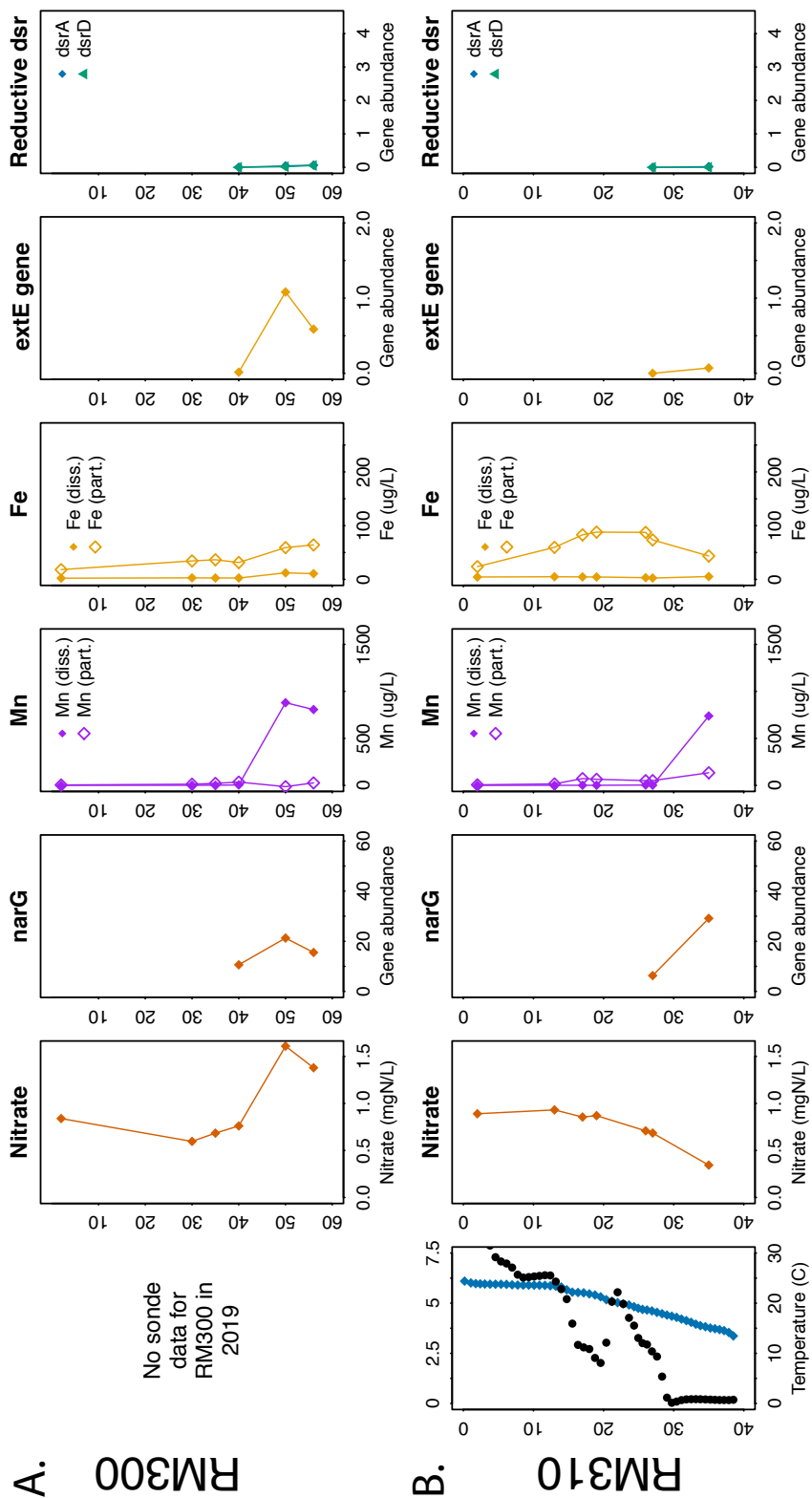


Figure S3.4

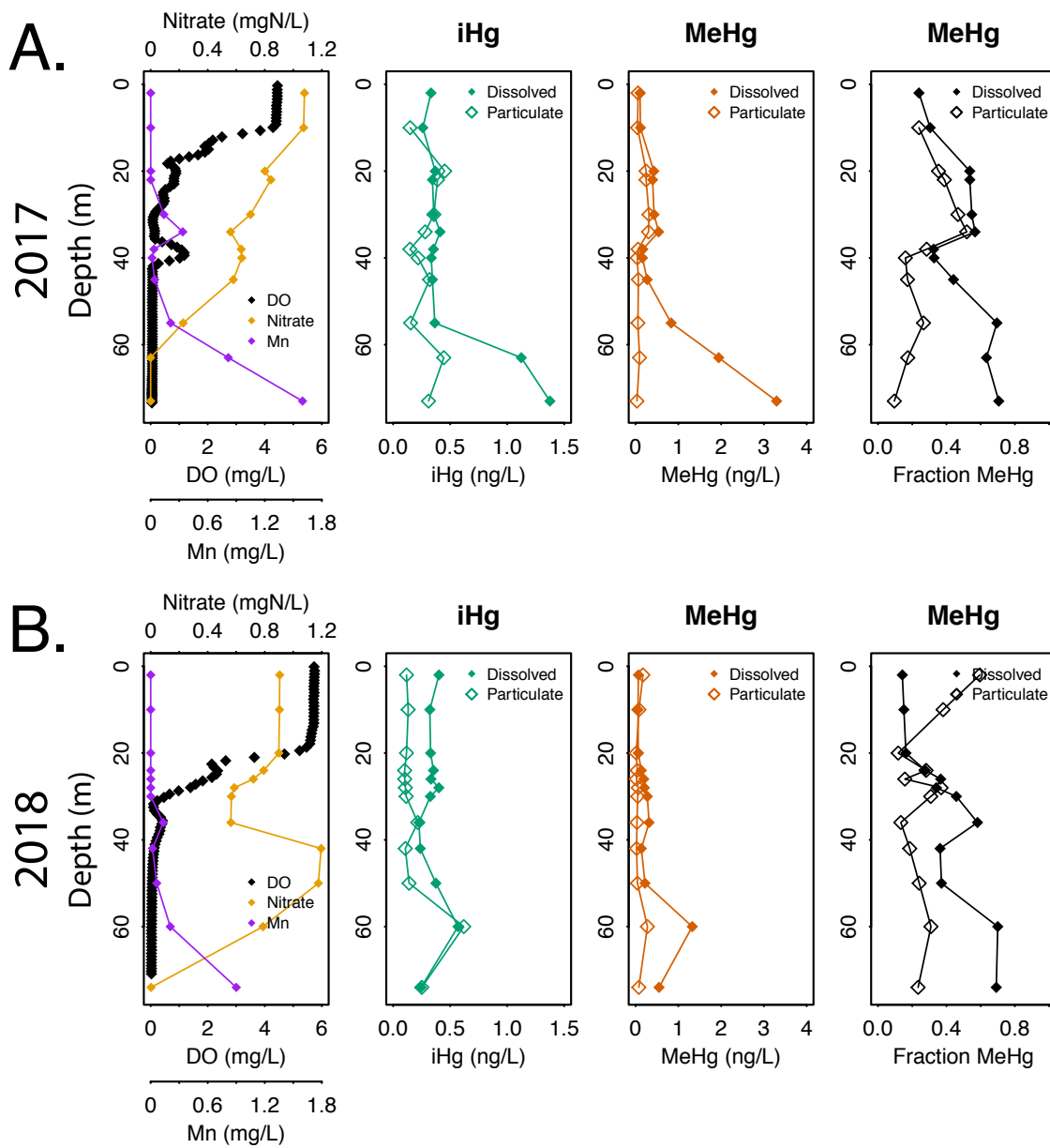


Figure S3.5

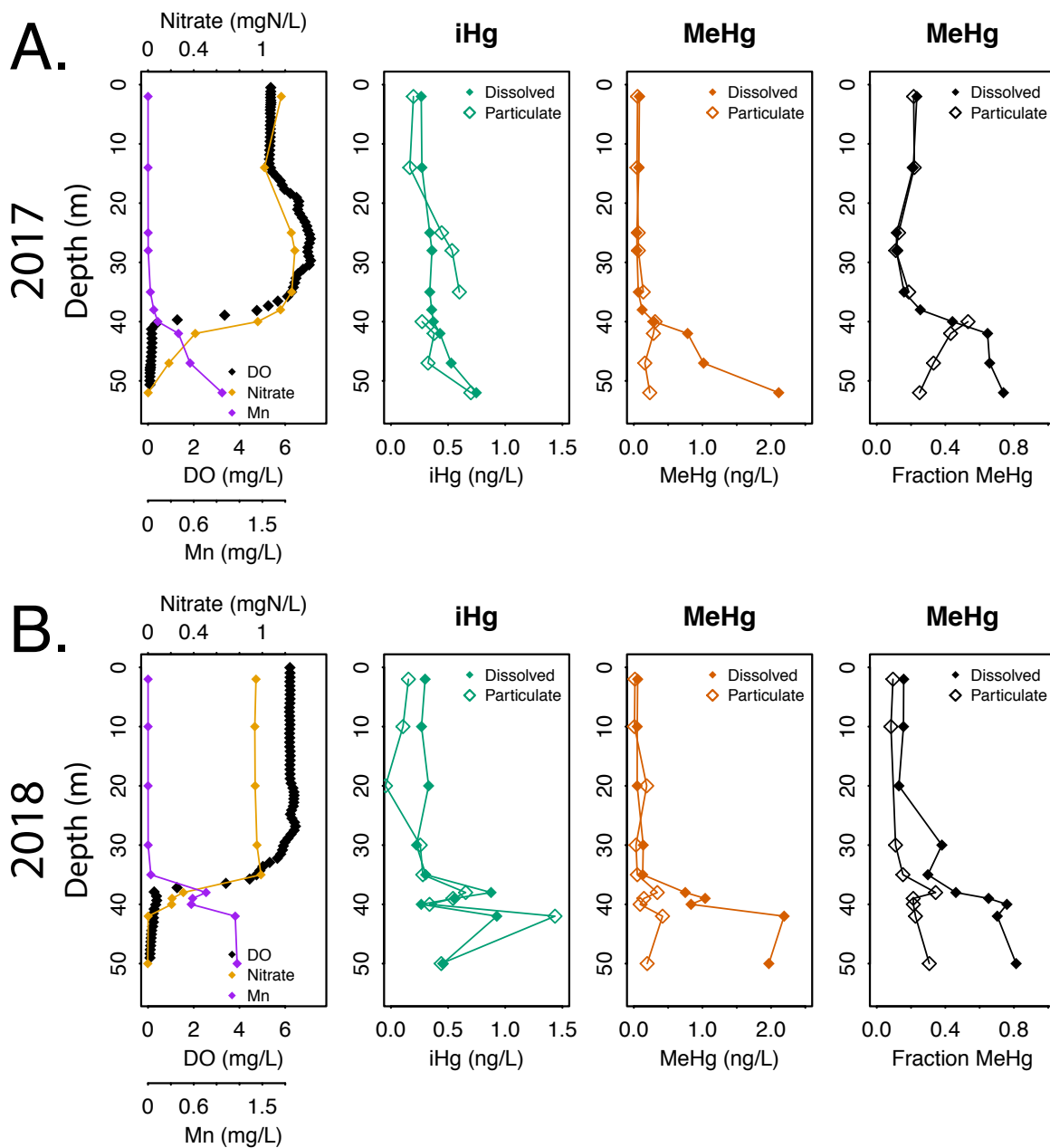


Figure S3.6

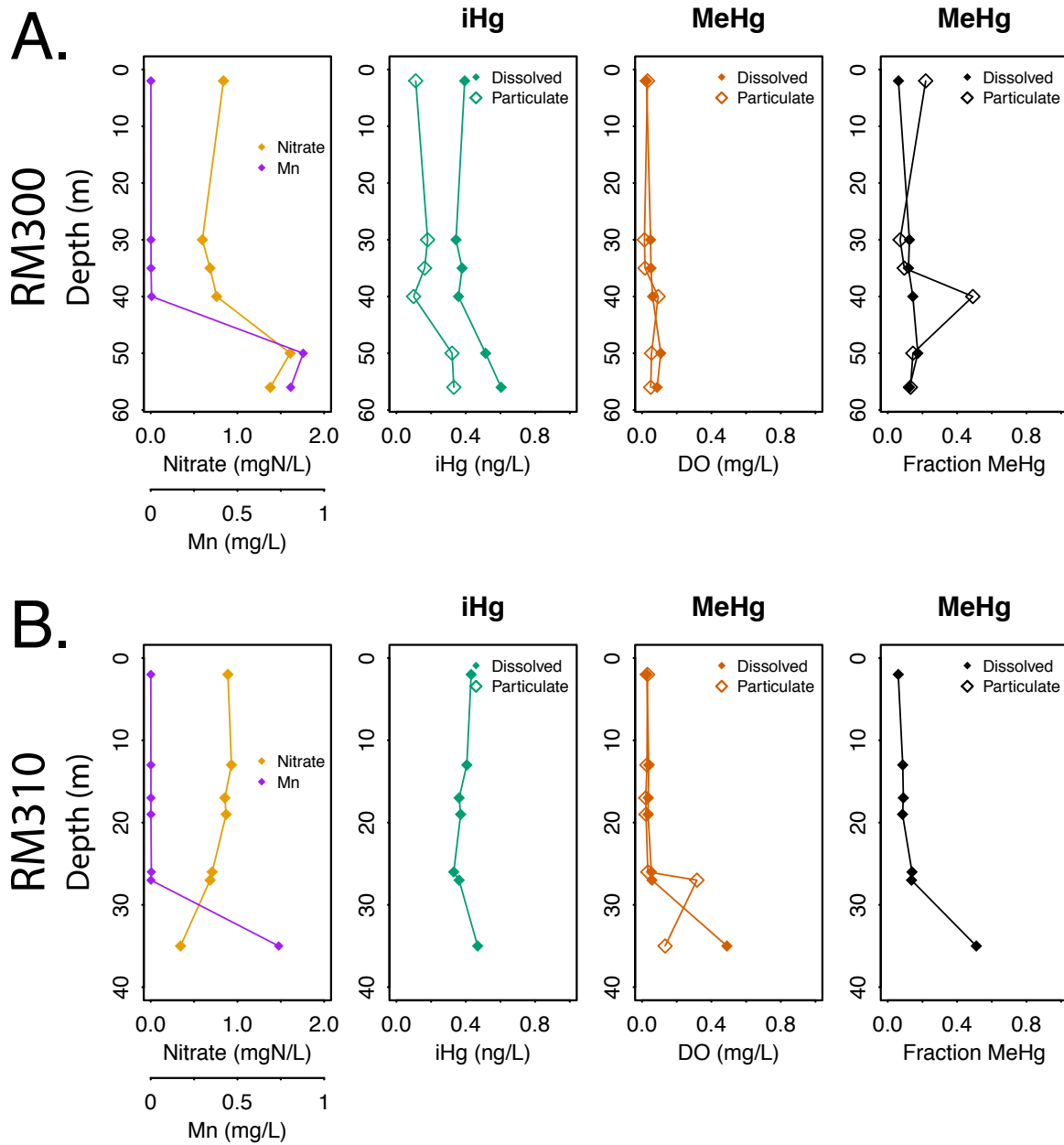


Figure S3.8

This study
Peterson et al, 2020
Jones et al, 2019
Hg-MATE references

0.5

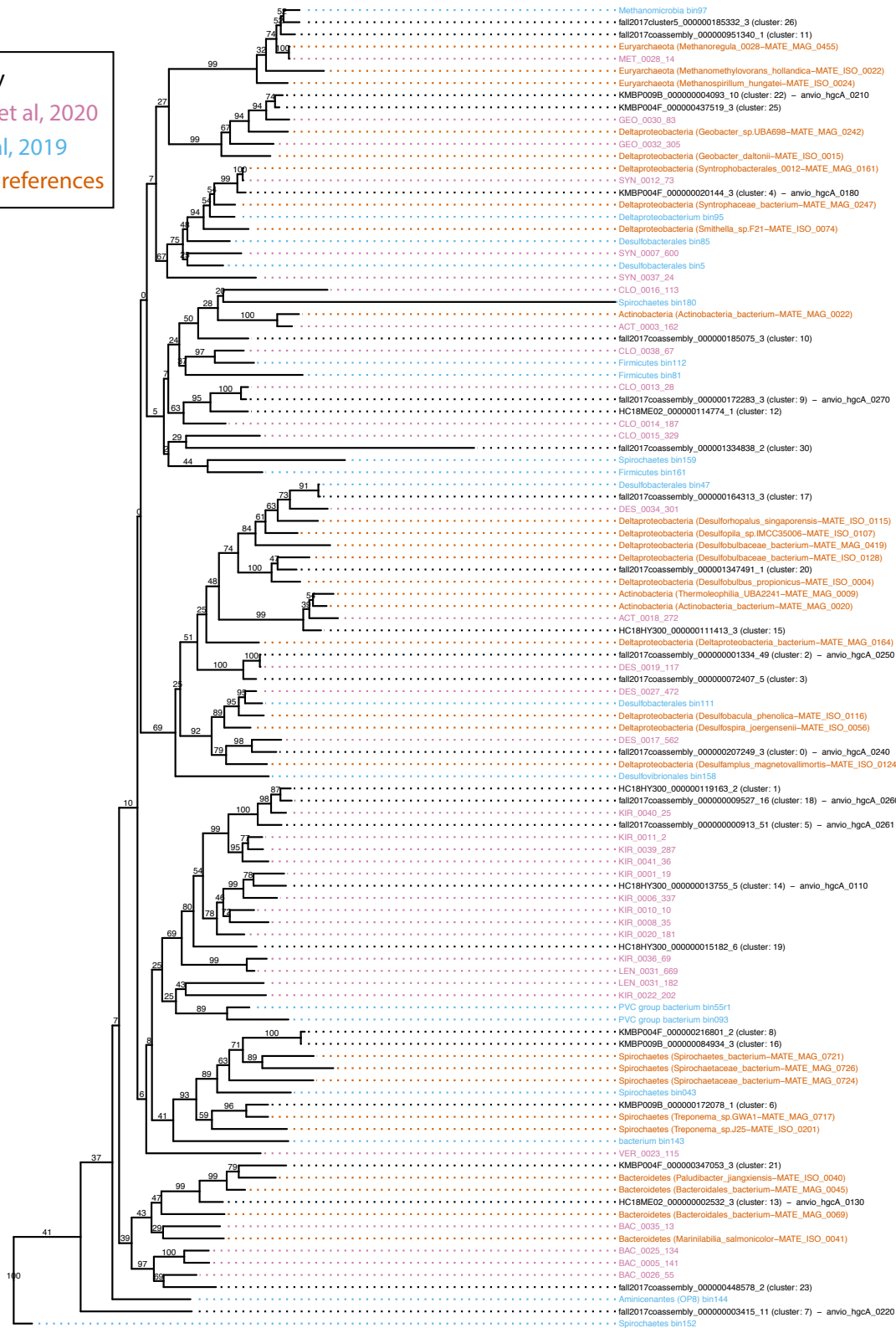


Figure S3.9

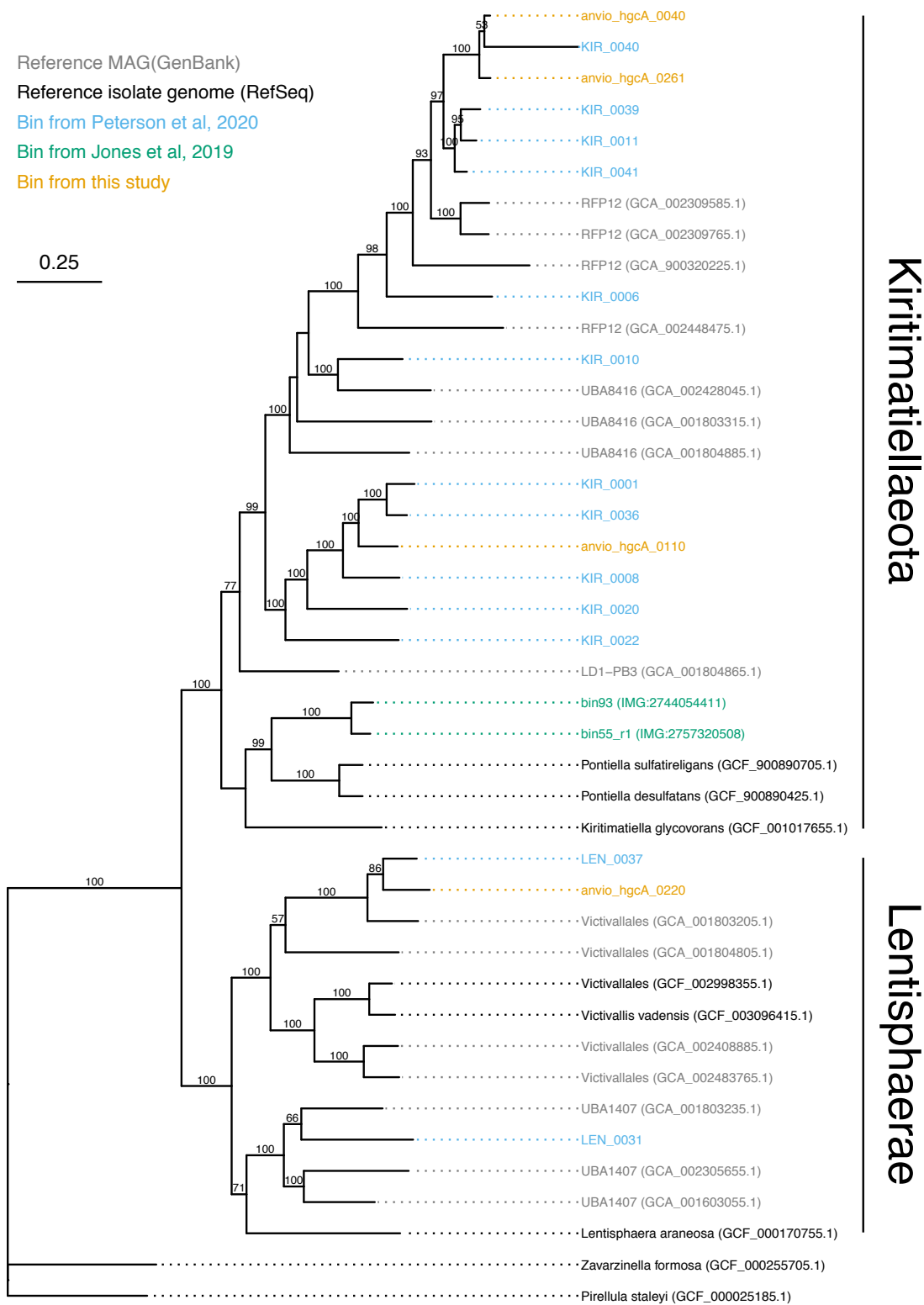


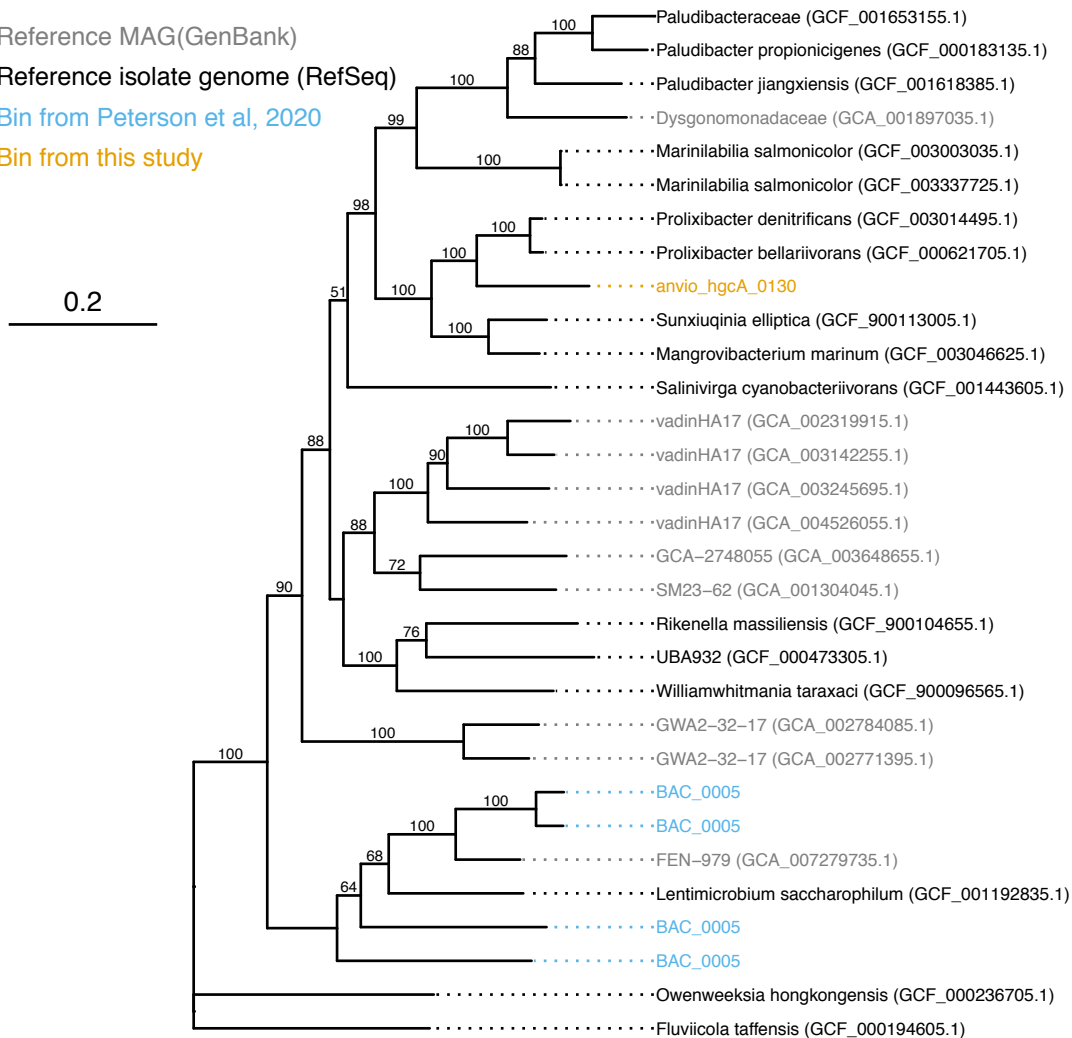
Figure S3.10

Reference MAG(GenBank)

Reference isolate genome (RefSeq)

Bin from Peterson et al, 2020

Bin from this study



Chapter 4: Microbial constraints on methylmercury production along a sulfate gradient in the Florida Everglades.

This chapter has been prepared as a manuscript for submission for peer review and publication.

Co-authored with Brett A. Poulin, David P. Krabbenhoft, and Katherine D. McMahon.

Abstract

Methylmercury (MeHg) production is constrained by both abiotic geochemical factors that control inorganic mercury (iHg) bioavailability to methylating organisms and biotic factors that control MeHg production. Geochemical influences on iHg bioavailability include inorganic sulfide levels and dissolved organic matter (DOM) composition, but the influence of the in situ microbial community on MeHg production is poorly understood. In this study, we used stable isotope-enriched Hg tracer incubations with an array of different porewaters used for tracer preparation. By using these multiple tracer preparations, we separately characterized the impact of the bioavailability of the Hg tracer due to porewater matrix composition and the Hg-methylating capacity of the microbial community in the sediment core on the production of MeHg. Incubations were paired with shotgun metagenomic sequencing to characterize the Hg-methylating community. The relative Hg methylation capacity increased as sulfate levels decreased and was significantly correlated with the relative abundance of the Hg-methylating gene *hgcA*. Hg-methylating organisms were dominated by methanogenic archaea and an array of non-traditional Hg-methylators, including some from Spirochaetes, Chloroflexi, and Aminicenantales. These results show that *hgcA* abundance can be a reliable marker for Hg-methylation capacity of microbial communities and that, at least in these sediments, Hg-methylation capacity of the microbial community is a limiting factor on MeHg production under high sulfide conditions, but not under low sulfide conditions. More broadly, this work provides a framework to measure the relative Hg-methylation capacity of the microbial community in isolation and probe the microbial community underlying that capacity using molecular sequencing tools.

Introduction

Methylmercury (MeHg) is produced under low-redox environments by organisms with the *hgcA* gene¹. MeHg is highly bioaccumulative and can cause Hg enrichment in the aquatic food web², leading to toxic levels in aquatic organisms.^{3,4} MeHg production is controlled primarily by two factors: the abiotic constraint on bioavailability of iHg for active and/or passive uptake by methylating organisms⁵⁻⁷ and the Hg-methylating potential of the microbial community⁸⁻¹¹. Either of these factors can be the rate-limiting step in MeHg production, depending on conditions.¹² *In situ*, these factors interact to produce patterns in MeHg loads in both the environment and the food web. For example, in sites with a large sulfate/sulfide gradient, MeHg often displays a “Goldilocks curve”, where there is high MeHg production at intermediate levels of sulfate and low MeHg at the high and low end.¹³ It is hypothesized that this curve is controlled by the interaction of increasing iHg bioavailability and decreasing microbial Hg-methylation activity along this gradient.¹⁴ The increased bioavailability is ascribed to smaller HgS aggregates as decreasing sulfide concentrations lead to reduced HgS polymerization. However, bioavailability is also controlled by dissolved organic matter (DOM) quantity^{15,16} and quality, such as the reduced S-content^{17,18} or the aromaticity^{19,20}, which complicate the relationship between water chemistry and MeHg production. The hypothesized decrease in microbial Hg-methylation activity is thought to be due to decreased activity of sulfate-reducing bacteria (SRB), often thought to be the dominant Hg-methylators in aquatic ecosystems^{1,21,22}.

The influence of microbial methylation capacity and local biogeochemical conditions on MeHg production is still poorly understood. Even in the lab, different microbes produce MeHg at drastically different rates^{8,9,23}, as do single cultures of microbes under different metabolic

conditions²⁴. In natural systems, using the *hgcA* gene as a marker for methylation capacity²⁵, the metabolic and phylogenetic diversity of potential Hg-methylating organisms is expansive.^{8,26,27} Even in sulfate-enriched sites, many of the microbes with *hgcA* (*hgcA*⁺) are not SRB but included fermentative organisms, putative syntrophs, methanogens, and iron/manganese reducers.²⁸⁻³¹ Reflective of this diversity is the site-specific response of MeHg production to molybdate inhibition³¹⁻³⁸ or sulfate amendment^{22,30}. In one sulfide-rich site, sulfate-induced reductions in MeHg production were attributed to decreases in *hgcA* diversity.³⁰ Surprisingly, some sites can show molybdate inhibition of MeHg production while identifying few SRB-associated *hgcA* at the same site.^{31,33} Thus, the relationship between the Hg-methylation capacity of the microbial community and sulfate reduction may be more complicated than previously expected. However, precise comparisons of the microbial methylation capacity across and within study systems is difficult due to the interacting effects of abiotic and biotic factors.

The Florida Everglades is an ideal site to study the impact of sulfate levels on MeHg production and accumulation in aquatic food webs. Abundant DOM and warm, shallow waters lead to prime biogeochemical conditions for the efficient transformation of iHg into MeHg.³⁹ This leads to elevated Hg in aquatic food webs, which subsequently results in fish consumption advisories for much of the Everglades system.³⁹ This efficient MeHg production has been linked to the sulfate gradient caused by sulfate-containing agricultural runoff in the northern Water Conservation Area (WCA) 2A, which is diluted as the Everglades become more ombrotrophic to the south in WCA-3A.¹⁴ MeHg levels exhibit the classic “Goldilocks curve”, with low MeHg levels at high and low sulfate concentrations but high MeHg at intermediate concentrations, along this gradient in the water column, peat cores, and aquatic food web.^{13,14} In addition to changes in sulfate and sulfide across this gradient, there are changes in the DOM’s S-content^{40,41}

and aromaticity⁴², suggesting a complex array of factors controlling bioavailability of Hg. Functional assays and *hgcA* amplicon sequencing suggest that Hg methylation is mediated by phylogenetically and metabolically diverse microorganisms throughout different ecological compartments in the Everglades,^{31,43} highlighting the need to identify the patterns in Hg methylation capacity that underlie the MeHg Goldilocks curve.

In this study, we set out to define shifts in the Hg methylation capacity of the microbial community independent of changes in bioavailability and to investigate how the Hg-methylating microbial community underlies these shifts. We used the results of a full-factorial Hg methylation experiment on the ability of different porewater matrices to quantify the relative Hg methylation potential (RMP) of microbial communities in peat across a sulfate gradient in the Florida Everglades. We then found a linear relationship between the RMP and relative *hgcA* abundance. We identified a consistent increase in the methylation capacity of the microbial community across the sulfate gradient, which correlated closely with an increase in the *hgcA* content of the microbial community. Genome reconstruction suggested that *hgcA* genes are dominated by those associated with methanogenic and fermentative organisms and did not include any SRB. This study indicates that the biotic and abiotic factors that underlie the MeHg Goldilocks curve are more complicated than previously described and that *hgcA* gene abundance may be a reliable marker for the relative methylation capacity of the microbial community. Overall, this study lays the groundwork for mechanistic studies of microbial communities' methylation capacity *in situ*.

Materials and methods

Study Site: Samples were collected along a hydrologic flow path in Water Conservation Areas 2A and 3A in December 2019 (Figure 1a). Agricultural run-off into the northern part of the Everglades results in high sulfate levels at the north end that decrease along the flow path. A separate control site was sampled in the Arthur R. Marshall Loxahatchee National Wildlife Refuge. Nineteen replicate sediment cores were collected at each site, 18 of which were dedicated to the factorial methylation experiment and the last for the metagenomic analysis. Each core was collected with a 10 cm diameter thin-walled lexan tube that had a medical-grade stainless steel cutting edge affixed to the downward end for cutting through the emergent grass roots. The core tubes had pre-drilled 1 mm diameter holes every 1 cm along its length, which were sealed with silicone glue. After the collection of each core, each end of the tube was quickly sealed with caps to minimize oxygen intrusion. The core for metagenomic sequencing was sealed and stored on ice until it could be frozen on dry ice within 12 hours. Porewater samples for geochemistry were collected using a solid Teflon sipper, constructed of 2.5 cm diameter Teflon rod that had a 0.5 cm hole bored out over its length and small diameter slits cut into the sides of the rod over the last 1 cm. The sipper was inserted into the peat to a depth of 5 cm to allow active but gentle pumping of porewater from the 4.5 to 5.5 cm depth interval at each site. Porewater to be used as a matrix for the spiking solution were collected from all six sampling stations and filtered through an in-line 0.45 μm poresize filter into N_2 -purged collection vessels. Water samples for sulfide analysis were preserved in sulfide anti-oxidant buffer and samples for anion analysis were frozen on dry ice. After collection, cores were sealed and stored in coolers in the dark until they could be frozen on dry ice within 24 hours of collection.

Hg methylation incubations: Filtered porewaters were purged with N₂ for 20 minutes back in the lab, then the enriched ²⁰¹Hg(II) tracer was added. The tracer was allowed to equilibrate for four hours before initiating injections of Hg tracers into each core. For each pair of porewater and sediment core (Fig. S4.2), equilibrated tracer was then injected into the center of the core at 1 cm intervals over the top 10 cm of the core. Cores were incubated for 24 hours, then frozen on dry ice. Back in the lab, the top 2 cm of the frozen sediment core was removed, the next 4 cm was homogenized and saved for analysis, and the rest was discarded. ²⁰¹HgT was quantified by oxidation with bromine monochloride and tin reduction coupled to cold vapor atomic fluorescence spectrometry.⁴⁴ Me²⁰¹Hg was analyzed by distillation, separation with gas chromatography, and quantification by isotope dilution using inductively couple plasma mass spectrometry.^{45,46}

DNA Extraction and Metagenomic Processing: Cores for sequencing were cut to match the analysis of the incubation cores. Frozen sediment was homogenized in a sterile bag. DNA was extracted using a modified phenol:chloroform extraction.⁴⁷ Briefly, cells were lysed using freeze:thaw cycles and a lysis buffer/SDS mix. Polyphenols and polysaccharides were precipitated out using PVPP and CTAB. DNA was extracted using phenol:chloroform and washed with 100% chloroform, then purified with isopropanol and ethanol precipitation then suspended in 100µl of nuclease-free water. Library preparation and shotgun sequencing was completed at QB3 Genomics at the University of California at Berkeley (Berkeley, CA). Libraries were prepared using a Kapa Biosystem Library Prep kit with a target insert length of ~600 bp (Kapa Biosystems, Wilmington, MA). Sequencing was done on an Illumina NovaSeq using the S4 kit to generate 150 bp paired reads (Illumina, Inc., San Diego, CA). Reads were trimmed and overlapping reads were merged using fastp (v0.20.1)⁴⁸. Metagenomes from the

same site were assembled using both MegaHit (v1.2.9)⁴⁹ and metaSPADes (v3.14.1)⁵⁰. Open reading frames (ORFs) were predicted using Prodigal (v2.6.3).⁵¹ Paired, single, and merged reads were all mapped back to contigs using bowtie2 (v2.4.2).⁵² Abundance values for all genes were normalized to the average abundance of 16 ribosomal proteins (rp16) within a metagenome. Manual binning of genomes with *hgcA* was based on differential coverage and tetranucleotide frequency and done using CONCOCT (v1.1.0)⁵³ and anvi'o (v6.2)⁵⁴, resulting in 11 medium-quality bins⁵⁵ with *hgcA*, including two with a fused *hgcAB*.

hgcA analysis: All *hgcA* genes were identified using hmmsearch (hmmer, v3.3.1)⁵⁶ with a custom Hidden Markov Model (HMM)²⁹. Putative HgcA sequences were manually confirmed to have the cap helix domain and at least 4 transmembrane regions at the C-terminus end.²⁵ Sequences downstream of a confirmed *hgcA* gene were searched for *hgcB* sequences, also using a custom HMM²⁹. Sequences were dereplicated across assemblies at 94% identity using CD-HIT (v4.6)⁵⁷. All HgcA sequences were automatically classified using the reference package from the Hg-MATE database with a custom workflow⁵⁸. The HgcA proteins sequences were then aligned to the Hg-MATE database (v1, accessed 2021-01-26)⁵⁹ using MUSCLE (v3.8.31)⁶⁰. The alignment was masked in Geneious at any residue with >50% gaps. A maximum-likelihood tree was generated in RAxML (v8.2.11)⁶¹ using the LG substitution matrix and 400 rapid bootstraps.

Additional metagenomic analyses: Microbial community coverage and diversity was estimated using Nonpareil (v3.304)⁶² in kmer mode with a kmer length of 32 and 100,000 reads as a query. 16S genes were identified and classified using GraftM (0.13.1)⁶³ with the Silva database (v132). Distance between metagenomes was estimated using Mash (v2.2.2)⁶⁴ with a sketch size of 100,000 and a kmer size of 21 and subsequently ordinated using Principal Coordinate Analysis implemented in R. Metabolic proteins were initially identified in the ORFs

from both the assemblies and the bins using HMM profiles from TIGRFAM, KOFAM, and PFAM. When needed, the identity of these proteins was confirmed using phylogenetic trees, gene neighborhood analysis, and custom scripts looking for conserved domains. Bin completeness and redundancy was estimated using the checkM (v1.0.11)⁶⁵ lineage_wf workflow and taxonomy was estimated using the GTDB-TK (v0.1.1)⁶⁶ classify_wf workflow. Inferred phylogeny of the bins was based on phylogenetic reconstruction of the rp16 proteins.^{67,68}

Statistical analyses: To standardize results across all incubations, Me²⁰¹Hg was standardized to the measured ²⁰¹HgT concentrations. A two-way analysis of variance (ANOVA) was performed to evaluate the impact of sediment core source and porewater source on MeHg production and test for any interaction between the two variables. To isolate the impact of the sediment source on Me²⁰¹Hg production, we calculated a relative methylation potential (RMP) for each incubation, normalizing the Me²⁰¹Hg production to the highest RMP value for an incubation using porewater from the same source (Fig. S4.2). A linear correlation implemented in R was used to test the relationship between the RMP and the Hg-methylator abundance. The normality of the Me²⁰¹Hg values and of the residuals for both the two-way ANOVA and the linear model were evaluated using the Shapiro-Wilkes test.

Results

Six sites were sampled along a flow path in the Florida Everglades (Fig. 4.1). Geochemical analyses confirmed the presence of a sulfate gradient in the Water Conservation Area (WCA) sites, with surface water sulfate levels over 30 mg/L at the 2A sites but substantially lower in WCA 3A (Fig. 4.1b). Surface water sulfide was very low or undetectable at all sites except for 2A-N at the north end of WCA-2A (Fig. S4.1a). Dissolved organic carbon

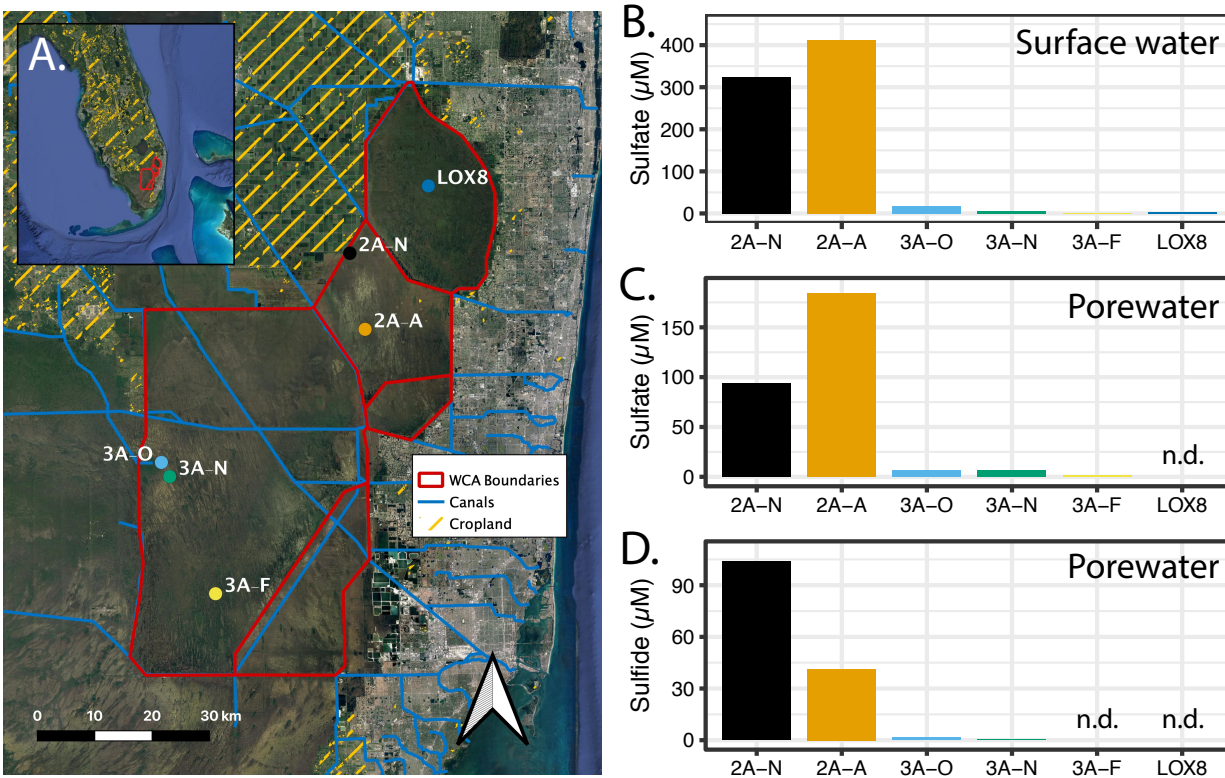


Figure 4.1: Sampling was conducted in the Water Conservation Areas (WCA) of the Florida Everglades, with one reference site in Loxahatchee (A). Sulfate-enriched runoff from the agricultural fields to the north drives a north-south gradient of sulfate in the surface water (B) and the porewater (C). This gradient is matched by the porewater sulfide levels (D).

(DOC) was highest in WCA 2A, ranging from 30-32 mg/L, but was consistently 17.8-21.6 mg/L through WCA 3A and at LOX8 (Fig. S4.1b). SUVA followed a similar trend, measuring 3.1-3.3 L/mg/m in WCA 2A and dropping to 2.1-2.4 L/mg/m in WCA 3A and LOX8 (Fig. S4.1c). Porewater sulfate was 9.0-17.7 mg/L in the porewaters in WCA 2A, dropping to 0.64 mg/L at 3A-O and continued to decrease at the more southern sites (Fig. 4.1c). Sulfate was not detectable in the porewater at LOX8. Sulfide levels in the WCA 2A porewater were 1.41-3.54 mg/L but dropped to 0.047 mg/L at 3A-O and continued to drop until it was below detection at 3A-F and LOX8 (Fig. 4.1d). Ambient MeHg levels in the sediment cores within the WCA exhibited the Goldilocks curve, with peak MeHg occurring at site 3A-O (Fig. 4.2a). LOX8 was an exception to this trend, where we recorded the highest MeHg levels despite porewater sulfate being below detection.

Next, we conducted MeHg production assays using a stable isotope-enriched Hg tracer. The tracer was pre-equilibrated with filtered porewater to allow the $^{201}\text{Hg}(\text{II})$ tracer to bind to the ligands in the filtered porewater before injection into sediment cores collected from each of the field sites. (Fig. S4.2). We then conducted a full-factorial experiment where duplicate cores from each site were injected with tracer that was pre-equilibrated using porewater from each site (Fig. S2). MeHg production was measured as a percent of the total ^{201}Hg pool (^{201}HgT) that was converted to MeHg. Me^{201}Hg production in the incubations ranged from 0% to 8% of ^{201}HgT (Fig S4.3). In the WCAs, Me^{201}Hg production assays under ambient conditions (when the porewater for equilibration was injected into a peat core from the same site) showed highest Me^{201}Hg production levels in the middle of the sulfate gradient at 3A-O, with lower levels at higher and lower concentrations of sulfate (Fig. 4.2b). LOX8 was the exception again, showing elevated Me^{201}Hg production despite below-detection levels of sulfate in the sediment.

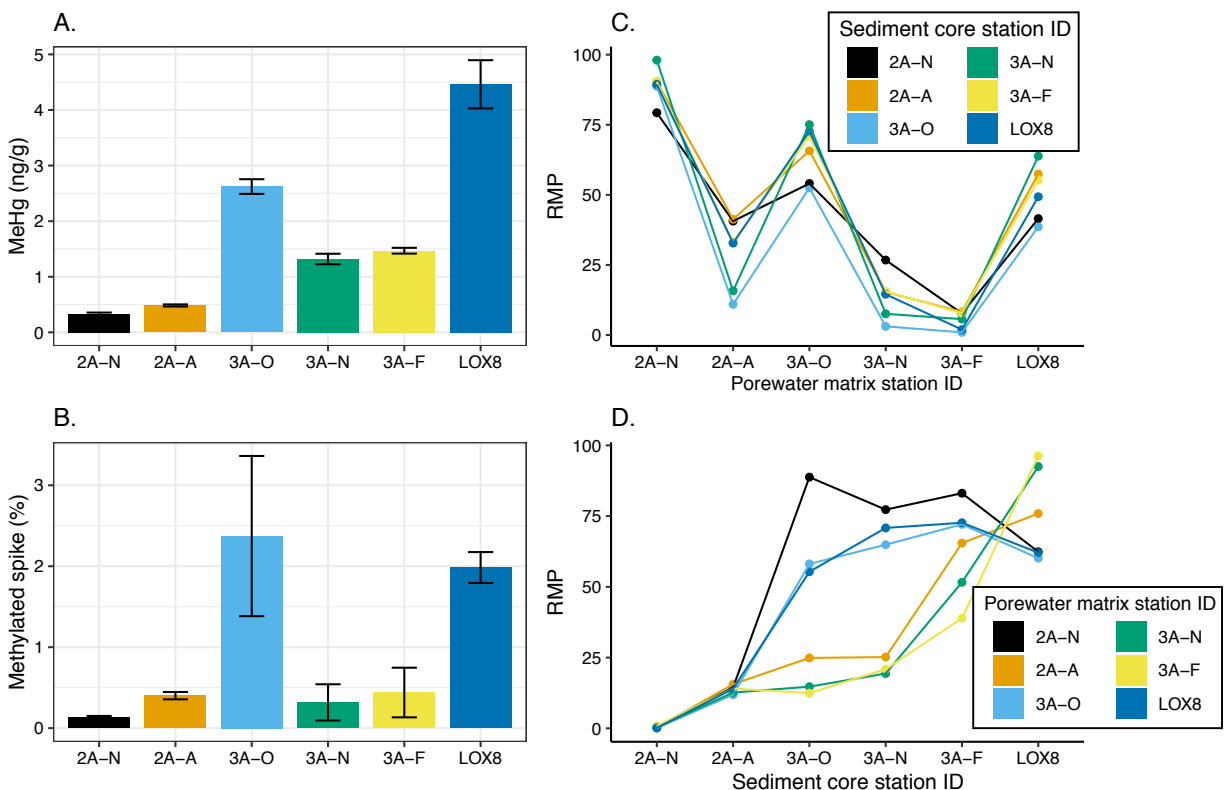


Figure 4.2: Ambient MeHg levels in the sediment cores used for incubation analysis show distinct peaks at 3A-O and LOX8 (A). MeHg production under ambient conditions, where the porewater matrix used for tracer equilibration was from the same station as the core, also shows distinct peaks at 3A-O and LOX8 (B). The relative methylation potential (RMP) of the porewaters used for tracer equilibration is highest at 2A-N, 3A-O, and LOX8 (C). RMP of the sediment cores from each station increases down the sulfate gradient (D). Three of the porewaters, however, lead to a plateau in RMP for the sediment cores over the 3A and LOX8 sites. Error bars in A and B represent the standard error.

We hypothesized that the bioavailability of the ^{201}HgT would be determined by the porewater matrix used for pre-equilibration, while the Hg methylation capacity was determined by the microbial community in the sediment core. If these two factors are mostly independent and neither is strictly rate-limiting, the influence of each variable on *in situ* Me^{201}Hg production could be isolated. We first needed to confirm that these effects were indeed independent. A two-way analysis of variance (ANOVA) with interaction showed a significant effect of both sediment core source ($p \ll 0.0001$) and porewater matrix source ($p \ll 0.0001$) on Me^{201}Hg production but no interaction effect ($p = 0.294$). However, the residuals of the model were not normally distributed ($p = 0.0016$), limiting our trust in this analysis. We then plotted the Me^{201}Hg production values, faceted by the sediment core source location (Fig. S4.3). Me^{201}Hg production responded consistently to different porewaters, across sediment cores from all stations. For example, pre-equilibration of the ^{201}Hg tracer with porewater from site 2A-N consistently resulted in the highest production of Me^{201}Hg , while using porewater from 3A-F resulted in the lowest Me^{201}Hg production (Fig. S4.3). To confirm this consistent response, we first grouped the Me^{201}Hg production values by the sediment core station of origin. Then, within each group, we normalized all Me^{201}Hg values to the highest Me^{201}Hg production. This confirmed that the Hg methylation rates responded consistently to different porewater matrices, regardless of the sediment core source. This observed consistency, combined with the limited interactive effect in the ANOVA, suggests that any interactive effect between the sediment core and porewater matrix on Me^{201}Hg production is relatively minor compared to the direct effects of the two variables. This allowed us to treat the variables as independent and quantify the impact of the microbial community source on Me^{201}Hg production.

We then investigated the relative Hg methylation capacity (RMP) of the microbial community in each of the sediment cores from each sampling station. We first plotted the Me²⁰¹Hg production data, faceted by the porewater matrix source. Clear and consistent trends in the Me²⁰¹Hg production of the sediment cores were observed, even when presented with ²⁰¹Hg pre-equilibrated with a wide range of porewaters (Fig S4.4). To quantify these trends, we grouped the incubations by porewater matrix source, then normalized the Me²⁰¹Hg production to the maximum Me²⁰¹Hg production in any incubation within that group. We refer to this value as the relative Hg methylation potential (RMP). The RMP of the sediment cores increased down the sulfate gradient (Fig. 4.2d), indicating an increased Hg methylation capacity in the microbial community at the low sulfate sites despite low Hg methylation under ambient conditions (Fig. 4.2a-b). In these results, however, we did observe some interaction effects between the sediment cores and the porewater (Fig. 4.2d). The RMP values of the cores followed two slightly different trajectories down the sulfate gradient depending on the porewater source (Fig. 4.2d). For incubations in three of the porewater groups (2A-A, 3A-N, and 3A-F), we observed a steady increase in the RMP of the sediment cores across the sulfate gradient. For the other three porewaters (2A-N, 3A-O, and LOX8), the RMP of the sediment cores increased from 2A-A to 3A-O but remained relatively consistent across 3A and LOX8 (Fig. 4.2d). These three porewater matrices showed the highest levels of Me²⁰¹Hg production, suggesting they resulted in highly bioavailable iHg (Fig. 4.2c).

To investigate the microbial community underlying these trends in methylation capacity over the sulfate gradient, we performed shotgun metagenomic sequencing in duplicate on sediment cores collected alongside the cores used for incubations (Table S2). It is typically difficult to attain high quality assemblies for sediment microbial communities. To address this,

we co-assembled duplicate metagenomes from each site using two assembly algorithms (Table S3). Ultimately, we generated a set of assemblies that collectively accounted for 24-44% of the metagenomic reads within each metagenome (Table S2). We identified *hgcA* and functional metabolic genes in each of the assemblies, then clustered them at 97% amino acid identity to avoid redundancy across assemblies (Table S4). To confirm phylogeny and predict metabolic function associated with different groups of *hgcA* sequences, we also reconstructed genomes of the Hg-methylating organisms by manually generating bins with *hgcA* (*hgcA*⁺) using *anvi'o*⁵⁴. One metagenome generated from the porewater at each site was used to improve the differential coverage for binning. We recovered 14 medium quality *hgcA*⁺ bins (Table S5).

***hgcA* gene identification:** We identified 91 unique *hgcA* genes in the assemblies and five paralogs of *hgcA* (Fig. S4.5; Table S3). Of these 91, four were fused *hgcAB* sequences, which were phylogenetically similar to previously described *hgcAB* sequences (Fig. S4.5).²⁶ The fused *hgcAB* genes were mostly present at 2A-N and 3A-O (Table S3). The one bin with a fused *hgcAB* gene is associated with a facultative aerobe in the Rokubacteriales order. The only organism with a fused HgcAB that has been tested for Hg methylation activity is incapable of MeHg production²⁶; thus, we did not include them in calculations of the overall *hgcA* abundance. Two HgcA sequences had mutations in the cap helix domain, but neither are suspected to interfere with Hg methylation activity⁶⁹, so they were included in all downstream analyses.

***hgcB* gene:** Seventy-four of these *hgcA* genes have a downstream *hgcB* gene (Table S4). Many of these were not predicted as ORFs by Prodigal, but alignments of DNA downstream from *hgcA* and subsequent 6-frame translations identified *hgcB* gene sequences. Other HgcB amino acid sequences were truncated due to incomplete assembly of the contig, but manual inspection of the truncated sequence suggested the gene was likely *hgcB*. Thirteen of the

remaining *hgcA* sequences were near or on the end of the contig and it is likely that the *hgcB* gene did not assemble into the contig. Only one *hgcA* gene, aside from the fused sequences, was located on a contig that had substantial DNA assembled downstream of the *hgcA* gene and did not include an *hgcB* gene. The phylogeny of the associated protein sequence suggested this *hgcA* gene is associated with Chloroflexi, but there were no closely related sequences from this study. As it has been shown that *hgcB* need not be directly downstream from *hgcA* for methylation to occur^{9,25,70}, we included this sequence in our abundance analyses.

***hgcA* abundance:** We assessed gene abundance by calculating the average number of reads mapping to each nucleotide residue in an entire contig containing the gene of interest. This coverage was normalized to the mean coverage of 16 ribosomal protein (rp16) genes (Fig. S4.6). Coverage of *hgcA* ranged from 1.4% to 17% of the rp16 coverage (Fig. 4.3a). Overall, *hgcA* relative abundance in the sediment increased consistently down the sulfate gradient (Fig. 34.a). The abundance of *hgcA* closely tracked with the increase in RMP of the microbial communities (Fig. 4.2d, 4.3a, S4.7). A linear regression of the log-log transformed data showed that RMP of the sediment core correlates significantly (adjusted $R^2 = 0.527$, $p \ll 0.001$) with sediment *hgcA* abundance (Fig. 4.3c, S4.7).

Taxonomic and metabolic analyses of Hg methylators: Phylogenetic analyses of the HgcA proteins and taxonomic and metabolic analyses of reconstructed genomes with *hgcA* (*hgcA*+ bins) suggested that the Hg-methylating organisms were primarily fermentative or methanogenic (Fig. 4.3a-b). Methanogenic archaea-associated *hgcA* genes account for 45% of the *hgcA* abundance across all samples, with relatively consistent coverage throughout the six different sites (Fig. 4.3b). Of these, 18 sequences, two of which are binned, are closely related and likely derived from organisms within the *Methanoregula* genus (Fig. S4.5). Two additional

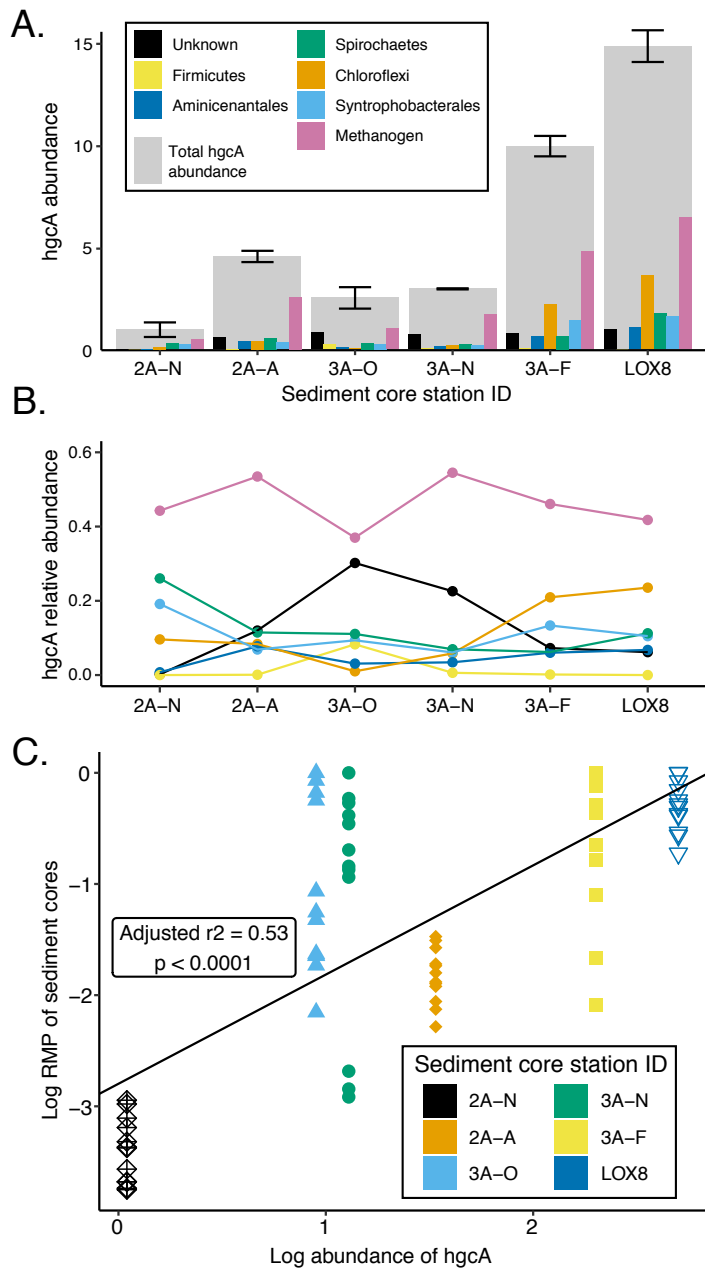


Figure 4.3: Abundance of *hgcA* gene correlates with relative Hg methylation potential (RMP) of sediment cores. Total *hgcA* abundance (in gray) increases down the sulfate gradient (A). Abundance of different taxonomic groups are color-coded in smaller bars. Error bars represent standard error. The taxonomic composition of *hgcA* was relatively consistent over the sulfate gradient (B), with the notable exception of Chloroflexi that increased in abundance at 3A-F and LOX8. The *hgcA* gene abundance was correlated to RMP on a log-log scale (C). RMP values are color coded by the station of origin for the sediment cores.

hgcA sequences and a third bin also associated with the Methanoregulaceae family (Fig. S4.5). These genes are primarily present at LOX8, but were found at 2A-A and 3A-F as well (Table S4). Seven *hgcA* genes, including 3 bins, associated with the family Methanocellaceae, were also detected and were most abundant at 3A-N and 3A-F. These are all within the Methanomicrobiales order, which represents CO₂-reducing methanogens that rely on hydrogen and occasionally formate. Indeed, the recovered bins from this group encode the pathways needed for hydrogenotrophic methanogenesis and contain no cytochromes. One *hgcA* sequence was identified as Methanomassiliicoccales. The associated bin contained multiple cytochromes, suggesting it corresponds to a methylotrophic methanogen, as predicted for this order.

Chloroflexi-associated *hgcA* sequences are the most abundant bacterial *hgcA* genes across the entire dataset, although most of their mapped reads originated from 3A-F and LOX8 (Fig. 4.3a, S4.7). We only recovered one bin with an *hgcA* gene from this cluster (Fig S4.5). This bin was classified in the Anaerolineae class (Table S4). It appears to correspond to either a facultative aerobe or an oxygen-tolerant fermentative organism, as it has a *cydAB* oxidase and the subunits for complex I of an electron transport chain (ETC). While it is missing some components of the ETC, because it is only 75% complete we cannot verify whether the organism has a complete ETC. It did not include genes mediating major terminal electron accepting processes other than the *cydAB* gene. Spirochaetes and Syntrophobacterales-associated *hgcA* genes were the next most abundant. These two both had a consistent relative abundance of *hgcA*, but accounted for slightly more of the relative abundance at 2A-N. We recovered one *hgcA*+ *Syntrophales* bins, which was predicted to correspond to an obligate fermenter or syntroph due to the lack of an ETC, multiheme cytochrome c proteins, or other genes that could mediate respiration with alternative terminal electron acceptors. It is likely tolerant of microaerobic

environments though as it has *cydAB* and *nrfA* genes. It appears particularly well-suited to ferment amino acids. We also identified *hgcA* genes associated with Aminicenantes and Firmicutes, each at relatively low abundance. We recovered a single Aminicenantes bin, which contained one of the most abundant *hgcA* genes in the whole dataset but was only present at LOX8. This bin contained the *coxAB* genes and genes for an aerobic ETC, suggesting it corresponds to a facultative aerobic organism.

Flanking microbial community: We used read-based taxonomic analyses and assembly-based metabolic protein analyses to investigate the microbial community beyond the Hg-methylating organisms. There was no significant difference in the Nonpareil diversity (one-way ANOVA, $F(5)=0.774$, $p = 0.602$) between sites (Fig. S4.8). A principal coordinates analysis of the kmer-based distances between metagenomes revealed distinct microbial communities at each site (Fig. 4.4a). The microbial community at LOX8 was separated from the communities in the WCA sites along the first axis, while the second axis separated the WCA communities along the sulfate/sulfide gradient, with 2A-A, 3A-O, and 3A-N clustering closely together between 2A-A and 3A-F. Along the third axis, 3A-O and 3A-N were clustered distinctly from 2A-A. The ordination is consistent with the positions along the sulfate gradient and the differences are visible at the phylum-level community composition of the 16S genes in the metagenome (Fig. S4.9). Most notably, archaeal phyla (Crenarchaeota and Euryarchaeota) were most abundant at the 3A-F and LOX8 sites, while the Proteobacteria decreased in abundance at that site. Rokubacteria and Gemmatimonadetes on the other hand were most abundant at 2A-N and decreased across the sulfate gradient. Other phyla, such as Chloroflexi, Proteobacteria, and Planctomycetes, were relatively consistent in abundance over the six different sites.

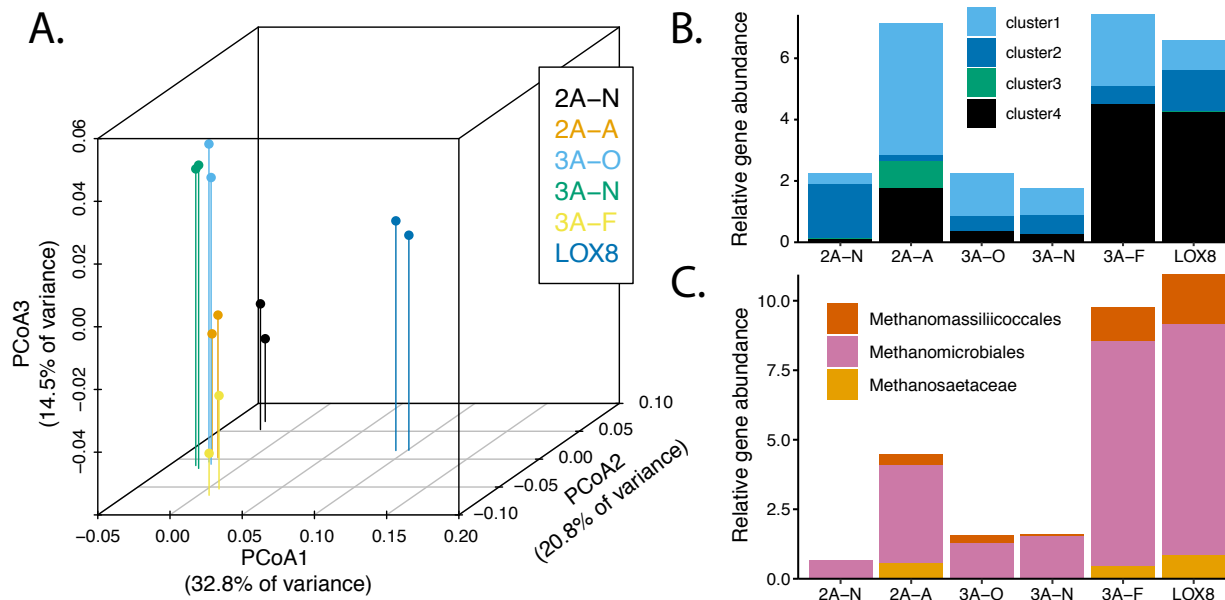


Figure 4.4: Microbial community composition exhibits distinct changes along sulfate gradient. The overall microbial community composition, as determined by 16S composition of the metagenomes, exhibits distinct differences along the gradient, as shown by the PCA plot (A). In particular, the LOX8 site is particularly unique, but the WCA sites fall out along the sulfate gradient on the second and third axes. Both *dsrA* (B) and *mcrA* (C), markers of sulfate-reduction and methanogenesis, respectively, are most abundant at 3A-F and LOX8, with an increase at 2A-A as well. The *dsrA* phylogenetic identity is distinct at 2A-A from the rest of the sites.

We then characterized the abundance of several metabolic genes across samples, starting with terminal respiratory proteins (Fig. 4.4b-c, S4.10). Reductive *dsrA* genes were most abundant at 2A-A, 3A-F, and LOX8 (Fig. 4.4b). This pattern was matched by the abundance of *dsrD*, another protein involved in sulfate reduction (Fig. S4.10a). Interestingly, the phylogenetic composition of *dsrA* at 2A-A was distinct from that at 3A-F and LOX8 (Fig. 4.4b). The methanogenic *mcrA* gene exhibited a similar distribution to the *hgcA* and *dsr* genes with peaks at 2A-A, 3A-F and LOX8 (Fig. 4.4c). As we observed with *hgcA*, the vast majority of *mcrA* genes were associated with the *Methanoregula* clade within the order Methanomicrobiales (Fig. 4.4c). A set of eight methanogenic markers corroborate the abundance distribution of the methanogens across the gradient (Fig. S4.10b). We identified periplasmic and membrane-bound nitrate reductases and terminal oxidases in the metagenomic assemblies. Abundances of *napA*, *narGHI*, *coxB*, and *ccoNOP* genes all show a marked drop in abundance at 3A-F and LOX8, even though those two sites are the only two without sulfide accumulation in the porewaters (Fig. S4.10c-d). These genes might be linked to the activity of sulfide-oxidizing bacteria, as we observed reverse *dsrA* and *sox* genes to be most abundant in the four WCA sites with detectable sulfide and drop off substantially at 3A-F and LOX8 (Fig. S4.10e-f).

Discussion

Our understanding of how the microbial community composition influences MeHg production *in situ* is still limited, due in part to the difficulty in separating the impact of the Hg methylation capacity of the microbial community from the effects of iHg bioavailability. Here, we attempted to isolate those two factors by pre-equilibrating the Hg tracer with filtered porewater collected at the different stations, thus establishing the bioavailability of the tracer

before injecting it into different peat cores. We then grouped the incubations by porewater source and normalized the data to the highest MeHg production in the group, thus assigning a relative Hg-methylation potential (RMP) to the cores from each station. This calculation makes several key assumptions. First, it assumes that the bioavailability of the Hg tracer does not change upon injection into the sediment core and interacting with the ambient porewater, mineral solid phases, and other potential binding sites or ligands. Kinetic limitations are thought to play a substantial role in iHg complexation^{71,72}, which would support long-lasting effects of pre-equilibration conditions. Other studies have shown notable differences in reactivity and/or bioavailability of Hg tracers in complex incubation matrices when the tracer was pre-equilibrated with different solid-phases and/or dissolved ligands⁷³⁻⁷⁵. In this study, if the complexation and bioavailability of the $i^{201}\text{Hg}$ tracer did undergo rapid isotope exchange and equilibrate with the binding sites in the sediment core, we would expect the Me^{201}Hg production to be nearly completely dependent on the sediment core that was used and all Me^{201}Hg production values would match those done in the sediment core under ambient conditions (Fig. 4.2b). However, Me^{201}Hg production varied more than an order of magnitude when using different porewaters for pre-equilibration (Fig. S4.4), suggesting that the speciation due to the pre-equilibration does control bioavailability of iHg, at least for the 24-hour time frame of these incubations. Second, it assumes that the porewater used for the Hg tracer matrix is not influencing the microbial metabolic activity, specifically the Hg-methylation capacity. If this were the case, we would expect sediment cores to respond differently to porewater injections with different chemical compositions, resulting in a strong interactive effect between porewater and sediment core. However, the Me^{201}Hg production responded similarly to each porewater matrix in all sediment cores (Fig. 4.2d, S4.3), with some exceptions discussed below. Overall, these data suggest limited interaction between

the effects of the porewater on bioavailability and the effect of the sediment core on Hg-methylation capacity.

We did observe two distinct patterns in the RMP of the sediment core community across the gradient depending on the porewater used (Fig. 4.2d). Half of the porewater matrices resulted in a plateau of Me²⁰¹Hg production across WCA-3A, while the other three resulted in a continual increase in RMP down the sulfate gradient. These three porewater did not have similar chemical compositions; in fact, there was one each from the top, middle, and bottom of the sulfate gradient (Fig. 4.2c). This makes it unlikely that the porewater matrix is stimulating or inhibiting the microbial community in such a way to cause this effect. Previous work has shown that the microbial community has a reduced effect on Hg methylation when bioavailability of iHg is low.^{12,75} However, the most notable similarity between these three porewaters (2A-N, 3A-O, and LOX8) is that they resulted in the highest levels of Me²⁰¹Hg production (Fig. 4.2c), ranging from approximately 2% to 4% Me²⁰¹Hg of the ²⁰¹HgT pool, suggesting bioavailability is not limiting here. In fact, these percentages match up with the maximum percentage of ambient MeHg in the same cores, which is around 2% at 3A-O and LOX8. This indicates these high-producing incubations could have reached an equilibrium point, or at least methylated most of a highly bioavailable pool of i²⁰¹Hg^{76,77}. Unfortunately, due to the very large number of cores used for this factorial experiment, it was not possible to also conduct multiple time-point assays to search for potential saturation/equilibrium effects, so we included all incubations in our final set of analysis. If there is such an effect occurring, it would mean we are likely underestimating the Hg-methylation capacity of the microbial communities at 3A-F and LOX8. Additional studies that further investigate the interaction between these two variables under an array of conditions will provide insight into the constraints on MeHg production in natural ecosystems.

The results shown here suggest that, under a range of geochemical conditions leading to large differences in bioavailability, the Hg-methylation capacity of the microbial community does influence Me²⁰¹Hg production rates. Even when the iHg tracer was pre-equilibrated with porewater from 3A-F, which led to the lowest iHg bioavailability (Fig 4.2c), the microbial community had a clear impact on Me²⁰¹Hg production (Fig. S4.4, bottom middle panel). Previous studies have suggested that the Hg-methylation capacity of the microbial community has a limited effect on MeHg production when the Hg tracer is limited in bioavailability.^{12,75,78} However, these studies used highly labile dissolved forms of the Hg tracer, such as Hg(NO₃)₂, or highly recalcitrant forms, such as nanoparticulate HgS. The range of bioavailability in the current study was much narrower and reflected the environmental conditions of the Everglades. Even in the high sulfide porewater used as matrices, kinetic limitations likely favored Hg-NOM complexes over the formation of recalcitrant particulate HgS, as those can take several days to form when dissolved organic matter is present.^{71,79,80} Previous work has shown that under conditions of low microbial methylation activity, changing the bioavailability of iHg has no effect on MeHg production.⁷⁹ However, we did not observe Hg-methylation capacity to be limiting either, with consistent effects of porewater on MeHg production even in cores from 2A-A, which had very low Me²⁰¹Hg production. This suggests that neither the Hg-methylation capacity nor the bioavailability of the iHg spike are strictly rate-limiting for Me²⁰¹Hg production at these stations, but rather that both play a role in determining extent of Hg methylation.

In this study, we identified increases in abundance and diversity of Hg-methylating organisms coincident with the increase in the relative Hg-methylation capacity. Abundance of *hgcA* did not correlate with MeHg levels in the sediment or MeHg production under ambient conditions. While some studies have shown correlations between MeHg concentrations and *hgcA*

abundance⁸¹⁻⁸³, others have shown no correlation^{84,85}, likely due to gradients in iHg bioavailability that were not quantified or examined. Decreases in MeHg production related to a decrease in diversity of *hgcA* sequences independent of changes in bioavailability have been documented in sulfate-enriched mesocosms.³⁰ In this study, *hgcA* abundance did correlate closely to the relative Hg-methylation capacity of the microbial community (Fig. 4.3B). This is a surprising considering that there are variable rates of MeHg production observed in culture^{8,9} and that we do not know which *hgcA*⁺ organisms are actively methylating in these natural systems. We also do not know how transcription and translation of *hgcA* are controlled in natural environments. Transcription of *hgcA* has been shown to be constitutive in response to Hg(II) exposure, at least under a narrow range of laboratory conditions.^{86,87} However, sequences homologous to the transcriptional regulator *arsR* were found near the *hgcA* gene in several recent studies^{27,88}, suggesting the gene may be under regulation in certain environments. This gene has also been identified in cultured *hgcA*⁺ organisms⁷⁰, which could be tested for regulatory activity. While only done in one ecosystem, the correlation observed here indicates that the abundance of *hgcA* may be a useful marker for determining the Hg-methylation capacity of the microbial community, regardless of the impact of geochemistry on iHg bioavailability or the observed MeHg production. By identifying the relationship between Hg-methylation capacity and *hgcA* in other systems, looking at *in situ* transcription and translation of *hgcA*, and identifying factors that mediate the relationship between these parameters and *hgcA*, we can begin to understand how the *hgcA*⁺ microbial community mediates the observed MeHg production.

There is very little evidence on how abundant Hg-methylating organisms are in the environment, as a fraction of the whole microbial community. Because *hgcA* is, to our

knowledge, always found in genomes in a single copy^{8,27}, by normalizing the *hgcA* abundance to the average abundance of several single copy genes, the 16 ribosomal protein genes in this case⁶⁷, we could estimate the fraction of the microbial community with the *hgcA* gene, which ranged from approximately 1-15% (Fig. 4.3a). This is consistent with other metagenomic studies looking at *hgcA* in anoxic environments when the *hgcA* abundance was reported as a fraction of the total community.^{28,29}

This study adds to an expanding body of literature suggesting that microbial Hg-methylators in the environment are far more diverse than previously suggested. While SRBs and methanogens are most often linked to MeHg production^{1,21,22}, the identification of *hgcA*²⁵ has drastically expanded the known phylogenetic and metabolic diversity of Hg-methylators in the environment.^{26,27} This holds true even in sulfate-rich systems^{28,29} and in highly reduced sediments²⁷. Here, we did not identify any *hgcA* sequences associated with SRBs. This is not due to a lack of SRBs, as we did identify *dsrA* and *dsrD* genes across the gradient (Fig. 4.4b, S4.10a). We observed that methanogens accounted for about 40-60% of the total methylating community, even under high-sulfate/sulfide conditions (Fig. 4.3b). At the bottom of the gradient, methanogens were still abundant, but we also observed a drastic increase in the abundance of Chloroflexi-associated *hgcA* sequences at this location. A wide range of *hgcA* sequences associated with other putative fermentative or syntrophic organisms, including Firmicutes, Spirochaetes, and Syntrophobacterales. Amplicon sequencing identified methanogens and syntrophs Hg-methylators along this same gradient, albeit at different sites and sampling different locations of the sediment core.³¹ The presence of the novel groups we identified in our study cannot be evaluated in this other study due to the likelihood that the PCR primers would not amplify highly divergent sequences. This suggests that fermentative and methanogenic

pathways are the primary drivers of MeHg production in the sediments, which could explain the lack of correlation between sulfide accumulation and Hg-methylation capacity. However, the abundance of the *dsr* genes concurrent with *hgcA* suggests SRB could still influence MeHg production, either by consuming fermentation products through sulfate respiration or by forming syntrophic partnerships with the methanogens under sulfate-limited conditions.²⁴ Incubations from a separate study done near the 3A-O and 3A-N sites showed a substantial effect of SRB on Hg methylation despite the dominance of Syntrophobacterales in the *hgcA* pool.³¹ While the Syntrophobacterales bin from the current study was not a SRB, other organisms within that order are SRB⁸⁹. This highlights the complexity of the *in situ* microbial community mediating MeHg production both directly and indirectly and underscores the need for targeted functional assays to identify the pathways leading to MeHg production in wetland sediments.

The metabolic gene information provides some interesting context for the Hg-methylating community, suggesting that in these sediment cores as we move down the sulfate gradient, there is a shift from sulfide-oxidation to sulfate-reduction and methanogenesis, which coincides with the increase in *hgcA* and the relative Hg-methylation capacity of the microbial community. This is not particularly surprising, as high concentrations of sulfide can inhibit sulfate reduction.⁵ Additionally, in sediments like these, there are often steep redox gradients that lead to changes in dominant TEAP activity. The sediments here were homogenized over a relatively large range, so the metagenomes are likely capturing a gradient of TEAP activity.

Finally, this work provides specific insights into the constraints on MeHg production in the sediment of the Everglades. Despite the lack of *hgcA*⁺ SRBs, there is extensive evidence linking MeHg production to sulfate levels in the Florida Everglades.³⁹ This, linked with the historic emphasis of sulfate reducers as the primary drivers of methylation^{21,22} and the known

role of sulfide in limiting iHg bioavailability⁵ has led to the Goldilocks hypothesis, which suggests that the peak in MeHg when the sulfate levels are “just right” is due to increasing bioavailability of iHg and decreasing Hg-methylator activity as we move down the gradient.^{13,14} This curve is reproduced here, apart from the high MeHg levels at LOX8 (Fig 4.2a-b). Overall, our results corroborate the Goldilocks curve hypothesis in that we observed that sites with high MeHg production and accumulation (3A-O and LOX8) had both porewater that promotes bioavailable iHg for uptake (Fig. 4.2c) and microbial communities capable of producing MeHg (Fig. 4.2d). The other sites had low rate of MeHg production under ambient conditions and correspondingly lower MeHg concentrations due to low microbial Hg-methylation capacity (2A-N), low bioavailability of iHg for uptake (3A-N, 3A-F), or both (2A-A). However, these data do contradict some of the previously stated mechanisms thought to underlie the Goldilocks hypothesis, as the porewater at 2A-N with high sulfide levels facilitates more MeHg production than the low sulfide porewaters at LOX8 or 3A-F (Fig. S4.3), despite overwhelming evidence that higher sulfide levels lead to inhibition of MeHg production by sequestering the iHg.⁵ This discrepancy could be due to kinetic limitations on HgS formation, as discussed above, in favor of Hg-complexation with sulfur moieties in DOM. Sulfurization of the DOM^{17,40} or higher SUVA content^{20,42} (Fig. S4.1c) could also drive increased bioavailability of MeHg at the sulfide-rich sites. It also could be simply that the sulfide levels were not high enough to cause inhibition of Hg methylation. On the other hand, Hg-methylation capacity increased down the sulfate gradient (Fig. 4.2d), backed up by data showing non-SRB were the dominant Hg-methylators in the sediment at these stations (Fig. 4.3). It is unclear why *hgcA* abundance would increase with decreasing sulfate, due in part to the unknown purpose of the *hgcA* gene. It is interesting to note that the sulfidic sites are also more eutrophic, which could play a role in the reduced *hgcA*

relative abundance and thus provide an alternative to the “biodilution” hypothesis for explaining reduced MeHg levels in fish under eutrophic conditions. Additional investigations into the mechanisms underlying these findings and the degree that they extend to other ecologically important compartments will further elucidate the mechanisms by which geochemical gradients in the Florida Everglades influence MeHg contamination in the ecosystem.

Acknowledgements

Funding for sampling, analysis and sequencing provided through the USGS Greater Everglades Priority Ecosystem Studies. Hg analyses were done by John DeWild and Jake Ogorek. Valuable feedback was provided by Bill Orem, Sarah Janssen, Chris Babiarz, Mike Tate.

References

1. Bodaly, R. A. *et al.* Bioaccumulation of mercury in the aquatic food chain in newly flooded areas. in *Metal ions in biological systems* vol. 34 259–288 (MARCEL DEKKER AG, 1997).
2. Brigham, M. E., Krabbenhoft, D. P., Olson, M. L. & DeWild, J. F. Methylmercury in flood-control impoundments and natural waters of northwestern Minnesota, 1997–99. **138**, 67–78 (2002).
3. Baldwin, A. K. *et al.* Seasonal Dynamics and Interannual Variability in Mercury Concentrations and Loads through a Three-Reservoir Complex. *Environ. Sci. Technol.* **54**, 9305–9314 (2020).
4. Clark, G. M. *et al.* Mercury cycling in the Hells Canyon Complex of the Snake River, Idaho and Oregon. (2016).
5. Friedl, G. & Wüest, A. Disrupting biogeochemical cycles – Consequences of damming. **64**, 11 (2002).
6. Willacker, J. J. *et al.* Reservoirs and water management influence fish mercury concentrations in the western United States and Canada. *Science of The Total Environment* **568**, 739–748 (2016).
7. Canavan, C. M., Caldwell, C. A. & Bloom, N. S. Discharge of methylmercury-enriched hypolimnetic water from a stratified reservoir. *The Science of The Total Environment* **260**, 159–170 (2000).
8. Kasper, D., Fernandes, E., Palermo, A., Branco, C. W. C. & Malm, O. Evidence of elevated mercury levels in carnivorous and omnivorous fishes downstream from an Amazon reservoir. *Hydrobiologia* **694**, 87–98 (2012).
9. Kasper, D. *et al.* Reservoir Stratification Affects Methylmercury Levels in River Water, Plankton, and Fish Downstream from Balbina Hydroelectric Dam, Amazonas, Brazil. *Environ. Sci. Technol.* **48**, 1032–1040 (2014).
10. Gilmour, C. C., Henry, E. A. & Mitchell, R. Sulfate stimulation of mercury methylation in freshwater sediments. *Environ. Sci. Technol.* **26**, 2281–2287 (1992).
11. Compeau, G. C. & Bartha, R. Sulfate-reducing bacteria: Principal methylators of mercury in anoxic estuarine sediment. *Appl Environ Microbiol* **50**, 498–502 (1985).
12. Fleming, E. J., Mack, E. E., Green, P. G. & Nelson, D. C. Mercury Methylation from Unexpected Sources: Molybdate-Inhibited Freshwater Sediments and an Iron-Reducing Bacterium. *Appl Environ Microbiol* **72**, 457–464 (2006).
13. Kerin, E. J. *et al.* Mercury methylation by dissimilatory iron-reducing bacteria. *Appl Environ Microbiol* **72**, 7919–7921 (2006).
14. Hamelin, S., Amyot, M., Barkay, T., Wang, Y. & Planas, D. Methanogens: principal methylators of mercury in lake periphyton. *Environ. Sci. Technol.* **45**, 7693–7700 (2011).
15. Gilmour, C. C., Bullock, A. L., McBurney, A., Podar, M. & Elias, D. A. Robust mercury methylation across diverse methanogenic *Archaea*. *mBio* **9**, 1–13 (2018).
16. Todorova, S. G. *et al.* Evidence for regulation of monomethyl mercury by nitrate in a seasonally stratified, eutrophic lake. *Environ. Sci. Technol.* **43**, 6572–6578 (2009).
17. Dent, S. R., Beutel, M. W., Gantzer, P. & Moore, B. C. Response of methylmercury, total mercury, iron and manganese to oxygenation of an anoxic hypolimnion in North Twin Lake, Washington. *Lake and Reservoir Management* **30**, 119–130 (2014).

18. Matthews, D. A. *et al.* Whole-lake nitrate addition for control of methylmercury in mercury-contaminated Onondaga Lake, NY. *Environmental Research* **125**, 52–60 (2013).
19. Vlassopoulos, D. *et al.* Manganese(IV) oxide amendments reduce methylmercury concentrations in sediment porewater. *Environ. Sci.: Processes Impacts* **20**, 1746–1760 (2018).
20. Gascón Díez, E. *et al.* Role of settling particles on mercury methylation in the oxic water column of freshwater systems. *Environ. Sci. Technol.* **50**, 11672–11679 (2016).
21. Eckley, C. S., Luxton, T. P., Knightes, C. D. & Shah, V. Methylmercury production and degradation under light and dark conditions in the water column of the Hells Canyon Reservoirs, USA. *Environ Toxicol Chem* etc.5041 (2021) doi:10.1002/etc.5041.
22. Gionfriddo, C. M. *et al.* Microbial mercury methylation in Antarctic sea ice. *Nature Microbiology* **1**, 1–12 (2016).
23. Tada, Y., Marumoto, K. & Takeuchi, A. Nitrospina-Like Bacteria Are Potential Mercury Methylators in the Mesopelagic Zone in the East China Sea. *Front. Microbiol.* **11**, 1369 (2020).
24. Lin, H. *et al.* Mercury methylation by metabolically versatile and cosmopolitan marine bacteria. *ISME J* (2021) doi:10.1038/s41396-020-00889-4.
25. McDaniel, E. A. *et al.* Expanded phylogenetic diversity and metabolic flexibility of mercury-methylating microorganisms. *mSystems* **5**, 1–21 (2020).
26. Jiménez Otero, F., Chan, C. H. & Bond, D. R. Identification of different putative outer membrane electron conduits necessary for Fe(III) citrate, Fe(III) oxide, Mn(IV) oxide, or electrode reduction by *Geobacter sulfurreducens*. *J Bacteriol* **200**, 1–20 (2018).
27. Lovley, D. R. & Phillips, E. J. P. Novel Mode of Microbial Energy Metabolism: Organic Carbon Oxidation Coupled to Dissimilatory Reduction of Iron or Manganese. *Applied and Environmental Microbiology* **54**, 1472–1480 (1988).
28. Peterson, B. D. *et al.* Mercury methylation genes identified across diverse anaerobic microbial guilds in a eutrophic sulfate-enriched lake. *Environ. Sci. Technol.* **54**, 15840–15851 (2020).
29. Capo, E. *et al.* Deltaproteobacteria and Spirochaetes-like bacteria are abundant putative mercury methylators in oxygen-deficient water and marine particles in the Baltic Sea. *Front. Microbiol.* **11**, 1–11 (2020).
30. Poulin, B. A. *et al.* *Chemical characterization of water and suspended sediment of the Snake River and Hells Canyon Complex (Idaho, Oregon)*. <https://doi.org/10.5066/P9DT2B6J> (2020).
31. Marvin-DiPasquale, M. *et al.* *Biogeochemical data for mercury and other constituents in surface sediment and deep cores from the Hells Canyon Reservoir Complex, Idaho and Oregon 2014-2018*. <https://doi.org/10.5066/P9L4XCD0> (2020).
32. Olson, M. L. & DeWild, J. F. Techniques for the collection and species-specific analysis of low levels of mercury in water, sediment, and biota. in *U.S. Geological Survey Water-Resources Investigations Report* vols 99-4018B (1999).
33. *U.S EPA Method 1631, Revision E: Mercury in Water by Oxidation, Purge and Trap, And Cold Vapor Atomic Fluorescence Spectrometry.* (2002).
34. Olund, S. D., DeWild, J. F., Olson, M. L. & Tate, M. T. Methods for the preparation and analysis of solids and suspended solids for total mercury. in *U.S. Geological Survey Techniques of Water-Resources Investigations, Book 5, Chapter A8* (2004).

35. DeWild, J. F., Olson, M. L. & Olund, S. D. *Determination of Methyl Mercury by Aqueous Phase Ethylation, Followed by Gas Chromatographic Separation with Cold Vapor Atomic Fluorescence Detection. Open-file Report.* (2002).
36. Horvat, M., Bloom, N. S. & Liang, L. Comparison of distillation with other current isolation methods for the determination of methyl mercury compounds in low level environmental samples. *Analytica Chimica Acta* **281**, 135–152 (1993).
37. Lepak, R. F. *et al.* Influence of *Cladophora*–quagga mussel assemblages on nearshore methylmercury production in Lake Michigan. *Environ. Sci. Technol.* **49**, 7606–7613 (2015).
38. Chen, S., Zhou, Y., Chen, Y. & Gu, J. fastp: an ultra-fast all-in-one FASTQ preprocessor. *Bioinformatics* **34**, i884–i890 (2018).
39. Ondov, B. D. *et al.* Mash: fast genome and metagenome distance estimation using MinHash. *Genome Biol* **17**, 132 (2016).
40. Nurk, S., Meleshko, D., Korobeynikov, A. & Pevzner, P. A. metaSPAdes: a new versatile metagenomic assembler. *Genome Research* **27**, 824–834 (2017).
41. Hyatt, D. *et al.* Prodigal: prokaryotic gene recognition and translation initiation site identification. *BMC Bioinformatics* **11**, 119 (2010).
42. Langmead, B. & Salzberg, S. L. Fast gapped-read alignment with Bowtie 2. *Nat Methods* **9**, 357–359 (2012).
43. Anantharaman, K. *et al.* Thousands of microbial genomes shed light on interconnected biogeochemical processes in an aquifer system. *Nat. Commun.* **7**, 1–11 (2016).
44. Sorek, R. *et al.* Genome-Wide experimental determination of barriers to horizontal gene transfer. *Science* **318**, 1449–1452 (2007).
45. Kang, D. D. *et al.* MetaBAT 2: an adaptive binning algorithm for robust and efficient genome reconstruction from metagenome assemblies. *PeerJ* **7**, 1–13 (2019).
46. Wu, Y.-W., Simmons, B. A. & Singer, S. W. MaxBin 2.0: an automated binning algorithm to recover genomes from multiple metagenomic datasets. *Bioinformatics* **32**, 605–607 (2016).
47. Sieber, C. M. K. *et al.* Recovery of genomes from metagenomes via a dereplication, aggregation and scoring strategy. *Nat Microbiol* **3**, 836–843 (2018).
48. Eren, A. M. *et al.* Anvi'o: an advanced analysis and visualization platform for 'omics data. *PeerJ* **3**, 1–29 (2015).
49. Chaumeil, P.-A., Mussig, A. J., Hugenholtz, P. & Parks, D. H. GTDB-Tk: a toolkit to classify genomes with the Genome Taxonomy Database. *Bioinformatics* **36**, 1925–1927 (2019).
50. Aramaki, T. *et al.* KofamKOALA: KEGG Ortholog assignment based on profile HMM and adaptive score threshold. *Bioinformatics* **36**, 2251–2252 (2020).
51. Eddy, S. R. *hmmer*. (2015).
52. Zhou, Z. *et al.* METABOLIC: High-throughput profiling of microbial genomes for functional traits, biogeochemistry, and community-scale metabolic networks. *bioRxiv (pre-print)* 30 (2020).
53. Fu, L., Niu, B., Zhu, Z., Wu, S. & Li, W. CD-HIT: accelerated for clustering the next-generation sequencing data. *Bioinformatics* **28**, 3150–3152 (2012).
54. Edgar, R. C. MUSCLE: a multiple sequence alignment method with reduced time and space complexity. *BMC Bioinformatics* **5**, 1–19 (2004).
55. Gionfriddo, C. M. *et al.* Hg-MATE-Db.v1.01142021. (2021).

56. Stamatakis, A. RAxML version 8: a tool for phylogenetic analysis and post-analysis of large phylogenies. *Bioinformatics* **30**, 1312–1313 (2014).
57. Schliep, K. P. phangorn: phylogenetic analysis in R. *Bioinformatics* **27**, 592–593 (2011).
58. Yu, G., Smith, D. K., Zhu, H., Guan, Y. & Lam, T. T. ggtree: an R package for visualization and annotation of phylogenetic trees with their covariates and other associated data. *Methods Ecol. Evol.* **8**, 28–36 (2017).
59. Gionfriddo, C. M. *et al.* An improved hgcAB primer set and direct high-throughput sequencing expand Hg-methylator diversity in nature. *Front. Microbiol.* **11**, 1–23 (2020).
60. Matsen, F. A., Kodner, R. B. & Armbrust, E. V. pplacer: linear time maximum-likelihood and Bayesian phylogenetic placement of sequences onto a fixed reference tree. *BMC Bioinformatics* **11**, 1–16 (2010).
61. Goñi-Urriza, M. *et al.* Genome insights of mercury methylation among *Desulfovibrio* and *Pseudodesulfovibrio* strains. *Research in Microbiology* **171**, 3–12 (2020).
62. Parks, J. M. *et al.* The genetic basis for bacterial mercury methylation. *Science* **339**, 1332–1335 (2013).
63. Ranchou-Peyruse, M. *et al.* Overview of mercury methylation capacities among anaerobic bacteria including representatives of the sulphate-reducers: implications for environmental studies. *Geomicrobiology Journal* **26**, 1–8 (2009).
64. Bowers, R. M. *et al.* Minimum information about a single amplified genome (MISAG) and a metagenome-assembled genome (MIMAG) of bacteria and archaea. *Nat Biotechnol* **35**, 725–731 (2017).
65. Levar, C. E., Chan, C. H., Mehta-Kolte, M. G. & Bond, D. R. An Inner Membrane Cytochrome Required Only for Reduction of High Redox Potential Extracellular Electron Acceptors. *mBio* **5**, e02034-14 (2014).
66. Levar, C. E., Hoffman, C. L., Dunshee, A. J., Toner, B. M. & Bond, D. R. Redox potential as a master variable controlling pathways of metal reduction by *Geobacter sulfurreducens*. *ISME J* **11**, 741–752 (2017).
67. Akhujkar, M. *et al.* The genome of *Geobacter bemidjiensis*, exemplar for the subsurface clade of *Geobacter* species that predominate in Fe(III)-reducing subsurface environments. *BMC Genomics* **11**, 490 (2010).
68. Jones, D. S. *et al.* Molecular evidence for novel mercury methylating microorganisms in sulfate-impacted lakes. *ISME J* (2019) doi:10.1038/s41396-019-0376-1.
69. Podar, M. *et al.* Global prevalence and distribution of genes and microorganisms involved in mercury methylation. *Sci. Adv.* **1**, 1–12 (2015).
70. Eckley, C. S. *et al.* Mercury methylation in the hypolimnetic waters of lakes with and without connection to wetlands in northern Wisconsin. *Can J Fish Aquat Sci* **62**, 400–411 (2005).
71. Watras, C. J. *et al.* Methylmercury production in the anoxic hypolimnion of a dimictic seepage lake. *Water, Air, and Soil Pollution* **80**, 735–745 (1995).
72. Lepak, R. F. *et al.* Factors affecting mercury stable isotopic distribution in piscivorous fish of the Laurentian Great Lakes. *Environ. Sci. Technol.* **52**, 2768–2776 (2018).
73. Ebel, W. J. & Koski, C. H. *Limnology of Brownlee Reservoir 1962 - 1964*. 42 (1964).
74. Watras, C. J. *et al.* Bioaccumulation of mercury in pelagic freshwater food webs. *Science of The Total Environment* **219**, 183–208 (1998).

75. Berg, J. S. *et al.* Intensive cryptic microbial iron cycling in the low iron water column of the meromictic Lake Cadagno: A cryptic microbial iron cycle. *Environmental Microbiology* **18**, 5288–5302 (2016).
76. Chadwick, S. P., Babiarz, C. L., Hurley, J. P. & Armstrong, D. E. Influences of iron, manganese, and dissolved organic carbon on the hypolimnetic cycling of amended mercury. *Science of The Total Environment* **368**, 177–188 (2006).
77. Liu, Y.-R. *et al.* Unraveling microbial communities associated with methylmercury production in paddy soils. *Environ. Sci. Technol.* **52**, 13110–13118 (2018).
78. Bravo, A. G. *et al.* Geobacteraceae are important members of mercury-methylating microbial communities of sediments impacted by waste water releases. *ISME J* **12**, 802–812 (2018).
79. Bravo, A. G. *et al.* Methanogens and iron-reducing bacteria: the overlooked members of mercury-methylating microbial communities in boreal lakes. *Appl Environ Microbiol* **84**, e01774-18, /aem/84/23/e01774-18.atom (2018).
80. Nealson, K. H. & Myers, C. R. Microbial reduction of manganese and iron: new approaches to carbon cycling. *Appl Environ Microbiol* **58**, 439–443 (1992).
81. Schaefer, J. K. & Morel, F. M. M. High methylation rates of mercury bound to cysteine by *Geobacter sulfurreducens*. *Nature Geosci* **2**, 123–126 (2009).
82. Gilmour, C. C. *et al.* Mercury methylation by novel microorganisms from new environments. *Environ. Sci. Technol.* **47**, 11810–11820 (2013).
83. Alpers, C. N. *et al.* Mercury cycling in agricultural and managed wetlands, Yolo Bypass, California: Spatial and seasonal variations in water quality. *Science of The Total Environment* **484**, 276–287 (2014).
84. Schaefer, J. K., Kronberg, R., Björn, E. & Skjellberg, U. Anaerobic guilds responsible for mercury methylation in boreal wetlands of varied trophic status serving as either a methylmercury source or sink. *Environ Microbiol* **22**, 3685–3699 (2020).

Appendix to Chapter 4: Supplementary tables and figures

Supplementary Tables: All supplementary data and tables can be found here:

<https://figshare.com/account/home#/projects/117342>

Supplementary Data 3.1: Includes all supplementary tables.

Table S1: Site coordinates for sampling locations.

Table S2: Metagenome metadata and statistics on reads counts, mapping, and coverage.

Table S3: Assembly statistics for all 12 assemblies used in analyses.

Table S4: *hgcA* information, including quality, classifications, binning, *hgcB* information and abundance.

Supplementary Figures:

Figure S4.1: Additional surface water geochemistry profiles along sulfate gradient in Everglades. Concentrations are shown for sulfide (A), dissolved organic carbon (DOC) (B), and SUVA, a measure of aromaticity of the dissolved organic matter (C). n.d. = no detection, sample below detection limit.

Figure S4.2: Conceptual diagram of sampling scheme and normalization methods. **A.** Sediment cores and filtered porewater samples were collected from all sampling stations. **B.** The inorganic ^{201}Hg -enriched tracer was pre-equilibrated with the filtered porewater for four hours. Then, equilibrated tracer was injected into duplicate sediment cores from each station. **C.** This resulted in a total of 72 incubations (2 duplicates x 6 stations for sediments cores x 6 stations for filtered porewater). **D.** To calculate the relative Hg methylation potential (RMP) values for each porewater matrix, incubations were grouped by the sediment core station (grouped by row, in C.). All Me^{201}Hg production values in that group were divided by the maximum Me^{201}Hg production value from that group, normalizing all values to a scale of 0 to 1. In this way, we had 12 RMP values for each porewater, since we had two replicates using each sediment core. To calculate the RMP values for each sediment core, we did the same normalization method except that we grouped the incubations by the porewater matrix source (grouped by column, in C.).

Figure S4.3: Me^{201}Hg production for each set of incubations, grouped by sediment source. The y-axis is the fraction of the ^{201}HgT pool present as Me^{201}Hg . The x-axis is the station where the porewater was collected and the plots are faceted by where the sediment core was collected. Error bars represent the standard deviation on duplicate samples.

Figure S4.4: Me^{201}Hg production for each set of incubations, grouped by porewater source. This is the same data as that shown in Fig. S4.3, but faceted differently to highlight the role of the microbial community in determining MeHg production. Error bars represent the standard deviation on duplicate samples.

Figure S4.5: Maximum likelihood phylogenetic tree of *HgcA* (A) from study with references. Tree was made with RAxML. Paralog sequences were included in tree generation and used as a

root. Relative abundance of each *hgcA* gene is shown in B. Abundance values have been normalized to mean coverage of 16 ribosomal proteins in the assemblies.

Figure S4.6: Abundance plots of 16 ribosomal protein genes (black dots) and the mean abundance for all 16 (red triangles) across all metagenomes. KMBP006 metagenomes are porewater metagenomes that were only used for binning purposes.

Figure S4.7: Relative methylation potential (RMP) of the sediment core plotted against the *hgcA* abundance in the sediments. Error bars represent the standard error for both RMP and *hgcA* abundance. Similar to Fig. 4.3 but without log-log transformation and including uncertainty for *hgcA* measurements.

Figure S4.8: Plot of nonpareil coverage curves (A) showed similar levels of coverage across all metagenomes. There was no significant difference in nonpareil diversity (B) of the microbial communities in the sediment of the six different stations.

Figure S4.9: Stacked bar chart of phylum-level taxonomic classification for 16S genes assembled from the metagenomes using GraftM. Phyla that did not account for more than 5% of the total abundance in any metagenome were removed.

Figure S4.10: Gene abundance for terminal electron accepting processes across all six sites. A. *dsrD* is a marker for sulfate-reduction. B. Black dots represent one of eight methanogenic markers from TIGRFAM, red triangles are the mean coverage of those eight. C. *narGHI* constitute the membrane-bound nitrate-reductase, while *napA* encodes the periplasmic nitrate reductase. *narG* and *napA* have been confirmed using phylogenetic trees. D. *ccoNOP* constitutes the *cbb₃*-type terminal oxidase. E. Reverse *dsrA* (*rdsrA*) is involved in oxidation of sulfur species, most often sulfide. *rdsrA* is identified using the *dsrA* HMM, then identified as *rdsrA* based on phylogeny. F. Individual genes within the *sox* operon that mediates sulfide oxidation.

Figure S4.1

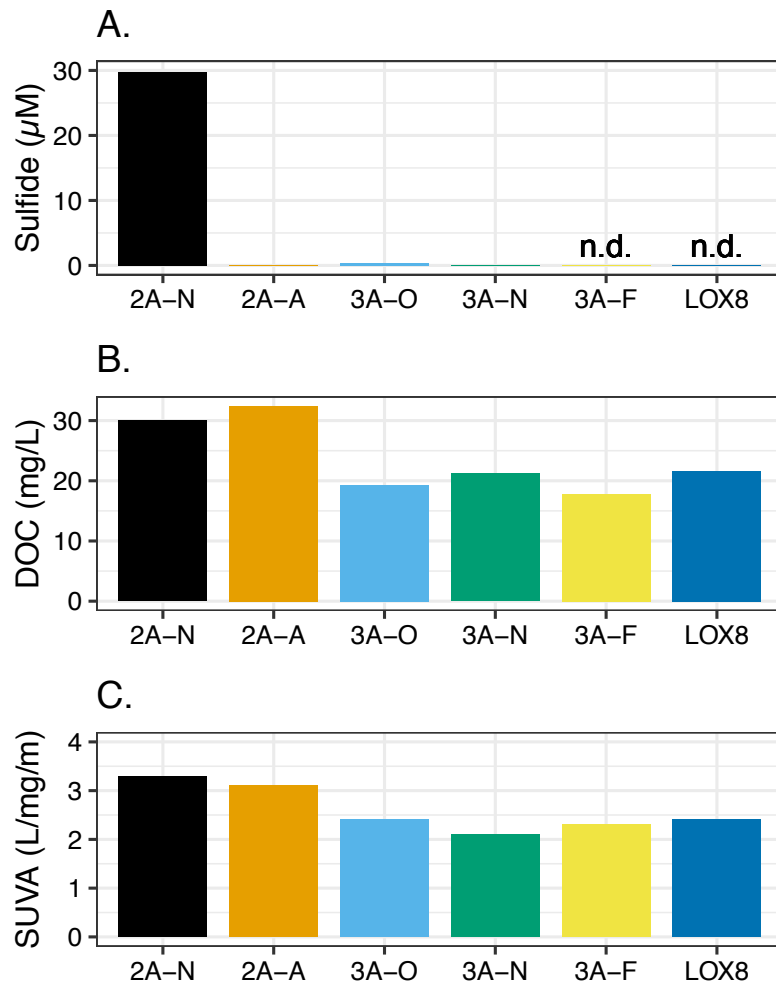


Figure S4.2

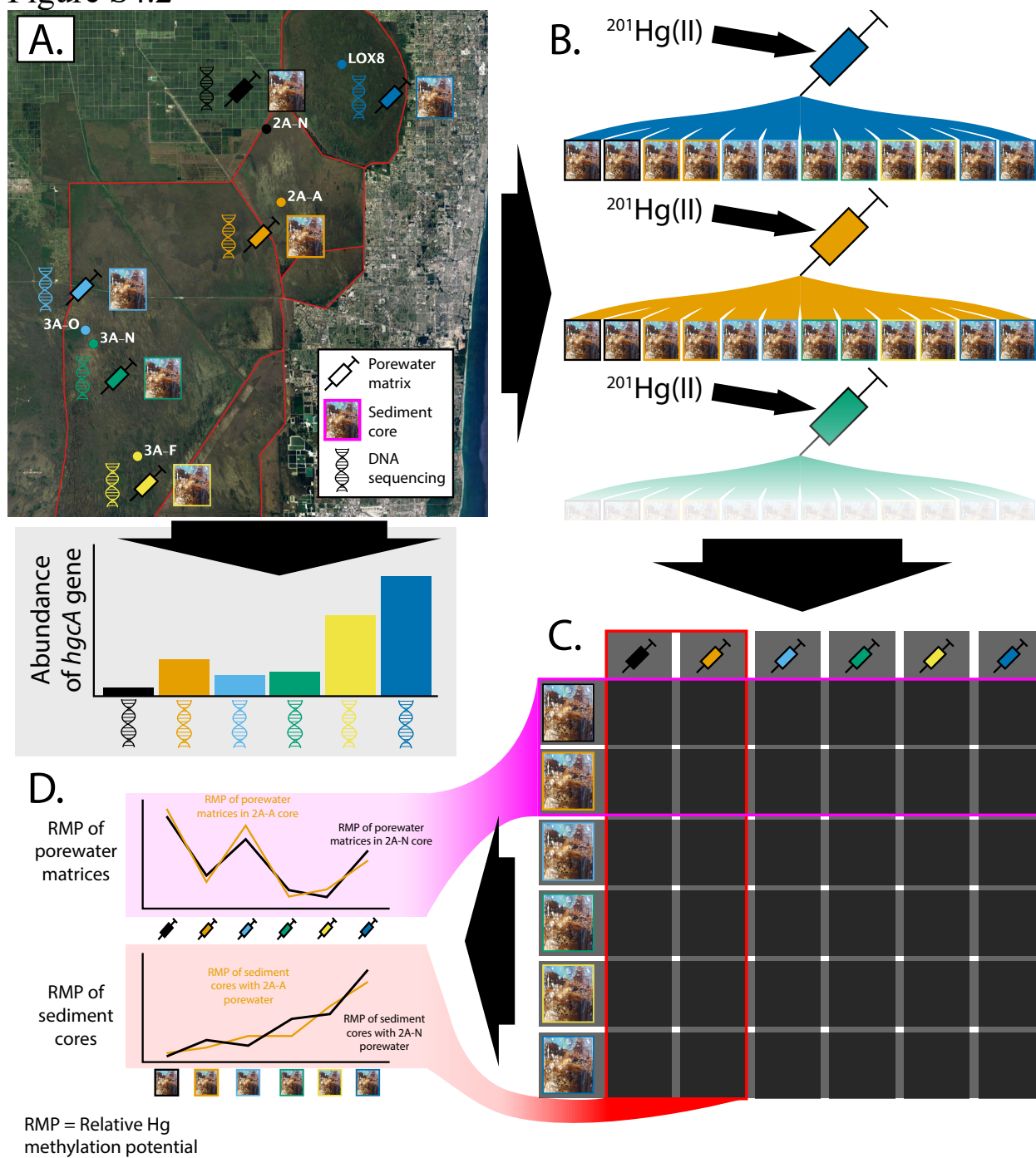


Figure S4.3

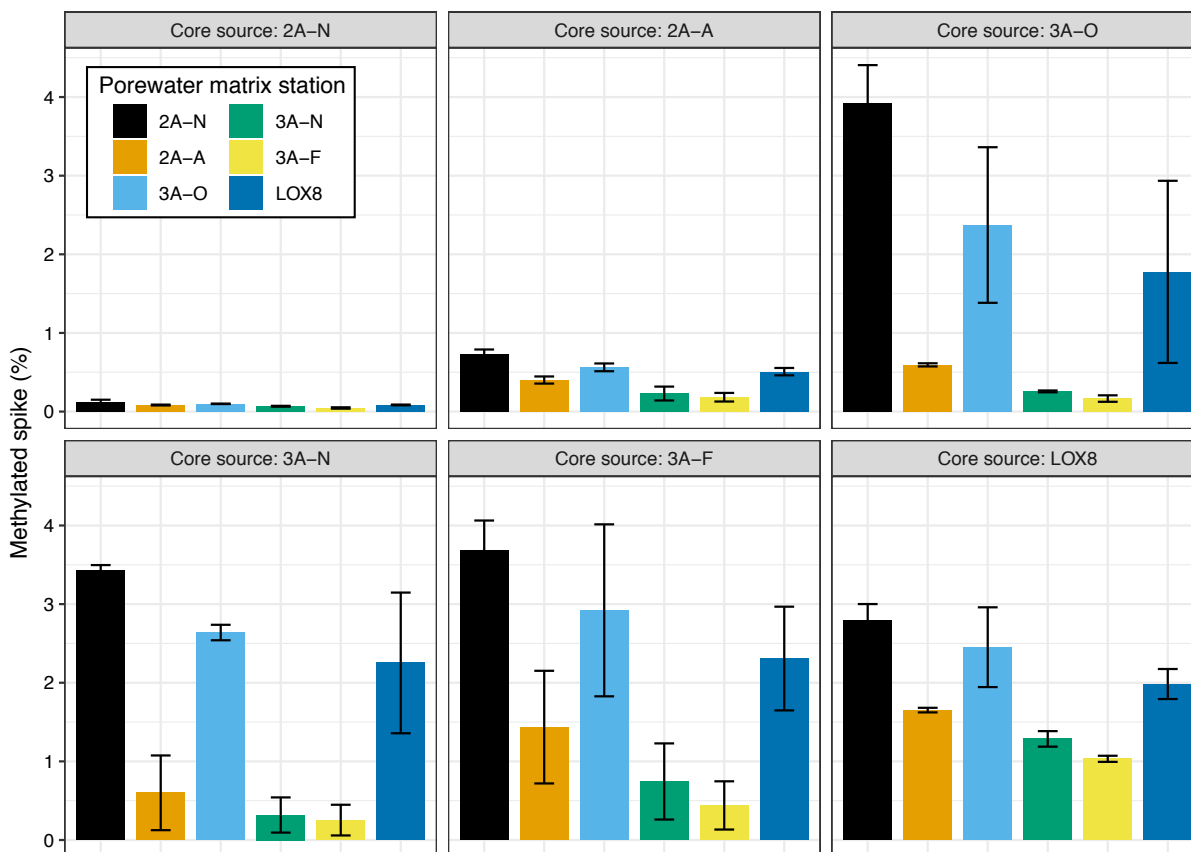


Figure S4.4

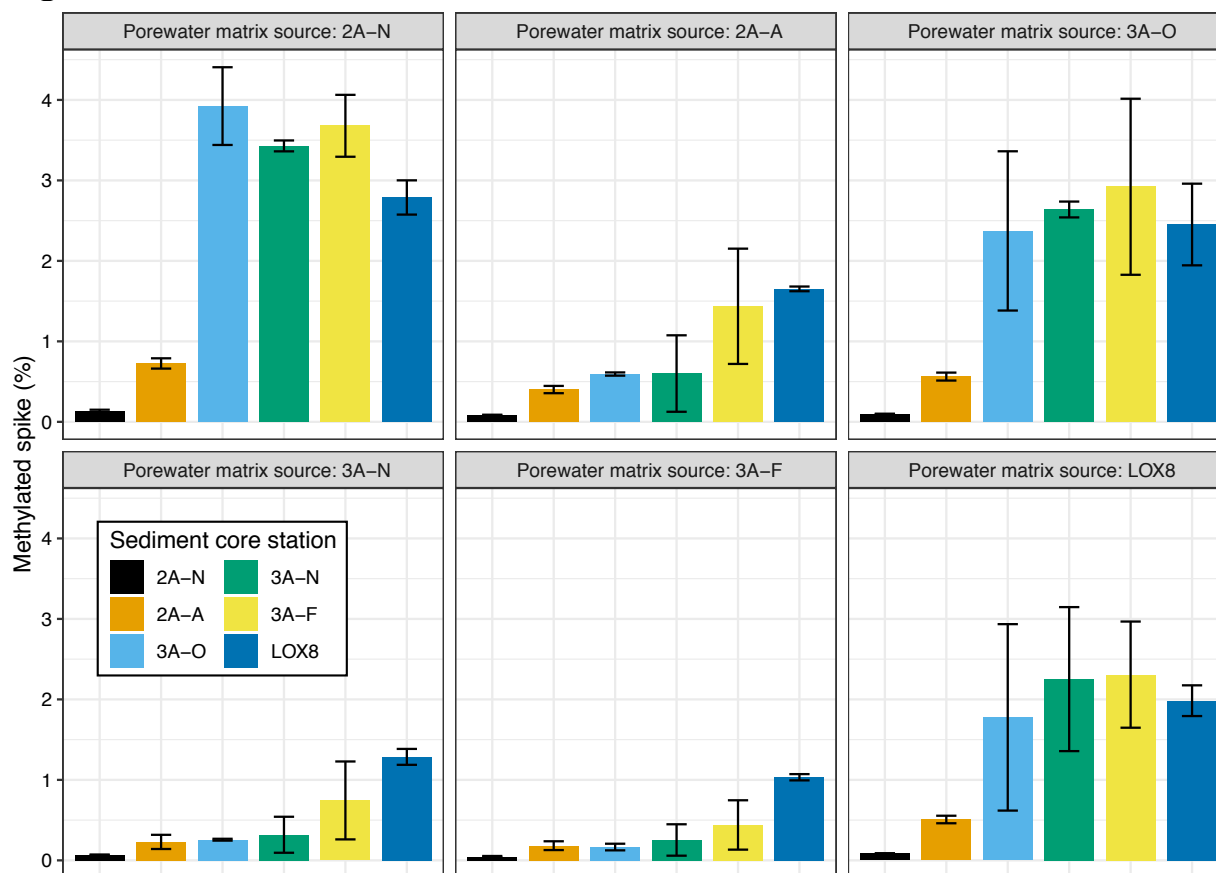


Figure S4.6

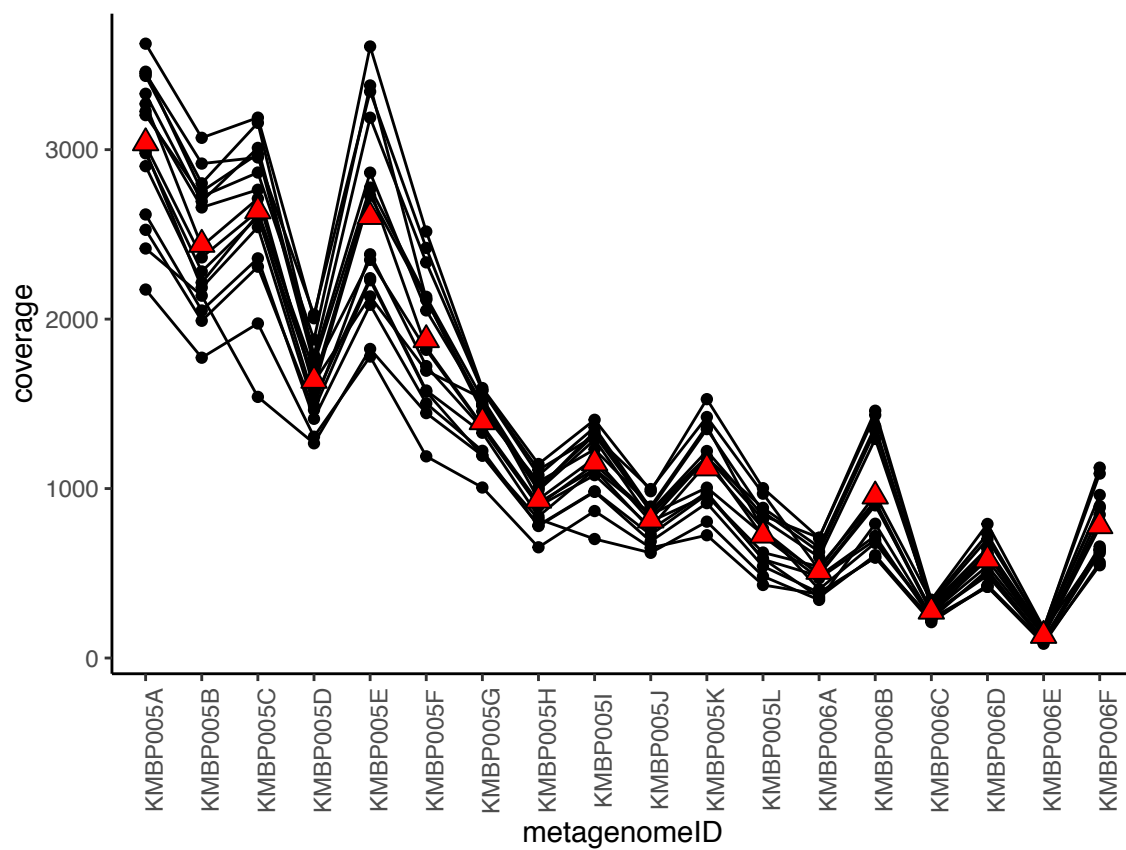


Figure S4.7

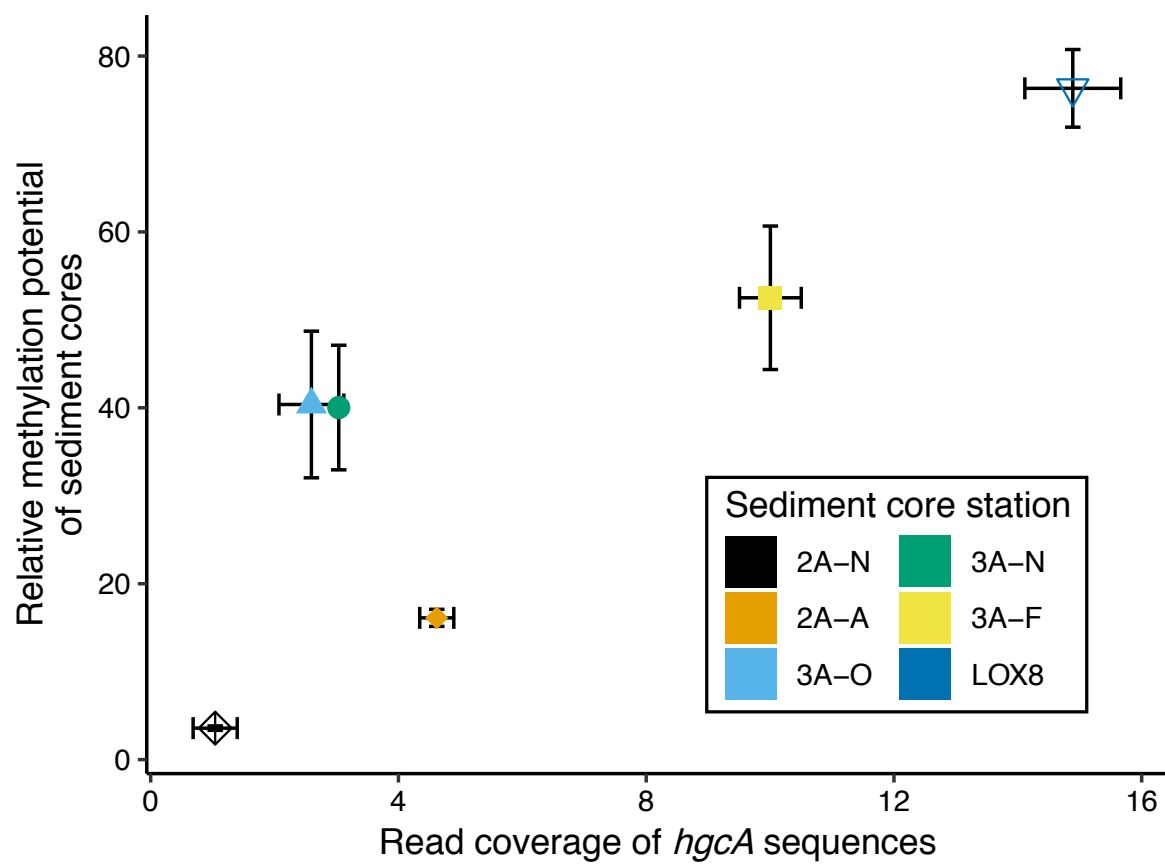


Figure S4.8

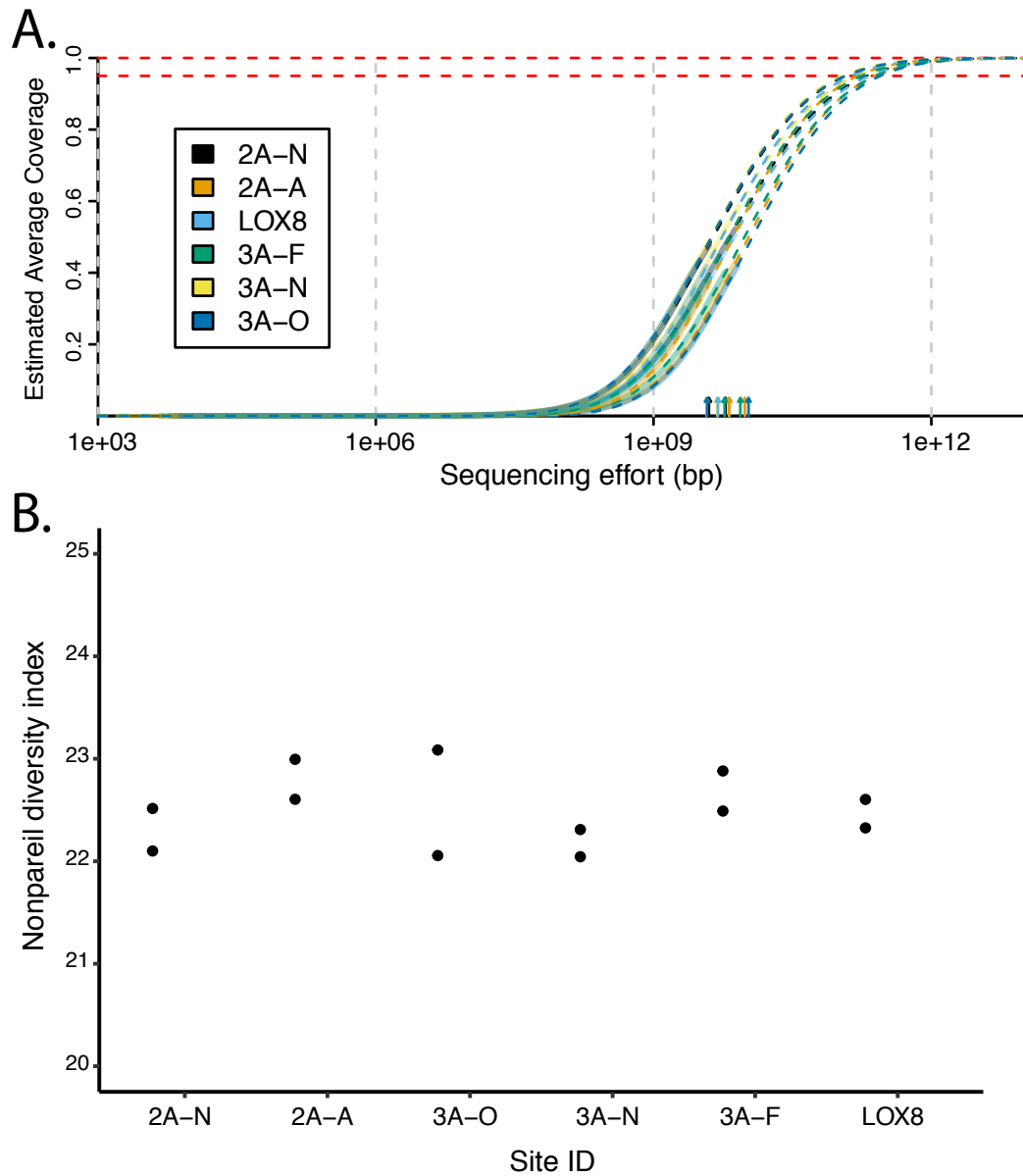


Figure S4.9

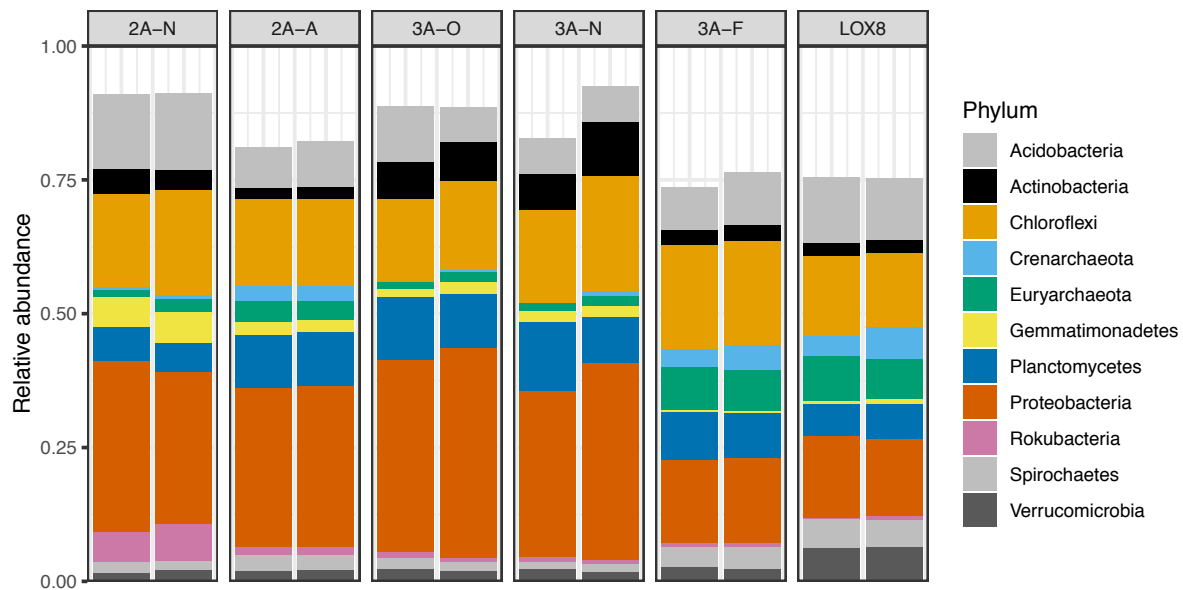
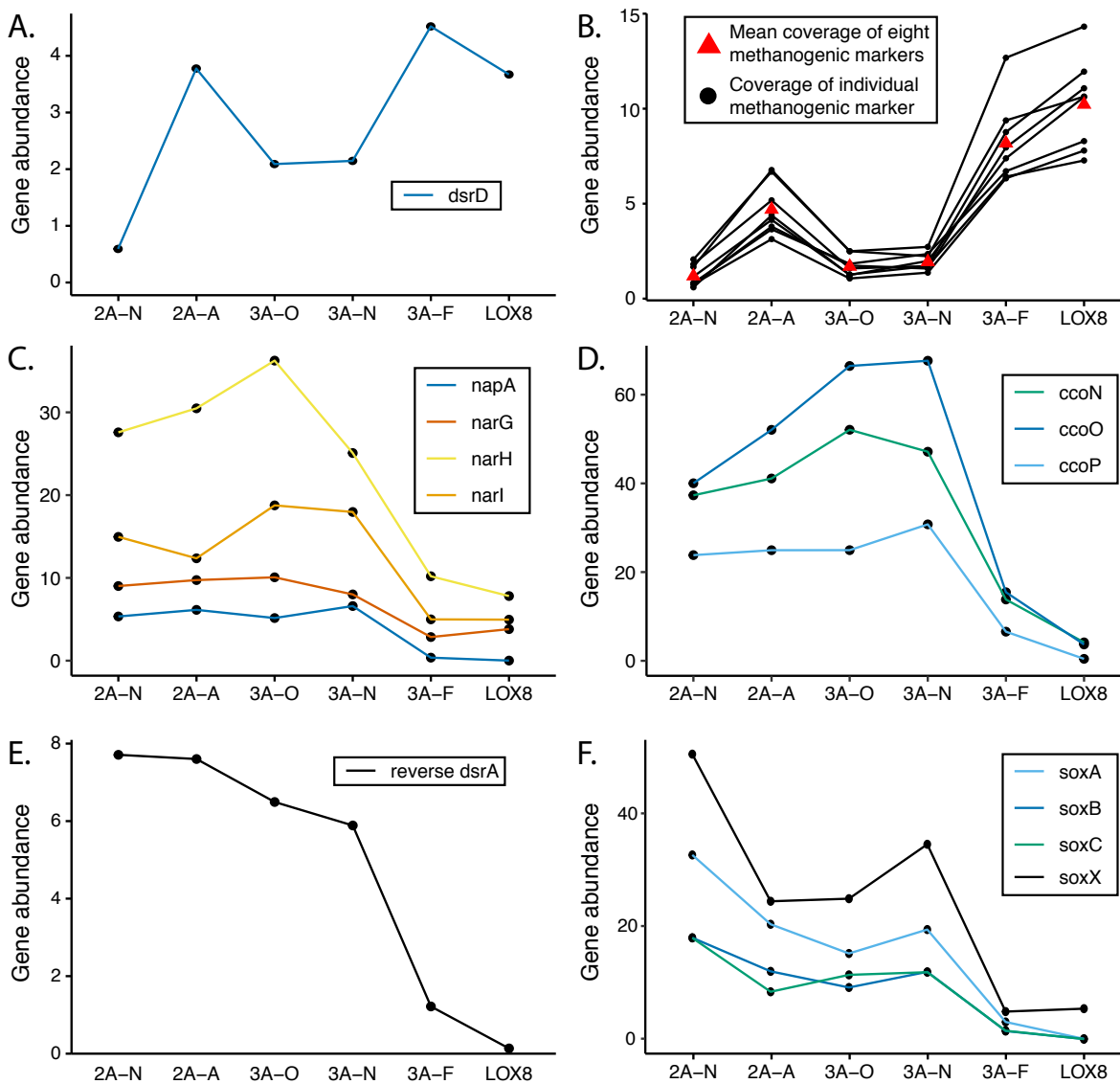


Figure S4.10



Chapter 5: Influence of sulfate reduction on methylmercury production
in a eutrophic freshwater lake.

This chapter is part of an ongoing study and will be incorporated into a future manuscript for publication.

Abstract

Sulfate-reducing bacteria (SRB) are linked to methylmercury production in many different environments. However, recent evidence has shown that SRB account for a small percentage of the microbial population carrying the mercury (Hg) methylation gene *hgcA*. In this study, we adapted and performed assays using a stable isotope enriched Hg tracer to measure MeHg production under ambient and molybdate-inhibited conditions across several spatial and temporal redox gradients in Lake Mendota. We also used shotgun metagenomic sequencing to identify both the Hg-methylating community and the flanking community. MeHg production was correlated to *hgcA* abundance, which was dominated by non-canonical Hg methylators, including fermentative Kiritimatiellaeota and respiratory Actinobacteria. While SRB accounted for less than two percent of the *hgcA* gene abundance, molybdate-inhibition reduced MeHg production by up to 71%. This work indicates that sulfate-reduction activity plays an outsized role in MeHg production relative to the abundance of SRB with *hgcA*. Future work on this study will investigate whether this is due to direct production of MeHg by the SRB Hg-methylators or to indirect anaerobic microbial food web effects in which SRB activity facilitates activity by the fermentative Hg methylators.

Introduction

Identifying the location and biogeochemical drivers of methylmercury (MeHg) production is an important step in understanding and possibly limiting MeHg accumulation in aquatic ecosystems. In freshwater ecosystems, MeHg production has been hypothesized to occur primarily in the sediments and then diffuse into the hypolimnion. However, recent studies, including chapters 2 and 3 of this thesis, have suggested that water column MeHg production is a major MeHg source to hypolimnion¹⁻³ and the aquatic food web⁴. This is partially due to the relative proximity of water column Hg methylation to the base of the aquatic food web, especially in lakes with a large anoxic hypolimnion. Despite this, biogeochemical drivers of Hg methylation in the water column are understudied relative to sediments.

Early work identified sulfate-reducing bacteria^{5,6} (SRB) and methanogens⁷ as the primary mediators of MeHg formation. Subsequently, the impact of sulfate reduction on MeHg production has been shown through correlations of MeHg and sulfide, MeHg production assays with molybdate inhibition or sulfate amendment, and isolation or sequencing of SRB with *hgcA*.^{8,9} This has led to efforts to mitigate Hg methylation of certain environments by increasing the redox state using nitrate or Mn oxide amendments¹⁰⁻¹². However, molecular sequencing of the Hg-methylating gene *hgcA* has revealed a vast metabolic diversity of putative Hg-methylators, including SRB, methanogens, fermenters, nitrate reducers, and/or Mn reducers across many different environments.¹³⁻¹⁶ This is echoed by diverse impact of SRB-inhibition on MeHg production across a range of environments.^{7,17-19} Attempts to link MeHg production to the *hgcA* community in the environment has highlighted the complexity of the relationship. For example, while we observed putative Hg methylating under suboxic conditions in Hells Canyon, the abundance of *hgcA*, both SRB- and non-SRB-associated, and MeHg concentrations increased

drastically when sulfide did appear (Chapter 3). In lake sediments, even when the *hgcA* gene pool does not include many sulfate reducers, inhibition of sulfate reduction has been observed¹⁸. On the other hand, sulfate enrichment can also reduce Hg methylation by reducing *hgcA* diversity and increasing the fraction of SRB Hg-methylators.²⁰ Collectively, this highlights the need to investigate the relationship between the microbial community and MeHg production under sulfate-reducing conditions.

In this study, we used a multi-pronged approach to link observed MeHg accumulation patterns along spatial and temporal redox gradients to the microbial community containing *hgcA*. Within Lake Mendota, SRB only accounted for a small percentage of the *hgcA* gene content, but MeHg accumulation increased drastically under sulfidic conditions (Chapter 2), suggesting that the true impact of SRB activity on MeHg production here is still poorly understood. In this chapter, our goal was to identify the role of sulfate reduction in the production of MeHg. We used an enriched stable isotope Hg tracer to measure MeHg production under ambient conditions and with molybdate inhibition across spatial and temporal redox gradients. We also performed shotgun metagenomic sequencing to identify and characterize the *hgcA*⁺ community and genes mediating common terminal electron accepting processes. Our results show that MeHg production occurs rapidly under ambient conditions and that *in situ* production is likely sufficient to explain MeHg accumulation in the water column. Molybdate inhibition resulted in decreased MeHg production, with the greatest decreases in the euxinic (samples with sulfide accumulation) deep hypolimnion. Despite this, *hgcA* genes were overwhelmingly associated with fermentative bacteria rather than sulfate-reducing organisms. This indicates that either the SRB have an outsized impact on MeHg production despite their low abundance or they have an impact on driving upstream metabolism. This study highlights the need for further work identifying the

mechanism for the role of sulfate reduction versus other forms of metabolism in driving MeHg production in aquatic ecosystems.

Materials and Methods:

Field site and sample collection: Sample collection was done at the deepest part of Lake Mendota, WI, USA, near the Long-Term Ecological Research buoy. Sampling was conducted during late stratification, in September and October. All sampling was done at night to minimize the incubation water exposure to sunlight. Temperature, dissolved oxygen, and turbidity profiles were collected using a multiparameter sonde (YSI, Yellow Springs, Ohio). Data was visualized in real time to guide adaptive sampling. All water samples were collected through a Teflon sampling line with a peristaltic pump. Samples for geochemical analyses were collected from throughout the metalimnion and hypolimnion. Samples for sulfide/sulfate analysis were preserved in 1% zinc acetate (ZnOAc). Samples for iron and manganese analysis were preserved in 2% nitric acid. Dissolved metal samples were filtered through a 0.45 μm poresize filter before acidification. From a subset of depths, we also collected water for MeHg production assays. At these depths, we filtered 460-580 ml of water onto a 0.2 μm poresize Sterivex filter, which were flash-frozen in liquid nitrogen within 90 seconds of collection. Water for Hg analysis was overfilled into a new 2L PETG bottle using the clean hands/dirty hands technique²¹ then double-bagged and stored on ice. Water was filtered within 24 hours onto a quartz fiber filter (QFF). The filtrate was preserved to 1% HCl and the QFF was frozen for particulate analysis.

Hg methylation incubations: Water samples for incubations were collected directly into trilaminate bags with a EVOH Coex liner suitable for trace metal sampling (ProAmpac, Rochester, NY). Filtered control bags were filtered in-line using a 0.2 μm poresize Sterivex filter

before collection in the bag. Bags were stored in a cooler in the dark during sample collection, then placed into a plastic bin with holes in it to allow water to flow through. The bins were resuspended in the lake at the original sampling depth for 24 hours before injection with the enriched stable isotope tracer. Filtered water from each depth was collected for use in preparing the stable isotope-enriched Hg tracer. This water was first stored in a cooler then wrapped in foil and stored in an anaerobic glovebox back in the lab. Five hours before injection into the bags, $^{198}\text{Hg}(\text{II})$ and Me^{204}Hg were added to the filtered water to a final concentration of ~ 100 ng/L and allowed to equilibrate with ambient ligands. A separate equilibrated tracer was prepared for each sampling depth, using water collected from that depth. Incubation bags were retrieved from the water column. Molybdate-inhibited incubations were injected with molybdate dissolved in N_2 -purged water, up to a concentration of 18 mg/L to match the maximum sulfate levels. All bags were then injected with 5 ml of equilibrated tracer per 500 ml of sample water, to a concentration of approximately 0.7-0.9 ng/L ^{198}Hg . All injections were done through the rubber outlet tubing on the bag and mixed into the system using a 60 ml syringe. Immediately after mixing the tracer into the sample, the t_0 sample was collected using a 50 ml syringe, stored in a new PETG bottle, and preserved in 1% HCl. This same sample collection was repeated at 24 (t_1) and 80 (t_2) hours. All incubations were carried out in triplicate, yielding a total number of 50 bags.

Geochemical analyses: Sulfide was quantified using the Cline's method with modifications for ZnAOc preservation.^{22,23} Sulfate was determined by ion chromatography using a Dionex 2100 with an AS9 column. Mn and Fe were quantified using inductively coupled plasma-mass spectroscopy (ICP-MS) on an Agilent 8900 Triple Quad. All Hg analyses were done at the U.S. Geological Survey's Mercury Research Lab (USGS MRL). For HgT analysis, samples were first treated with bromine monochloride to oxidize all Hg, then reduced using tin

chloride and quantified using cold vapor atomic fluorescence spectroscopy.^{24,25} MeHg samples, both filters and waters, were first distilled then quantified using isotope dilution with ICP-MS, following a modified U.S. EPA method 1630.^{26–28} MeHg and HgT analyses all passed all quality-controlled benchmarks set by the USGS MRL.

Incubation calculations and statistics: Relative rate constants (K_{metR}) were calculated using the following equation: $K_{\text{metR}} = (\text{Me}^{198}\text{Hg}_{\text{t1}} - \text{Me}^{198}\text{Hg}_{\text{t0}}) / (\text{number of days}) / {}^{198}\text{HgT}_{\text{t0}}$. We refer to this calculated value as a relative rate constant because we use only one time point in this calculation and because the added ${}^{198}\text{Hg(II)}$ is unlikely to exactly match the bioavailability of the ambient Hg(II), even with the pre-equilibration. Additionally, changes in the concentration of the reactant, ${}^{198}\text{Hg(II)}$, due to conversion to Me^{198}Hg and the loss of ${}^{198}\text{HgT}$ reduce certainty in the rate calculation. A two-way ANOVA was used to test for significant differences in K_{metR} between treatments and sample date/depth. Planned comparisons between the two treatments at each sampling location were completed using the emmeans package in R.

DNA extraction and sequencing: Sterivex filters were cut open using a PVC cutter and the filter removed. Half of the filter was placed in a bead-beating tube. Cells were lysed using both lysozyme and protease mixtures and through bead-beating. Polysaccharides and polyphenols were removed using CTAB and PVPP. DNA was then extracted twice using phenol:chloroform:IAA and washed with chloroform. DNA was then purified using alcohol precipitation and resuspended in nuclease-free water. Library prep was done using ~400 bp inserts with the Kapa Biosystem Library Prep kit at the Functional Genomics Lab at QB3 (Berkeley, CA). Sequencing was done at the Vincent J. Coates Genomics Sequencing Lab (QB3, Berkeley, CA) on an Illumina NovaSeq to generate 150 bp paired-end reads. 16S sequencing was done at the Biotech Center at the University of Wisconsin-Madison using the V3-V4 primers.²⁹

Bioinformatics processing for molecular sequencing: The fastp program was used to quality trim reads and merge overlapping pairs.³⁰ Metagenomes were assembled individually and coassembled using metaSPADes.³¹ Contigs shorter than 1000 bp were removed using anvi'o.³² Prodigal³³ was used on the metagenome mode to predict open reading frames (ORFs) and bowtie2³⁴ was used with the default settings to map reads to contigs. The raw gene abundance is calculated as the average number of reads mapping to each nucleotide within the gene. The abundance of each gene was normalized to the average abundance of 16 ribosomal protein (rp16) genes. Metabat2³⁵ and MaxBin2³⁶ were used to generate bins. These bins were aggregated using Das Tool.³⁷ The final set of bins were automatically generated using CONCOCT³⁸, then *hgcA*+ bins were manually curated in anvi'o³². Bins from different assemblies that shared 97% ANI and had 50% alignment were grouped into metagenome operational taxonomic units (mOTUs). Bin taxonomy was assigned using GTDB-TK³⁹. HgcA was identified in the ORFs from all assemblies using a custom HMM²³ and manually confirmed to have the requisite cap-helix domain and transmembrane domains near the C-terminus.¹³ CD-HIT⁴⁰ was used to cluster HgcA sequences at 97% identity across different assemblies and one representative from each cluster was selected. HgcA sequences from this study, Peterson et al²³, Jones et al⁴¹, and from the Hg-MATE database⁴² were aligned using MUSCLE⁴³. Residues with 50% gaps in the alignments were trimmed using trimal⁴⁴. A maximum-likelihood tree was generated using RAxML⁴⁵ with the LG substitution model. Support values for the branches were generated through 300 rapid bootstrap replicates. The tree was rooted using two paralogs of *hgcA*. The tree was visualized using the ggtree⁴⁶ package with RStudio. Hidden Markov Models (HMMs) were used with hmmer⁴⁷ to identify metabolic genes in the assemblies, which were confirmed using reference sequences and phylogenetic approaches. Metabolic annotations of the bins were done using

convergent approaches, including HMMs with hmmer, kofamscan⁴⁸, METABOLIC⁴⁹, and FEET. Phylogenetic reconstruction using FastTree⁵⁰ was used to confirm annotations of genes encoding TEAPs. 16S sequences were quality trimmed in mothur⁵¹ and classified using the Greengenes⁵² and FreshTrain⁵³ databases.

All the code used in this paper is available on GitHub:

<https://github.com/petersonben50/BLiMMP>.

Results:

Site description and geochemical profiles: Lake Mendota receives substantial nutrient input from the watershed and thermally stratifies early in the summer, leading to a succession of terminal electron acceptors in the hypolimnion (Fig. 1). Previous work has suggested water column Hg methylation is an important source of water column MeHg, especially starting in late August (Chapter 1). Thus, we focused our sampling on the water column in September and October. Thermal stratification began in mid-May and anoxia developed in the deep hypolimnion in 2020 by early June (Fig. S5.1). By mid-July, the entire hypolimnion was anoxic, which continued through until turnover (Fig. S5.1, 5.1a,d). While we did not measure nitrate in this study, data from the North Temperate Lakes – Long Term Ecological Research station have shown that nitrate is consistently depleted in the metalimnion and hypolimnion by early September.⁵⁴ In September, particulate manganese (Mn) levels peaked at 0.55 μM three meters below the oxycline, below which the Mn pool was exclusively in the dissolved form, accumulating to over 6 μM (Fig. 5.1b). In October, the redox gradient was compressed⁵⁵ due to the descending thermocline, and particulate Mn reached 1.3 μM immediately below the oxycline (Fig. 5.1e). This particulate Mn coincided with the peak in turbidity, which we targeted during

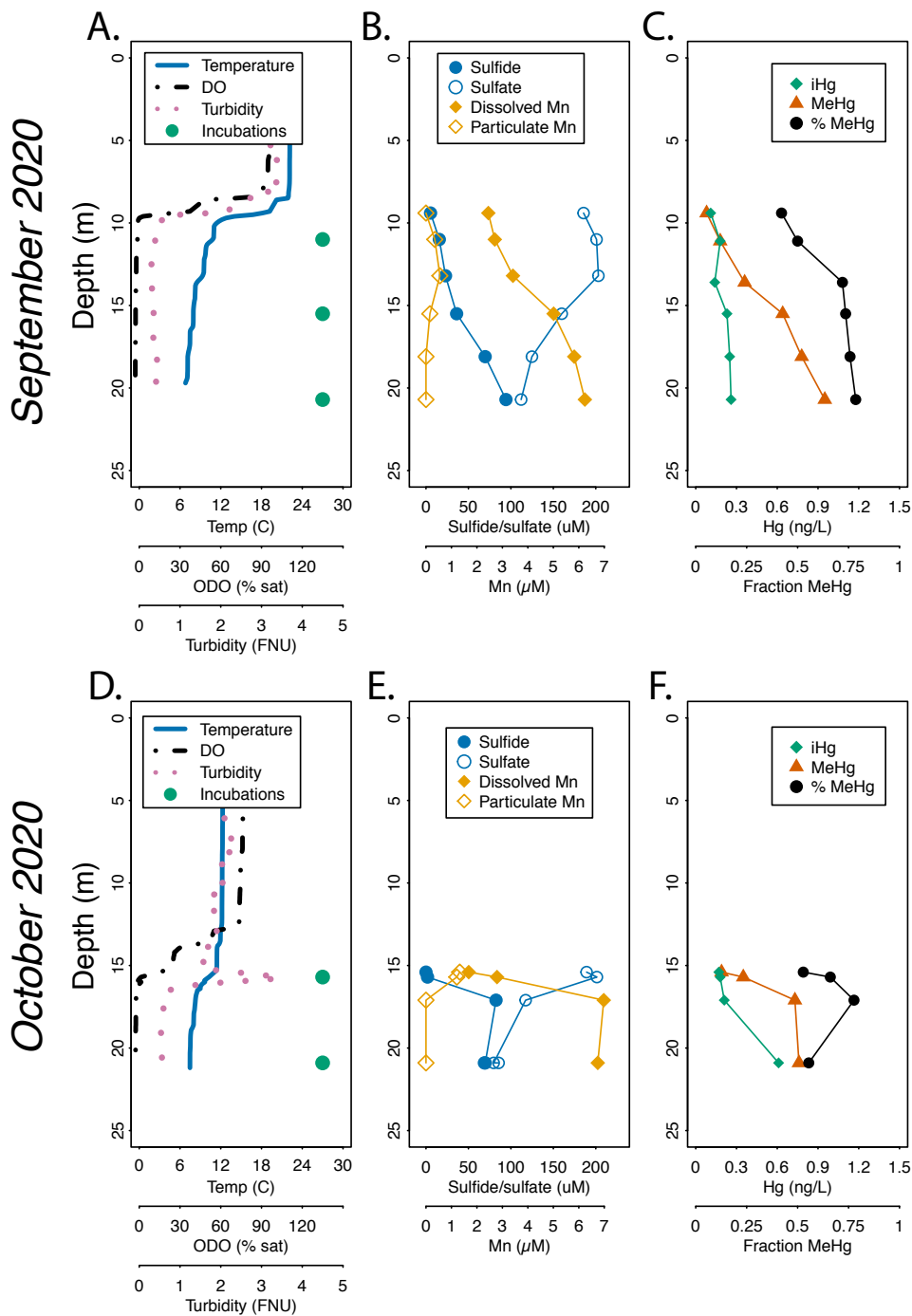


Figure 5.1: Physical, geochemical, and Hg profiles from two sampling dates. Green dots in A. and D. indicate where the Hg methylation assays were conducted. DO = dissolved oxygen, Mn = manganese, iHg = inorganic Hg, MeHg = methylmercury.

our sampling efforts (Fig. 5.1d,e). Fe concentrations were much lower than Mn, never reaching above 0.7 μM for the particulate phase and even less for the dissolved phase (Figure S5.2b,i). In September, sulfide levels were highest, nearly 100 μM , just above the sediment-water interface and non-detectable at the metalimnion (Fig. 5.1b). This trend was mirrored by the sulfate levels, which peaked in the metalimnion near 200 μM and decreased linearly down the water column to just over 100 μM above the sediment water interface. While sulfate showed a similar trend in October as in September, sulfide peaked at 83 μM in the upper hypolimnion before dropping to about 69 μM just above the sediment water interface (Fig. 5.1e). We also measured dissolved organic carbon (DOC) levels, suspended particulate matter (SPM), and bacterial carbon production (BCP) at a subset of the sampling locations (Fig. S5.2e,l). SPM and DOC did not change much within a profile, but in October, BCP was approximately four times higher near the oxic-anoxic interface than in the deeper hypolimnion.

Hg profiles: We focused our analysis on the dissolved fractions of the Hg species, since that is the fraction most likely interacting with the Hg-methylating organisms. Profiles of particulate Hg species are included in Fig. S5.2g,n. We define iHg here as the total Hg (HgT) minus MeHg. In September, iHg was consistent throughout the water column, ranging from 0.11 ng/L in the metalimnion to 0.26 ng/L in the deep hypolimnion (Fig. 5.1c). In October, iHg remained in this range in the upper hypolimnion and metalimnion but increased at the deepest depth to 0.61 ng/L (Fig. 5.1f). MeHg values were more variable in September, ranging from 0.08 ng/L in the metalimnion to 0.95 ng/L at the deepest depth (Fig. 5.1c). The percent of HgT present as MeHg (%MeHg) was higher in the lower hypolimnion (~75%) than the area just under the oxic-anoxic interface (~40-50%) (Fig. 5.1c). In October, MeHg reached a peak of 0.73 ng/L

in the upper hypolimnion and plateaued down to the bottom (Fig. 5.1f). Due to the elevated iHg in the deep hypolimnion, the percent MeHg peaked in the upper hypolimnion at 78% (Fig. 5.1f).

Sample depth selection: Five depths across the two sampling dates were selected based on the temperature, DO, and turbidity for use in shotgun metagenomic sequencing and MeHg production assays (Fig. 5.1a,d). Two of these depths (11 m in September and 15.7 m in October) had detectable particulate Mn and low sulfide levels and will be referred to as the “suboxic” samples. Two other samples (20.7 m in September, 20.9 m in October) were deeper in the hypolimnion and had undetectable particulate Mn and high sulfide concentration and will be referred to as the “euxinic” samples. The remaining sample, 15.5 m in September, had low particulate Mn but some sulfide accumulation as well and will be referred to as the “redox transition” sample.

Incubation results: Each incubation bag was injected with 0.80 ± 0.13 ng/L of $^{198}\text{Hg}(\text{II})$ (Fig. S5.3). Incubations were sampled three times: at 0 (t_0), ~24 (t_1) and ~80 (t_2) hours after adding the equilibrated isotope-enriched Hg and MeHg tracers. ^{198}HgT levels decreased consistently across most incubations, with an average decrease at t_1 of $13 \pm 9\%$ /day (mean \pm standard deviation) and a maximum decrease of 23% (Fig. S5.3). HgT loss slowed after the first 24 hours, averaging only $5 \pm 3\%$ /day from t_1 to t_2 . HgT loss was less pronounced during the October incubations than it was in September. Because of these decreases in HgT, we used the HgT concentrations from t_0 to calculate the rate constants below. At t_0 , there was only detectable Me^{198}Hg in one of the 50 incubations (Fig. S5.4). Additionally, no detectable Me^{198}Hg was produced in any of the filtered controls at any time point. There was detectable Me^{198}Hg production under ambient conditions and molybdate-inhibition for each location, with only some incubations from the suboxic region in September having undetectable Me^{198}Hg production.

Despite the high levels of Me¹⁹⁸Hg production and moderate loss of ¹⁹⁸HgT, which together indicate a substantial decrease in ¹⁹⁸Hg(II) in several incubations, we observed nearly linear Me¹⁹⁸Hg production through 80 hours (Fig. S5.4).

We used the Me¹⁹⁸Hg concentrations at t_1 and the ¹⁹⁸HgT concentrations at t_0 to calculate a relative Hg methylation rate constant (K_{metR}) for each incubation under ambient conditions and molybdate-inhibition (Fig. 5.2). For incubations under ambient conditions, K_{metR} ranged from 0.003 to 0.185 day⁻¹, with higher K_{metR} in the euxinic samples than the high redox and suboxic samples (Fig. 5.2, 5.3a). The highest K_{metR} values were observed in the October incubations from 20.9 m. At each depth, the K_{metR} values for the molybdate-amended samples were lower than the K_{metR} values under ambient conditions. A two-way ANOVA test revealed a significant effect of treatment conditions, sample location and an interaction of the two on the K_{metR} values ($p < 0.0001$). Planned comparisons of the treatments within a sample location revealed significant differences in K_{metR} between molybdate-inhibited and ambient incubations for the two euxinic samples ($p < 0.0001$). The difference between ambient conditions and molybdate-inhibited samples at the redox-transition sample was nearly significant ($p = 0.07$), while the two suboxic samples showed no significant difference ($p > 0.35$). We did not quantify the effect of molybdate on Me¹⁹⁸Hg production in the suboxic samples due to the lack of a significant difference between ambient and molybdate-inhibited conditions and to the Me¹⁹⁸Hg concentrations being below the limit of quantitation. For the other three samples, however, we calculated the percent reduction in Me¹⁹⁸Hg production due to molybdate amendment. Molybdate-amendment reduced the K_{metR} values by 71% in the two euxinic samples, while it only reduced K_{metR} by 44% in the redox-transition sample (Fig. 5.4b).

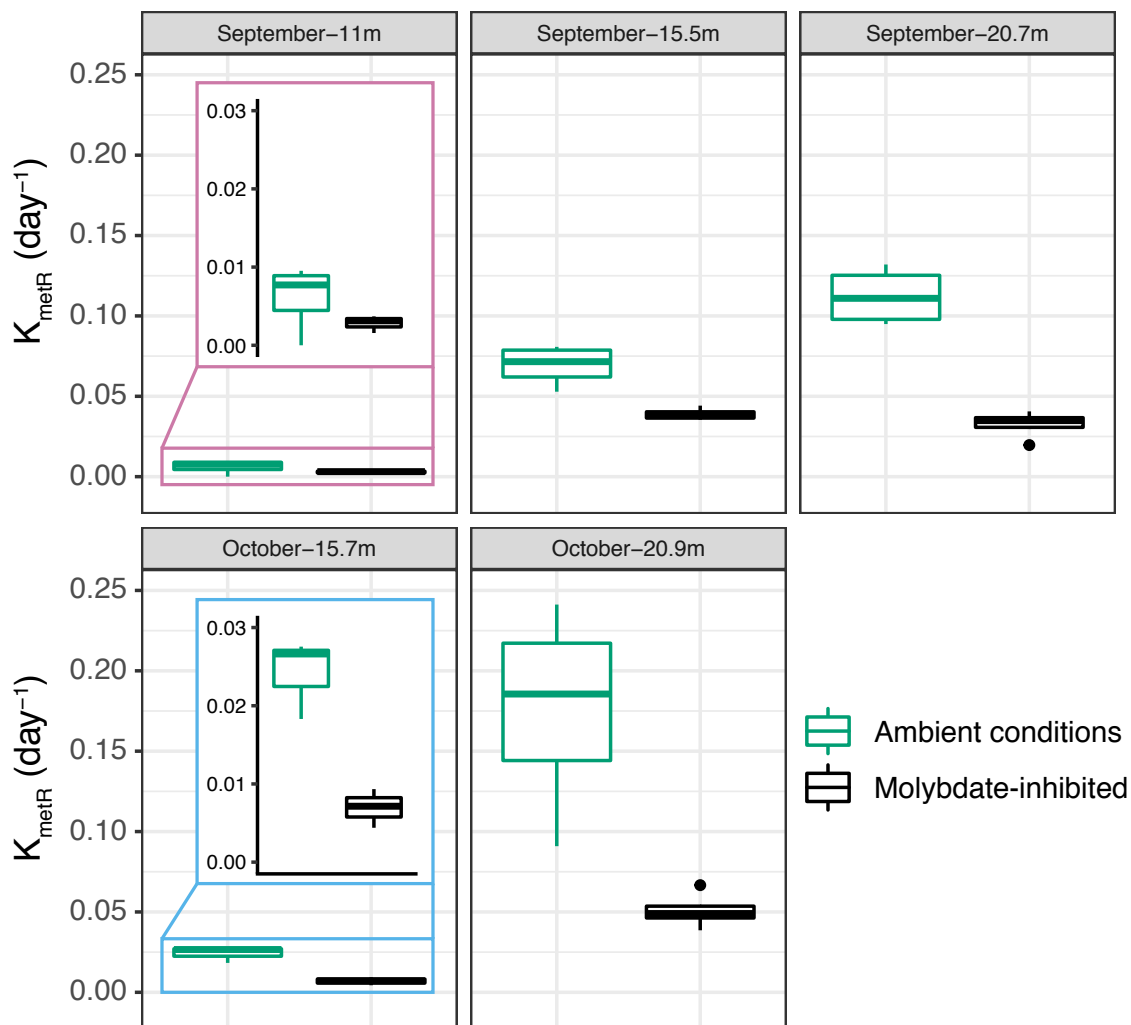


Figure 5.2: Inhibition of SRB reduces Me^{198}Hg production. Calculated K_{metR} values for ambient- and molybdate-inhibited microbial communities at all five sampling locations.

***hgcA* genes:** Across the five metagenomes, we identified 32 *hgcA* gene sequences. All *hgcA* genes encoded proteins with the requisite cap-helix domain and transmembrane domains at the C-terminus end. All *hgcA* genes with assembled DNA downstream of *hgcA* included an *hgcB* gene. Abundance of *hgcA* ranged from 4 to 17% of the rp16 coverage and was highest in the euxinic samples and lowest in the suboxic samples, with the redox transition sample in the middle (Fig. 5.3b). Thus, *hgcA* abundance increased with increasing K_{metR} values (Fig. 5.3a-b, S5.5). Phylogenetic analysis revealed that most identified *hgcA* genes were closely related, in some cases identical, to *hgcA* genes recovered in a previous study on the lake from 2017²³, suggesting a consistent methylator population from year to year (Fig. S5.6). Each sequence was assigned a taxonomic classification based on these phylogenetic similarities and, if no related sequence was found, reference sequences from the Hg-MATE database⁴².

Fermentative Hg-methylators: The *hgcA* gene pool was dominated by sequences from obligately fermentative organisms. The Kiritimatiellaeota-associated *hgcA* sequences were by far the most abundant, accounting for 60-78% of the *hgcA* abundance in all samples (Fig. 5.3). We successfully reconstructed one Kiritimatiellaeota-associated bin (BLI20_KIR), which was highly abundant in the September profile at the redox transition and the euxinic regions with 48 and 30%, respectively, of the total *hgcA* gene abundance. BLI20_KIR corresponded to an obligately fermentative organism with a high number of glycoside hydrolases. We recovered many other, lower abundance, *hgcA* sequences that are predicted to be from obligately fermentative organisms, including from Spirochaetes, Clostridia, Verrucomicrobia, and Lentisphaerae. All of these *hgcA* clusters except Spirochaetes had a closely related *hgcA* gene in a bin corresponding to an obligate fermenter from a previously study from this lake (Fig S5.6).²³

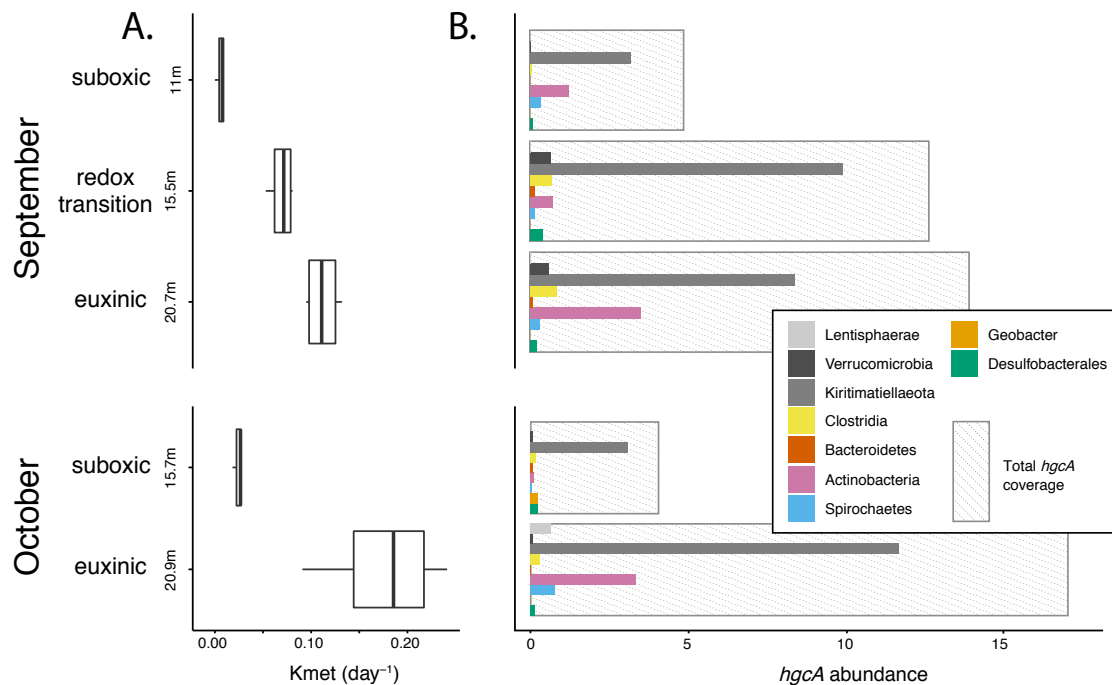


Figure 5.3: K_{metR} values (A) track closely with *hgcA* abundance (B). Large bars shaded gray show total *hgcA* coverage. Bars shaded with different colors inside those bars correspond to coverage of different taxonomic groups.

Respiratory Hg-methylators: The *hgcA* sequences from organisms predicted to have respiratory metabolisms were less abundant overall. Actinobacteria-like *hgcA* sequences were the second most abundant sequences, accounting for 3-25% of *hgcA* abundance across all samples (Fig 5.3b). We recovered one *hgcA*⁺ Actinobacteria-affiliated bin (BLI20_ACT), which contained a partial electron transport chain and had five multiheme cytochrome c proteins, which suggest it may be capable of respiratory metabolism. However, we did not identify any well-characterized genes used in major TEAPs in this bin. One *hgcA* gene shared 90% amino acid sequence identity with an *hgcA* gene from a Bacteroidetes bin (BAC_0005) reconstructed from this lake in 2017 (Fig S5.6).²³ This bin, along with several other closely related *hgcA*⁺ Bacteroidetes bins, contained an electron transport chain, putative external electron transfer genes, and some polysulfide reductases, suggesting these Hg methylators are also reliant on an array of respiratory pathways. Several *hgcA* associated with putative sulfate-reducing Desulfobacterales were present, but only accounted for a small percentage of the *hgcA* abundance, with a maximum of 6% of the total *hgcA* abundance at 15.7 m in October (Fig 5.3b, 5.4c). We also recovered a single *hgcA* sequence, only present at 15.7 m in October, that shared 99% sequence identity with an *hgcA* sequence from a putative Mn-reducing *Pelobacter* bin recovered in a previous study on this lake. Overall, these putative respiratory *hgcA*⁺ bins only accounted for less than 5% of the *hgcA* abundance in all samples except for the suboxic samples in October.

Sulfate reduction: Reductive *dsrA* and *dsrD*, both associated with sulfate reduction, increased from the metalimnion/upper hypolimnion on both dates (Fig. 5.4F). These *dsr* genes are present at low abundances, ranging from < 0.1% to 1.5% of the microbial community. None of these sequences were binned so we could not classify the SRB bacteria present. From a

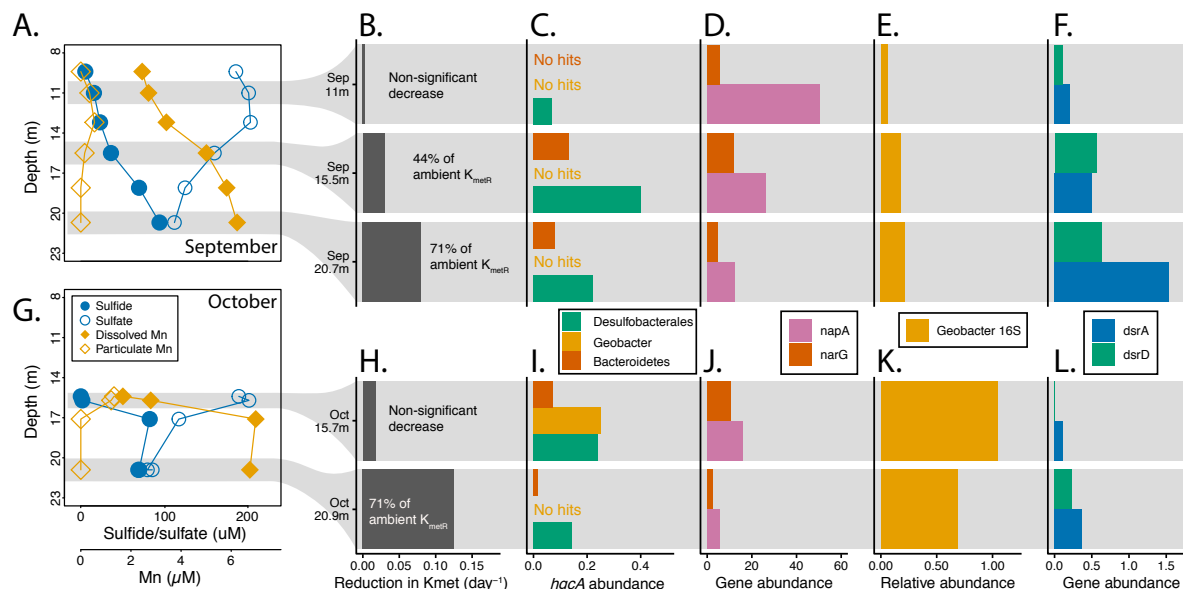


Figure 5.4: Profiles of TEAP markers in the water column from the two sampling dates. Profiles of sulfate, sulfide, and particulate/dissolved Mn are shown for reference in A and G. B and H profiles show the reduction in K_{metR} in response to molybdate inhibition. For those that we calculate the fraction inhibition, the values are written on the plot. Abundance of *hgcA* sequences associated with respiratory organisms are shown in C and I. Remaining plots show abundance of nitrate reductase genes *narG* and *napA* (D, J), the relative abundance of 16S sequences associated with *Geobacter* in an amplicon sequencing library (E, K) and the abundance of dissimilatory sulfite reductase subunits *dsrA* and *dsrD*. The *dsrA* subunits only include sequences associated with reductive *dsrA* branches and not the reverse *dsrA* branch. All gene abundances are normalized to the mean abundance of 16 ribosomal proteins.

previous study, eight bins were identified as SRB out of 228 bins. To further explore the SRB community, we mapped the reads from this study to this set of bins. SRB bins accounted for 0.5% to 1.1% of the total mapped reads, with Desulfobacterales bins the most abundant SRB, followed by Syntrophobacterales.

Metabolic genes: We also searched for additional genes that could be mediating TEAPs in these samples. Abundance of the periplasmic nitrate reductase *napA* decreased from the suboxic regions to the euxinic samples on both dates, while in September the *narG* nitrate reductase peaked in the upper hypolimnion (Fig. 5.4D). We could not identify any porin-cytochrome c complexes homologous to those involved in mediating Mn oxide reduction through external electron transfer (EET) in *Geobacter*. This does not imply an absence of any genes capable of EET, however, as that process is likely mediated by a wide array of yet unidentified genes. Using 16S amplicon sequencing, we identified sequences associated with the Geobacteraceae family (Fig. 5.4E). Previous metagenomes from this lake included several Geobacteraceae-associated bins, all of which had EET pathways.²³ Geobacteraceae was low in abundance in September, but increased to 1% of the total microbial community in the suboxic region by October. We searched for *mcrA*, *mtrA*, and several other methanogenic markers but did not find any.

Discussion:

Here, we adapted a stable isotope-enriched Hg tracer method to measure the Hg methylation potential of depth-discrete water samples from a freshwater lake reliably and consistently.^{1,56} For each incubation with detectable MeHg production, we calculated a relative rate constant (K_{metR}) for MeHg production (Fig. 5.2). These K_{metR} values are best thought of as a

potential rather than a true rate constant⁵⁷, for several reasons. First, we only calculated K_{metR} over one time interval (t_0 to t_1). Sampling and analytical constraints hampered more frequent sampling under 24 hours and the continued loss of HgT and high MeHg production rates indicated that by 80 hours the reactant concentration had decreased substantially. However, the near linearity of Me¹⁹⁸Hg production through both time intervals (Fig. S5.4) suggests that we are measuring an ongoing rate rather than having a burst of production at the start of the incubation, which is consistent with previous studies in freshwater lakes that have observed linear MeHg production for at least 24 hours^{1,58}. Second, there was some loss of tracer during the incubation period, likely due to sorption to the EVOH Coex walls of the bags. We did not extract and quantify the Hg from the walls, and thus cannot comment on the ratio of iHg to MeHg lost. By using the ¹⁹⁸HgT concentration from t_0 we assumed that all of the lost ¹⁹⁸Hg was iHg and available as a reactant for methylation. These are conservative assumptions in this calculation; therefore, the calculated relative rate constants are lower bound estimates of the true rate constants with respect to reactant concentration and product loss. Third, while we pre-incubated the tracer with filtered water to allow the ¹⁹⁸iHg tracer to bind to ambient ligands, we acknowledge that the availability of the tracer is likely still different than that of the ambient Hg. Especially in the euxinic samples, it is possible that kinetic constraints on iHg complexation limit the formation of recalcitrant HgS particles in favor of more bioavailable Hg-DOM complexes.^{59,60} This likely means that the K_{metR} values are overestimations of the true rate constants with respect to bioavailability constraints. Despite these limitations, however, K_{metR} values were consistent across replicates for each of the different sampling depths, time, and across treatments, suggesting it is a valuable approach for measuring differences in MeHg production potential in response to changes in geochemistry or to inhibitor amendment.

The high rates of MeHg production observed here support the hypothesis that *in situ* production can be a major source of MeHg in the water column of freshwater lakes, as opposed to strictly from diffusion from the sediments.² Concentration gradients of MeHg leading out of the sediments, as observed in the September profile (Fig. 5.1c), are often interpreted to mean that MeHg accumulation in the hypolimnion is largely due to MeHg production in the sediments that subsequently diffuses into the hypolimnion. However, here we observe that Me¹⁹⁸Hg production in the deeper euxinic samples is also higher. At the euxinic depths, up to 50% of the original enriched isotope spike had been converted into MeHg after 80 hours. This is surprisingly high, considering that only 50% of the ambient Hg pool is MeHg at that location. The consistent low levels of iHg throughout the water column (Fig. 5.1c,f), around 0.25 ng/L, also suggest high levels of MeHg water column Hg methylation. The one exception to this is the higher levels of iHg in the deep euxinic sample in October (Fig. 5.1f). Additionally, the correlation of MeHg production with *hgcA* suggests *in situ* production as a dominant source of MeHg (Fig. S5.5). Collectively, these data suggest that high rates of MeHg production in the water column produce or at least maintain the high levels of MeHg in the hypolimnion. The water column Hg methylation rates observed here are higher than, but comparable to, K_{metR} values from a number of different oligotrophic, mesotrophic, eutrophic, and dystrophic lakes.^{1,41,57,61,62}

This study highlights the likely role of fermentative organisms in MeHg production in the hypolimnion. Under euxinic conditions, when sulfate reduction is predicted to be the dominant TEAP, Me¹⁹⁸Hg production continued with a K_{metR} of 0.03 to 0.05 day⁻¹ in the bags with molybdate amendments (Fig. 5.2). Because this rate continued throughout the entire incubation, at both 24 and 80 hours (Fig. S5.4), it is likely that this production is entirely independent of sulfate-reduction rather than occurring before sulfate reduction was fully inhibited. This SRB-

independent MeHg production is likely due to the abundant obligately fermentative Hg methylators we observed at all depths. These fermentative putative Hg methylators, particularly the Kiritimatiellaeota, have been identified as major constituents of the *hgcA* population across multiple marine⁶³ and freshwater⁴¹ environments, including chapters 2 and 3 of this thesis. While the partial or non-existent inhibition of MeHg production in response to molybdate is often attributed to Hg methylation by methanogens or iron-reducers, the results here suggest fermentative organisms may play a role as well.^{18,19,64} Efforts to stimulate MeHg production by adding fermentative end-products such as acetate or lactate often show no increase or an inhibitory effect on MeHg production, which could be linked to inhibition of fermentative organisms by increasing the concentration of the end product.^{65,66} While many of these organisms have not been experimentally verified to produce MeHg, the functional assays combined with the molecular sequencing provides evidence that they are environmentally relevant Hg-methylators.

Despite the low abundance of SRB with *hgcA*, sulfate reduction still clearly plays an important role in MeHg production. Molybdate inhibition eliminates 71% of the Me¹⁹⁸Hg production in the euxinic samples and 44% in the redox transition zone (Fig. 5.4c). This is not particularly surprising, as at least partial inhibition of MeHg production in response to molybdate amendment has been observed in many environments, including in lake sediments^{5,6,18}, the water column of freshwater lakes⁵⁷, settling particles in a lake⁶², wetland sediments⁶⁷, and periphyton^{17,68}. While inhibition of SRB has the potential to impact bioavailability in addition to microbial Hg methylation capacity, the effect in this study was likely due to changes in microbial metabolism, as there was no detectable difference in sulfide accumulation between t_0 and t_2 in the incubation under ambient conditions or molybdate inhibition. Changes in MeHg production

in response to altered sulfate reduction dynamics, independent of changes in bioavailability, have been shown in sulfate-enriched sediments as well.²⁰ However, this molybdate-induced inhibition of Hg methylation was surprising considering that SRB only accounted for 0.8-3% of the *hgcA* abundance in these samples (Fig. 5.3b). While few studies have examined both the impact of SRB inhibition on Hg methylation activity and searched for *hgcA* sequences, amplicon sequencing of *hgcA* has shown limited presence of suspected SRB-associated *hgcA* genes in boreal lake sediments and wetland sediments where MeHg production was inhibited by molybdate amendment.^{18,67} However, the limitations on amplicon sequencing make it difficult to evaluate the true abundance of SRB with *hgcA* in these studies.

The first potential explanation for the observed discrepancy between molybdate-inhibition of MeHg production and the relative lack of SRB-associated *hgcA* sequences is that the small number of SRB Hg methylators are directly producing a high fraction of the MeHg. SRB Hg-methylators from Deltaproteobacteria are thought to be particularly efficient at producing MeHg, at least under laboratory conditions, but there is substantial variation between different organisms.^{14,69-71} Many of the abundant *hgcA* sequences associated with fermentative organisms are from taxa (Kiritimatiellaeota, Lentisphaerae) that have not been tested in the lab for MeHg production, thus we know little about their Hg methylation capacity. In the environment, there are many factors that could modulate a specific organism's Hg methylation capacity. While we know that *hgcA* transcription in *Desulfovibrio desulfuricans* and translation in *Geobacter sulfurreducens* PCA is not induced by Hg(II) exposure^{72,73} and *hgcA* transcription in *Desulfovibrio dechloroacetivorans* strain BerOcl is not induced by varying carbon substrates and terminal electron acceptors⁷⁴, the presence of putative transcriptional regulators, including some similar to arsenic resistance operon regulators, upstream from many *hgcA* sequences

suggests some form of regulation is likely in some organisms.^{16,75} RNA expression of *hgcA* from non-experimentally verified Hg methylators has been documented in two different systems^{16,76}, but how these transcriptional levels compare to other Hg methylators, particularly those from different metabolic guilds, is unknown. Differences in Hg(II) uptake mechanisms^{8,77} or preferential selection of different iHg pools⁷⁸ could also lead to varying MeHg production capacity between organisms in the environment. Additionally, carbon flow to Hg might be different in different organisms. The use of a methylated tetrahydrofolate (THF) molecule during methylation links *hgcA* to the THF cycle^{13,79}, which is involved in an array of biosynthetic, energy-conserving, and carbon-fixing pathways used under an array of different metabolic conditions.⁸⁰ These links may mediate the observed impacts of *hgcA* deletion on the redox state of the cell, single carbon metabolism^{73,81}, and outer membrane cytochrome expression⁷³. Understanding why the organisms produce MeHg and how it relates to the overall metabolic strategy of these organisms, alongside field studies using functional measurements combined with RNA sequencing or metaproteomics, will help us understand the direct contribution of different functional guilds to MeHg production in the environment.

Second, any SRB, even ones without *hgcA*, could influence MeHg production indirectly by modulating the metabolic activity of fermentative Hg-methylating organisms. The degradation of carbon molecules in anoxic environments is mediated by a consortium of microorganisms, often referred to as the anaerobic microbial food web through which carbon flows from top to bottom. In this study and in previous studies, putative Hg methylating organisms have been identified representing each of the functional guilds found in this conceptual microbial food web (Fig. 5.3).^{23,41} In these food webs, microbes are reliant on organisms “above” or “below” them in the food web to produce needed substrates or consume

products to drive their metabolism. If one organism is mediating a rate-limiting step in the process, changes in that organism's metabolism can have upstream or downstream effects on the other microbial community members. These processes have mostly been studied in lab-scale reactors and marine sediments, where hydrolysis of large carbon compounds at the "top" of the food web is often thought to be the major rate-limiting step in this process^{82,83}, but in several environments, terminal respiration can be a major bottleneck in community metabolism.^{84,85} Lake Mendota is a highly productive eutrophic lake with a highly labile organic carbon pool⁸⁶, which may suggest that carbon hydrolysis is not the rate limiting step. If so, by blocking sulfate-reduction we may also be inhibiting organisms reliant on the SRB to consume fermentation products such as formate, acetate, or hydrogen. This food web stimulation of MeHg production can be seen in the impact of non-Hg-methylating syntrophic partners⁶⁹ and the enhanced effect of stimulating both fermenters and SRB on Hg methylation⁸⁷. The geochemical (Fig. 5.1) and metabolic gene profiles (Fig. 5.4) suggest that sulfate reduction was the dominant respiratory pathway consuming fermentation products. Thus, the molybdate-induced reduction in Me¹⁹⁸Hg production at the euxinic depths could be due to greater reliance of the microbial community on SRB to drive community metabolism. Future experiments on MeHg production paired with broad-scale measurements of community metabolism and respiration and with RNA sequencing or metaproteomics will be critical for developing an accurate picture of how biogeochemical cycles and the microbes that mediate them influence the production of MeHg.

Acknowledgements

Funding for this project was provided by the National Science Foundation (NSF) through CBET Environmental Engineering. Graduate student funding for Benjamin Peterson was provided through the NSF Graduate Research Fellowship Program. This project would not have been possible without extensive assistance from the USGS Mercury Research Lab. Thanks to Dave Krabbenhoft and Sarah Janssen for extensive help on protocol development and data interpretation. Thanks to Jake Ogorek for assistance in protocol development and analytical support. Thanks to John DeWild and Mike Tate for helpful feedback on data interpretation. This would also not have been possible without an army of volunteers for fieldwork. Thanks especially to Amber White for her inability to tell me no when I ask for help with sampling. Thanks also to Marissa Kneer, Elizabeth McDaniel, Tylor Rosera, Hannah Tepsa Peterson, Anna Schmidt, Robert Marick, Riley Hale, Matt Scarborough, Kevin Walters, Charles Olmsted, Vince Butitta, Tedward Erker, Angie Buch, Kathryn Schmidt, Julian McMahon, and to anyone else I may have missed for coming out onto the lake in the middle of the night helping. Thanks to Frank Colombo of PacTech for helping with the incubation bag design.

References

1. Eckley, C. S. *et al.* Mercury methylation in the hypolimnetic waters of lakes with and without connection to wetlands in northern Wisconsin. *Can J Fish Aquat Sci* **62**, 400–411 (2005).
2. Watras, C. J. *et al.* Methylmercury production in the anoxic hypolimnion of a dimictic seepage lake. *Water, Air, and Soil Pollution* **80**, 735–745 (1995).
3. Poulin, B. A. *et al.* *Chemical characterization of water and suspended sediment of the Snake River and Hells Canyon Complex (Idaho, Oregon)*. <https://doi.org/10.5066/P9DT2B6J> (2020).
4. Lepak, R. F. *et al.* Factors affecting mercury stable isotopic distribution in piscivorous fish of the Laurentian Great Lakes. *Environ. Sci. Technol.* **52**, 2768–2776 (2018).
5. Compeau, G. C. & Bartha, R. Sulfate-reducing bacteria: Principal methylators of mercury in anoxic estuarine sediment. *Appl Environ Microbiol* **50**, 498–502 (1985).
6. Gilmour, C. C., Henry, E. A. & Mitchell, R. Sulfate stimulation of mercury methylation in freshwater sediments. *Environ. Sci. Technol.* **26**, 2281–2287 (1992).
7. Hamelin, S., Amyot, M., Barkay, T., Wang, Y. & Planas, D. Methanogens: principal methylators of mercury in lake periphyton. *Environ. Sci. Technol.* **45**, 7693–7700 (2011).
8. Hsu-Kim, H., Kucharzyk, K. H., Zhang, T. & Deshusses, M. A. Mechanisms regulating mercury bioavailability for methylating microorganisms in the aquatic environment: A critical review. *Environ. Sci. Technol.* **47**, 2441–2456 (2013).
9. Regnell, O. & Watras, Carl. J. Microbial mercury methylation in aquatic environments: A critical review of published field and laboratory studies. *Environ. Sci. Technol.* **53**, 4–19 (2019).
10. Todorova, S. G. *et al.* Evidence for regulation of monomethyl mercury by nitrate in a seasonally stratified, eutrophic lake. *Environ. Sci. Technol.* **43**, 6572–6578 (2009).
11. Matthews, D. A. *et al.* Whole-lake nitrate addition for control of methylmercury in mercury-contaminated Onondaga Lake, NY. *Environmental Research* **125**, 52–60 (2013).
12. Vlassopoulos, D. *et al.* Manganese(IV) oxide amendments reduce methylmercury concentrations in sediment porewater. *Environ. Sci.: Processes Impacts* **20**, 1746–1760 (2018).
13. Parks, J. M. *et al.* The genetic basis for bacterial mercury methylation. *Science* **339**, 1332–1335 (2013).
14. Gilmour, C. C. *et al.* Mercury methylation by novel microorganisms from new environments. *Environ. Sci. Technol.* **47**, 11810–11820 (2013).
15. Podar, M. *et al.* Global prevalence and distribution of genes and microorganisms involved in mercury methylation. *Sci. Adv.* **1**, 1–12 (2015).
16. McDaniel, E. A. *et al.* Expanded phylogenetic diversity and metabolic flexibility of mercury-methylating microorganisms. *mSystems* **5**, 1–21 (2020).

17. Cleckner, L. B., Gilmour, C. C., Hurley, J. P. & Krabbenhoft, D. P. Mercury methylation in periphyton of the Florida Everglades. *Limnol Oceanogr* **44**, 1815–1825 (1999).
18. Bravo, A. G. *et al.* Methanogens and iron-reducing bacteria: the overlooked members of mercury-methylating microbial communities in boreal lakes. *Appl Environ Microbiol* **84**, e01774-18, /aem/84/23/e01774-18.atom (2018).
19. Schaefer, J. K., Kronberg, R., Björn, E. & Skjellberg, U. Anaerobic guilds responsible for mercury methylation in boreal wetlands of varied trophic status serving as either a methylmercury source or sink. *Environ Microbiol* **22**, 3685–3699 (2020).
20. Jones, D. S. *et al.* Diverse communities of *hgcAB*⁺ microorganisms methylate mercury in freshwater sediments subjected to experimental sulfate loading. *Environ. Sci. Technol.* acs.est.0c02513 (2020) doi:10.1021/acs.est.0c02513.
21. Olson, M. L. & DeWild, J. F. Techniques for the collection and species-specific analysis of low levels of mercury in water, sediment, and biota. in *U.S. Geological Survey Water-Resources Investigations Report* vols 99-4018B (1999).
22. Cline, J. D. Spectrophotometric determine of hydrogen sulfide in natural waters. *Limnol Oceanogr* **14**, 454–458 (1969).
23. Peterson, B. D. *et al.* Mercury methylation genes identified across diverse anaerobic microbial guilds in a eutrophic sulfate-enriched lake. *Environ. Sci. Technol.* **54**, 15840–15851 (2020).
24. *U.S EPA Method 1631, Revision E: Mercury in Water by Oxidation, Purge and Trap, And Cold Vapor Atomic Fluorescence Spectrometry.* (2002).
25. Olund, S. D., DeWild, J. F., Olson, M. L. & Tate, M. T. Methods for the preparation and analysis of solids and suspended solids for total mercury. in *U.S. Geological Survey Techniques of Water-Resources Investigations, Book 5, Chapter A8* (2004).
26. DeWild, J. F., Olson, M. L. & Olund, S. D. *Determination of Methyl Mercury by Aqueous Phase Ethylation, Followed by Gas Chromatographic Separation with Cold Vapor Atomic Fluorescence Detection. Open-file Report.* (2002).
27. Horvat, M., Bloom, N. S. & Liang, L. Comparison of distillation with other current isolation methods for the determination of methyl mercury compounds in low level environmental samples. *Analytica Chimica Acta* **281**, 135–152 (1993).
28. Lepak, R. F. *et al.* Influence of *Cladophora*–quagga mussel assemblages on nearshore methylmercury production in Lake Michigan. *Environ. Sci. Technol.* **49**, 7606–7613 (2015).
29. Parada, A. E., Needham, D. M. & Fuhrman, J. A. Every base matters: assessing small subunit rRNA primers for marine microbiomes with mock communities, time series and global field samples: Primers for marine microbiome studies. *Environ Microbiol* **18**, 1403–1414 (2016).
30. Chen, S., Zhou, Y., Chen, Y. & Gu, J. fastp: an ultra-fast all-in-one FASTQ preprocessor. *Bioinformatics* **34**, i884–i890 (2018).

31. Nurk, S., Meleshko, D., Korobeynikov, A. & Pevzner, P. A. metaSPAdes: a new versatile metagenomic assembler. *Genome Research* **27**, 824–834 (2017).
32. Eren, A. M. *et al.* Anvi'o: an advanced analysis and visualization platform for 'omics data. *PeerJ* **3**, 1–29 (2015).
33. Hyatt, D. *et al.* Prodigal: prokaryotic gene recognition and translation initiation site identification. *BMC Bioinformatics* **11**, 119 (2010).
34. Langmead, B. & Salzberg, S. L. Fast gapped-read alignment with Bowtie 2. *Nat Methods* **9**, 357–359 (2012).
35. Kang, D. D. *et al.* MetaBAT 2: an adaptive binning algorithm for robust and efficient genome reconstruction from metagenome assemblies. *PeerJ* **7**, 1–13 (2019).
36. Wu, Y.-W., Simmons, B. A. & Singer, S. W. MaxBin 2.0: an automated binning algorithm to recover genomes from multiple metagenomic datasets. *Bioinformatics* **32**, 605–607 (2016).
37. Sieber, C. M. K. *et al.* Recovery of genomes from metagenomes via a dereplication, aggregation and scoring strategy. *Nat Microbiol* **3**, 836–843 (2018).
38. Alneberg, J. *et al.* Binning metagenomic contigs by coverage and composition. *Nat Methods* **11**, 1144–1146 (2014).
39. Chaumeil, P.-A., Mussig, A. J., Hugenholtz, P. & Parks, D. H. GTDB-Tk: a toolkit to classify genomes with the Genome Taxonomy Database. *Bioinformatics* **36**, 1925–1927 (2019).
40. Fu, L., Niu, B., Zhu, Z., Wu, S. & Li, W. CD-HIT: accelerated for clustering the next-generation sequencing data. *Bioinformatics* **28**, 3150–3152 (2012).
41. Jones, D. S. *et al.* Molecular evidence for novel mercury methylating microorganisms in sulfate-impacted lakes. *ISME J* (2019) doi:10.1038/s41396-019-0376-1.
42. Gionfriddo, C. M. *et al.* Hg-MATE-Db.v1.01142021. (2021).
43. Edgar, R. C. MUSCLE: a multiple sequence alignment method with reduced time and space complexity. *BMC Bioinformatics* **5**, 1–19 (2004).
44. Capella-Gutiérrez, S., Silla-Martínez, José. M. & Gabaldón, T. trimAl: a tool for automated alignment trimming in large-scale phylogenetic analyses. *Bioinformatics* **25**, 1972–1973 (2009).
45. Stamatakis, A. RAxML version 8: a tool for phylogenetic analysis and post-analysis of large phylogenies. *Bioinformatics* **30**, 1312–1313 (2014).
46. Yu, G., Smith, D. K., Zhu, H., Guan, Y. & Lam, T. T. ggtree: an R package for visualization and annotation of phylogenetic trees with their covariates and other associated data. *Methods Ecol. Evol.* **8**, 28–36 (2017).
47. Eddy, S. R. *hmmer*. (2015).
48. Aramaki, T. *et al.* KofamKOALA: KEGG Ortholog assignment based on profile HMM and adaptive score threshold. *Bioinformatics* **36**, 2251–2252 (2020).

49. Zhou, Z. *et al.* METABOLIC: High-throughput profiling of microbial genomes for functional traits, biogeochemistry, and community-scale metabolic networks. *bioRxiv (pre-print)* 30 (2020).
50. Price, M. N., Dehal, P. S. & Arkin, A. P. FastTree 2 – approximately maximum-likelihood trees for large alignments. *PLoS ONE* **5**, e9490 (2010).
51. Schloss, P. D. *et al.* Introducing mothur: open-source, platform-independent, community-supported software for describing and comparing microbial communities. *Appl Environ Microbiol* **75**, 7537–7541 (2009).
52. DeSantis, T. Z. *et al.* Greengenes, a chimera-checked 16S rRNA gene database and workbench compatible with ARB. *Appl Environ Microbiol* **72**, 5069–5072 (2006).
53. Newton, R. J., Jones, S. E., Eiler, A., McMahon, K. D. & Bertilsson, S. A guide to the natural history of freshwater lake bacteria. *Microbiology and Molecular Biology Reviews* **75**, 14–49 (2011).
54. Magnuson, J., Carpenter, S. R. & Stanley, E. H. North Temperate Lakes LTER: Chemical Limnology of Primary Study Lakes: Nutrients, pH and Carbon 1981 - version 52. (2020).
55. Chadwick, S. P., Babiarz, C. L., Hurley, J. P. & Armstrong, D. E. Influences of iron, manganese, and dissolved organic carbon on the hypolimnetic cycling of amended mercury. *Science of The Total Environment* **368**, 177–188 (2006).
56. Hintelmann, H. & Evans, R. D. Application of stable isotopes in environmental tracer studies - Measurement of monomethylmercury (CH₃Hg⁺) by isotope dilution ICP-MS and detection of species transformation. *Fresenius' Journal of Analytical Chemistry* **358**, 378–385 (1997).
57. Eckley, C. S., Luxton, T. P., Knightes, C. D. & Shah, V. Methylmercury production and degradation under light and dark conditions in the water column of the Hells Canyon Reservoirs, USA. *Environ Toxicol Chem* etc.5041 (2021) doi:10.1002/etc.5041.
58. Xun, L., Campbell, N. E. R. & Rudd, J. W. M. Measurements of Specific Rates of Net Methyl Mercury Production in the Water Column and Surface Sediments of Acidified and Circumneutral Lakes. *Can. J. Fish. Aquat. Sci.* **44**, 750–757 (1987).
59. Zhang, T., Kucharzyk, K. H., Kim, B., Deshusses, M. A. & Hsu-Kim, H. Net Methylation of Mercury in Estuarine Sediment Microcosms Amended with Dissolved, Nanoparticulate, and Microparticulate Mercuric Sulfides. *Environ. Sci. Technol.* **48**, 9133–9141 (2014).
60. Miller, C. L., Southworth, G., Brooks, S., Liang, L. & Gu, B. Kinetic Controls on the Complexation between Mercury and Dissolved Organic Matter in a Contaminated Environment. *Environ. Sci. Technol.* **43**, 8548–8553 (2009).
61. Eckley, C. S. & Hintelmann, H. Determination of mercury methylation potentials in the water column of lakes across Canada. *Science of The Total Environment* **368**, 111–125 (2006).

62. Gascón Díez, E. *et al.* Role of settling particles on mercury methylation in the oxic water column of freshwater systems. *Environ. Sci. Technol.* **50**, 11672–11679 (2016).
63. Capo, E. *et al.* Deltaproteobacteria and Spirochaetes-like bacteria are abundant putative mercury methylators in oxygen-deficient water and marine particles in the Baltic Sea. *Front. Microbiol.* **11**, 1–11 (2020).
64. Fleming, E. J., Mack, E. E., Green, P. G. & Nelson, D. C. Mercury Methylation from Unexpected Sources: Molybdate-Inhibited Freshwater Sediments and an Iron-Reducing Bacterium. *Appl Environ Microbiol* **72**, 457–464 (2006).
65. Christensen, G. A. *et al.* Carbon Amendments Alter Microbial Community Structure and Net Mercury Methylation Potential in Sediments. *Appl Environ Microbiol* **84**, e01049-17, /aem/84/3/e01049-17.atom (2017).
66. Kucharzyk, K. H., Deshusses, M. A., Porter, K. A. & Hsu-Kim, H. Relative contributions of mercury bioavailability and microbial growth rate on net methylmercury production by anaerobic mixed cultures. *Environ. Sci.: Processes Impacts* **17**, 1568–1577 (2015).
67. Bae, H.-S., Dierberg, F. E. & Ogram, A. Syntrophs dominate sequences associated with the mercury methylation-related gene *hgcA* in the Water Conservation Areas of the Florida Everglades. *Appl Environ Microbiol* **80**, 6517–6526 (2014).
68. Achá, D. *et al.* Sulfate-Reducing Bacteria in Floating Macrophyte Rhizospheres from an Amazonian Floodplain Lake in Bolivia and Their Association with Hg Methylation. *Appl Environ Microbiol* **71**, 7531–7535 (2005).
69. Yu, R.-Q., Reinfelder, J. R., Hines, M. E. & Barkay, T. Syntrophic pathways for microbial mercury methylation. *ISME J* **12**, 1826–1835 (2018).
70. Ekstrom, E. B., Morel, F. M. M. & Benoit, J. M. Mercury methylation independent of the acetyl-coenzyme A pathway in sulfate-reducing bacteria. *Appl Environ Microbiol* **69**, 5414–5422 (2003).
71. Ranchou-Peyruse, M. *et al.* Overview of mercury methylation capacities among anaerobic bacteria including representatives of the sulphate-reducers: implications for environmental studies. *Geomicrobiology Journal* **26**, 1–8 (2009).
72. Gilmour, C. C. *et al.* Sulfate-reducing bacterium *Desulfovibrio desulfuricans* ND132 as a model for understanding bacterial mercury methylation. *Appl. Environ. Microbiol.* **77**, 3938–3951 (2011).
73. Qian, C. *et al.* Quantitative proteomic analysis of biological processes and responses of the bacterium *Desulfovibrio desulfuricans* ND132 upon deletion of its mercury methylation genes. *Proteomics* **18**, 1700479 (2018).
74. Goñi-Urriza, M. *et al.* Relationships between bacterial energetic metabolism, mercury methylation potential, and *hgcA/hgcB* gene expression in *Desulfovibrio dechloroacetivorans* BerOc1. *Environ Sci Pollut Res* **22**, 13764–13771 (2015).

75. Gionfriddo, C. M. *et al.* Genome-resolved metagenomics and detailed geochemical speciation analyses yield new insights into microbial mercury cycling in geothermal springs. *Applied and Environmental Microbiology* **86**, 1–20 (2020).
76. Lin, H. *et al.* Mercury methylation by metabolically versatile and cosmopolitan marine bacteria. *ISME J* (2021) doi:10.1038/s41396-020-00889-4.
77. Schaefer, J. K. *et al.* Active transport, substrate specificity, and methylation of Hg(II) in anaerobic bacteria. *Proceedings of the National Academy of Sciences* **108**, 8714–8719 (2011).
78. Janssen, S. E., Schaefer, J. K., Barkay, T. & Reinfelder, J. R. Fractionation of Mercury Stable Isotopes during Microbial Methylmercury Production by Iron- and Sulfate-Reducing Bacteria. *Environ. Sci. Technol.* **50**, 8077–8083 (2016).
79. Choi, S.-C., Chase, T. & Bartha, R. Metabolic pathways leading to mercury methylation in *Desulfovibrio desulfuricans* LS. *Appl Environ Microbiol* **60**, 4072–4077 (1994).
80. White, D., Drummond, J. & Fuqua, C. *The Physiology and Biochemistry of Prokaryotes*. (Oxford University Press, 2012).
81. Qian, C. *et al.* Global proteome response to deletion of genes related to mercury methylation and dissimilatory metal reduction reveals changes in respiratory metabolism in *Geobacter sulfurreducens* PCA. *J. Proteome Res.* **15**, 3540–3549 (2016).
82. Beulig, F., Røy, H., Glombitza, C. & Jørgensen, B. B. Control on rate and pathway of anaerobic organic carbon degradation in the seabed. *Proc Natl Acad Sci USA* **115**, 367–372 (2018).
83. Noike, T., Endo, G., Chang, J.-E., Yaguchi, J.-I. & Matsumoto, J.-I. Characteristics of carbohydrate degradation and the rate-limiting step in anaerobic digestion. *Biotechnol. Bioeng.* **27**, 1482–1489 (1985).
84. Burdige, D. J. & Gardner, K. G. Molecular weight distribution of dissolved organic carbon in marine sediment pore waters. *Marine Chemistry* **62**, 45–64 (1998).
85. Arnosti, C., Repeta, D. J. & Blough, N. V. Rapid bacterial degradation of polysaccharides in anoxic marine systems. *Geochimica et Cosmochimica Acta* **58**, 2639–2652 (1994).
86. Ostapenia, A. P., Parparov, A. & Berman, T. Lability of organic carbon in lakes of different trophic status. *Freshwater Biology* **54**, 1312–1323 (2009).
87. Desrochers, K. A. N., Paulson, K. M. A., Ptacek, C. J., Blowes, D. W. & Gould, W. D. Effect of Electron Donor to Sulfate Ratio on Mercury Methylation in Floodplain Sediments under Saturated Flow Conditions. *Geomicrobiology Journal* **32**, 924–933 (2015).

Appendix to Chapter 5: Supplementary figures

Supplementary Figures:

Figure S5.1: Heatmaps of temperature (A) and dissolved oxygen (B) at the sampling location in Lake Mendota over most of the ice-free season in 2020 (x-axis is time). The vermillion diamonds in each figure correspond to the date and depths where the incubations were conducted. The black line in A corresponds to the thermocline.

Figure S5.2: Profiles of dissolved oxygen (DO), temperature and turbidity (A, H); dissolved and particulate iron (Fe) (B, I); dissolved and particulate manganese (Mn) (C, J); sulfate and sulfide (D, K); dissolved organic carbon (DOC), suspended particulate matter (SPM), and bacterial carbon production (BCP), which is a measure of community heterotrophy (E, L); dissolved inorganic Hg (iHg), dissolved methylmercury (MeHg), and percent MeHg in dissolved phase (F, M); and particulate inorganic Hg (iHg), particulate methylmercury (MeHg), and percent MeHg in particulate phase (G, N) for both September and October sampling trips.

Figure S5.3: Total excess ^{198}Hg levels for all five sets of incubations. The bin holding the incubation bags at 15.7 m in October was lost between t_1 and t_2 .

Figure S5.4: Excess Me^{198}Hg plots over three time points for three depths in September (A) and two depths in October (B). Plots with zoomed-in y-axis are shown in C for the two suboxic incubations due to their lower Me^{198}Hg production. The bin holding the incubation bags at 15.7 m in October was lost between t_1 and t_2 , so there's no data for t_2 for that location.

Figure S5.5: Plot of the K_{metR} values for incubations under ambient conditions vs. the *hgcA* abundance at that location. Gene abundance is normalized to the abundance of 16 ribosomal protein genes.

Figure S5.6: Maximum likelihood tree of identified *hgcA* sequences from this study (in orange) with reference sequences from Peterson et al, 2020; Jones et al, 2019; and the Hg-MATE database. Heatmap shows the abundance of each *hgcA* sequence identified in this study in each metagenome. The *hgcA* gene abundance is expressed as a percentage of the mean abundance of 16 ribosomal protein genes.

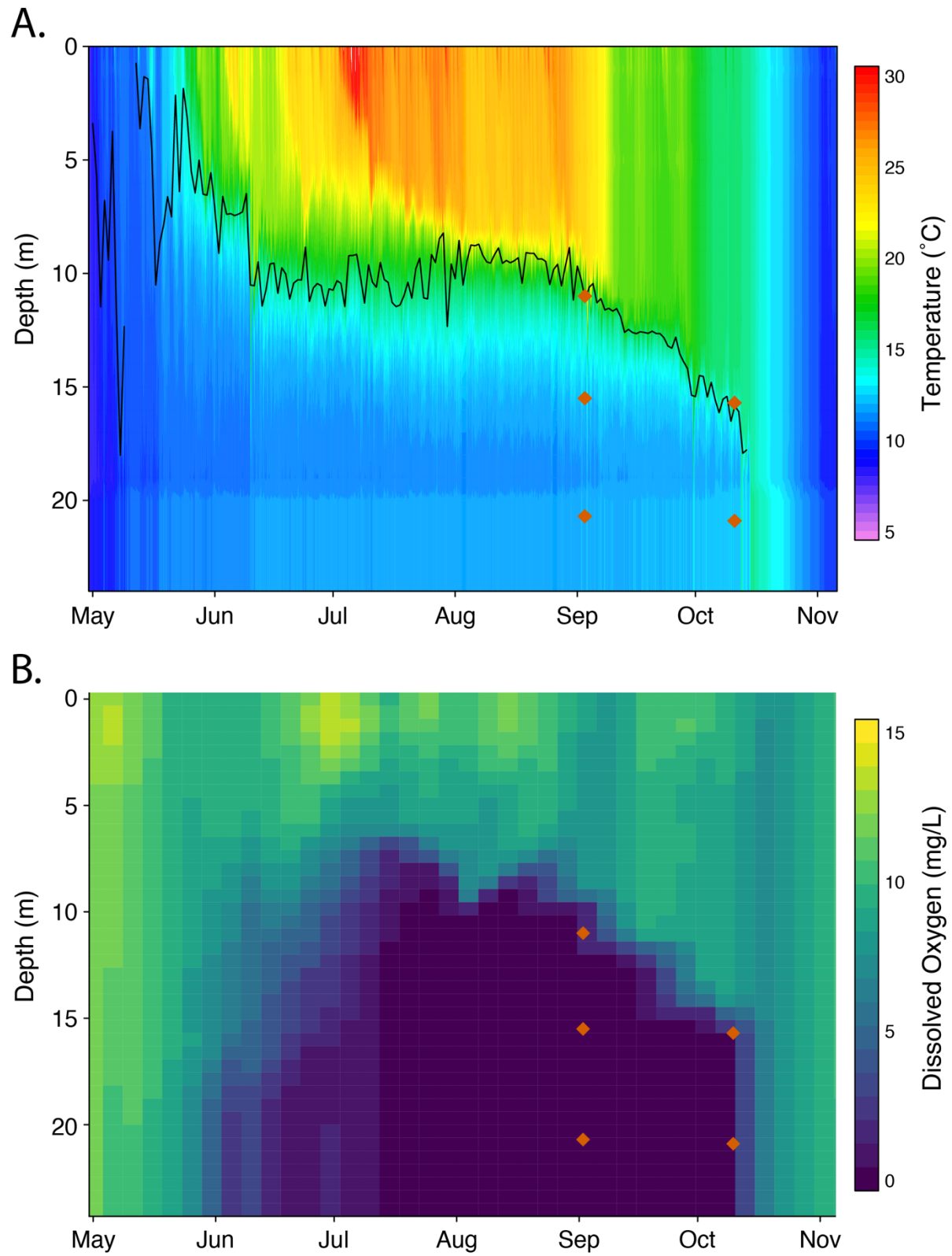
Fig. S5.1

Fig. S5.2

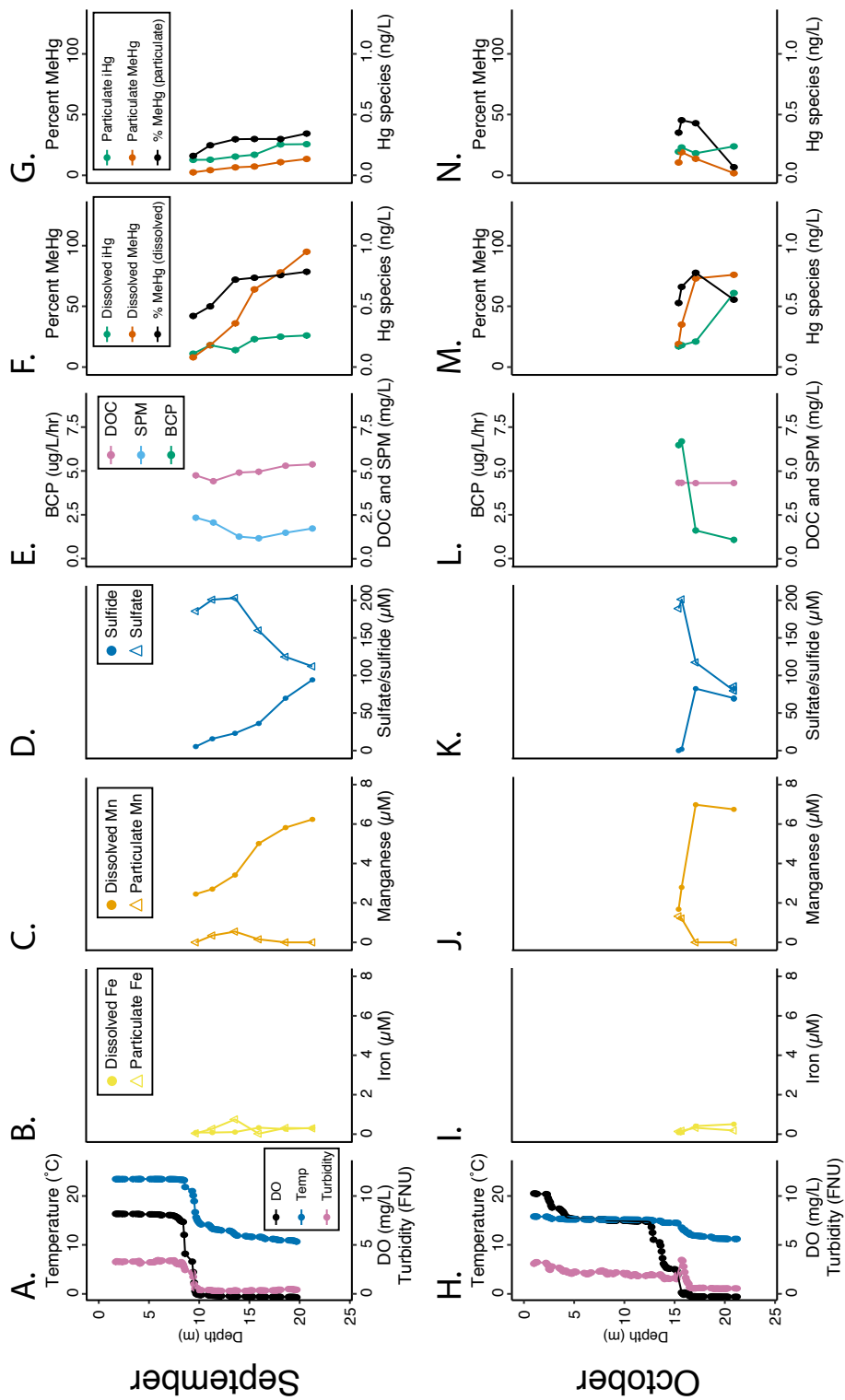


Fig. S5.3

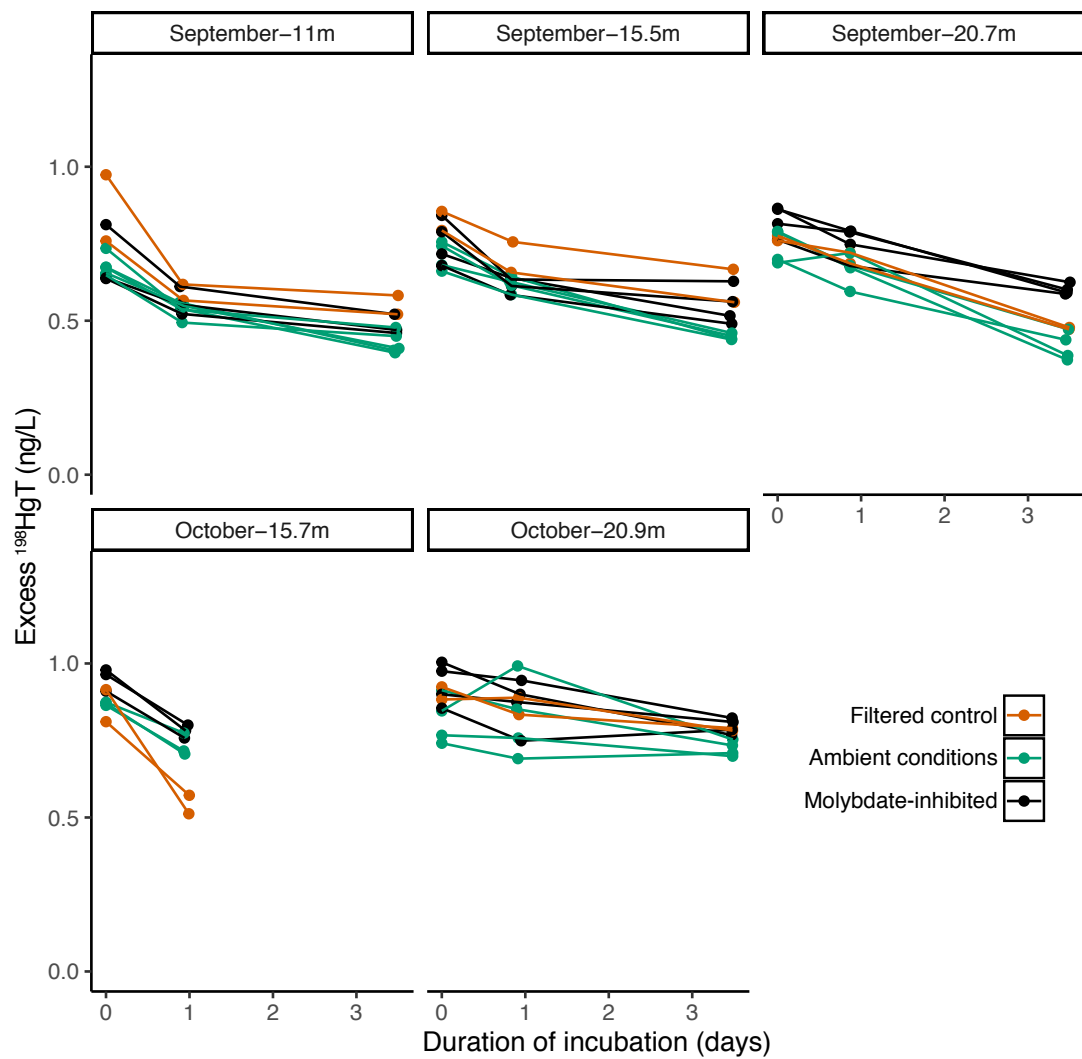


Fig. S5.4

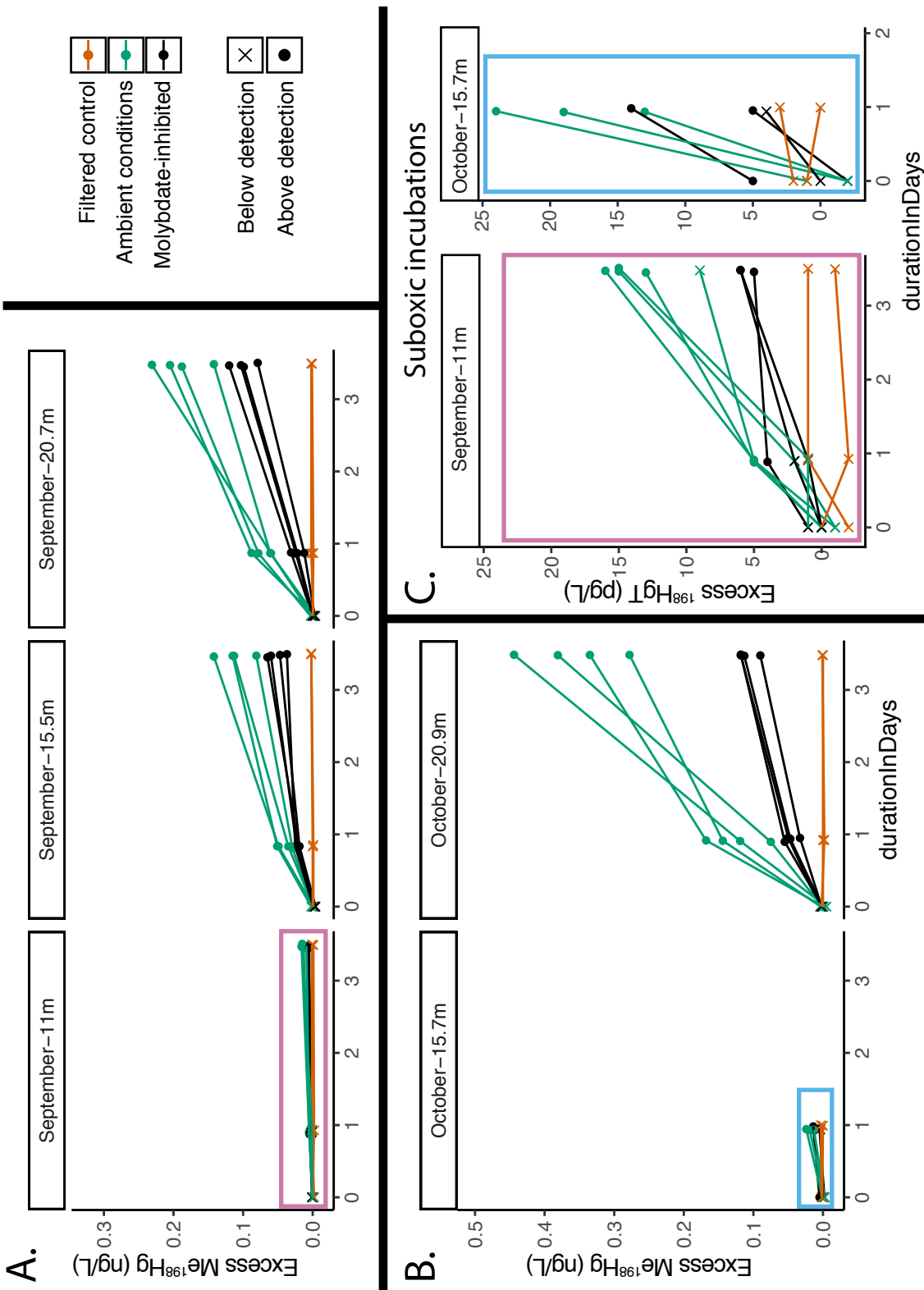


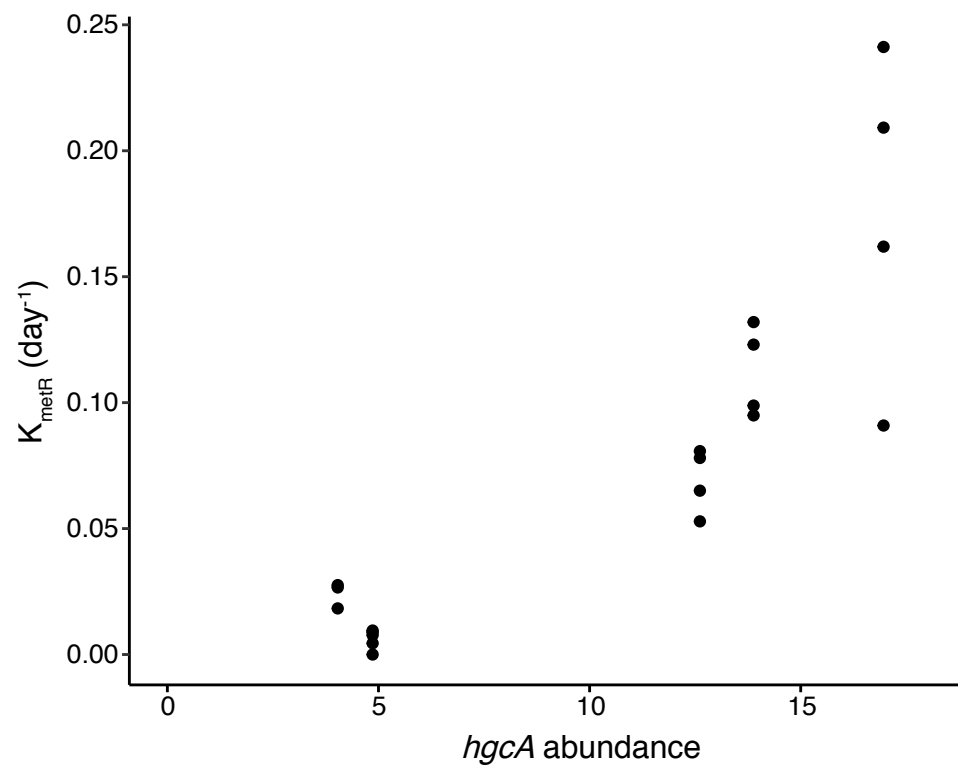
Fig. S5.5

Fig. S5.6

This study

Peterson et al, 2020

Jones et al, 2019

Sequences from Hg-MATE database

0.5



Chapter 6: Conclusions and future directions.

Several common themes appeared over the four research chapters in this thesis. In this chapter, I briefly summarize the major findings and propose future work that will expand upon these results.

1. Fermentative organisms constitute large fraction of Hg-methylator diversity across multiple aquatic systems.

Each of the research chapters in this thesis joins a rapidly growing body of literature highlighting the metabolic and taxonomic diversity of the organisms carrying *hgcA*. In particular, obligately fermentative Hg methylators were abundant across all study sites. In both Lake Mendota and Brownlee Reservoir, we identified organisms with *hgcA* (*hgcA*⁺) associated with the Kiritimatiellaeota phylum as the most abundant Hg-methylators, among many other obligately fermentative organisms (Chapters 2, 3, and 5). These organisms have been previously identified in another freshwater lake, but not as high in abundance.¹ They were present in the sediment cores from the Everglades, but at a lower relative abundance, suggesting they may be specifically suited to living in the water column (Chapter 4). We also observe a number of organisms that appear to be facultatively aerobic with *hgcA*, within phyla such as Actinobacteria or Chloroflexi (Chapters 4 and 5). It is uncertain what their active metabolic pathways are at these depths, but the lack of oxygen at the depths where they were found would indicate that these organisms are living fermentatively. This, together with the observed MeHg production under inhibition of sulfate reduction, shows that there may be a common group of organisms mediating Hg methylation in freshwater lakes and that fermentative organisms in general may play a large role in MeHg production across an array of ecosystems.

Expanding the use of metagenomic sequencing for *hgcA* identification or the use of improved PCR primers will help identify how widespread these divergent *hgcA* sequences are. Verification of these organisms as functional and relevant Hg-methylators is a key next step as well. In the field, performing RNA sequencing would identify which *hgcA*⁺ organisms were transcriptionally active, which metabolic pathways were active, and whether or not the *hgcA* gene was actively transcribed. While the HgcA amino acid sequences have the necessary conserved residues² and protein modeling of other non-canonical HgcA proteins^{3,4} suggests that these novel *hgcA* sequences are capable of Hg methylation, ensuring that these microbes are actually capable of taking up iHg and converting it to MeHg is a necessary step. Analyses have identified non-canonical Hg-methylators in culture^{5,6}, which offers an opportunity to experimentally verify these new Hg-methylators.

2. Water column Hg-methylation is likely to be important source of MeHg.

Our results from Lake Mendota and Brownlee Reservoir corroborate past literature suggesting that MeHg accumulation in the anoxic hypolimnion can often be attributed to *in situ* production rather than diffusion from the sediments (Chapters 2, 3, and 5).^{7,8} In Mendota, we observed profiles that were inconsistent with diffusion from the sediments and high rates of MeHg production that matched up with the *hgcA* abundance. In Brownlee, we also saw mid-column peaks in MeHg and percent MeHg, and here we also saw a correlation between *hgcA* abundance and MeHg concentrations in the water column. This corroborates with gradients just above the sediment-water interface that indicate that MeHg was not diffusing out of the sediments.⁹ Curiously, at both sites the inorganic Hg (iHg) levels were approximately 0.2 ng/L with a few exceptions in the deepest, most reduced samples. One potential explanation for this is

that high rates of MeHg production will methylate nearly all of the bioavailable Hg and that any iHg is inaccessible for uptake and subsequent methylation. In this case, water column Hg methylation is more limited by the appearance of bioavailable iHg, which would explain the similar levels of MeHg accumulation despite large differences in Hg methylation capacity (Chapter 5).

Much remains uncertain about how MeHg accumulation occurs in the hypolimnion. Improving the stable isotope enriched Hg tracer incubations to allow for quantification of Hg methylation in ecosystems with a different trophic status and lower MeHg production, such as Brownlee Reservoir, will enable studies to see if rapid conversion of iHg to MeHg in the water column is widespread. Equally importantly will be determining the source, transport, and complexation of iHg that leads to the observed bioavailability in these systems. The complexity of these interactions highlights the value of focusing on a small number of locations using large-scale, intensive studies using a multi-pronged, interdisciplinary approach. Incorporating new techniques and methods, such as the corewater sampling⁹ or MeHg-specific stable isotope analysis¹⁰, will further enhance our ability to identify the source and transport of MeHg in the hypolimnion.

3. Abundance of *hgcA* can be a valuable indicator of Hg methylation capacity.

We've shown that in various conditions and environments, *hgcA* gene presence can be representative of MeHg accumulation, MeHg production, and/or microbial Hg methylation capacity. In Brownlee Reservoir, where hypolimnetic and metalimnetic MeHg accumulation were thought to be driven by water column Hg methylation, we observed a linear correlation between *hgcA* and MeHg (Chapter 3). The lack of sulfide accumulation and relative

homogeneity of the DOM composition and concentration suggests that bioavailability of iHg may not change much over these conditions and that MeHg production levels is mostly reliant on Hg methylation capacity. On the other hand, *hgcA* abundance did not correlate well with MeHg levels in Lake Mendota (Chapter 2 and 5), but it did correlate well with relative Hg methylation rates (Chapter 5). The very high rates of Hg methylation we observed, the high fraction of MeHg, and the consistent iHg concentrations across a range of conditions may suggest that nearly all bioavailable Hg has been methylated, meaning that MeHg levels are limited more by the available iHg pool rather than the rate of MeHg production. While *hgcA* abundance was unrelated to MeHg levels overall or MeHg production values under ambient conditions in sediment cores of the Florida Everglades, by isolating the effect of the Hg methylation capacity of the microbial community from the effect of iHg bioavailability, we showed that *hgcA* correlates well with the calculated Hg methylation capacity under a broad range of iHg bioavailability (Chapter 4). Collectively, these data show that *hgcA* can be a valuable tool in separating the impact of the microbial Hg methylation capacity from the array of other factors that influence MeHg accumulation in freshwater ecosystems.

There remains a great deal of work to be done to evaluate the influence of the Hg methylation capacity of a microbial community on the final observed levels of MeHg in the environment. In particular, using the methods described in Chapter 4 to examine the Hg methylation capacity of the microbial community under a range of realistic iHg bioavailability conditions and compare that to the microbial community with *hgcA* across multiple environments will help provide insight into how MeHg concentrations are controlled *in situ*.

4. Hg methylation can be active under suboxic conditions.

Hg methylation is historically associated with sulfidic conditions, but the data presented here, particularly from Brownlee Reservoir, strongly suggests that MeHg production is possible under suboxic conditions. Sulfide production was rare during our sampling efforts in Brownlee, yet MeHg accumulation was common. MeHg production in oxic or suboxic environments has previously been ascribed to sulfate reduction occurring in euxinic niches¹¹; however, the sulfate reduction genes only appeared when sulfide was present and some organisms with *hgcA* carried respiratory pathways for nitrate or Mn reduction, suggesting that this Hg methylation was a truly suboxic process (Chapter 3). In Mendota, MeHg was highest when sulfide was present, but the abundance of *hgcA*⁺ Geobacteraceae with external electron pathways co-localized with elevated particulate manganese (Mn) levels suggests that Mn reduction could be playing a role in MeHg production in this lake as well (Chapter 2).

Experimentally confirming MeHg production activity under these suboxic conditions is a critical next step. Testing *hgcA*⁺ cultures that operate under suboxic conditions, such as nitrate reducers or Mn reducers under conditions similar to those found in the environment will be an important step in confirmed that this process works under these conditions. Additionally, demonstrating reduced MeHg production under inhibition of both sulfate-reducing bacteria (SRB) and methanogens and enhanced MeHg production in response to nitrate and/or Mn amendment will help evaluate the environmental relevance of suboxic MeHg production. RNA sequencing or metaproteomics done in parallel with these experiments could be used to identify the expression of *hgcA* under these conditions and identify the active metabolic pathways in these Hg-methylating organisms to further confirm links between nitrate or Mn reduction and MeHg production.

5. The relationship between Hg methylation capacity and sulfate reduction varies widely between ecosystems.

The results from this study highlight the complex relationship between sulfate reduction activity and the Hg methylation capacity of the microbial community. In the two freshwater water column ecosystems, we observed substantial increases in *hgcA* levels under sulfidic conditions (Chapters 2, 3 and 5). While this would suggest that most *hgcA*⁺ organisms are SRB, they actually accounted for a small percentage of the overall *hgcA* population. The *hgcA* gene is not known to confer any competitive advantage or Hg detoxification under laboratory condition. However, the appearance of *hgcA* under sulfidic conditions, coupled with the observations that HgT accumulates in the water column under more reduced conditions due to diffusion or diagenesis¹² and that MeHg is rapidly exported from the cell¹³, suggests that rapid Hg methylation and export of Hg is a favorable trait under these conditions. While many studies have searched for *hgcA*, very few have done so in way that allows for the calculation of Hg-methylator abundance as a fraction of the total microbial community, limiting our ability to comment on the selection of the trait within these communities. However, in one study, the relative abundance of *hgcA*⁺ organisms, not just *hgcA*⁺ SRB, was higher in high sulfide samples.¹ On the other hand, in the sediments of the Florida Everglades, *hgcA* increased substantially as sulfide declined, suggesting that this trend does not hold up in sediment communities, possibly due to the lower bioavailability of iHg under these conditions (Chapter 4).

Understanding the role of *hgcA* in microbial physiology will go a long way towards explaining the observed distribution of the gene in the environment. In the lab, further characterization of the links between *hgcA* activity and the THF cycles¹⁴⁻¹⁶ and the possible interaction with divalent metal uptake¹⁷ may provide insight into the conditions under which

hgcA increases microbial fitness. In the environment, additional exploration of *hgcA* abundance and diversity using shotgun metagenomics along sulfide gradients will illuminate the conditions under which these trends hold true. Furthermore, RNA sequencing data from these same gradients will identify whether or not the *hgcA* is expressed under changing conditions and provide additional insight into the active metabolic pathways for these Hg-methylating organisms.

6. Sulfate reduction can have major influence on MeHg production capacity independent of *hgcA*+ SRB abundance.

The results from Chapter 5 show that even when SRB with *hgcA* are low in abundance, sulfate reduction plays a substantial role in the Hg methylation capacity of the microbial community. This could be due to direct impacts of the SRB Hg-methylators, in which this small community of methylators accounts for a large percentage of the MeHg production. Differences in Hg methylation efficiency in laboratory experiments do indicate that such a difference is possible. SRB could also influence MeHg by driving overall food web activity. While polymer hydrolysis is often regarded as the rate-limiting step in anaerobic carbon degradation, it may not be true in ecosystems with a high level of labile carbon, such as Lake Mendota. In such a system, respiration processes such as sulfate reduction are likely to drive community metabolism, and inhibition of these pathways is likely to slow down upstream fermentation pathways. If these fermentative organisms are the primary Hg-methylators, this will decrease MeHg production capacity.

While directly testing the Hg-methylating capacity of different metabolic guilds in a complex community is not currently possible, indirect measurements to estimate microbial

activity, such as RNA sequencing or metaproteomics, could indicate the relative *hgcA* expression or general metabolic activity of different guilds and suggest which are producing MeHg. As discussed previously, the Hg methylation activity of many of the non-canonical *hgcA*⁺ organisms have not yet been tested. Even laboratory measurements of their MeHg production efficiency might provide an indication of the relative contribution of different guilds to the Hg methylation rates *in situ*. On the other hands, identifying potential indirect effects of SRB on MeHg production will require further investigation into the basic structure of the anaerobic food web in the system of interest. Measuring the community metabolism response to SRB inhibition, through leucine uptake assays or BONCAT, in parallel to MeHg production assays could provide insight into the shifts in community metabolism underlying the changes in Hg methylation activity. More targeted analysis could be done as well by using ¹³C-labeled substrates to track changes in both the rate of consumption of the substrate and in the wiring of the microbial network that is degrading it through stable isotope probing.

References

1. Jones, D. S. *et al.* Molecular evidence for novel mercury methylating microorganisms in sulfate-impacted lakes. *ISME J* (2019) doi:10.1038/s41396-019-0376-1.
2. Smith, S. D. *et al.* Site-directed mutagenesis of *hgcA* and *hgcB* reveals amino acid residues important for mercury methylation. *Appl. Environ. Microbiol.* **81**, 3205–3217 (2015).
3. Lin, H. *et al.* Mercury methylation by metabolically versatile and cosmopolitan marine bacteria. *ISME J* (2021) doi:10.1038/s41396-020-00889-4.
4. Gionfriddo, C. M. *et al.* Microbial mercury methylation in Antarctic sea ice. *Nature Microbiology* **1**, 1–12 (2016).
5. McDaniel, E. A. *et al.* Expanded phylogenetic diversity and metabolic flexibility of mercury-methylating microorganisms. *mSystems* **5**, 1–21 (2020).
6. Gionfriddo, C. M. *et al.* Hg-MATE-Db.v1.01142021. (2021).
7. Watras, C. J. *et al.* Methylmercury production in the anoxic hypolimnion of a dimictic seepage lake. *Water, Air, and Soil Pollution* **80**, 735–745 (1995).
8. Eckley, C. S. *et al.* Mercury methylation in the hypolimnetic waters of lakes with and without connection to wetlands in northern Wisconsin. *Can J Fish Aquat Sci* **62**, 400–411 (2005).
9. Poulin, B. A. *et al.* *Chemical characterization of water and suspended sediment of the Snake River and Hells Canyon Complex (Idaho, Oregon)*. <https://doi.org/10.5066/P9DT2B6J> (2020).
10. Rosera, T. J. *et al.* Isolation of methylmercury using distillation and anion-exchange chromatography for isotopic analyses in natural matrices. *Anal Bioanal Chem* **412**, 681–690 (2020).
11. Gascón Díez, E. *et al.* Role of settling particles on mercury methylation in the oxic water column of freshwater systems. *Environ. Sci. Technol.* **50**, 11672–11679 (2016).
12. Chadwick, S. P., Babiarz, C. L., Hurley, J. P. & Armstrong, D. E. Influences of iron, manganese, and dissolved organic carbon on the hypolimnetic cycling of amended mercury. *Science of The Total Environment* **368**, 177–188 (2006).
13. Schaefer, J. K. *et al.* Active transport, substrate specificity, and methylation of Hg(II) in anaerobic bacteria. *Proceedings of the National Academy of Sciences* **108**, 8714–8719 (2011).

14. White, D., Drummond, J. & Fuqua, C. *The Physiology and Biochemistry of Prokaryotes*. (Oxford University Press, 2012).
15. Parks, J. M. *et al.* The genetic basis for bacterial mercury methylation. *Science* **339**, 1332–1335 (2013).
16. Choi, S.-C., Chase, T. & Bartha, R. Metabolic pathways leading to mercury methylation in *Desulfovibrio desulfuricans* LS. *Appl Environ Microbiol* **60**, 4072–4077 (1994).
17. Schaefer, J. K., Szczuka, A. & Morel, F. M. M. Effect of Divalent Metals on Hg(II) Uptake and Methylation by Bacteria. *Environ. Sci. Technol.* **48**, 3007–3013 (2014).